universität wien

DISSERTATION / DOCTORAL THESIS

Titel der Dissertation /Title of the Doctoral Thesis

Circuit mechanisms of hierarchical interactions in affective learning

verfasst von / submitted by

Dominic Kargl, MSc

angestrebter akademischer Grad / in partial fulfilment of the requirements for the degree of

Doctor of Philosophy (PhD)

Wien, 2020 / Vienna 2020

Studienkennzahl lt. Studienblatt / degree programme code as it appears on the student record sheet:	A 794 685 490
Dissertationsgebiet lt. Studienblatt / field of study as it appears on the student record sheet:	Molekulare Biologie
Betreut von / Supervisor:	Dr. Wulf Haubensak

Acknowledgements

I owe tremendous thanks to Wulf Haubensak for the opportunity to do my PhD work in such a vibrant and exciting field of science. The last years strongly shaped my personality and opened my eyes to what neuroscience is and should be. Your incessant enthusiasm along with enabling free exploration and independence were key drivers of this project.

I want to express my gratitude to all past and present members of the Haubensak group for the exceptionally supportive environment you managed to create inside and outside of the lab, not to mention the fun trips and parties! Yet, I want to particularly thank Joanna Kaczanowska for her never-ending efforts in making our collaboration this supportive. I'm especially grateful to you for your patience and of course for coloring the countless hours in the basement. Likewise, I'm thankful to Johannes Griessner for the stimulating and entertaining (scientific) discussions over coffee.

Thank you Inês Crisóstomo for creating this supportive environment at the VBC, this is making a great difference for PhD students on campus.

I want to thank all collaborators, especially Ornella Valenti for the fun hours while introducing me to the power of *in vivo* electrophysiology and constant advice. Special thanks to all the support facilities, especially Martin Colombini for pioneering electrode construction at the IMP.

I cannot thank the Sparverein enough for keeping my spirit up throughout the years. You were indeed an indispensable source of energy! A great share of this goes to Eva for her remarkable skill in cheering me up, not to mention the invaluable life support at (many) times.

Finally, I want to thank Jana for her endless patience, understanding and love. Seeing you at the end of a hard day means the world to me.

The research in this thesis was supported by the Research Institute of Molecular Pathology (IMP), Boehringer Ingelheim, the Austrian Research Promotion Agency (FFG), and a grant from the European Community's Seventh Framework Programme (FP/2007-2013) / ERC grant agreement no. 311701.

Abstract

Brains aim to predict the future based on their sensory past. In Pavlovian learning (PL) salient sensory stimuli in the environment, such as conditioned (CS) and unconditioned stimuli (US), become associated to reduce uncertainty about CS value and adapt behavior. Functional neuroanatomy identified diverse neural substrates across cerebral hierarchies to facilitate PL, including cortical, striatal and brain stem circuits, suggesting distributed processing of Pavlovian stimuli. The encoding of complementary stimulus features and their interaction might therefore constitute a synergistic property of neural systems for optimal performance. Moreover, the underlying information flow between hierarchical levels at defined PL stages is largely unknown.

This thesis seeks to (i) allocate the hierarchical encoding of distinct stimulus features, such as valence and salience in cortico-limbic networks and (ii) establish causal interactions of network elements in the context of PL to derive generalizable principles for the etiology of psychiatric conditions with aberrant hierarchical circuit interaction.

By using functional MRI, *in vivo* activity recordings and neuronal circuit manipulation during a discriminatory PL task this work identified a circuit module resolving uncertainty about CS value by exploiting instructive interoceptive information. In this framework, the central amygdala (CE) crucially employs bottom-up signaling via the cholinergic basal forebrain to recruit stimulus-associated interoceptive models in the insular cortex to support CE CS discrimination. In turn, top-down–instructed stimulus-behavior associations are retained in CE circuitry as long-term memory by a permissive US-dependent positive prediction error signal ascending from dopaminergic ventral periaqueductal gray and dorsal raphe neurons (vPAG/DR).

Collectively, this thesis depicts PL as a gradual model-building process, engaging distinct hierarchical levels, encompassing the IC, CE and vPAG/DR, to incorporate interoception-based value information into exteroceptive stimulus representations. In this process, distributed stimulus features synergize to allow for adaptive behavioral responding. Furthermore, this work provides a mechanistic account for dysfunctional network integration possibly underpinning intolerance to uncertainty, a hallmark of autism and related psychiatric disorders.

Zusammenfassung

Gehirne versuchen die Zukunft auf der Grundlage ihrer sensorischen Vergangenheit vorhersagen. Beim Pawlowschen Lernen (PL) werden hervorstechende Sinnesreize in der Umwelt, wie konditionierte (CS) und unkonditionierte Stimuli (US), in Zusammenhang gebracht, um die Unsicherheit über den Wert des CS für den Organismus zu reduzieren und das Verhalten dementsprechend anzupassen. Die funktionelle Neuroanatomie identifizierte verschiedene neuronale Substrate über zerebrale Hierarchien hinweg, die für PL notwendig sind. Diese schließen kortikale, striatale und Hirnstammregionen mit ein, was auf eine verteilte Verarbeitung von Pawlowschen Stimuli schließen lässt. Die Kodierung von komplementären Eigenschaften dieser Stimuli und deren Interaktion könnte daher eine synergistische Eigenschaft neuronaler Systeme für deren optimalen Funktion darstellen. Darüber hinaus ist der zugrundeliegende Informationsfluss zwischen hierarchischen Ebenen in definierten PL-Phasen weitgehend unbekannt.

Ziel dieser Arbeit ist es, (i) die hierarchische Kodierung verschiedener Reizeigenschaften, wie z.B. Valenz und Salienz kortiko-limbischen Netzwerken zuzuordnen und (ii) kausale Interaktionen von Netzwerkelementen im Kontext des PL zu etablieren, um verallgemeinerbare Prinzipien für die Ätiologie psychiatrischer Zustände mit abweichender hierarchischer Schaltkreisinteraktion abzuleiten.

Durch die Verwendung von funktioneller MRT, in vivo Aktivitätsaufzeichnungen und neuronaler Schaltkreismanipulation während eines diskriminatorischen PL-Prozesses wurde in dieser Arbeit ein Schaltkreismodul identifiziert, welches die Unsicherheit über den Wert des CS durch die Nutzung instruktiver interozeptiver Informationen auflöst. Dabei löst die zentrale Amygdala (CE) entscheidende Bottom-Up-Signale über das cholinerge basale Vorderhirn aus, um Stimulus-assoziierte interozeptive Modelle im insularen Kortex zu rekrutieren, die die CS-Diskriminierung in der CE erlauben. Zusätzlich wird diese Top-Down-instruierte Assoziation von Stimulus und Verhalten durch ein permissives, US-abhängiges und positives Vorhersagefehlersignal im Langzeitgedächtnis der CE gespeichert, welches von dopaminergen Neuronen im ventralen periaquäduktalen Grau und dorsalen Raphe-Kern (vPAG/DR) zur CE aufsteigt.

Zusammengefasst stellt diese Arbeit PL als einen graduellen Modellbildungsprozess dar, der verschiedene hierarchische Ebenen umfasst (IC, CE und vPAG/DR), um interozeptionsbasierte Wertinformationen in exterozeptive Stimulusrepräsentationen zu integrieren. In diesem Prozess wirken verteilte Stimuluseigenschaften synergistisch

zusammen, um eine adaptive Verhaltensreaktion zu ermöglichen. Darüber hinaus liefert diese Arbeit ein mechanistisches Modell einer dysfunktionalen Netzwerkintegration, welche möglicherweise der Intoleranz gegenüber Unsicherheit, ein Kennzeichen von Autismus und verwandten psychiatrischen Störungen, zu Grunde liegt.

Table of Contents

Introduction

Origins of affect

Emotions determine individual survival by tagging features in the environment with meaning. For this purpose, brains (learn to) tune to cues linked to pleasure or pain to ultimately guide approach or avoidance behavior, respectively. Emotional states are internal drivers for action and bring about the physiological, cognitive and motivational resources of an individual to cope or exploit challenges or opportunities provided by its environment, respectively (LeDoux, 1995). Environmental cues engage multiple sensory modalities and thus are inherently complex and multi-dimensional. Therefore, neural systems need to reduce these dimensions to a common motivational metric (e.g. hedonic scale) to allow for binary approach/avoidance decisions, the essential consequence of an emotional state (Shizgal, 1999).

Initially, portrayed as tampering with human rationality and reason by the ancient Greeks, emotion's constructive function in perception, attention, memory and decision-making has now been recognized by observations of the predominantly advantageous biasing of each of the above cognitive processes (Cacioppo and Gardner, 1999; Dolan, 2002). Consequently, the conceptual separation of emotion and cognition into different faculties is being increasingly abandoned (Pessoa, 2008). Despite no consensual definition on emotions exists yet, it is widely accepted that they exist across a wide range of phylogeny and therefore were subject to evolutionary forces (Darwin, 1872). Interestingly, James Darwin did not view emotional expressions as functionally adaptive per se, rather as vestiges of ingrained habitual behaviors, once useful in the evolutionary past (Barrett, 2011). Over the last centuries many theories on the origin of emotion have emerged. These can be broadly categorized into the 'Basic Emotion' (Ekman, 1992), the 'Appraisal' (Arnold, 1960) and the 'Constructionist' (Wundt, 1894) domains. Basic emotion theory predicts automatic responses/expressions to environmental cues which are hardwired in the brain and therefore have a biological origin. It posits that basic categories are universal and the same category (e.g. 'fear') would elicit homologous responses with similar behavioral patterns within any given species. Appraisal theories depict emotions as intentional states that follow cognitive evaluation of sensory cues which ultimately instantiates meaning. They explicitly state the absence of reflexes or habits and require conscious awareness (Gendron and Barrett, 2009). Early psychological

constructionist theories attempted to deconstruct emotions into their basic components (‘dimensions’). These propositions introduced ‘valence’ and ’arousal’ as the two major factors constituting an emotion. Central to these proposals were antagonistic motivational systems, engaged by the appetitive or aversive (valence) nature of stimuli and modulated by the level of activation (arousal) (Dickinson and Pearce, 1977; Konorski, 1967). Accordingly, every emotion could be described by unique mapping onto these dimensions. In psychology, this model was successful in capturing the subjective (human) experience across modalities (e.g. faces, images, words). In this regard, one of the most influential studies by James Russell gave rise to the two-dimensional circumplex model of affect, in which self-reported judgement of stimuli based on their affective value was in agreement with the two-factor model (Russell, 1980). Although this descriptive classification of subjective experience of human affect by these principal components formalize the diversity of emotions to some extent, it remains unclear how these dimensions would be implemented in the brain and therefore they may not be inherent to affect itself. Based on current evidence it is unknown whether valence and arousal themselves map onto discrete neural elements. It follows that a focus on mechanisms should prevail over purely mental categories (Barrett, 2017; Calder et al., 2001). This applies especially to emotion research on animal models, where verbal reports on emotion categories are unavailable.

One of the most influential theories from the constructionists was put forward in 1884 by William James and independently from Carl Lange in 1885, which has been rediscovered more recently due to the surging interest in the role of signals from the viscera in aspects of cognition (Azzalini et al., 2019).
The central statement in James’ proposition “*What is an emotion?*” was as follows:

> *Our natural way of thinking about these standard emotions is that the mental perception of some fact excites the mental affection called the emotion, and that this latter state of mind gives rise to the bodily expression. My thesis on the contrary is that the bodily changes follow directly the perception of the exciting fact, and that our feeling of same changes as they occur is the emotion.*
>
> - William James, 1884

According to the James-Lange theory and contrary to intuition, he conceived that upon encounter of affective sensory stimuli bodily arousal occurs first and the secondary central interpretation of bodily changes would be perceived as the affective value. As a corollary, he

stated that we are sad because we cry and afraid because we tremble (James, 1884). This concept was challenged by several contemporaries, such as Walter Cannon and Charles Sherrington on various grounds (Cannon, 1927). Most of which are unfounded considering current knowledge, including the (at that time) assumption of the autonomic nervous system being predominantly efferent, comprising very few afferent connections. In addition, these afferences would be too undifferentiated to give rise to different emotions (Cannon, 1931). In fact, afferences vastly outnumber efferences in the vagus nerve, the 10th cranial nerve connecting the heart, lungs and digestive organs to the brain (Berntson et al., 2018) and furthermore, different tastes of disgust are separable by simultaneous neuroimaging and physiological recordings (Harrison et al., 2010).

A prominent extension to the James-Lange concept, having physiological arousal at its core, is the two-factor theory of affect (Schachter and Singer, 1962). While in both theories bodily arousal initiates emotional experience, the important difference between the two resides at the level of value attribution. James-Lange suggested the affective value being primary to the afferent visceral information, whereas Schachter and Singer introduce an intermediate appraisal level, where physiological arousal would be ambiguous at first and cognitively labelled with value *post hoc* only after integrating it with other sensory modalities. This take bridges the Appraisal and Constructionist theories on emotion, however, still represents a peripheral theory of emotion.

Currently both models are valuable, as they may apply to different stages of learning/development. It is well conceivable that initially visceral information has to be learnt to be meaningfully interpreted, alluding to a possible plasticity of their meaning (pertaining to Schachter-Singer), while in a learnt state, those signals may be stereotypic and readily interpreted as carrying affective value (James-Lange).

Interoception

The term “interoceptor” has first been coined by Sir Charles Sherrington and classically refers to sensing the physiological state of the body (Sherrington, 1907). This function serves the primary purpose to maintain bodily parameters, such as blood pressure, metabolic state and body temperature at physiological levels and deviate upon demand (e.g. during exercise or sickness). This broad collection of functions has been integrated into the term ‘homeostasis’, coined by Walter Cannon and defining the desired state of the body (Cannon, 1939). By its initial definition by Sherrington, interoception described the process of sensing

the state of the inner surfaces of the body, so from a current perspective the modern equivalent and more accurate term used is ‘viscerоception’, as it refers to signals from the viscera only. This is complemented by exteroception, which refers to sensing the surfaces facing the exterior milieu. According to Sherrington, vision, audition, olfaction, gustation and mechanosensation would constitute the exteroceptive senses, including ambient temperature and pain, while interoception and proprioception concern the viscera and skeletal muscle/vestibular system, respectively (Ceunen et al., 2016).

The intuitive segregation of afferents into exteroceptive versus interoceptive, based on stimulus origin located exogenously versus endogenously with respect to body surface, cannot always be readily made. This conceptual distinction has been revised, mostly based on anatomical tracing studies. These have led to the incorporation of nociceptive, temperature, as well as information about the internal chemical environment into the process of interoception. At the level of the spinal cord the central nervous system (CNS) differentiates between inside and outside of the body developmentally and anatomically. Large diameter afferent fibers, conveying exteroceptive and proprioceptive information to the deep laminae, develop during the first wave of spinal cord innervation by dorsal root ganglion cells. Secondarily, small diameter Aδ- and C-fiber innervation, coincident with the population with spinal lamina I neurons, establish interoceptive sensing of temperature, metabolic, chemical, mechanical states (Craig, 2002). Furthermore, the ascending pathways conveying this information terminate in the insular cortex (including pain), the primary interoceptive cortex, not in the somatosensory cortex. This system represents the basic ‘homeostatic afferent pathway’ (Craig, 2003).

Moreover, the classically viewed exteroceptive chemical senses olfaction and gustation constitute the ‘special visceral afferents’ (SVAs), as they share neuronal pathways and genetic markers with the autonomic nervous system and general visceral afferents (GVAs), also exemplified by the primary gustatory cortex located within the insula (Saper, 2002). From a bodily perspective this organization can be explained, as despite the ligands of SVAs are exogenous, they act on interior surfaces and therefore have immediate consequences for the integrity of the body. This may have led to the convergence of olfactory and gustatory information onto similar neural pathways as the gut, thoracic, abdominal and pelvic afferents (GVAs).

As for segregating senses into exogenous/endogenous, the differentiation of interoceptive afferents into somatic or visceral origin for all tissues in the body is not always possible. A useful proposition is a differentiation by efferent innervation (Ceunen et al., 2016). In this

case, tissues innervated by the autonomic nervous system originate visceral afferents, whereas somatic nervous system-innervated tissues originate somatic afferents. By this definition only the skin, esophagus and lung represent ‘ambiguous’ sources, originating somatic and visceral afferents, while vascular afferents, sensing blood pressure via peripheral baroreceptors are visceral.

Anatomical organization of primary visceroception

Maintaining bodily homeostasis is the main driver of behavior, which necessitates sensing of deviations from the desired state to restore homeostasis. There are three main pathways conveying visceral information to the CNS (Fig. 1).

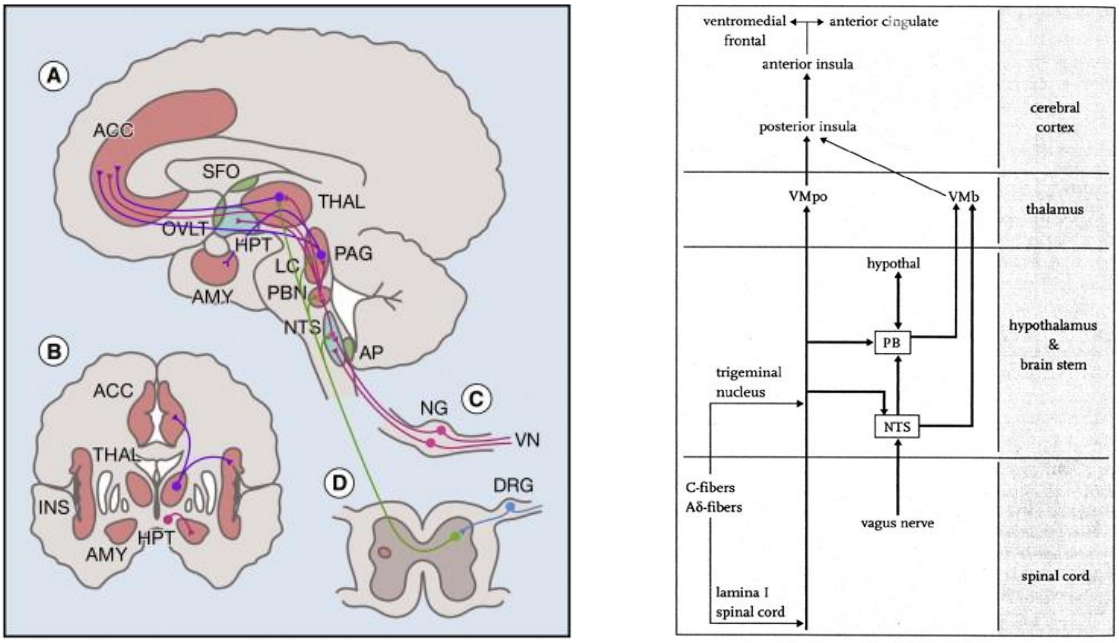

Figure 1 | Visceral afferents of the human brain. (Left) A. Sagittal and B. coronal section of the human brain. C. Nodose ganglion of the vagus nerve. D. Coronal section of the spinal cord. Pathways depicted: spinothalamic (light green), vagal (pink) and humoral (dark green). Reprinted by permission from Elsevier: Cell Press, Neuron, Critchley and Harrison, 2013. **(Right)** Schematic depiction of structures and pathways involved in visceroception. Reprinted by permission from John Wiley and Sons: Wiley, Annals of the New York Academy of Sciences, Damasio, 2003. Abbreviations: DRG - dorsal root ganglion. THAL - viscerosensory thalamus, NTS - nucleus of the solitary tract, PB - parabrachial nucleus, PAG - periaqueductal gray, VN - vagus nerve, NG - nodose ganglion. HPT - hypothalamus, AMY - amygdala, ACC - anterior cingulate cortex, INS – insula, LC - locus coeruleus, AP - area postrema, OVLT - organum vasculosum of lamina terminalae, SFO - subfornical organ, VMpo - ventromedial posterior nucleus of the thalamus;

The cranial pathway (i.), containing the glossopharyngeal (IX. cranial nerve) and vagus nerve (X. cranial nerve), the spinal afferent pathway, including the lamina 1 spinothalamic tract (ii.) and the humoral pathway (iii.), predominantly fulfilled by the circumventricular organs,

which directly sense the hormonal, immunological and chemical status of the body via fenestrated epithelia around the ventricles (Critchley and Harrison, 2013).

i. The cranial pathway provides basic homeostatic information on hunger, satiety, thirst and respiration, among others. It ascends via the cranial nerves to the nucleus of the solitary tract (NTS) via and in parallel to brain stem nuclei towards the hypothalamus. These viscerosensory regions connect to higher areas as the amygdala and insular cortex (IC).
ii. The spinothalamic pathway conveys mechanical and chemical information from the viscera. In addition, slow unmyelinated Aδ- and C-fiber input to the lamina 1 of the spinal cord transmits pain and temperature information, which again reaches the NTS to finally terminate in the IC after brain stem and thalamic intermediates. (Craig, 2002)
iii. The humoral pathway senses circulatory molecules to probe the immunological, hormonal, metabolic and osmotic status of the body. Gathered by the subfornical organ, area postrema and organum vasculosum of the lamina terminalae, located around the third and fourth ventricle, this information reaches the IC via hypothalamic and thalamic nuclei. In addition, the brain harbors chemosensory receptors and non-neuronal agents within its parenchyma for molecules that either diffuse or are actively transported into the brain, most notably microglia (Critchley and Harrison, 2013).

Although viscerotopy is preserved to some extent in the early stages of interoception from NTS to hypothalamus (‘labelled lines’), arguing for a representational function of regions involved, there is early integration and cross-talk between the diverse modalities. This architecture may facilitate cross-modal reflexes for efferent autonomic regulation, but also generate integrated pictures of the body state in early stages of processing, akin to a hedonic/homeostatic scale (Cabanac, 2002). The apex of viscerosensory processing is represented by the anterior cingulate cortex (ACC) and IC (Fig. 1), the latter integrating all visceroceptive modalities and thereby generating the most holistic representation of the body state. This is supported by early cortical stimulation experiments by Wilder Penfield in awake humans, who reported visceral sensations and symptoms upon electrical stimulation of the IC (Penfield and Faulk, 1955). Later cortical stimulation experiments delineated a small area in the posterior IC and parietal operculum to also produce painful sensations. These could never be observed upon stimulation of any other

area of the human cortex, including areas consistently activated by painful stimuli, such as the ACC or somatosensory areas (Mazzola et al., 2012). These experiments are complemented by numerous functional imaging studies, showing activation of the IC in various interoceptive tasks (see Craig, 2002 for a general overview and Segerdahl et al., 2015 specifically for pain).

More recent semantic evolution of *interoception* has led to conceptual broadening of its definition. Illustrated by the blurry segregation of somatic versus visceral afferents (e.g. skin, lung), and ultimate convergence after spinal cord in areas as the thalamus and earlier, Craig (2002) argued from a bodily perspective to include any modality that is informative about the current state of the body as contributing to interoception. By inference, it is a cross-modal process, in which integrated sensory modalities imply relevance for being informative about the body state (Ceunen et al., 2016; Critchley and Garfinkel, 2017). This framework incorporates exteroceptive signals and projects increasingly cross-modal representations onto the IC from its primary sensory posterior towards its anterior portion (Fig. 2), in accord with increasing domain-general processing in frontal cortices (Badre, 2008). By extrapolating this gradient, it was suggested that the most anterior IC (aIC) contributes to (human) perceptual awareness (Craig, 2009).

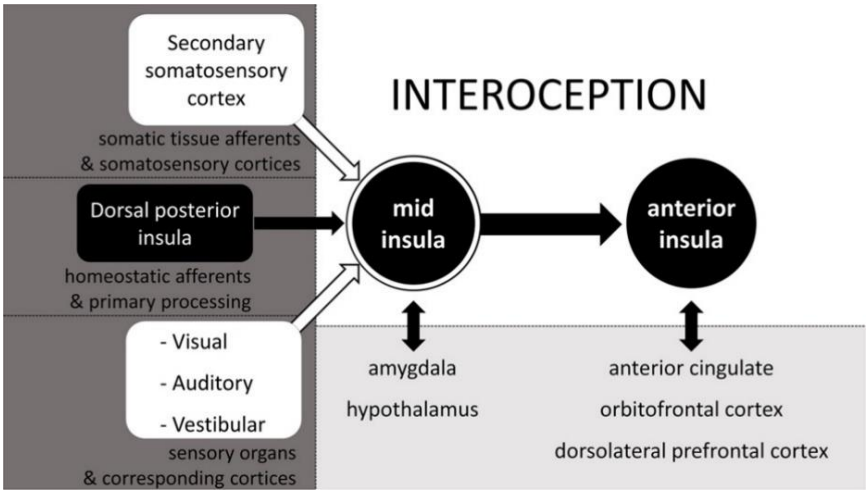

Figure 2 | The most inclusive definition of interoception projected onto the rostro-caudal axis of the IC. Interoception is conceived as the construction of an increasingly integrated, crossmodal representation of the bodily state, involving all sensory systems relevant for maintaining the integrity of the body. Image taken from (Ceunen et al., 2016) This work is licensed under the Creative Commons Attribution 4.0 International License. http://creativecommons.org/licenses/by/4.0

Affective interoception – Case studies

Emotions are intricately linked with bodily changes and perception. Evidence from (functional) anatomy portrays the IC as the central hub for visceral processing. In keeping with the proposition of bodily signals constituting emotional experiences (Lamm and Singer, 2010), there is evidence for overlapping representations of emotional and interoceptive processing in the aIC (Craig, 2002; Zaki et al., 2012). Consequently, functional uncoupling of brain and bodily afferents should result in altered emotional experience. Indeed, there are numerous examples of aberrant/absent ascending autonomic nervous system information contributing to emotional dysfunction. These originate from surgical interventions, degenerative pathologies, or yet idiopathic origin:

- In patients treated with endoscopic thoracic sympathectomy for neuropathic pain (Mailis-Gagnon and Furlan, 2002) or autonomic disorders, such as hyperhidrosis. After surgery the latter patient specifically reported profound personality changes, manifested in “emotional blunting” and an “indifference towards prior aspirations”, as well as a “lack of fear” and absence of motivation to engage socially (Berntson et al., 2018).
- Similar consequences on emotional experience are observed in the condition pure autonomic failure (PAF), which is a degenerative disorder of the autonomic nervous system. Due to peripheral autonomic denervation, patients suffer physically from the inability to modulate blood pressure and heart rate upon behavioral demand. However, in consequence, PAF also eliminates afferent feedback reporting the bodily state.
- Alexithymia is a sub-clinical condition in which individuals display impaired capacity in perceiving, distinguishing and regulate one’s own emotion, as well as recognizing other’s emotions (Nemiah et al., 1976). It affects 10% of the population and the affective deficit has vast consequences for the life of these individuals. The reduced capacity in understanding emotion of others is associated with the lack of altruistic behaviors, resulting in difficulties maintaining interpersonal relationships (Griffith, 1998; Hesse and Floyd, 2008). Importantly, a number of psychiatric conditions are comorbid with alexithymia, most commonly the autism spectrum (Hill et al., 2004), but also major depression (Leweke et al., 2011), eating and personality disorders (Nowakowski et al., 2013; Van Der Velde et al., 2015) are overrepresented. Furthermore, overconsumption of psychoactive substances is more frequently

observed (Lyvers et al., 2014; Thorberg et al., 2009). Importantly, affected individuals were assessed for their interoceptive accuracy (IA), the ability to perceive their interoceptive state. IA is routinely quantified by the heartbeat perception task (HPT), where the performance of individuals in accurately reporting the occurrence of one's heartbeat is assessed (Schandry, 1981). There is substantial variability in task performance within the general population, however, there is an intricate link between alexithymia and interoceptive deficits. Specifically, interoceptive awareness is a negative predictor for alexithymia based on HPT performance (Herbert et al., 2011). Beyond HPT, there is preliminary evidence that this phenomenon might extend to other domains of basic interoception (e.g. hunger, thirst, nausea), indicating increased perceptual similarity between basic bodily modalities and emotional states, potentially resulting in 'interoceptive confusion', underpinning alexithymia (Shah et al., 2016).

Despite conflicting studies reporting spinal cord-injured patients devoid of obvious emotional deficits (Cobos et al., 2002), examples above warrant an implication of basic interoception as a core component of emotional experience and awareness. Functional neuroanatomy has delineated regions in the CNS involved in IA. Human subjects directing attention towards their interior (by means of the HPT), contrasted to exterior attention, showed enhanced activity in the limbic cortices IC and ACC, as well as in somatomotor/sensory areas, among few others. Importantly, correlating activity and grey matter volume of these regions with actual IA performance highlighted the right aIC with the strongest positive relationship to IA (Critchley et al., 2004). This stresses the IC as a potential entry point of interoceptive signals into conscious awareness and furthermore links it functionally and morphometrically to perceptual accuracy and affective experience (Craig, 2011).

A functional dissociation between IC and ACC emerges when assessing activity by functional imaging in acquired lesion and PAF cases. In humans, volitional exercise and stressor tasks trigger autonomic arousal and show increased activity in the dorsal ACC (Critchley et al., 2000a), while in ACC lesioned patients autonomic responses, such as cardiovascular or galvanic skin conductance responses (SCR) are absent (Critchley, 2005; Tranel and Damasio, 1994). Moreover, in patients suffering from peripheral denervation, who cannot mount this autonomic response, the ACC and pons in brainstem are hyperactive. This compensatory activity is being attributed to absent visceral feedback and is contrasted by blunted IC activity in PAF (Critchley et al., 2001, 2002). This suggests the ACC as a visceromotor cortex (or 'limbic motor cortex'), complemented by the

viscerosensory/interoceptive IC (‘limbic sensory cortex’). Notably, this architecture is mirrored functionally by their brainstem equivalents periaquedactal grey (PAG, homeostatic motor area) and parabrachial nucleus (PB, homeostatic sensory area) (Craig, 2003).

In summary, above phenomena provide a case for an intricate link between the perception of bodily signals and affective experience and thereby make a case for incorporating affective states into basic homeostasis. Furthermore, powerful neuroimaging technology in humans (fMRI, PET) allowed for a delineation of a homeostatic system, centered around the ACC and IC with interoception at its core.

Interoception in decision-making

It is consensus that emotions are mental states that bring about the physiological, motivational and behavioral changes needed to instantiate action. The interest in the relationship between peripheral theories on emotion and motivational decision-making was sparked by observations when subjecting human patients suffering from prefrontal/orbitofrontal cortex damage to cognitive testing. Although generally intelligible and highly functional on standard cognitive tasks, they were severely dysfunctional in real-life decision-making (Eslinger PJ and Damasio AR, 1985; Shallice and Burgess, 1991), as well as suffering from repeated disadvantageous decisions (Bechara et al., 1994).

The latter phenomenon was reproduced in the laboratory by the Iowa gambling task (IGT), invented by the group of Antonio Damasio (Damasio, 1994). Since its inception it has given rise to an extensive body of literature on economic decision-making in (psycho)pathological, physiological and pharmacological states (see Dunn et al., 2006 for critical review). The IGT aims to reproduce real-life decision-making in conditions of reward and punishment under uncertainty (thereby emulating approach-avoidance behavior), where subjects learn to maximize monetary gain by drawing from different decks of cards, even though an exact calculation of the gains and losses is not accessible, hence remains a long-term estimation. Each deck is associated with fixed amounts and probability of gain, resulting in net ‘advantageous decks’ and ‘disadvantageous decks’. Over time neurotypical subjects learn to choose decks associated with the best net long-term gain. However, patients suffering from a prefrontal cortex lesion perform consistently worse, by choosing more disadvantageous decks (Bechara et al., 1994). This was interpreted as being either a defect in working memory, as patients could be unable to integrate outcomes over multiple trails or alternatively, a defect in value attribution, where patients fail in marking decks with positive or negative affective

value to guide decisions. The latter possibility was supported by preliminary evidence at the time and led to the development of the 'somatic marker hypothesis' (SMH) (Damasio, 1994). Extending these findings, galvanic skin conductance responses (SCR) during the task were assessed and used as a signature of autonomic arousal. Interestingly, all subjects developed SCRs over the course of learning upon receiving reward or punishment, however only control subjects developed anticipatory SCRs before the actual decision, as opposed to patients with a prefrontal lesion. Moreover, the magnitude of the SCR correlated with task performance (Bechara et al., 1996). This represents a physiological correlate of economic performance and suggests that the brain factors in bodily signals/somatic markers into the decision-making process. Colloquially referred to as 'gut feelings', the anticipatory SCRs also preceded conscious conceptualization of the task, meaning subjects were unaware of the advantageous strategy, while already biasing their decisions towards the advantageous decks (Bechara et al., 1997).

The initial concept of the limbic system was proposed as the system of convergent viscero- and exteroceptive stimuli to give rise to emotions (MacLean, 1949). Despite initially focused on the prefrontal cortex (PFC), the SMH expanded on the limbic system and integrated structures as the somatosensory, IC, basal ganglia as neural substrates to mediate SM (Damasio, 1998). Neuroimaging studies assessed brain activity during the (modified) IGT and found a network consisting of orbitofrontal cortex (OFC), PFC, ACC, aIC, predominantly in the right hemisphere. Importantly, task performance and SCR correlated with activity in PFC and aIC, among few others (Critchley et al., 2000b; Ernst et al., 2002), congruent with similar evidence from the HPT (see above).

While evidence for the validity of the SMH remains correlative, further criticism was raised upon the accumulation of notable counterintuitive evidence regarding SMH predictions. PAF or spinal cord-damaged patients, for example, show no deficits in the IGT. However, this was explained by the intact non-spinal ascending pathways (e.g. the vagus nerve) (Heims et al., 2004). Furthermore, it was speculated that negative results in above conditions may result from either compensatory mechanisms occurring in these long-term disorders, as well as the possible usage of acquired strategies by means of SM prior condition onset (Dunn et al., 2006). The role of working memory (WM) for task performance is also ambiguous. While reports of WM independence from the original authors was demonstrated in patients with dlPFC and vmPFC lesions (Bechara et al., 1998), others show mixed results, depending on the specific lesion area (Manes et al., 2002). It seems as lesions affecting WM exacerbate IGT performance in addition to proposed SM deficits, where WM is mainly affected by

dorsal PFC lesions. The ambiguity in these results may not be surprising as independence of WM and SM domains is hardly imaginable in decision-making. Finally, Damasio originally argued himself, that SM may be engaged in the early learning phase where task contingencies are complex and uncertain. In this formulation, SM themselves may initially guide attention and thereby WM towards favorable outcomes, which might later give rise to declarative knowledge on the task (Bechara, 2004; Damasio, 1994). This take is intriguing given the role for attention and salience ascribed to the interoceptive IC more recently based on neuroimaging (Chen et al., 2015; Menon and Uddin, 2010; Uddin, 2014). The aIC in humans was demonstrated to be a causal outflow hub and coordinator between two large-scale brain networks, the default mode (DMN) and the central executive network (CEN) (Fig. 4, left) (Sridharan et al., 2008). These two antagonistic networks mediate attention towards the exterior (CEN, green) and interior (DMN, yellow), where the proposed "salience network" (SN, blue), consisting of the right fronto-insular (rFIC) and ACC, serves as an arbitrator and switch, coordinating attention between external and internal saliency (e.g. cognitive, homeostatic). Notably, within the SN the rFIC/aIC displays the greatest net Granger causal outflow, suggesting a hierarchically superior and putatively causal position within the SN, DMN and CEN (Fig. 4, right).

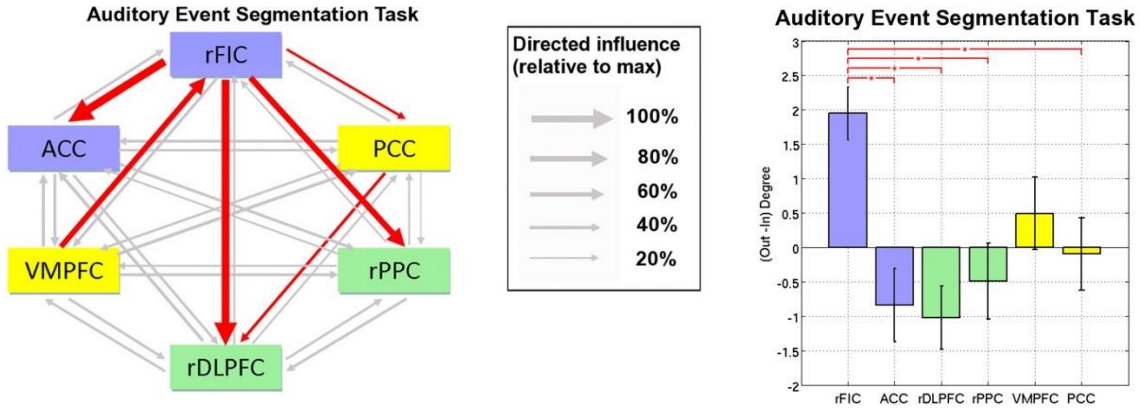

Figure 3 | Granger causality analysis (GCA)-inferred information flow. (Left) GCA during an auditory event segmentation task on a network of two components of each the salience network (SN. blue), central executive network (CEN, greem) and default mode network (DMN, yellow). Thickness represents the strength of the connection, normalized to the maximum. Significant causality depicted in grey, red arrows indicate dominant directional influecne. **(Right)** Causal Granger output determined by the difference between outward and inward causality during an auditory event segmentation task. Abbreviations: rFIC - right fronto-insular cortex, ACC - anterior cingulate cortex, PCC - posterior cingulate cortex, VMPFC - ventromedial prefrontal cortex, PPC - right posterior parietal cortex, rDLPFC - right dorsolateral prefrontal cortex; Figure taken from Sridharan et al., 2008; Copyright 2008 National Academy of Sciences.

The non-declarative basis of decision-making suggested by the SMH resonates with more recent description of emotions as highly abstracted states, embodied in models of the world that are rooted in the internal physiology. These early models are thought to then instigate cognitive states to decide advantageously independent from conscious awareness. Consequently, awareness of a successful strategy would only emerge after (iteratively) observing one's own actions and outcomes, a sequence pattern reminiscent of the James-Lange theory of emotion. The implementation of 'good enough' abstractive neural architecture might be efficient and preserve resources at the expense of more accurate models (Barrett, 2017). An instance of a model-type mechanism was formulated along with the SMH in the form of the 'body loop' (Bechara and Damasio, 2005). Accordingly, in the process of decision-making, the body loop is engaged to re-enact the physiological state of the body, which then feeds back to engage neuromodulators as dopamine (DA) and acetylcholine (ACh) to bias decision-making. This requires the existence of an existing representation of that state, a model, in order to instantiate it. A parallel proposal was the 'as-if loop', where similar representations and neurotransmitter systems would be triggered, however the body proper could be bypassed, and cortico-subcortical-brainstem loops replace the actual afferent body input to 'simulate' the body. The as-if loop conveniently explains the absence of IGT performance deficits in PAF and lesioned subjects, although the validity of this model requires testing. However, both loops provide a theoretical framework for model-based decision-making, having bodily signals at its core, and directly tie into a modern constructivist explanation of emotions.

Allostasis through interoceptive predictive processing

Allostasis

Compared to virtually all senses, interoception provides the most reliable and continuous stream of information to the brain, while at the same time the body demands incessant regulation. Stemming from optimal control theory, it is suggested that the regulation purely based on homeostatic control loops ('stability through constancy') is problematic due to the inherent inefficiency of simple error-correction (Sterling, 2012). While this does not preclude homeostatic mechanisms, allostasis on the other hand describes the process of predictive regulation of (bodily) needs upon changing parameters. The benefits of allostasis lie in the facilitation of trade-offs for energy efficiency (e.g. the antagonistic sympathetic and

parasympathetic nervous systems) and in the minimization of deviations from desired states by anticipation thereof through engagement of other modalities. Prominent examples of allostatic mechanisms are the circadian regulation of physiology by which excess metabolic capacity is prevented ahead of predicable periods of dormancy (Schulkin, 2019). Furthermore, anticipated osmotic stress upon food consumption is curtailed by prandial drinking, independent from actual osmotic state (Zimmerman et al., 2016). Even this basic phenomenon requires the prior 'knowledge', an internal model, for that food consumed will affect osmotic load in the future and require fluid intake. This knowledge is instantiated by a projection from the hypothalamus to the subfornical organ, driving drinking behavior upon food consumption. When zooming out, nervous systems can be viewed as a collection of superimposed, hard-wired and learnt allostatic loops, with the cerebral cortex allowing for the construction of the most flexible and complex loops to govern and maintain a functional body. Given the ubiquity of allostatic mechanisms, ill-based models may lead to dysregulation and underpin a range of conditions, such as hypertension or obesity, however the very same principles may apply to psychiatric illnesses such as mood and anxiety disorders (Schulkin, 2019).

Predictive processing

Classically, brain function has been described in terms of stimulus and response, whereby a given environmental cue elicits cascading feed-forward activity from subcortical areas via primary sensory and associative cortices to motor regions to mount a behavioral response. This view relies fully on bottom-up signaling for perception and was in part fueled by the discovery of the receptive field by Hubel and Wiesel (Hubel and Wiesel, 1959). However, numerous perceptual phenomena are at odds with this notion, for example the evident differentiation between self-generated and externally generated input, pointing towards a more proactive generative process governing perception and action by the brain (Engel et al., 2001). Accordingly, these fundamental processes are not purely stimulus-driven, but emerge from the interaction of sensory input with internal models built on accumulated prior experience. The crucial advantage of an internal model, sufficiently descriptive of the world, is that it endows neural systems with predictive over purely reactive capacity (Barrett, 2017).
The conception of brains as predictive machines dates to work of Hermann von Helmholtz in the 19th century (Helmholtz, 1867). He reasoned that the brain is contained within a skull in darkness and therefore has no direct access to the actual causes of its sensations. Because the

physical origins of its activity remain hidden to the brain as the observer, the only strategy it can employ to understand the world is to infer the state of the environment from the activity that was caused in context of a model and construct perception accordingly. 'Perceptual inference' is an inverse inference problem neural systems are facing and made Helmholtz speculate that perception is just a best guess given the noisy sensory data at hand. Elaborating on this view, the brain is a statistical organ that continuously computes a multitude of probability distributions for future sensory input (Ma et al., 2006). These are compared to actual sensory input and given the current context, the most probable option wins and instantiates perception. It is therefore not a process of sensing how the world actually is, but rather how it relates to previous experience, our priors, which are highly individual and culturally determined (Clark, 2013; see Tse and Cavanagh, 2000 for cultural determinsim of perception). These principles rest on the existence of an internal generative model (GM), which over time is constructed by extraction of statistical structures and relationships in the world and is embodied in the connectome of the brain. Intuitively, in the visual system statistical structures may be as simple as prevalent co-occurring edges in the visual scene, oriented in a certain direction relative to each other. Subsequently, the occurrence of one edge makes the perception of the other edge in the expected direction more likely. In other words, the brain attempts to synthetize the sensations caused by the two edges to generate structure and apply this model to future sensory input, and in this way crucially shape how we perceive the world (de Lange et al., 2018).

This principle is the fundamental cause of pervasive (visual) illusions perception is vulnerable to. Probably one of the most intuitive example is the famous 'light from above' prior, which describes the perception of convex or concave patches, depending on whether a patch is illuminated from above or below, respectively (Ramachandran, 1988). This perceptual illusion rests on an internal model incorporating our extensive prior experience that light in the environment predominantly comes from above. However, even this profound prior, acquired over a lifetime, can be rapidly altered by relatively minimal training in humans, demonstrating the adaptability of internal models to altered environmental contingencies (Adams et al., 2004). Further evidence for GMs comes from activity recordings in the visual system, showing that spontaneous activity in the absence of visual stimulation resembles activity evoked by natural scenes, reflecting the statistics of the environment. Remarkably, this resemblance increases with age, pointing towards a continuous maturation of internal models towards optimality (Berkes et al., 2011).

A GM embodies predictions of what to expect next, therefore sufficient accuracy thereof will reflect the environment and be adaptive for the agent immersed in it. Consequently, it is of fundamental importance to biological agents to minimize prediction errors (PEs) and maintain the body in the expected state in order to survive (formalized in the free-energy principle in Friston, 2003, 2005, 2006, 2009, 2010). To achieve PE minimization there are essentially two major possible strategies:

(1) Perceptual plasticity: Update the internal model to match it to the unexpected sensory input

(2) Active inference: Act on the world to change sensory input according to the internal model

Intriguingly, this concept unifies perception and action into the very same computation, as the only relevant difference between the two strategies within the predictive processing framework lies in how PE are utilized. In the first case, the occurrence of PE/surprises challenge the validity of the model and are subsequently incorporated by synaptic plasticity, resulting in better predictions (Friston, 2005). Conversely, in the case of active inference, PE are not used to update the GM, but directly serve as motor commands until predictions are met and (e.g. proprioceptive) PE disappear (Adams et al., 2013a; Friston, 2003). This may represent the fundamental difference between sensory (1) and motor areas (2), possibly reflected in their different architecture. The motor cortex exhibits a less developed thalamo-recipient layer 4, compared to sensory areas, and thereby may be less receptive for PE rendering its output more deterministic (Shipp et al., 2013). Interestingly, the similar architecture found in the interoceptive system led to the speculation that interoception might operate in a similar fashion as the motor system (Barrett and Simmons, 2015). Consistent with brain architecture, the predictive processing framework is embedded in a hierarchically organized circuitry where predictions and PE flow in dedicated directions across hierarchical levels, allowing for testable hypotheses of the predictive processing framework (Friston, 2008)

Hierarchical predictive processing

The brain is organized in a hierarchical multi-level architecture (Felleman and Van Essen, 1991; Harris et al., 2019; Hochstein and Ahissar, 2002). There are many principles proposed to construct hierarchies (Rauss and Pourtois, 2013), ranging from rigid anatomical principles (Barbas and Rempel-Clower, 1997) to a flexible and dynamic one depending on task

demands (Engel et al., 2001). Importantly, the predictive processing framework does not rely on a specific principle, however, suggests that hierarchical organization reflects gradients of functional separation to integration from bottom to top levels, respectively. Accordingly, the lowest areas contain rather domain-specific areas within a given processing modality (e.g. subcortical, cerebellar systems), which are subsumed and converge in increasing domain-general modules towards the top (e.g. limbic cortices, association areas) (Badcock et al., 2019). This principle is supported by functional neuroimaging studies (Pendl et al., 2017; Sepulcre et al., 2012) and resonates with the anatomical organization of hierarchical brain systems for e.g. memory and executive functions (Collin et al., 2015; Koechlin, 2006).

Classically, bottom-up (synonymous with 'feedforward') and top-down ('feedback') describe information flow between levels where the former labels the ascending sensory input (see Fig. 2 for interoceptive bottom-up pathways) and the latter descending modulatory feedback (Zhang et al., 2014). Originally feedforward/bottom-up information flow was thought to be at large responsible for transforming sensation into perception. However, it appears that rather the top-down descending activity is doing the "perceptual work" and thus predictions constructing subjective reality (Clark, 2013; Hohwy, 2007). Highlighted by the observation that top-down usually greatly outnumber bottom-up connections between bidirectionally connected regions (Peters et al., 1994), the brain seems to invest the bulk of available resources in modeling the world, rather than accurately representing it.

The core of predictive processing rests on the specific roles ascribed to top-down and bottom-up information flow. The goal of a GM embodied at a given hierarchical level is to predict the activity of the hierarchically lower level by means of its top-down connections. The lower area matches these incoming predictions with ascending bottom-up sensory input to disambiguate and interpret the sensory data. Importantly, in this way sensory data that has been successfully predicted is being 'explained away' by the GM above. Any residual from bottom-up input, unaccounted for by the GM above, generates a PE propagating up the hierarchy to update the GM and minimize future PE signaling (in the case of perceptual learning). Phenomena supporting this view can be observed in the most basic sensory cortices and seem to be a generalizable cortico-cortical computation between hierarchies (Fig. 4 for a schematic representation) (Keller and Mrsic-Flogel, 2018; Den Ouden et al., 2012). These include expectation suppression, where the response upon the presentation of an expected stimulus is dampened (Todorovic and de Lange, 2012). Also more difficult to reconcile with strictly bottom-up processing are omission responses, where activity in sensory areas can be

observed upon the unexpected omission of a stimulus (PE), emphasizing the presence of model-driven predictions (Den Ouden et al., 2009).

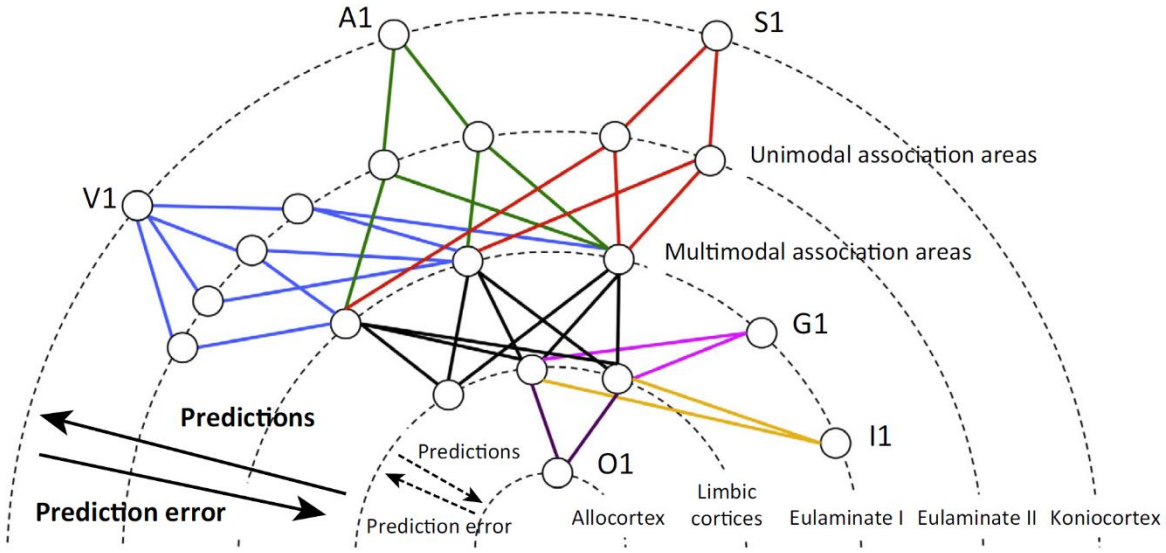

Figure 4 | Scheme of the hierarchical organization of cortical sensory systems. The outermost circle represents the lowest hierarchical level, containing the exteroceptive primary sensory areas of the visual (V1), auditory (A1) and somatosensory (S1) systems. Moving towards the center, bottom-up information carrying PEs ascends via association areas towards multimodal limbic cortices, such as the aIC. Predictions flow in the opposite direction. Note the more intermediate processing devoted to the exteroceptive senses, while viscerosensory cortices like the primary interoceptive (I1) or gustatory cortex (G1) exhibit fewer hierarchical levels, likely owing to their lower complexity. The specific order reflects the cytoarchitecture in primates, with the primary exteroceptive areas featuring the most elaborate laminar differentiation (koniocortices). which becomes more undifferentiated in association areas (eulaminate cortices). This pattern is reinforced in the limbic cortices, where in addition the granular layer disappears (agranular cortices). Within this scheme the olfactory cortex is a special case, due its more ancient origin it only exhibits 3 layers (allocortex) and does not follow the connectional logic of the other sensory systems. Furthermore, the olfactory system avoids white matter tracts and lacks thalamic structures. Reprinted by permission from Elsevier: Cell Press, Trends in Cognitive Sciences, Chanes and Barrett, 2016.

Uncertainty and attention

Noise and uncertainty are immanent in sensory information. Predictive processing must account for this in balancing the effect of predictions and PEs. Given an ambiguous sensory context, predictions are less reliable and, in consequence, also emerging PEs, which means immediate model update or action must be suppressed. Theoretically, this is implemented by ‘precision’ signaling, essentially representing a scaling factor for the gain of PEs (Feldman and Friston, 2010). Accordingly, high context ambiguity results in high model uncertainty, ensuing low precision and PE signaling. Conversely, high certainty of GM validity should put high weight on incidental PE and prompt model update or action more potently. Importantly,

accepting this concept implies that attention is an analogous mechanism to precision, by which (synaptic) gain on PE (equivalent to actual bottom-up information) signaling is adjusted, similar to stimuli modulated by attention. The neurobiological implementation for precision is still unclear, however, neuromodulators have been suggested as potential mediators, most prominently dopaminergic and cholinergic signaling (Friston et al., 2012; Moran et al., 2013; Parr et al., 2017).

Interoceptive predictive processing

Helmholtz states inference as the only strategy accessible to the brain to generate meaning by internalizing the relationship between brain activity and the outside world. There is apt evidence for the implementation of predictive processing in all exteroceptive senses (Akatsuka et al., 2007; Baldeweg, 2006; Bar et al., 2006), however purely detecting statistical regularities across senses is futile in the absence of value, which underlies motivational drive to seek or evade. Maintaining the integrity of the body has upmost priority for all organisms, making it a legitimate strategy for the brain to root predictive processing in the internal physiology. Interoceptive predictive processing (IPP) suggests the integration of external senses with an interoceptive GM to generate predictions for potential physiological change (e.g. pain, satiety), which may constitute the very emotions themselves (Fig. 5) (Seth et al., 2012). These predictions should then drive perceptual plasticity, after comparing it to bottom-up information; or active inference, to avert actual deviations from the desired physiological state by e.g. increasing heart rate and blood pressure for imminent behavioral flight, or restore the desired physiological state by inducing autonomous salivation upon encountering food cues. (Pavlov, 1911). Along these lines, the (predicted) magnitude of deviations from a state of homeostasis was suggested to be essentially captured by the affective quantity of valence, being negative or positive for a departure from or return to the desired state, respectively (Joffily, 2013).

Due to the similarity in agranular architecture between motor cortex and interoceptive cortex (aIC), it was speculated that, just as motor predictions may be fulfilled by secondary proprioceptive PE, output from the interoceptive system may be conceptualized likewise as (viscero)motor predictions (e.g. heart rate rises) that are fulfilled by interoceptive PE (e.g. heart rate does not rise) (Barrett, 2015; Chanes, 2016; Seth, 2016). In this case any emotional response would represent an instance of active inference resulting in predictions enacted by the interoceptive system and fulfilled by lower (viscero)motor regions like the midbrain PAG

until any mismatch between predicted and actual heart rate are resolved by PAG visceromotor activity. Consequently, an emotional state is a high-level allostatic loop engaging multiple modalities to preserve body integrity.

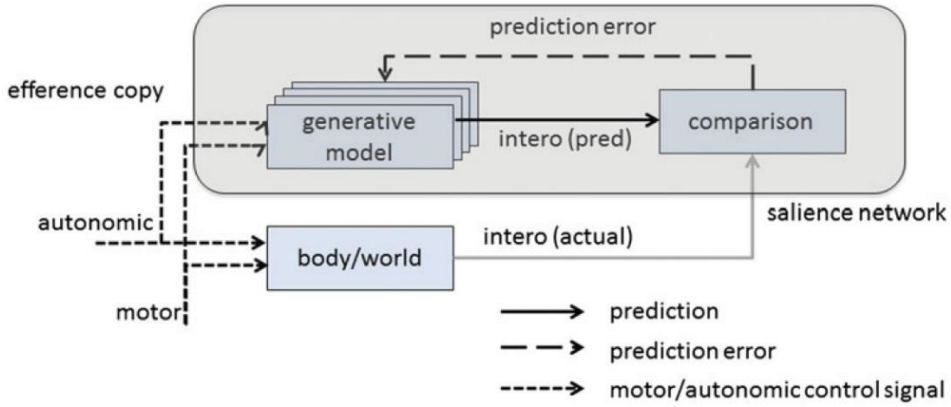

Figure 5 | Hierarchical interoceptive predictive processing. The salience network as a potential site of implementation of IPP proposes modules for the encoding of a GM, issuing predictions (pred) regarding the interoceptive state to lower hierarchies, the comparator. In turn, predictions are compared to actual sensory input (intero), upon any residuals (PE) will propagate back to the GM upstream in the hierarchy. Reprinted by permission from Cambridge University Press: Behavioral and Brain Sciences, Taken from Seth and Critchley, 2013.

Despite intact sensation, an inability to build GMs renders agents blind to experience and deprived of meaning. Constructing a GM to bind an assortment of edges into an object, might be the very same mental operation as assigning affective value to that object, with the fundamental difference that the latter process turns the object into an entity relevant to allostasis (Barrett, 2017). In order to construct the affective value categories of appetitive/aversive, an interoceptive model must embody these categories to guide action. As opposed to all other sensory systems, this is a unique property of interoception as it provides the fundamental reference points the brain can utilize to navigate the environment by explaining value of sensory data by the inferred states about the possible consequences for the body (‘interoceptive inference’, Seth, 2013). Interoceptive signals, such as quenched thirst or pain, may therefore represent ultimate priors that provide the base for a maturing cross-modal GM over the course of life.

Thesis objectives and neural substrates

Although affective states are inherently linked to bodily changes, the role of interoceptive GMs in affective learning and their possible recruitment for resolving value uncertainty are not understood. Similarly, the neural pathways mediating interoceptive affective decision-making, and the potential underlying information exchange between these elements are still unclear, despite prominent theories like the SMH (Damasio, 1994).

To address the possible integration of interoceptive states with exteroceptive stimuli in affective learning, Pavlovian conditioning provides a paradigm by which initially neutral conditioned stimuli (CS), such as sounds, acquire access to affective states commonly elicited by unconditioned stimuli (US), such as primary reward and punishment (Fig. 6) (LeDoux, 2000). The temporal pairing of CS and US triggers the formation of memory traces throughout the brain and the resulting expression of affective responses upon CS presentation (approach or avoidance behavior) can be viewed as a correlate of overcome value uncertainty towards the meaning of the CS for allostasis. In humans, the aIC has been found to be engaged in states of categorization uncertainty, suggesting an involvement of interoceptive states in difficult decision-making (Grinband et al., 2006). Furthermore, the extensively shared functional neural architecture, between affective states in general (Phan et al., 2002), as well as aversive conditioning specifically (Buchel et al., 1998) and interoceptive areas warrants to take the interoceptive system, notably the IC, as an entry point to explore mechanisms of affective decision making for mediating allostasis.

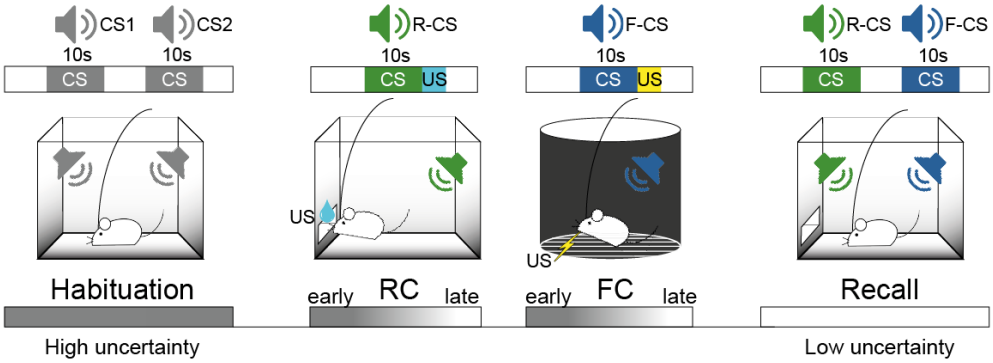

Figure 6 | Scheme of the discriminatory auditory Pavlovian conditioning paradigm. Water-deprived mice undergo a habituation session where two different neutral sounds are presented (CS1, CS2). Thereafter, CS1 is repeatedly paired with the delivery of an appetitive water drop for several reward conditioning (RC) sessions. This is followed by a single fear conditioning (FC), where CS2 is paired with an aversive foot-shock. Uncertainty about CS value is reduced over the course of conditioning and the presentation of the R-CS (reward-CS) and F-CS (fear-CS) should elicit affective approach or avoidance behavior, respectively. This is tested in a separate recall session, where CSs are again presented without reinforcement.

In an attempt to establish an integral allostatic-interoceptive network in humans, similar to other sensory modalities, the IC was shown to be functionally coupled to subcortical areas, such as the amygdala and midbrain PAG, two hierarchically distinct visceromotor areas (Kleckner et al., 2017). The amygdala is a primary site of plasticity for affective memories (LeDoux, 2003; Sigurdsson et al., 2007), required for acquisition and behavioral expression of affective responses (Goosens, 2001). Human lesion cases revealed an important dissociation as to the type of memory being stored in the amygdala. Subjected to an aversive conditioning paradigm, hippocampus-lesioned subjects failed to remember the actual conditioning procedure, however acquired an autonomous SCR upon CS presentation after CS-US pairing. Strikingly, bilateral amygdala damage impaired the SCR specifically, while leaving declarative memory intact (Bechara et al., 1995). This has contributed to the view that the amygdala is a site of implicit memory storage, indexing percepts with affective value to drive downstream circuits to elicit affective responses (Haubensak et al., 2010; LeDoux et al., 1988; Penzo et al., 2014) and importantly, also apply its index to bias upstream regions involved in perception towards stimuli relevant to affect (Anderson and Phelps, 2001). Notable downstream structures of the CE implicated in the above processes are the PAG and Nucleus Basalis of Meynert (NBM), respectively.

Objective 1 –

Learning establishes GMs in IC subregions

The IC varies smoothly along its antero-posterior axis in its cytoarchitecture (Morel et al., 2013), structural (Ghaziri et al., 2018) and functional connectivity (Deen et al., 2011) across species with the extent of architectural differentiation increasing from mouse to human (Nieuwenhuys, 2012). The gradual change of agranular architecture in the aIC towards dysgranular and granular architecture in the posterior pIC is roughly comparable between primates and mouse. Interestingly, these features covary with a functional dissociation, where pIC activity linearly tracks an interoceptive stimulus, while the aIC contextualizes and therefore correlates with subjective stimulus ratings (Craig et al., 2000; Geuter et al., 2017). Consistent with cytoarchitecture, the pIC exhibits primary sensory properties whereas an integrative re-representation of objective stimulus-features towards the anterior renders the limbic aIC more associative (Critchley et al., 2001). Collectively, the functionally and structurally divergent properties of aIC and pIC provide the opportunity to test the IPP

framework in a possibly hierarchical system, as well as the role of GMs in affective decision-making.

Hypothesis 1

aIC and pIC form a hierarchical system, which is reflected in their encoded GM and communication across PL stages. (see limbic cortex (aIC) and I1 (pIC) in the hierarchical scheme in Fig. 4).

Objective 2 –

PE signaling in vPAG/DR–CE–IC pathways drives affective learning

The central amygdala (CE) is a crucial site for Pavlovian plasticity, and CE neurons respond to appetitive and aversive CSs upon conditioning (Shabel and Janak, 2009). The discovery of genetic markers delineating separate cell types and associated functions established a key role of the CE for amygdala output and gating function. It was mainly work on FC that gave insight into the synaptic remodeling of CE circuitry (Duvarci et al., 2011; Fadok et al., 2017; Li et al., 2013; Sanford et al., 2017). Pairing a CS with an aversive US leads to a reconfiguration of a basolateral amygdala (BLA) to CE pathway to bias the input from the BLA towards somatostatin^{+} (SST^{+}) and corticotropin-releasing factor^{+} (CRF^{+}) neurons and away from protein-kinase Cδ^{+} (PKCδ^{+}) neurons in the CE (Hartley et al., 2019; Li et al., 2013). Accordingly, the integrity and plasticity of this pathway is necessary for regulating affective responses in humans and rodents (Terburg et al., 2018). Along with BLA–CE reconfiguration, CE cell types acquire differential response profiles upon CS presentations (Fig. 7), which are instrumental to the behavioral gating function. (Cai et al., 2014; Ciocchi et al., 2010; Fadok et al., 2017; Haubensak et al., 2010; Li et al., 2013).

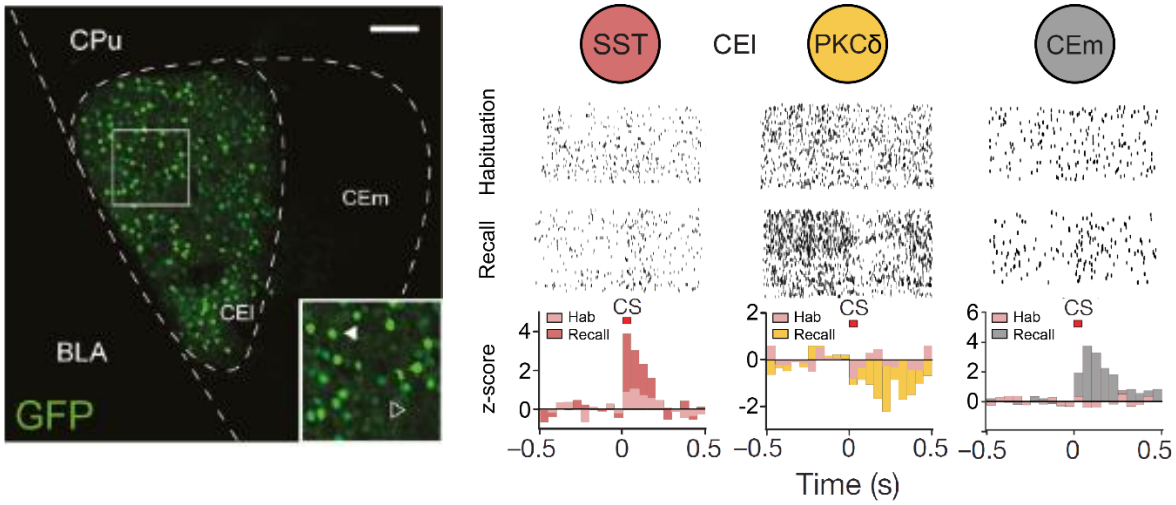

Figure 7 | CE cell types acquire differential response profiles after FC. (Left) Coronal section of the CE, virally transduced to Cre-dependently express GFP in a mouse expressing Cre in the PKCδ^{+} neurons. PKCδ expressing cells mark ~50% of the cells in the lateral CE (CEl) (SST marking PKCδ^{-} neurons) and are the predominant cell type co-expressing the oxytocin receptor (Haubensak et al., 2010). Full arrow in inset indicates a PKCδ^{+}, hollow arrow a PKCδ^{-} (by inference SST^{+}) neuron. **(Right)** SST^{+} neurons in the CEl and neurons in the medial portion of the CE (CEm) acquire excitatory responses upon presentation of an aversive CS, whereas PKCδ^{+} neurons are suppressed. Left image from supplementary Fig. 5 of Manuscript 1. Right figure adapted by permission from Springer Nature: Nature, from Haubensak et al., 2010 (SST, PKCδ) and from Ciocchi et al., 2010 (CEm). Abbreviation: CPu - Caudate-Putamen;

Pavlovian plasticity in the CE implies the generation of stimulus-bound GMs upon learning. However, in early learning stages the affective value of CSs (CS1/2 in Fig. 6) is inherently uncertain and therefore should attract attention (Barto et al., 2013). Novel stimuli represent PEs as their occurrence cannot not be predicted. The NBM is implicated in signaling novelty and salience (Hangya et al., 2015; Zhang et al., 2019), suggesting the CE–NBM pathway may be engaged during novelty/uncertainty to signal insufficient evidence about CS value in the CE. Interestingly, the integrity of this pathway has been shown to interfere with attentional processes (Han et al., 1999).

Response plasticity upon PL in the CE requires permissive signals for circuit rearrangement. PE are major drivers for plasticity. Pain, as an intrinsically salient event (US), may provide a necessary PE signal to drive GM update within the CE. Pain information ascends via the DRG to also reach the PAG (Fig. 1, left) and indeed, PE signals have been described in the PAG (Roy et al., 2014). The vPAG/DR region harbors a population of dopaminergic (DA) neurons, representing a potential source for a teaching signal, driving learning about salient events in the CE (Cho et al., 2017).

Hypothesis 2

The CE–NBM pathway recruits the interoceptive IC to link CE CS uncertainty with upstream interoceptive GMs.

Hypothesis 3

The ascending vPAG/DR–CE provides a bottom-up teaching signal for Pavlovian associative learning in the CE.

Objective 3 –

IC–CE–vPAG/DR pathways control affective decision-making and learning

This serial model of BLA–CE affective processing ascribes distinct roles to the BLA and CE, where the BLA encodes actual sensory features of the stimulus, while the affective and motivational properties associated with the CS are encoded in the CE (Balleine and Killcross, 2006). Evidence from appetitive conditioning supports this functional segregation and implies that sensory-specific affective and motivational features may originate from other brain areas (Corbit, 2005).

The CE was shown to gate a diverse array of behaviors, including innate and learned freezing, predatory behavior, mother-pup interactions, feeding behavior and addiction (Cai et al., 2014; Ciocchi et al., 2010; Gallagher et al., 1990; Han et al., 2017; Haubensak et al., 2010; Isosaka et al., 2015; Li et al., 2013; Murray et al., 2015; Rickenbacher et al., 2017), Importantly, common overarching features implemented in the limited number of (known) CE cell types across behaviors, which allow for the implementation of diverse gating functions are currently lacking. The CE shows intrinsic functional connectivity to the IC, making it a prominent candidate pathway to integrate interoceptive information for affective learning (Gorka et al., 2018). The CE might serve as a site of convergence of interoceptive predictions associated with above affective states.

The CE sends a descending projection to the vPAG, which has been shown to control motor responses like freezing (Haubensak et al., 2010). However, the DAergic system has been proposed to incorporate a wide array of top-down information (Cohen et al., 2012), which may collectively give rise to the encoding of predicted states of the world. As CE acquires CS responses over the course of learning, the top-down CE–vPAG/DR projection may therefore exert negative feedback by signaling successfully acquired CS properties by CE.

Hypothesis 4

The cortico-striatal IC-CE pathway extracts explicit stimulus features from IC GMs to control affective behavior and learning in CE.

Hypothesis 5

We hypothesize top-down projections from CE to vPAG/DR contribute to a dopaminergic belief state about CS properties.

Manuscripts

Manuscript 1

Title: The amygdala instructs insular interoceptive feedback for affective learning

Authors: Dominic Kargl[1]*, Joanna Kaczanowska[1]*, Florian Groessl[1], Lukasz Piszczek[1], Sophia Ulonska[2], Jelena Lazovic[3], Katja Bühler[2], Wulf Haubensak[1]

Affiliations: [1]Research Institute of Molecular Pathology (IMP), Vienna Biocenter (VBC), Campus-Vienna-Biocenter 1, 1030 Vienna, Austria

[2]VRVis Research Center, Donau-City Strasse 11, 1220 Vienna, Austria

[3]Preclinical Imaging Facility (pcIMAG), Vienna Biocenter Core Facilities (VBCF), Vienna, Austria

*These authors contributed equally to this work

Correspondence to: wulf.haubensak@imp.ac.at

Abstract: Brains integrate environmental predictors with salient events to minimize uncertainty about the future. Interestingly, features of predictive stimuli are encoded across cerebral hierarchies. However, the purpose of this distributed organization remains unclear. Mapping complementary stimulus features onto a hierarchical cortico-limbic network, we here uncover a process mechanism where uncertainty about stimulus value at lower hierarchies exploits top-down feedback of interoceptive models to improve behavioral performance. We found that the amygdala itself instructs the bottom-up recruitment of a cortico-limbic loop between the insula and central amygdala via the basal forebrain to promote discriminatory Pavlovian conditioning. Learning links intra-insular unconditioned stimulus (US) representations of bodily states with conditioned stimuli (CS) to support central amygdala CS discrimination. Consequently, experimental uncoupling of directional information flow between hierarchical levels disrupts learning. We suggest that dysfunctional hierarchical interactions may underlie the intolerance to uncertainty observed in autism and related psychiatric conditions.

Main

Brains function as predictive machines, building internal models of the world to generate hypotheses about future sensory input[1]. In Pavlovian learning (PL) the brain utilizes predictive models for CSs to optimize behavioral outcomes. Learning updates these CS models with its predictive value for unconditioned rewarding or threatening stimuli (US)[2,3]. Previous research has successfully identified regions, neuronal populations and mechanisms underlying this form of associative learning[4,5]. These networks encode CS and US features at multiple hierarchies, from brainstem and amygdala to higher cortical associative areas[6–8].

During human brain development, functional hierarchies mature over the first two years of life, marked by the step-wise convergence of sensory modalities and emergence of hub-like nodes[9]. Particularly, limbic cortices represent the apex of sensory integration, which may encode the most holistic model of the (task) world[10,11]. Importantly, aberrations in hierarchical structure likely underlie conditions like autism, which is marked by dysfunctional network integration (e.g. Default Mode Network)[12]. This highlights the necessity for tight coordination of hierarchical communication for cognitive function, as seen in cortico-striatal motor processing[13]. The analogies between the motor and interoceptive system in circuit architecture[14,15] suggest that the hierarchical recruitment of interoceptive models built on stimulus values, as they emerge over training, drive affective decision-making and learning. Due to its fundamental role in interoception[16–19], the insular cortex (IC) may bind the CS to bodily states to resolve uncertainty about their value and guide future behavioral responses. Notably, interoceptive models are central to psychological theory, most prominently the recruitment of somatic markers for behavioral decision-making[20]. Therefore, we propose that such cross-hierarchical interactions with IC circuitry effectively integrates such bodily representations to guide affective decisions and learning. Interestingly, the human IC displays coupling to the striatal-like central nucleus of the amygdala (CE) in resting state functional MRI (RS-fMRI)[21,22]. The CE is a major gate for generating affective behavior[23–25], suggesting the IC–CE network might operate as a hierarchical system that integrates interoceptive models and affective behavioral decisions.

However, how this distributed CS and US information is used to build predictive models to solve PL tasks is unknown. Likewise, it is unclear which circuits and mechanisms integrate models into behavioral decisions to resolve uncertainty. These complex emergent functions are difficult to study in isolated elements, and therefore remained largely uncharted. We here

set out to map the network-wide organization of complementary CS features (value uncertainty, interoceptive model) to unmask hierarchical process mechanisms underlying PL.

To first address whether the IC and CE form a functional network, we performed resting state functional MRI (RS-fMRI) in wild-type mice. Seed-based brain-wide correlation of the IC blood oxygenation level dependent (BOLD) signal revealed coupling of the IC to the CE (Fig. 1a, n=4, see Supplementary Fig. 1a/b for seed placement/correlation matrix and Supplementary Table 2 for ROIs). Conversely, CE seed-based analysis showed coupling with the anterior portion of the IC (aIC), the posterior insular cortex (pIC) and the basal forebrain (BF). These brain-wide unbiased approach delineated a dedicated network that functionally interconnects the interoceptive insular cortex with the CE.

Previous work in humans established a rostro-caudal gradient in domain-general processing in frontal areas for abstract rule learning and cognitive control[26–28]. This principle may transfer to the IC, as aIC and pIC have been shown to functionally diverge[29]. Therefore, we recorded activity from the aIC and pIC using *in vivo* electrophysiology (Supplementary Fig. 2) and from the lateral and medial divisions of CE (CEl/CEm) using genetically encoded calcium indicators GCaMP6f/m (Fig. 1b, *top*). We sampled from somatostatin^{+} (SST::Cre, CE^{SST}), protein kinase C-δ^{+} (PKCδ::Cre, CE^{PKCδ}) and CEm neurons (wild type; Supplementary Fig. 3)[24,25]. CE^{PKCδ} and CE^{SST} are critical components for fear and reward learning and behavioral gating, which may depend on emotional state. So, we speculated that the CE network should encode features of a CS and US model, both within and among CE^{PKCδ}, CE^{SST} and CEm populations, for proper behavioral responding in a PL task[25,30,31]. On average, we recorded from 113 neurons in aIC (n=6 mice), 98 neurons in pIC (n=7) and 48 units in CE^{SST} (n=4), 54 in CE^{PKCδ} (n=5) and 29 in CEm (n=4) per session from the right hemisphere and extracted calcium events. These cohorts were water-deprived and subjected to a discriminatory auditory reward-fear PL paradigm. After habituation in Context A, CS1 (10s, 50ms white-noise pips at 0.9Hz) was paired with an unconditioned appetitive stimulus (R-US, water reward) in the reward conditioning sessions (RC) in Context A (R-CS). Then, mice underwent fear conditioning (FC), which paired CS2 (10s, 3kHz-constant) with an unconditioned aversive stimulus (F-US, foot-shock) in Context B (F-CS), followed by a non-reinforced recall stage in Context A (Fig. 1b, *bottom*). Importantly, this discriminatory PL approach allowed for deconstructing stimulus value into its underlying valence and salience components (which is not possible with single-valenced fear/reward-only designs), while allowing to extract interoceptive model building from US onto CS mapping (see below). We

propose that the encoding of task parameters across cortico-striatal hierarchies are shaped by associating CS-US contingencies, gradually reducing uncertainty about CS value. To test this, we trained a classifier to decode CSs in IC and CE activity across PL stages (see Methods). By iteratively drawing neurons from each population at every stage, we found that information on CS increased in the IC and CE network over time compared to shuffled data (Fig. 1ci, di, see Supplementary Fig. 4a for valence-resolved decoding).

Learning systems should discriminate between stimuli based on their predicted outcomes. To test whether IC and CE discriminate between R-CS and F-CS, we trained classifiers to decode R-CS or F-CS from the other CS. We found that IC and specifically $CE^{PKC\delta}$ progressively dissociate CSs with learning (lower accuracy – lower similarity, Fig. 1cii, dii). These data suggest that the IC–CE network maps additional features onto external stimuli during associative learning. A potential scenario is a direct transfer of US properties onto the CS. To test this, we trained a classifier on US responses (Supplementary Fig. 4bi) and decoded from the respective CS. We found the IC projected US properties onto an US-predictive CS (higher accuracy – higher similarity, Fig. 1ciii), endowing CS representations with interoceptive value (i.e. somatic markers[20]). In this process, the aIC exhibited early valence-domain generality, which pIC acquires in the late stage of conditioning (Supplementary Fig. 4bii). Interestingly, IC subregions dissociated the primary valence of USs, indicated by differential population responses upon R-US and F-US in aIC and pIC (Supplementary Fig. 7a). This highlights a valence gradient from positive to negative along the IC antero-posterior axis.

Conversely, CE subpopulations differentially utilized US properties. While CE^{SST} explicitly transferred US properties onto CSs, US and CS features in $CE^{PKC\delta}$ did not share representations, while CEm remained neutral with learning (Fig. 1diii). Notably, all CE populations responded to both USs (Supplementary Fig. 7f). Therefore, CE responses alone may not offer relational contrast for US value discrimination and thus are tuned to stimulus salience. In conclusion, our data support a model, whereby CE^{SST} and CEm differentiate intrinsic stimulus salience, which becomes indifferent upon acquisition of US salience in both valence domains (Supplementary Fig. 4bii). In contrast, valence discrimination is facilitated by $CE^{PKC\delta}$ (Fig. 1dii).

Top-down interoceptive models facilitate stimulus-behavior associations

Functional coupling of divergent stimulus features representing the same contingency may be an emergent property of learning systems, suggesting exchange of information in the IC–CE

network facilitates sensory integration and stimulus-behavior association in PL. To ask whether this transition requires information transfer across cortico-limbic hierarchies, we first assessed synaptic connectivity between a/pIC and CEl populations by retrograde tracing (Supplementary Fig. 5ai) and slice electrophysiology (Fig. 2a, Supplementary Fig. 5aii). We found that aIC and pIC innervate CEl subpopulations symmetrically (Fig. 2b, see 'IC-CE circuit architecture' in Supplementary Notes, 92% of PKCδ$^+$ vs 91% of SST$^+$ responsive for aIC/ 100% of PKCδ$^+$/SST$^+$ for pIC input).

We then trained a random forest (RF) classifier to assess network performance in representing the specific task parameter in random draws of 100 neurons from IC and CE. An episode was considered 'correct' during presentation of the respective CS versus 'incorrect' if it occurred before CS onset. This analysis showed that successful encoding of the association between CS and behavior was linked to correct trial performance (see Supplementary Fig. 6ai). We then probed information exchange between the top (IC) and bottom (CE) hierarchies in this network by quantifying the transfer entropy (TE) from event (spike or calcium transient)-aligned 1s-binned activity (Supplementary Fig. 6bi)[32], centered around the onset of behavioral episodes (port visits for R-CS; freezing onsets for F-CS). We note that stimuli or behavior evoke a state that is generalizable across individuals within our circuit architecture, which makes such approaches feasible[33]. After exploring TE parameter space by considering all possible neuron pairs within CS and stage as well as within and across regions, we applied the peak TE from a 1s history for all subsequent analyses (Supplementary Fig. 6bii). This analysis revealed significant information transfer from IC to CE for correct behavioral associations (Fig. 2ci, Decoder accuracy (Da) of RF shown above network and feature importance (FI) projected onto network elements). Specifically, a subnetwork-specific transfer for correct port visits from aIC to CE^{PKCδ} and CE^{SST} (Fig. 2ci, green), as well as from pIC to CE^{SST}, for correct freezing onsets (Fig. 2ci, blue). Importantly, this top-down information transfer was absent in behavioral episodes occurring outside the CS presentation (Fig. 2cii). Taken together, these data emphasized a specific role of the IC–CE network for stimulus-behavior associations, the ultimate purpose in PL tasks. Moreover, these results support biased US representations along the antero-posterior axis of the IC (Supplementary Fig. 7a) reflecting a positive-negative antero-posterior valence gradient shaped by US-evoked responses, which also determined later CS-specific responses in the task (Supplementary Fig. 7c-e, see 'IC-CE circuit architecture' in Supplementary Notes).To experimentally test behavioral consequences predicted by TE maps, we subjected a cohort of mice to the PL task while we temporally uncoupled the IC from CE. Mice received bilateral injection of adeno-

associated virus (AAV) carrying the optogenetic inhibitor archaerhodopsin (syn-Arch) or GFP as controls (syn-GFP) into aIC or pIC with and bilateral fiber-optic cannulas placed above CE (Fig. 2di, Supplementary Fig. 5b). The respective IC–CE projection was optogenetically inhibited specifically during CS presentation at training. This design specifically interfered with the predicted value of a task model in IC corresponding to the CS-associated expectation. In this context, such an approach interrogated the function of predictive interoceptive states and their contribution to stimulus-behavior associations. Mice receiving aIC–CE inhibition during CS periods throughout conditioning showed impaired stimulus-behavior association, indicated by a lower number of port visits in RC and exacerbated freezing in FC compared to control animals (Fig. 2dii). In contrast, we observed the opposite pattern for pIC–CE manipulation (Fig. 2dii, Supplementary Fig. 8a for raw data).

To test for an effect on memory formation, mice underwent a recall session where both sounds were presented without manipulation. The aIC–CE manipulation not only interfered with stimulus-behavior association at conditioning but also manifested in behavioral performance at recall (Fig. 2diii, *left*). While optogenetic pIC–CE uncoupling was successful during conditioning, it was insufficient to last into recall (see Supplementary Fig. 8bi,ii for raw data). However, memory deficits at recall resulted from potentially stronger DREADD (designer receptor exclusively activated by designer drug)-based perturbation of the pIC–CE pathway at conditioning (Fig. 2diii *right*, see Supplementary Fig. 8c/biii,iv for learning curves/raw data). Specifically, to achieve tonic silencing, wild-type mice received bilateral injections of retrograde canine-adenovirus carrying a construct coding for Cre-recombinase (CAV::Cre) into the CE and an AAV carrying Cre-dependent inhibitory hM4 receptor into the pIC bilaterally or Cre-dependent GFP in controls (hM4(pIC)-CE, GFP controls; Supplementary Fig. 5c). Collectively, these data demonstrated a functional role of IC–CE interaction in both reward and fear PL in line with the underlying information flow predicted from TE. We showed that interoceptive IC innervates CE subpopulations symmetrically, while IC subregions drive stimulus-behavior transitions antagonistically. Both projections implement Pavlovian memory to adapt behavior for future encounters of sensory cues.

Basal forebrain NBM mediates bottom-up recruitment of IC activity

Previous work has implicated cortico-striatal loops to gate information flow[34]. Aside from IC, our fMRI survey identified strong coupling from CE to corticopetal basal forebrain

cholinergic nuclei like the Nucleus Basalis of Meynert (NBM) (Fig. 1a, *right*). Since electrical stimulation of CE via basal forebrain[35] and activation of putative PKCδ^{+} neurons[36] triggered cortical arousal, we hypothesized that the CE–NBM pathway may facilitate IC coupling to CE. The topological organization of NBM projections suggests that distinct subareas innervate specific cortical patches[37], which potentially allows NBM inputs to coordinate arousal in selected cortical regions. To test this, we lesioned CE bilaterally by injecting N-methyl-D-aspartate (NMDA, n=3, Supplementary Fig. 1c) to identify regions displaying depleted BOLD signal coupling to NBM compared to CE sham-lesioned control animals (correlation matrix in Supplementary Fig. 1d). NBM-seeded global brain correlations in CE-NMDA-lesioned animals showed decreased coupling of the right aIC, suggesting that CE innervation of NBM selectively triggers NBM–aIC interactions (Fig. 3a, Supplementary Fig. 1a for seed placement). To explore this possibility, we assessed synaptic connectivity between CEl populations and NBM neurons by retrograde tracing (Supplementary Fig. 9a) and slice electrophysiology (Fig. 3b, Supplementary Fig. 9b, see 'CE-NBM circuit architecture' in Supplementary Notes). We found that (mostly GABAergic[38]) CEl subpopulations primarily innervate putatively local parvocellular (pc) interneurons (IN) versus corticopetal magnocellular (mc) neurons, supporting a disinhibitory mechanism of CE input gating the NBM output.

To characterize this pathway *in vivo*, two aIC-pIC multi-site implanted animals (PKCδ::Cre, Fig. 1b) received an injection of DIO-ChR2 into the right CE and a fiber-optic cannula above the right NBM. This approach permitted directly assessing the effects of CE^{PKCδ}-NBM stimulation on aIC and pIC (Fig. 3ci). Animals received 5ms 470nm laser pulses, which elicited pronounced LFP depolarization in aIC and to a lesser extent in pIC (Fig. 3cii, *left/right*, comparison of minima of aIC and pIC in Fig. 3ciii), and 405nm laser pulses as control stimuli, as ChR2 is insensitive to this wavelength[39]. This stimulation also increased single unit spiking in IC (Supplementary Fig. 10), indicating CE activity may recruit the IC. Possible disinhibition of ChAT^{+} neurons implies a dependency on cholinergic signaling in the IC. Therefore, a cholinergic antagonist should attenuate cortical depolarization. Indeed, systemic administration of the muscarinic 1 receptor antagonist telenzepine (TZP) mitigated CE^{PKCδ}-NBM induced cortical depolarization by approximately 50%, demonstrating involvement of muscarinic signaling (Fig. 3cii, insets for comparison of minima). Collectively, these data support a model where CE input predominantly inhibits putative GABAergic IN to disinhibit corticopetal ChAT$^{+/-}$ mc neurons (Fig. 3d). Importantly, this

identifies a missing link by which the IC–CE pathway is recruited into behavioral decisions[40,41].

Learning establishes an intra-cortical hierarchy and task model

Stimuli must acquire meaning to establish a behavioral response. Therefore, neural systems require elements signaling insufficient evidence about stimulus value (which should then drive learning by recruiting additional information). To probe for network-level signatures of uncertainty, we quantified TE between network elements at the time of CS presentation during learning, when uncertainty should be high. We observed extensive bottom-up TE from CE to IC, indicating potential recruitment of IC by CE (Fig. 4ai, see 'Control' in Supplementary Fig. 6aiii for graphical depiction of Da and FI). Importantly, extensive top-down TE from IC to CE suggests a cross-hierarchical transfer of a (bottom-up-recruited) task model.

The success of a task model may relate to the probability of correct behavioral responses. To address this, we next sought to separate CS-driven networks generated from CS periods that lead to a correct response (port visit during R-CS/freezing episode during F-CS) from CS periods with an incorrect behavioral decision (unspecific or absent behavior). This analysis showed that a successful task model is characterized by bottom-up and top-down TE from aIC to pIC (Fig. 4aii). These characteristics were different in unsuccessful trials, where despite preserving bottom-up TE, any top-down transfer was missing (Fig. 4aiii). This is paralleled by worse Da on CSs not containing correct behavioral episodes (Supplementary Fig. 6aii for graphical depiction of Da and FI).

Despite no clear directionality in IC communication in humans[42], our data places aIC above pIC in an interoceptive hierarchy. Top-down processes can ascribe predictions based on models of sensory input to lower elements in the hierarchy, which may place constraints onto bottom-up information to facilitate its interpretation[43]. To test these predictions *in vivo*, we simultaneously recorded from aIC and pIC during the PL task (Fig. 4bi). We related local spikes with distant local field potentials (LFPs) for assessing coherence, a proposed mechanism through which neuronal networks exchange information by adjusting gain[44]. Since performance should scale with model accuracy, we chose the best performer in the fear domain at the recall stage (Supplementary Fig. 7c, 'MS1'). Spike-triggered averages (STAs) of pIC LFP were generated around spikes from aIC to reveal oscillatory synchronization. During habituation, this showed similar STA amplitudes during CS presentation compared to a 10s period immediately preceding sound onset (preCS) (Fig. 4bii). Strikingly, during recall

we observed a stimulus-induced increase in STA amplitude (Fig. 4biii). To eliminate potential changes in total LFP amplitudes, we normalized the STA spectrum to the absolute pIC LFP amplitude, yielding spike-field coherence (SFC). During habituation, we found SFC peaks in the β- and γ-range for preCS, which decreased during CS presentation (Fig. 4Civ). However, at recall we observed CS-specific tuning of aIC spikes to pIC LFP with maximum SFC at 33Hz (Fig. 4bv). Notably, SFC was stronger in the negative valence domain, indicating asymmetry of aIC–pIC communication (Supplementary Fig. 11a). Importantly, synchronization was not present in worse performers (Supplementary Fig. 11b) or when performing the converse analysis (pIC-aIC, Supplementary Fig. 11c). As CE–NBM activity-induced depolarization of IC LFP was partially dependent on M1R signaling, we tested for M1R dependency of interareal coherence. We performed recall sessions after systemic TZP administration, which was interspersed with recall sessions in control conditions. M1R antagonism abolished stimulus-induced SFC, demonstrating that cholinergic signaling via M1R receptor mediates cortical gain control in the IC (Fig. 4biii,v, dashed lines). Taken together, these data reveal experience- and performance-dependent and stimulus-driven top-down gain modulation within aIC–pIC networks. We propose this phenomenon as a neural correlate of a task model predicted by the TE maps.

To determine the functional relevance of aIC–pIC binding, we trained animals in the PL paradigm that expressed hM4 (or GFP for controls) in aIC neurons projecting to pIC by injection of CAV::Cre into the pIC and an AAV carrying Cre-dependent hM4 (or Cre-dependent GFP for controls) into aIC (both bilaterally) (hM4(aIC)-pIC, Supplementary Fig. 5c). We systemically administered CNO to both groups at the RC and FC stages and tested their memory during drug-free recall (see Supplementary Fig. 8c for learning curves). We found that inhibiting the projection from aIC to pIC specifically during training impaired Pavlovian fear learning (Fig. 4cii, see Supplementary Fig. 8d for raw data). These results provide evidence for top-down gating of associative plasticity in the IC and support valence-asymmetric gain control established by SFC.

Our data suggest that the acquisition of a domain-general task model in the aIC is required for PL performance. To test whether this is reflected in the distribution of PL features, we contrasted the FI between correct/incorrect CSs or behavioral episodes (Fig. 2cii/4aiii, Supplementary Fig. 6aii/ii). Indeed, FI in aIC was reduced compared to correct CS presentations (Fig. 4di), as well as for CS-unspecific behavioral episodes (Fig. 4dii), indicating impaired recruitment of an interoceptive model.

The CE–NBM pathway promotes interoceptive top-down models for PL

In PL USs serve as primary PE signals to update the model about the CS as a US predictor. TE of the post-US period revealed recurrent dynamics between and within CE populations, as well as bottom-up TE from primary sensory pIC to multimodal aIC. Interestingly, we found bottom-up recruitment of the $CE^{PKC\delta}$ to aIC pathway, which linked hierarchies during an instructive US (Fig. 5a). Collectively, an impinging PE largely uncoupled the network compared to a CS (Fig. 4ai), while shifting network TE toward bottom-up signaling (pIC-aIC; see 'Control' in Supplementary Fig. 6aiv for graphical depiction of Da and FI). To test whether this phenomenon is solely attributed to primary reinforcement or whether network dynamics represents a general feature of sensory uncertainty, we examined CS presentations where information on valence was low but relative salience was high. These conditions are best satisfied during habituation, as RF mean accuracy for CS detection was significantly higher in habituation compared to conditioning (Supplementary Fig. 6c). CS-aligned TE networks during this stage resembled US-aligned networks remarkably well, suggesting that the CE–NBM–aIC pathway was engaged under conditions of uncertainty (Fig. 5b).

To further validate these predictions, we recorded from IC (Fig. 1b) in mice undergoing habituation and conditioning stages when $CE^{PKC\delta}$ was chemogenetically silenced. To recalculate the TE networks, neural activity from aIC and pIC was replaced with their respective activity from recordings when $CE^{PKC\delta}$ was silenced (aIC', pIC'; hM4($CE^{PKC\delta}$), Fig. 5c). In these networks, we still found bottom-up TE from CE to IC. However, recruitment of top-down transfer from IC to CE was absent, reminiscent of network TE during an incorrectly assigned CS (Fig. 4aiii). These results indicate CE (and $PKC\delta^+$ neurons therein) may be required for IC recruitment. In addition, intra-insular communication displayed pIC to aIC directionality, resembling US/habituation networks (Fig. 5a/5b). This suggests CE (and $PKC\delta^+$ neurons) activity facilitates top-down information transfer, while bottom-up signaling predominates during $CE^{PKC\delta}$ inhibition (Fig. 5c). Notably, RF decoding revealed a shift in FI from aIC to pIC (Fig. 5c, Supplementary Fig. 6aiii), which is fully recapitulated by the US (Supplementary Fig. 6di, FI: Supplementary Fig. 6aiv) and partially for CS in habituation (Supplementary 6dii)

Since our data suggest that uncertainty evokes CS-associated information flow within the IC–CE network, artificially reducing uncertainty should interfere with updating a task model and learning. Predictions from TE maps point towards bottom-up cross-hierarchical interactions triggered by CE (Fig 5b) via NBM (Fig. 3). We tested this in a cohort of mice in the PL task with selectively blocked $CE^{PKC\delta}$-NBM communication during CS presentations at training.

For this, PKCδ::Cre animals were bilaterally injected with Cre-dependent Halorhodopsin or Archaerhodopsin (DIO-NpHR3.0/DIO-Arch) into the CE and implanted with fiber-optic cannulas above the NBM (Fig. 5di; Supplementary Fig. 5d). Mice receiving optogenetic inhibition of $CE^{PKC\delta}$-NBM during all CS periods of conditioning indeed displayed aberrant Pavlovian associations during manipulation-free recall. This was evident by low number of port visits and reduced freezing levels compared to control animals (Fig. 5dii; see Supplementary Fig. 9c/d for learning curves/raw data). Together, these data reproduce impaired memory formation observed in aIC– and pIC–CE manipulations (Fig. 2d). Of note, optogenetic interference with the SST^{+} projection to NBM had no effect on PL (Supplementary Fig. 9e,f; Supplementary Fig. 5d).

Since IC contributes to successful stimulus-behavior associations, we hypothesized that an interoceptive model could facilitate CS discrimination for CE in PL. To test the functional consequence of silencing the interoceptive model, we took animals initially used for CE recordings (Fig. 1d) and performed bilateral chemogenetic inhibition of aIC followed by reassessment of CS representation and discrimination in CE population activity (Fig. 5ei, hM4(aIC), Supplementary Fig. 3b). We focused on neurons most engaged at respective tasks by selection of highest Da through single-neuron decoding (best neurons, see Methods), potentially representing functional ensembles (see Supplementary Fig. 4c and Supplementary Table 3). Silencing the top of the interoceptive hierarchy markedly impaired CS representation in CE^{SST} (Fig. 5eii) and reduced CS discrimination by $CE^{PKC\delta}$ to chance level (Fig. 5eii, CE^{SST} and CEm revert to discrimination levels at habituation, Fig. 1dii: see Supplementary Fig. 4biii for valence-resolved transfer). This implies functionally independent IC-CE pathways channeling CS information via CE^{SST} and CS discrimination via $CE^{PKC\delta}$. Strikingly, aIC silencing revealed a disinhibition of salience transfer from US to CS during conditioning, providing a potential mechanistic explanation for the emergence and role of IC-CE pathways in PL. In the absence of an interoceptive model, the CE by default maps stimulus salience onto CS representations, obstructing stimulus discrimination by $CE^{PKC\delta}$. In contrast, successful model recruitment confers valence discrimination through $CE^{PKC\delta}$ (Fig. 5eiii) to enable correct behavioral responding (Fig. 4aii, Fig. 2c).

Discussion

Our study successfully integrated brain wide network analysis from high field small animal fMRI with circuit physiology and mapped the IC↔CE/NBM network as an own-standing functional unit, also supporting previous findings on IC–CE function[40,41,45]. This approach uncovered a basic functional motif, which encodes complementary stimulus features at different hierarchies and stages of PL. This design establishes a process mechanism for PL, where stimulus value at lower-levels updates top-level interoceptive models in IC; this information feeds back to CE to reassemble valence and salience dimensions of the predictor (CS) to guide behavioral decisions (Supplementary Fig. 12).

Theories on affect propose that interoceptive signals modulate decision-making and emotional learning[20]. Accordingly, USs evoke innate representations of affective states that then bias decision-making. We found a rostro-caudal distribution of IC value responses of which magnitude predicts behavioral performance and CS responses at recall. Our data showed that IC not only represents sensory cues[46], but generates (CS-associated) allostatic states instructing lower hierarchies about CS valence to guide behavioral responding and memory formation. Thus, our study identifies a cortico-striatal hierarchy linking interoceptive models to decision making. This implements theories integrating bodily states into affective decisions (Somatic Marker Hypothesis[20]). Representations of CS, US and uncertainty synergize across IC–CE hierarchies for PL to optimize behavioral outcomes, potentially showcasing a general phenomenon in cortico-limbic interaction.

We identified an uncertainty-driven ascending IC↔CE/NBM pathway as a critical mechanism for driving IC–CE signaling. Lesion studies have linked the connection between CE and NBM to enhanced surprise/PE-triggered learning[47,48], whereby introduction of inconsistency into CS-US contingencies, which increases uncertainty, enhanced the CS association and learning, supporting the Pearce-Hall model for PL[49]. Although we did not explicitly operationalize probabilistic conditioning in our PL task, the CE–NBM pathway could instantiate precision signaling as neural gain control of top-down models from higher order areas (aIC) to primary sensory areas (pIC)[50]. This striatal coordination of cortical hierarchies may also be computationally advantageous, e.g. as for gating working memory[51]. *In vitro* experiments indicate that ACh can favor associative to primary sensory cortex communication[52]. Therefore, we speculate a similar mechanism may gate associative plasticity in the interoceptive system[53] (Fig. 4c), as ACh has been linked to learning rate and certainty[54,55]. Basal forebrain cholinergic neurons rapidly respond to reinforcement feedback

in both valence domains[56]. Since, neurons in CE are unlikely to mediate NBM responses to USs, we instead speculate that the CE–NBM axis integrates primary reinforcement signals with information on novelty, confidence and expectation[57], which is broadcasted to the IC. Interestingly, in humans these higher-order PE incorporating hierarchical probability distributions have been mapped onto the basal forebrain[58].

Cognitive function requires balanced top-down/bottom-up signaling, while its dysregulation may underlie conditions like autism and schizophrenia[59,60]. Along these lines, we propose that disrupted functional connectivity in IC↔CE/NBM networks might contribute to those conditions. First, deficits in model-building might lead to augmented bottom-up processing and associated symptom domains. This relates to humans diagnosed with autism as they rely less on prior beliefs, suggesting they may predominantly utilize bottom-up signaling in perception[61], which could be explained by augmented salience (at the expense of valence) in the absence of the interoceptive model (Fig. 5eiii,iv). This phenomenon is congruent with TE networks generated from data under conditions of $CE^{PKC\delta}$ inhibition, where CS-driven networks revert to uncertain/surprise states (Fig. 5c). Our observation of enhanced accuracy of encoding exteroceptive stimuli in the network, along with a relative shift of FI towards primary sensory pIC, resonates with fundamentally different cognitive strategies ascribed to autism. Weak central coherence and enhanced perceptual functioning represent hallmarks of biases towards details and impaired abstraction[62]. Interestingly, these studies show dominance of posterior networks in perceptual tasks[63]. Thus, we propose that CE–NBM signaling is central for hierarchical information flow during uncertainty and the inability to resolve it (Fig. 5d), as seen in autism[64] and comorbid anxiety[65]. Second, disruptions in hierarchical processing (Fig. 4d, 5c) analogous to human patients[12] might explain the absence of affective models in autism and the resulting behavioral difficulties with uncertainty and affective interactions.

In conclusion, we describe distributed neural ensembles in a cortico-limbic network that resolves uncertainty about the value of sensory cues and drives affective learning by recruiting interoceptive models in IC. Under states of uncertainty, lower hierarchies (CE) drive bottom-up recruitment of IC via NBM. This, in turn, integrates stimuli with bodily states to build interoceptive models in IC, which then feed back to the CE to control behavioral decisions. Overall, we propose that the inability to establish or recruit hierarchically organized interoceptive predictions in IC↔CE/NBM circuitry based on the present sensory environment contribute to symptoms of autism spectrum or schizophrenia.

Methods

Animals

Male mice aged between 2-6 months were group housed in a colony on a 14h light/10h dark period, allowed water and food ad libitum, unless noted otherwise. Animal procedures were performed in accordance with institutional guidelines and were approved by the 4 respective Austrian (BGBl nr. 501/1988, idF BGBl I no. 162/2005) and European authorities (Directive 86/609/EEC of 24 November 1986, European Community) and covered by the license M58/002220/2011/9. Wild-type C57BL/6J mice were in-house bred and provided by the Research Institute of Molecular Pathology animal facility or ordered from Charles River Laboratories (strain C57BL/6J). Transgenic animals (Prkcd::GluClα::Cre^{24} BAC transgenic mice, PKCδ::Cre and SOM-IRES::Cre transgenic mice, SST::Cre; stock no: 013044, Jackson Laboratory) were maintained on the C57BL/6J background. All mice were handled by the experimenters for several days prior starting any behavioral procedures.

Stereotactic surgery for virus/toxin injections, fiber-optic cannula/lens/electrode implantations

Mice were deeply anesthetized with isoflurane and maintained at 1.5-2% throughout the procedure (Univentor 400). Animals were mounted in a stereotactic frame (Kopf), while body temperature kept constant at 36°C via a rectal temperature-controlled heating pad (FHC). Before skin incision, local anesthesia was provided underneath the skin by injection of 0.1ml of lidocaine (Xylanaest, 1%). The exposed skull was drilled through above area of interest, relative to bregma (Franklin & Paxinos 2007). Post-surgery animals were provided analgesics (250mg/ml Carprofen; Rimadyl, Pfizer) and antibiotics (400 mg/l Enrofloxacin; Baytril, KVP pharma) via drinking water for 7 days. For optogenetic experiments, animals were bilaterally injected with respective viruses (CEl 80nl, AP -1.38, ML ±2.9, DV -4.85mm; aIC 100nl, AP +1.54, ML ±3.17, DV -3.55; pIC 80nl, AP -0.7, ML ±4.2, DV -4mm) and implanted bilaterally with fiber-optic cannulas (Doric Lenses, 200-400µm, NA 0.37-0.53) 0.5mm above target coordinates (CEl AP -1.38, ML ±2.9, DV -4.35mm; NBM AP -0.4, ML ± 1.6, V -4.3mm). For chemogenetic inhibition, we used Cre-dependent hM4 DREADD system (AAV::DIO-hM4) injected bilaterally to aIC (100nl) or pIC (80nl), the Cre-expressing construct was delivered bilaterally to pIC or CEl. For Ca^{2+} imaging mice were unilaterally injected with an AAV carrying a Ca^{2+} indicator into CEm (60nl, AAV::GCaMP6m; AP -1.06, ML +2.25, DV -4.5mm) or in CEl (50 nl, AAV::DIO-GCaMP6f; AP -1.38, ML +2.9, DV -4.85mm). At least 4 weeks after injection, a lens was implanted above the injection site (Inscopix microendoscope 0561 Part ID:1050-002182). After a one-week recovery period, baseplate was cemented onto the skull (Inscopix microscope baseplate V2, Part ID:1050-002192). For in vivo electrophysiology silicon probes (single-site; Neuronexus) or custom-built tetrodes (multi-site; 30µm Nichrome wires, California Fine Wire; 2 bundles per site) affixed on fiber-optic cannulas were implanted. Ground screws were mounted above the contralateral prefrontal cortex and cerebellum. All implants were fixed to the skull with dental cement (SuperBond C&B kit, Prestige Dental Products).

Resting state functional Magnetic Resonance Imaging (RS-fMRI)

MRI was performed on a 15.2 T Bruker system (Bruker BioSpec, Ettlingen, Germany) with 23 mm quadrature birdcage coil. Prior to imaging, all mice were anesthetized with 4% isoflurane, while care was taken to adjust the isoflurane levels immediately so that respiration did not go below 140 breaths per minute (bpm) at any time. During imaging, respiration was

kept between 140-160 bpm. For resting state fMRI study, single shot echo planar imaging (EPI) sequence with spin echo readout was used (TR=3000ms, TE= 19.7ms, FOV=16 X 16 mm^2, voxel size =250 X 250 μm^2, 30 slices 0.5mm thick, 1 average, 240 repetitions, 12 minutes total imaging time). Following resting state scan, a high-resolution T1-weighted anatomical scan was acquired using gradient echo sequence (TR=500ms, TE=3ms, FOV=16 X 16 mm^2, voxel size=125 X 125 μm^2, 30 slices 0.5mm thick, 4 averages).

Data processing for RS-fMRI

Resting state fMRI data were processed using the Data Processing Assistant for Resting-state fMRI Advanced Edition (DPARSF-A) toolbox, which is part of the Data Processing and Analysis of Brain Imaging (DPABI) toolbox version 2.1 (http://rfmri.org/dpabi,[66]). The first 10 volumes were removed from each data set, to assure that steady state magnetization was reached. Data were processed in series of steps that included slice-timing correction, realignment, co-registration, normalization and segmentation using in-house created mouse masks for cerebrospinal fluid (CSF), white matter (WM) and gray matter (GM). Nuisance covariates related to motion were regressed out using Friston 24-parameter model[67]. In addition, WM and CSF mean time-series were used as nuisance regressors in the general linear model to reduce influence of physiological noise[68]. Data were analyzed with and without linear regression of global signal[69–71]. Data were smoothed spatially with a 2.4 pixel full-width half-maximum Gaussian kernel. A narrow band pass filter (0.054-0.083 Hz) suggested by[72] was used, following nuisance regression. All data were co-registered to the in-house generated mouse atlas with 80 distinct brain regions. For the seed-based functional connectivity analysis, the mean time series signal from the region of interest (seed) was calculated and correlated with the time series signal from each pixel of the brain. Between group comparison was done using pairwise t-test followed by Gaussian Random Field (GRF) Theory Multiple Comparison Correction (voxel-level p-value=0.05, cluster-level p-value=0.05). Within group comparison was done using one-sample t-test followed by GRF multiple comparison correction (voxel-level p-value=0.05, cluster-level p-value=0.05).

For the functional connectivity matrix, mean time course signal from 80 brain region was calculated. Fisher's z-transformed Pearson correlation coefficients between each pair of brain regions were calculated for all groups[73]. One-sample t-test was used to find a significant pair of brain regions within a group, $p<0.05$ was considered significant. All analyses were performed using freely available R-project software[74].
Resting state fMRI results shown here use global signal regression (GSR). An alternative approach for noise correction was performed as well[75], and no significant differences among results were found (data not show). We chose to interpret results following GSR, as this approach was shown to improve specificity of positive correlations[76,77] and aided predicting symptoms following focal brain lesions in humans[78].

Combined Pavlovian reward and fear conditioning for behavioral cohorts

Animals from all experimental cohorts were water deprived for 16h at all stages of the experiment, while their weight was continuously monitored and ensured that it never fell below 80% of their initial weight. Prior conditioning experiments animals underwent a port training session where they learned to associate the port with the delivery of a water drop in context A (light on, water delivery port, neutral grid). Only after successful port training the animals proceeded to reward conditioning (RC). All cohorts underwent at least 8 RC sessions in context A, where they received between 12 and 24 pairings of a neutral sound (50ms white

noise, 0.9Hz for 10s at 70dB, 'R-CS') with the subsequent delivery of a water drop (port opened for 1s). Thereafter mice underwent a single fear conditioning (FC) session in context B (no light, port removed, shock grid) where they received 5 pairings of a different neutral sound (3kHz continuous for 10s at 70dB, 'F-CS') with the delivery of a mild 1s foot shock (0.5mA, Coulbourn). Memory test was conducted in context A by presenting both unreinforced sounds four times each interleaved in blocks of two (2x(2R-CS + 2F-CS)). Reward-specific behavior was scored when a mouse broke the IR beam while entering the port ('port visits'), whereas freezing behavior was scored on recorded videos with Ethovision v12.0 (Noldus) offline (1s minimum time immobile, <0.5% area change for a 1s sliding window).

In vivo electrophysiology acquisition and data analysis

Mice were handled and habituated to the recording room for several days prior experimental recordings. Implanted electrodes were connected via an Omnetics connector to a 16-channel unity-gain headstage (Plexon), and mice were left in the homecage for 10min thereafter. The headstage was connected to a pre-amplifier where the signal was band-pass filtered (3Hz-1khz) and amplified. Neural activity was digitized at 40kHz and highpass-filtered for spikes (800Hz) and LFPs (3-200Hz) for offline analysis. Spikes were sorted with Offline Sorter v4 (OFS, Plexon). All recording sessions per mouse were merged and principal component (PC) analysis was performed on unsorted waveforms. Spikes were manually sorted with OFS. Single units were sorted manually in 3D PC feature space per session and declared a single unit if the spike cluster was separable from noise and other clusters and no refractory period infringements were detected. To avoid multi-sampling of single units, cross-correlograms of units from adjacent channels were inspected for co-firing and respective units removed from analysis.

Behavioral design for *in vivo* electrophysiological experiments

Mice underwent 3 habituation sessions (6 presentations per CS in blocks of 2) and 3 port training sessions (random water delivery at the port), each 30 min after i.p. injection of either PBS, CNO or TZP (treatment order counterbalanced). For RC, mice were separated into a PBS and a CNO group, receiving respective i.p. injections daily. After 8-12 RC sessions (20 CS-US pairings), mice were subjected to a FC session (3-4 CS-US pairings), receiving the same treatment as in RC. After 3-4 recall sessions (same treatments as in habituation, 4-6 presentations per CS in blocks of 2), mice underwent single RC and FC sessions with the respective converse treatment (PBS or CNO), followed by 3 recall sessions, each with a different treatment (PBS,CNO,TZP). Reward-specific behavior was scored when a mouse broke the IR beam while entering the port ('port visits'), whereas freezing onsets were scored (1s minimum time immobile, 1s sliding window, Motion Threshold=80) on recorded videos with Cineplex Editor v3.6 (Plexon) and aligned to electrophysiological data offline.

Behavioral design for Ca^{2+} imaging experiments

Mice underwent 2 habituation sessions with 4 presentations of each CS in blocks of 2 and 2 port training sessions (random water delivery in the port), 30 min before each session mice received i.p. injection of either PBS or CNO (treatment order was counterbalanced). Then all mice underwent 6-10 RC sessions with 12 CS-US pairings, receiving a daily i.p. injection of PBS before RC sessions and one with a prior CNO injection. Next, mice were subjected to 2 FC sessions with 2 CS-US pairings each, receiving either injection of PBS or CNO (balanced order). Thereafter, all mice were subjected to 4 recall sessions (2 PBS and 2 CNO sessions).

Reward-specific behavior was scored when a mouse broke the IR beam while entering the port ('port visits'), whereas freezing onsets were scored on recorded videos with Ethovision v12.0 (Noldus) offline (1s minimum time immobile, <0.5% area change for a 1s sliding window).

Ca^{2+} imaging acquisition and data processing

Deep-brain calcium imaging was performed with an *in vivo* miniature endoscope (Inscopix). Mice were handled and habituated to the mounted microscope for several days prior experimental recordings. nVista HD System v2.0.32 (Inscopix) was used for acquisition of Ca^{2+} signals. Images were obtained at 20 fps with automatically set exposure time, 3.25 gain and LED power set to 40%. Data was processed and analyzed with Mosaic v1.2.0 software (Inscopix). The aligned videos were down-sampled 2x2 (time x space) and the Ca^{2+} signal was calculated as the relative change of fluorescence over the entire recording session ($\Delta F(t)/F0=(F(t)-F0)/F0$). The individual neurons and their Ca^{2+} traces were extracted by applying PCA-ICA analysis. Spatial filters obtained by PCA-ICA were then manually selected to avoid duplicates or false units in further analysis. Ca^{2+} traces were then filtered (0.5 Hz low pass filter) and automated Ca^{2+} event detection was applied ($\Delta F(t)/F0 > 3$xMAD (median absolute deviation), $\tau_{off}=0.2$ s). All normalized Ca^{2+} signal values, traces and events, are reported in SD units. Exported traces and events were further analyzed with Neuroexplorer software v5.114 (Plexon).

Peri-event time histogram (PETH) analysis of neural recordings

Data from in vivo electrophysiology and calcium recordings were processed in Neuroexplorer. Neuronal firing and calcium signals were extracted as 500ms binned events. Neuronal events were then exported as PETH and z-scored per recording stage. Only data within -8 – 18s relative to CS onset was considered and smoothed with Gaussian filter (degree=5 for IC and 8 for CE data). The electrical shock artefact was masked and neural activity originating from a channel showing prolonged LFP black-out at a given trial was replaced with the population average of the same bin.

Neural decoding

Neural decoding was performed on raw recorded neural data X to determine the representation of stimuli y within the recorded brain regions. We reasoned that operations on raw data while not maximizing decoder accuracy will allow for more straight-forward comparisons between conditions, as non-linearities introduced by independent data pre-processing steps are minimized. Decoding was done by solving classification problems $y=f(X)$ with classes y (defined for Task 1 "CS": bins before CS onset, bins during CS; and for Task 2 "US": bins before CS, bins during US).

Three different types of computations were done: (1) Single-region decoding, (2) identification of similarity of neural activity patterns for single regions and (3) multi-region decoding. The computations were done using Jupyter Notebooks, Python 3 and the scikit-learn package[79]. 1s bin data was used for all of the above.

(1) Single-region decoding

The neural data matrix X was defined by "region": per treatment, region, sound, stage and day, all available neural data of the different mice were combined. The alignment was done

based on the classification goal y. Before the classification, the data was z-scored and balanced by undersampling. The Multi-layer Perceptron classifier was used. A 5-fold cross validation was performed, and the procedure was repeated 40 times. As criterion for decoder performance the average of the accuracy of all iterations was taken. The best single neurons in CE were defined as those reaching highest accuracy when X consisted of this single neuron only (see Supplementary Table 3 for all neurons). For region-wise decoding, neuron selection versions were applied according to maximum number of neurons available to allow meaningful comparisons between treatments and stages and are indicated in the respective figure legends. As a control, the classification procedure was applied to shuffled class vectors y per task.

(2) Similarity of neural activity patterns

To evaluate the similarity of the representation of conditioned and unconditioned stimuli within the neuronal activity over time, decoders trained on one stimulus were applied to another stimulus within the same stage. The combinations (i) lick on R-CS, (ii) shock on F-CS, (iii) R-CS on F-CS and F-CS on R-CS were performed. For each combination, a decoder was trained ten times on one stimulus and applied on the second one. The trained classifier was applied to shuffled target class vectors y as a control.

(3) Multi-region decoding

For the multi-region decoding neural data matrices X of "network" were defined: per stimulus and stage, where all available neuronal data were combined. As for the "region", the alignment was done based on the classification goal. Two different treatments were investigated: (i) Control: only data from control sessions (PBS), (ii) hM4($CE^{PKC\delta}$): only data from CNO sessions for regions aIC and pIC, $CE^{PKC\delta}$, CE^{SST} and CEm as in control. Prior the Random Forest classification, the data were z-scored and balanced by undersampling. A 5-fold cross validation was performed, and the procedure was repeated 40 times. Apart from the average classification accuracy of all iterations, the averaged feature performance of all single neurons per region was computed.

Transfer entropy

Transfer entropy $\boldsymbol{TE_{n_1-n_2}}$ between neurons n_1 and n_2 was computed using the Python package PyInform (https://github.com/ELIFE-ASU/PyInform), which is a wrapper of the inform library using Jupyter Notebooks and Python 3. Per treatment, sound and stage "network" (as for the multi-region decoding) were created with 1s bin data. Afterwards 500 neurons were drawn randomly from this matrix, taking into account the percentage distribution between the regions. The TE was computed locally and pairwise between all neurons. The local maximum per pair was taken. Additionally, only the upper 50% of all pairs per region combination were considered. TE between regions was defined by the average TE of neurons belonging to the regions as in[33]. Significance was tested similarly to Timme and Lapish[80]. The null hypothesis was that $\mathbf{n_2}$ does not depend on $\mathbf{n_1}$. 1000 surrogate datasets were created by shuffling the time-series and computing the region-wise TE. As p-value for significance testing ($\alpha<0.05$), the proportion of $TE_{surrogate}>=TE_{real}$ was taken.

$$\boldsymbol{TE_{k,v}\,(n_1 - n_2) = \langle TE_k\,(n_{1,i} - n_{2,j})\rangle_{i,j}}\ ,$$

Where *k* refers to past states and *i* and *j* label the sample subset of $R_{a,i}$ and $R_{b,j}$ of size *v* in each region.

Optogenetic manipulations

Mice were handled and habituated to attachment of the fiber-optic patch cord (Doric Lenses) to the fiber implants for several days prior experiment. For behavioral cohorts, activation of Channelrhodopsin-2 (ChR2) was achieved with a 473nm laser, delivering 10ms pulses at an intensity of 10mW at the fiber tip at a stimulation frequency of 20Hz for IC projections to CE. Neuronal inhibition was achieved by activation of Halorhodopsin or Archaerhodopsin using an 489nm laser at constant 7-8mW light intensity at the fiber tip. Intensity was adjusted before experiments with a power meter (Thorlabs, PM100D). The laser was triggered by a custom Matlab (v2014b) script during conditioning experiments for conditioned stimulus (CS) periods only. CE–NBM stimulation during *in vivo* electrophysiological recordings was performed with 5ms pulses from a 470nm LED (Doric Lenses).

Chemogenetic/pharmacological manipulations

Mice were handled and habituated to intraperitoneal PBS injections for 3 days. PBS, TZP (Sigma) and CNO (Sigma) injections were timed 30min prior experiment start and mice returned to their homecage after injection. Volume was adjusted to 0.1ml and a final dosage of 3mg/kg was used for TZP and 5mg/kg of CNO for all chemogenetic experiments other than RC sessions, for which the dosage was adjusted to 2.5mg/kg.

Brain slice preparation and electrophysiology

Three weeks prior to electrophysiological recordings, male WT mice received injections of AAV-ChR2 in the IC, whereas transgenic SST- and PKCδ::Cre mice injections of AAV-DIO-ChR2 in the CE. At the age of 2-3 month, mice were deeply anesthetized with isoflurane, decapitated and their brains quickly chilled in sucrose-based dissection buffer, bubbled with 95% O_2/5% CO_2 containing the following (in mM): 220 Sucrose, 26 $NaHCO_3$, 2.4 KCl, 10 $MgSO_4$, 0.5 $CaCl_2$, 3 Sodium Pyruvate, 5 Sodium Ascorbate and 10 glucose. Transverse coronal brain slices (300µm) were cut in dissection buffer using a Vibratome (Leica, VT1000S) and immediately incubated for 15 min recovery phase in oxygenated artificial cerebrospinal fluid (aCSF) 126 NaCl, 2.5 KCl, 1.25 NaH_2PO_4, 26 $NaHCO_3$, 2.5 $CaCl_2$, 2.5 $MgCl_2$, and 25 glucose in 95% O_2/5% CO_2 at 32°C. This was followed by a slice resting phase with oxygenated aCSF for at least 45 min at room temperature (RT).
Individual brain slices containing target regions (CE for IC injections, NBM for CE injections) were placed on the stage of an upright, infrared-differential interference contrast microscope (Olympus BX50WI) mounted on a X-Y table (Olympus) and visualized with a 40x water immersion objective by an infrared sensitive digital camera (Hamamatsu, ORCA-03). Slices were fully submerged and continuously perfused at a rate of 1-2 ml per min with oxygenated aCSF. Patch pipettes were pulled on a Flaming/Brown micropipette puller (Sutter, P-97) from borosilicate glass (1.5mm outer and 0.86mm inner diameter, Sutter) to final resistances ranging from 3 to 5MΩ. Internal solution for recording responses to optogenetic stimulation of PKC-δ/SST neuronal input to NBM contained (in mM): 135 KCl, 0.2 EGTA, 10 HEPES, 2 MgATP, 0.5 Na_2GTP, and 10 Na_2phosphocreatine 0.2% (w/w) Biocytin and for recording responses to optogenetic stimulation of IC neuronal input in CE (in mM): 135 K-Gluconate, 5 KCl, 10 HEPES, 2 $MgCl_2$, 0.2 EGTA, 1 Na_2ATP, 0.4 NaGTP, 10 Na_2Phosphocreatine, 0.2% (w/w) Biocytin, 280-290 mOsmol. Membrane currents were recorded with a Multiclamp 700B amplifier (Molecular Devices). Electrophysiological signals were low pass filtered at 3kHz, sampled at 10 kHz (Digidata 1440A, Axon Instruments) and further analyzed with pClamp 10 software (Molecular Devices).

Recordings started 5 minutes after letting the cell reestablish constant activity post break-in. Inputs from IC to CE or CE to NBM respectively, were stimulated in voltage-clamp (-70mV) with 20ms blue light pulses through a 40x electrophysiology microscope objective, driven by a 120W mercury lamp (X-Cite 120 PC Q). The amplitude of 4 pulses, 1 second apart, was averaged as postsynaptic responses of specific cell types in the CE or NBM. Cell identity was confirmed with the help of biocytin and post hoc immunohistochemistry.

Histological evaluation

For verification of injection targeting, implant placement and virus expression, mice were deeply anesthetized by an intraperitoneal injection of a mixture of Ketamine (10mg/ml, OGRIS Pharma) and Medetomidine (Domitor, ORION Pharma) in phosphate-buffered saline (PBS) and transcardially perfused with cold 10ml PBS and 30ml of 4% Paraformaldehyde (PFA). Brains were immediately removed and post-fixed overnight in 4% PFA at 4°C. 20µm cryo-sections were obtained from brains from all cohorts except animals subjected to electrophysiological recordings or Ca^{2+} imaging, for which 80µm thick vibratome sections were collected.

Immunohistochemistry

Sections were permeabilized with PBS-T (0.1% Triton X-100 in PBS or 0.2% for *ex vivo* electrophysiology sections) and subsequently blocked with 2% bovine serum albumin (BSA, in PBS-T) for 1h to attenuate unspecific binding. Slides were incubated overnight with primary antibodies (Methods Table 2) in BSA at 4°C. Then, slides were washed in PBS-T and incubated with fluorescently conjugated secondary antibodies (Invitrogen, Methods Table 2) in BSA for 2h at room temperature. After washing, slides were mounted with fluorescence mounting medium (Dako) and images acquired on a confocal microscope (Zeiss) and slide scanner (3DHistech).

Data analyses and statistical tests

All statistical tests were performed using Graph Pad Prism ® (version 7 & 8) or custom R code (for ANOVA>250 data points). Significant results are indicated on the graphs or tables and are described in the figure legends.

Data and code availability

All data and custom codes are available upon request.

Methods Table 1.

Viral vectors

Abbreviation	Construct	Manufacturer	Titer (GC/ml)
DIO-GFP	AAV5.EF1a.DIO.GFP.WPRE	IMP	9.73E+10
syn-GFP	AAV5.hsyn.eGFP.WPRE	Penn Vector Core	1.15E+13
syn-ChR2	AAV5.hsyn.hChR2(H134R).eYFP.WPRE	Penn Vector Core	1.87E+13
DIO-ChR2	AAV5.EF1a.DIO.hChR2(H134R).eYFP.WPRE	Penn Vector Core	1.30E+13
syn-Arch	AAV5.hsyn.ArchT.YFP.WPRE	Penn Vector Core	4.68E+12
DIO-Arch	AAV5. Ef1a.DIO.eArch.eYFP.WPRE	BI Biberach	6.00E+12
DIO-NpHR	AAV5.Ef1a.DIO.eNpHR3.0-eYFP.WPRE	Penn Vector Core	2.59E+12

GCaMP6m	AAV9.hsyn.GCaMP6m.WPRE	BI Biberach	1.00E+12
DIO-GCaMP6f	AAV1.hsyn.DIO.GCaMP6f.WPRE.	Penn Vector Core	1.00E+13
AAV::Cre	AAV5.CMV.Cre	Vector Biolabs	1.00E+12
CAV::Cre	CAV2.Cre	Montpellier Vector Platform	5.50E+12
DIO-hM4	AAV5.hsyn.DIO.hM4D.mCherry.WPRE	Penn Vector Core	1.01E+13

Methods Table 2.

Primary antibodies

Antigen	Species	Dilution	Catalog #	Lot #	Supplier
PKC-δ	Mouse	1:1000	610398	4080743	BD Biosciences
FOXO3/NeuN	Chicken	1:500	ab131624	GR88877-12	Abcam
ChAT	Goat	1:200	AB144P	2280814	Millipore

Secondary antibodies

Antigen	Species	Dilution	Catalog #	Lot #	Supplier
Mouse	Goat	1:1000	A21052	1712097	Life technologies
Chicken	Goat	1:1000	A11041	1383072	Life technologies
Goat	Donkey	1:500	A11057	819578	Abcam

Acknowledgments

We thank Manuel Pasieka from Bioinformatics and Scientific Computing, Vienna Biocenter (VBC) for development of software used in behavioral experiments video recording and custom Matlab code for behavioral and neuronal data analysis. We also thank Lydia Zopf and Peter Opriessnig from Preclinical Imaging, Vienna BioCenter Core Facilities (pcIMAG, VBCF) for fMRI data acquisition and analysis. We thank Tamara Engelmaier and Mihaela Zeba from Histopathology (VBCF) for tissue processing. Additionally, we want to acknowledge Thomas Lendl from BioOptics (IMP) for generating custom Java scripts for histological image analysis and Maria Novatchkova from BioInformatics (IMP) for statistical analysis. We thank Life Science Editors for editing assistance. This research was supported by the Research Institute of Molecular Pathology (IMP), Boehringer Ingelheim, the Austrian Research Promotion Agency (FFG), and a grant from the European Community's Seventh Framework Programme (FP/2007-2013) / ERC grant agreement no. 311701.

Author Contributions

DK and JK performed neuronal activity recordings, behavioral experiments and analyzed the data. FG did electrophysiological slice recordings. LP and SU analyzed neuronal activity data, JL performed fMRI experiments and data analysis. DK, JK and WH wrote the manuscript. KB and WH supervised the study.

Competing Interests Statement

The authors declare no competing interests**.**

References

1. Friston, K. A theory of cortical responses. *Philos. Trans. R. Soc. B Biol. Sci.* **360,** 815–836 (2005).
2. Schultz, W. & Dickinson, A. Neuronal Coding of Prediction Errors. *Annu. Rev. Neurosci.* (2000). doi:10.1146/annurev.neuro.23.1.473
3. Groessl, F. *et al.* Dorsal tegmental dopamine neurons gate associative learning of fear. *Nat. Neurosci.* **21,** 952–962 (2018).
4. LeDoux, J. E. Emotion circuits in the brain. *Annu. Rev. Neurosci.* **23,** 155–84 (2000).
5. Grewe, B. F. *et al.* Neural ensemble dynamics underlying a long-term associative memory. *Nature* **543,** 670–675 (2017).
6. Likhtik, E., Stujenske, J. M., A Topiwala, M., Harris, A. Z. & Gordon, J. A. Prefrontal entrainment of amygdala activity signals safety in learned fear and innate anxiety. *Nat. Neurosci.* **17,** 106–113 (2013).
7. Karalis, N. *et al.* 4-Hz oscillations synchronize prefrontal–amygdala circuits during fear behavior. *Nat. Neurosci.* **19,** 605–612 (2016).
8. Saez, R. A., Saez, A., Paton, J. J., Lau, B. & Salzman, C. D. Distinct Roles for the Amygdala and Orbitofrontal Cortex in Representing the Relative Amount of Expected Reward. *Neuron* **95,** 70–77 (2017).
9. Pendl, S. L. *et al.* Emergence of a hierarchical brain during infancy reflected by stepwise functional connectivity. *Hum. Brain Mapp.* **38,** 2666–2682 (2017).
10. Chanes, L. & Barrett, L. F. Redefining the Role of Limbic Areas in Cortical Processing. *Trends Cogn. Sci.* **20,** 96–106 (2016).
11. Pezzulo, G., Rigoli, F. & Friston, K. J. Hierarchical Active Inference: A Theory of Motivated Control. *Trends in Cognitive Sciences* (2018). doi:10.1016/j.tics.2018.01.009
12. Hong, S. J. *et al.* Atypical functional connectome hierarchy in autism. *Nat. Commun.* (2019). doi:10.1038/s41467-019-08944-1
13. Turner, R. S. & Desmurget, M. Basal ganglia contributions to motor control: A vigorous tutor. *Current Opinion in Neurobiology* (2010). doi:10.1016/j.conb.2010.08.022
14. Shipp, S., Adams, R. A. & Friston, K. J. Reflections on agranular architecture: Predictive coding in the motor cortex. *Trends Neurosci.* **36,** 706–716 (2013).
15. Barrett, L. F. & Simmons, W. K. Interoceptive predictions in the brain. *Nat. Rev. Neurosci.* **16,** 419–429 (2015).
16. Critchley, H. D., Wiens, S., Rotshtein, P., Öhman, A. & Dolan, R. J. Neural systems supporting interoceptive awareness. *Nat. Neurosci.* **7,** 189–195 (2004).
17. Craig, A. D. How do you feel? Interoception: the sense of the physiological condition of the body. *Nat. Rev. Neurosci.* **3,** 655–666 (2015).
18. Segerdahl, A. R., Mezue, M., Okell, T. W., Farrar, J. T. & Tracey, I. The dorsal posterior insula subserves a fundamental role in human pain. *Nat. Neurosci.* **18,** 499–500 (2015).
19. Avery, J. A. *et al.* Convergent gustatory and viscerosensory processing in the human dorsal mid-insula. *Hum. Brain Mapp.* **38,** 2150–2164 (2017).
20. Bechara, A. & Damasio, A. R. The somatic marker hypothesis: A neural theory of economic decision. *Games Econ. Behav.* **52,** 336–372 (2005).
21. Gorka, A. X., Torrisi, S., Shackman, A. J., Grillon, C. & Ernst, M. Intrinsic functional connectivity of the central nucleus of the amygdala and bed nucleus of the stria terminalis. *Neuroimage* (2018). doi:10.1016/j.neuroimage.2017.03.007
22. Schultz, D. H., Balderston, N. L. & Helmstetter, F. J. Resting-state connectivity of the amygdala is altered following Pavlovian fear conditioning. *Front. Hum. Neurosci.* (2012). doi:10.3389/fnhum.2012.00242
23. Goosens, K. A. & Maren, S. Contextual and auditory fear conditioning are mediated by the lateral, basal, and central amygdaloid nuclei in rats. *Learn. Mem.* **8,** 148–155 (2001).
24. Haubensak, W. *et al.* Genetic dissection of an amygdala microcircuit that gates conditioned fear. *Nature* **468,** 270–276 (2010).
25. Li, H. *et al.* Experience-dependent modification of a central amygdala fear circuit. *Nat. Neurosci.* (2013). doi:10.1038/nn.3322
26. Badre, D. & D'Esposito, M. FMRI evidence for a hierarchical organization of the prefrontal cortex. *J. Cogn. Neurosci.* **19,** 1–18 (2007).
27. Bahlmann, J., Blumenfeld, R. S. & D'Esposito, M. The Rostro-Caudal Axis of Frontal Cortex is Sensitive to the Domain of Stimulus Information. *Cereb. Cortex* **25,** 1815–1826 (2015).
28. Koechlin, E. & Jubault, T. Broca's Area and the Hierarchical Organization of Human Behavior. *Neuron* **50,** 963–974 (2006).
29. Geuter, S., Boll, S., Eippert, F. & Büchel, C. Functional dissociation of stimulus intensity encoding and

predictive coding of pain in the insula. *Elife* **6,** 1–22 (2017).
30. Kim, J., Zhang, X., Muralidhar, S., LeBlanc, S. A. & Tonegawa, S. Basolateral to Central Amygdala Neural Circuits for Appetitive Behaviors. *Neuron* **93,** 1464–1479.e5 (2017).
31. Fadok, J. P., Markovic, M., Tovote, P. & Lüthi, A. New perspectives on central amygdala function. *Curr. Opin. Neurobiol.* **49,** 141–147 (2018).
32. Magrans, I., Abril, D., Yoshimoto, J. & Doya, K. Connectivity inference from neural recording data : Challenges , mathematical bases and research directions. *Neural Networks* **102,** 120–137 (2018).
33. Lizier, J. T., Heinzle, J., Horstmann, A., Haynes, J. D. & Prokopenko, M. Multivariate information-theoretic measures reveal directed information structure and task relevant changes in fMRI connectivity. *J. Comput. Neurosci.* (2011). doi:10.1007/s10827-010-0271-2
34. Chatham, C. H., Frank, M. J. & Badre, D. Corticostriatal output gating during selection from working memory. *Neuron* **81,** 930–942 (2014).
35. Kapp, B. S., Supple, W. F. & Whalen, P. J. Effects of electrical stimulation of the amygdaloid central nucleus on neocortical arousal in the rabbit. *Behav. Neurosci.* **108,** 81–93 (1994).
36. Gozzi, A. *et al.* A neural switch for active and passive fear. *Neuron* **67,** 656–666 (2010).
37. Zaborszky, L. *et al.* Neurons in the basal forebrain project to the cortex in a complex topographic organization that reflects corticocortical connectivity patterns: An experimental study based on retrograde tracing and 3D reconstruction. *Cereb. Cortex* **25,** 118–137 (2015).
38. Cassell, M. D., Freedman, L. J. & Shi, C. The intrinsic organization of the central extended amygdala. *Ann. N. Y. Acad. Sci.* **877,** 217–241 (1999).
39. Nagel, G. *et al.* Channelrhodopsin-2, a directly light-gated cation-selective membrane channel. *Proc. Natl. Acad. Sci.* **100,** 13940–13945 (2003).
40. Gehrlach, D. A. *et al.* Aversive state processing in the posterior insular cortex. *Nat. Neurosci.* (2019). doi:10.1038/s41593-019-0469-1
41. Venniro, M. *et al.* The Anterior Insular Cortex→Central Amygdala Glutamatergic Pathway Is Critical to Relapse after Contingency Management. *Neuron* **96,** 414–427.e8 (2017).
42. Almashaikhi, T. *et al.* Intrainsular functional connectivity in human. *Hum. Brain Mapp.* **35,** 2779–2788 (2014).
43. Kok, P., Failing, M. F. & de Lange, F. P. Prior expectations evoke stimulus templates in the primary visual cortex. *J. Cogn. Neurosci.* (2014). doi:10.1162/jocn_a_00562
44. Fries, P. Rhythms for Cognition: Communication through Coherence. *Neuron* **88,** 220–235 (2015).
45. Schiff, H. C. *et al.* An Insula–Central Amygdala Circuit for Guiding Tastant-Reinforced Choice Behavior. *J. Neurosci.* (2018). doi:10.1523/JNEUROSCI.1773-17.2017
46. Livneh, Y. *et al.* Homeostatic circuits selectively gate food cue responses in insular cortex. *Nature* **546,** 611–616 (2017).
47. Holland, P. C. & Gallagher, M. Different roles for amygdala central nucleus and substantia innominata in the surprise-induced enhancement of learning. *J. Neurosci.* **26,** 3791–3797 (2006).
48. Han, J. S., Holland, P. C. & Gallagher, M. Disconnection of the amygdala central nucleus and substantia innominata/nucleus basalis disrupts increments in conditioned stimulus processing in rats. *Behav. Neurosci.* **113,** 143–151 (1999).
49. Pearce, J. M. & Hall, G. A model for Pavlovian learning: Variations in the effectiveness of conditioned but not of unconditioned stimuli. *Psychol. Rev.* (1980). doi:10.1037/0033-295X.87.6.532
50. Feldman, H. & Friston, K. J. Attention , uncertainty , and free-energy. **4,** 1–23 (2010).
51. Frank, M. J. & Badre, D. Mechanisms of hierarchical reinforcement learning in corticostriatal circuits 1: Computational analysis. *Cereb. Cortex* **22,** 509–526 (2012).
52. Roopun, A. K. *et al.* Cholinergic neuromodulation controls directed temporal communication in neocortex in vitro. **4,** (2010).
53. Caras, M. L. & Sanes, D. H. Top-down modulation of sensory cortex gates perceptual learning. *Proc. Natl. Acad. Sci.* **114,** 9972–9977 (2017).
54. Doya, K. Metalearning and neuromodulation. *Neural Networks* **15,** 495–506 (2002).
55. Yu, A. J. & Dayan, P. Uncertainty, neuromodulation, and attention. *Neuron* **46,** 681–92 (2005).
56. Hangya, B., Ranade, S. P., Lorenc, M. & Kepecs, A. Central Cholinergic Neurons Are Rapidly Recruited by Reinforcement Feedback. *Cell* **162,** 1155–1168 (2015).
57. Martinez-Rubio, C., Paulk, A. C., McDonald, E. J., Widge, A. S. & Eskandar, E. N. Multimodal Encoding of Novelty, Reward, and Learning in the Primate Nucleus Basalis of Meynert. *J. Neurosci.* **38,** 1942–1958 (2018).
58. Iglesias, S. *et al.* Hierarchical Prediction Errors in Midbrain and Basal Forebrain during Sensory Learning. *Neuron* **80,** 519–530 (2013).
59. Lawson, R. P., Rees, G. & Friston, K. J. An aberrant precision account of autism. *Front. Hum. Neurosci.* **8,** 1–10 (2014).

60. Friston, K., Brown, H. R., Siemerkus, J. & Stephan, K. E. The dysconnection hypothesis (2016). *Schizophr. Res.* **176,** 83–94 (2016).
61. Lawson, R. P., Mathys, C. & Rees, G. Adults with autism overestimate the volatility of the sensory environment. *Nat. Neurosci.* **20,** 1293–1299 (2017).
62. Happé, F. & Frith, U. The weak coherence account: Detail-focused cognitive style in autism spectrum disorders. *J. Autism Dev. Disord.* **36,** 5–25 (2006).
63. Koshino, H. *et al.* Functional connectivity in an fMRI working memory task in high-functioning autism. *Neuroimage* **24,** 810–821 (2005).
64. Vasa, R. A., Kreiser, N. L., Keefer, A., Singh, V. & Mostofsky, S. H. Relationships between autism spectrum disorder and intolerance of uncertainty. *Autism Res.* **11,** 636–644 (2018).
65. Simonoff, E. *et al.* Psychiatric disorders in children with autism spectrum disorders: prevalence, comorbidity, and associated factors in a population-derived sample. *J. Am. Acad. Child Adolesc. Psychiatry* (2008). doi:10.1097/CHI.0b013e318179964f

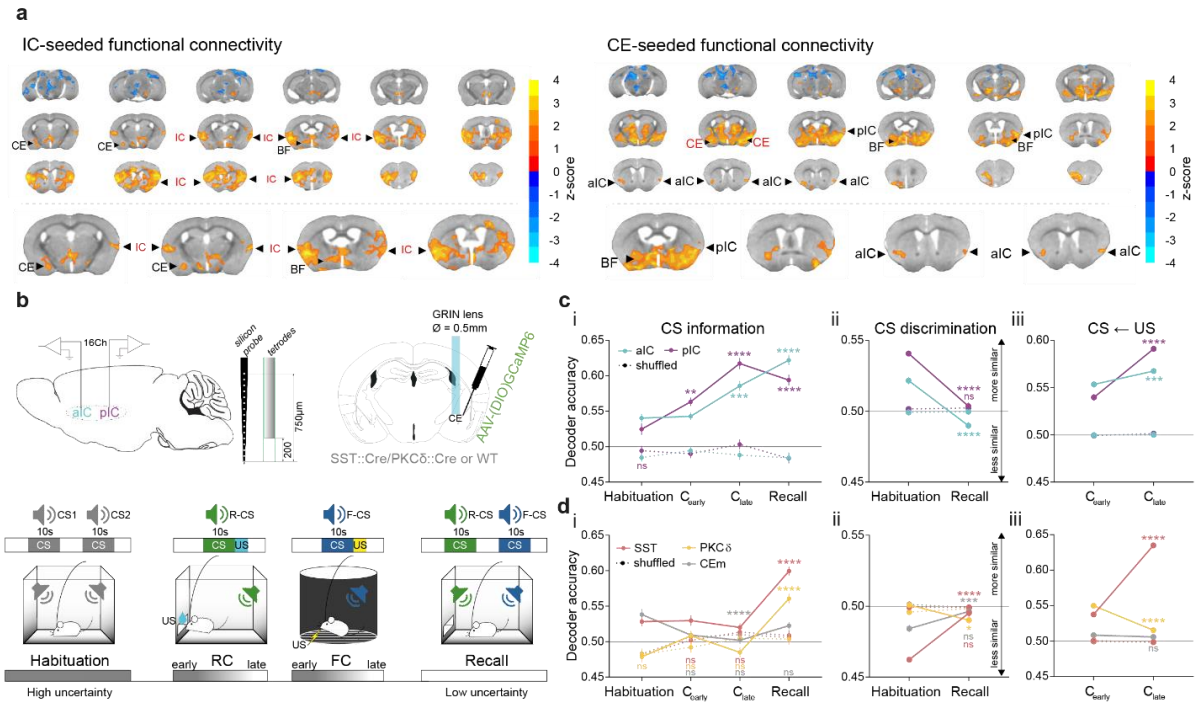

Fig. 1 | A coupled IC–CE network builds a model of task parameters. a, Seed-based functional connectivity of bilateral IC (left) showed coupling to central amygdala (CE) and basal forebrain (BF). A seed in the CE (right) showed coupling to interoceptive IC (anterior and posterior IC, aIC and pIC) and BF (radiological view, see Methods). Significant z-scored correlations to seed nodes are displayed in orange (positive) and blue (negative). **b**, Schematic depiction of experimental recordings, where mice were chronically implanted with single-site silicon or multi-site tetrode probes in aIC and pIC (top, left); SST::Cre, PKCδ::Cre, or wild-type mice were chronically implanted with a GRIN lens above CE in animals injected with AAVs carrying GCaMP6 (top, right). Experimental timeline of the 4-stage discriminatory PL paradigm (bottom). **c**, (i) Decoder accuracy (Da) of a multi-layer perceptron classifier (MLP) trained to detect CS information in activity of 200 random draws of 40 neurons per IC subregions for each CS (CS average is shown). * indicate significant differences to the respective habituation stage. (ii) CS-averaged Da of a MLP trained on activity of the 40 neurons (see section 'Single-region decoding' in Methods) to detect R(F)-CS applied on F(R)-CS in the habituation and recall stage. * indicate significant differences to the habituation stage. (iii) Averaged Da of a MLP trained on activity of random 40 neurons to detect R-US or F-US applied on R-CS or F-CS in the early (C_{early}) and late (C_{late}) phase of conditioning. * indicate significant differences to C_{early} stage. **d**, (i) Da of a MLP trained to detect CS information in activity of 200 draws of random 30 neurons per CE^{SST} and $CE^{PKC\delta}$ (and 7 neurons for CEm) and stage upon CS presentation (CS average is shown). * indicate significance as in c. (ii) CS-averaged Da of a MLP trained on activity of random 30 neurons of CE^{SST} and $CE^{PKC\delta}$ and 7 of CEm to detect R(F)-CS applied on F(R)-CS at habituation and recall. (iii) CS-averaged Da of an MLP trained on activity random 30 neurons of CE^{SST} and $CE^{PKC\delta}$ and 10 from CEm to detect R-US or F-US applied on R-CS or F-CS in the C_{early} and C_{late}. Holm-Sidak post hoc for all analyses, ****p<0.0001. All data presented as mean±SEM. Full statistical report in Supplementary Table 1.

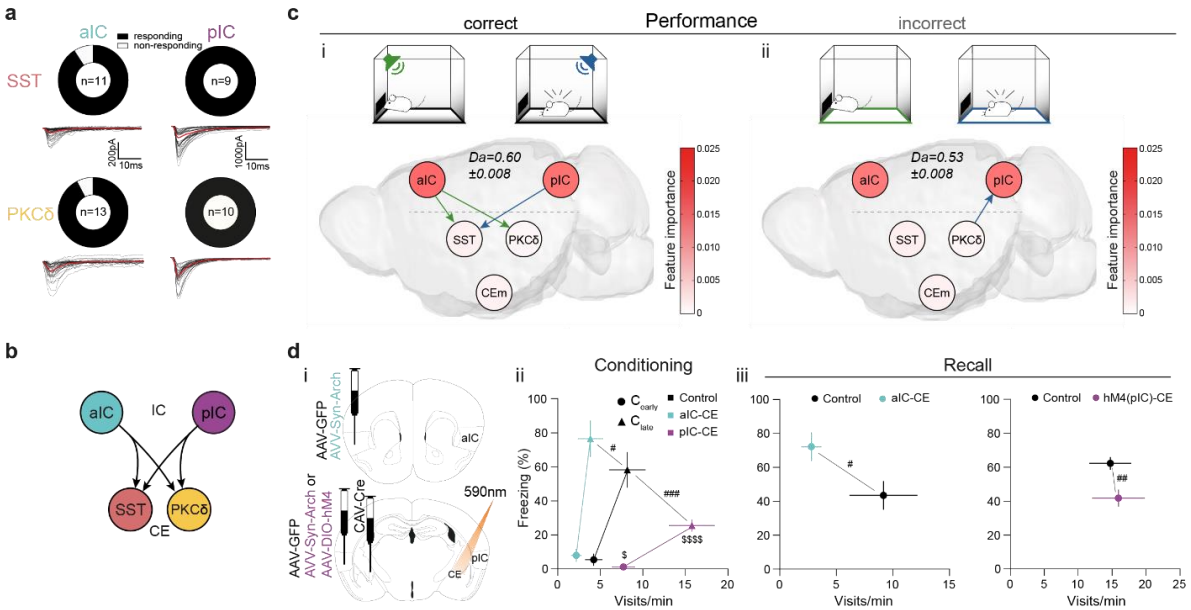

Fig. 2 | Top-down interoceptive models facilitate stimulus-behavior associations. a, Fraction of SST$^+$ and PKCδ$^+$ neurons in CE responding with IPSCs upon optogenetic stimulation of aIC or pIC input. **b**, Scheme for IC inputs to CE populations. **c**, Performance dependent transfer entropy (TE) between IC and CE nodes for (i) correct (port visits during R-CS and freezing episodes during F-CS) and (ii) incorrect (port visits or freezing outside of corresponding CS) behavioral episodes (±2s of bin containing behavioral episode onset). Nodes are colored according to the feature importance (FI) from a RF classifier (see Supplementary Fig. 6i). **d**, (i) Experimental approach to functionally dissect aIC and pIC inputs to CE during a PL task. (ii) Behavioral performance of optogenetic experimental groups in C_{early} and C_{late}. (iii) Behavioral performance of the optogenetic (left) and chemogenetic (hM4(pIC)–CE, right) IC–CE treatment cohorts during manipulation-free recall. Data shown as mean±SEM. n_{GFP}=9/12 $n_{aIC–CE}$=7, $n_{pIC–CE}$=9/8. Holm post hoc as difference to control as #, between manipulation groups as $. #/$p<0.05, ##/$$p<0.01, ###p<0.001, $$$$p<0.0001. Full statistical report in Supplementary Table 1.

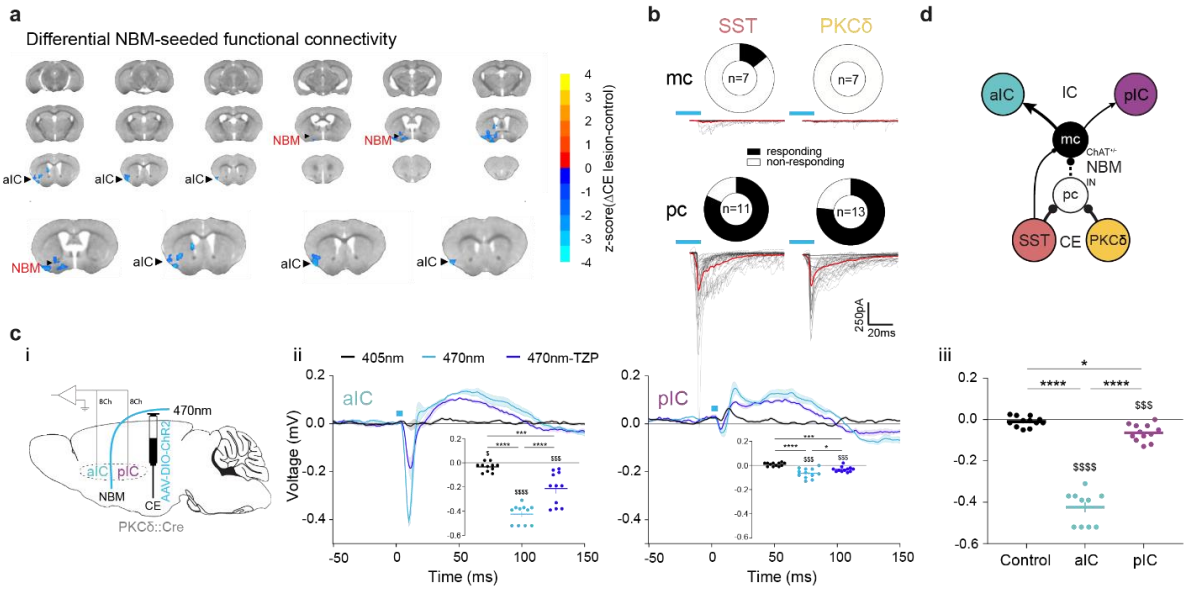

Fig. 3 | Basal forebrain NBM mediates bottom-up recruitment of IC activity. a, Chronic NMDA-lesion of CE reduced NBM RS functional connectivity with right aIC compared to sham-lesioned control group. Two-sample t-test between control (n=4) and CE-lesion (n=3) groups, followed by Gaussian Random Field Theory Multiple Comparison Correction (voxel-level p-value=0.05, cluster-level p-value=0.05). Differential z-score of CE lesion and control groups indicates depleted correlation (blue). **b**, Fraction of mc/pc neurons in NBM responding with IPSCs upon optogenetic stimulation of CE^{SST} or $CE^{PKC\delta}$ input. **c**, (i) *In vivo* optogenetic stimulation of the right CE–NBM pathway in two IC multi-site recorded, freely moving animals. (ii) Peri-laser stimulus time histograms of aIC (left) and pIC (right) channel-averaged LFP traces averaged over 60 (405, 470nm) and 40 (470nm-TZP) laser pulses for each channel. Traces represent averages of all available channels in aIC (11Ch) and pIC (12Ch). Insets depict respective minima of LFP traces within 20ms after laser pulse onset. (iii) Quantification of IC LFP minima upon CE–NBM stimulation under control conditions. All data presented as mean±SEM. Holm-Sidak post hoc analysis was used for comparison between treatments/regions and one-sampled t-test for individual differences to zero */$p<0.05, ***/$$$p<0.001, ****/$$$$p<0.0001. Full statistical report in Supplementary Table 1. **d**, Circuit model of the IC↔CE/NBM pathway consistent with experimental data. Dotted line represents connection not assessed, but consistent with previous studies.

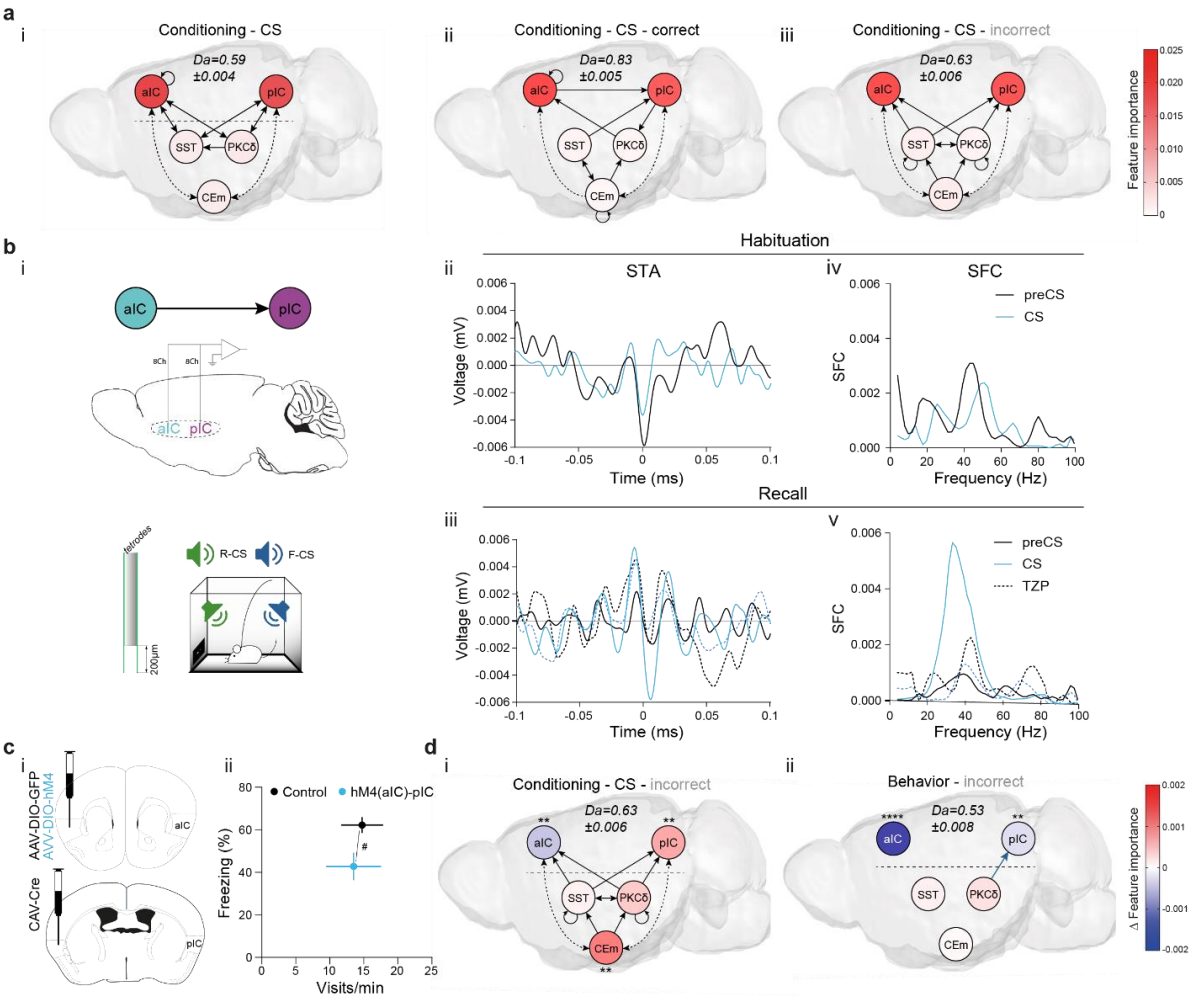

Fig. 4 | Learning establishes an intra-cortical hierarchy and task model. a, (i) Network depicting significant TE during CSs generated from data acquired from RC and FC. TE networks generated from CSs during which correct (ii) and incorrect/no (iii) behavior occurred during CS trials. Nodes are colored according to the FI from RF classification. **b**, (i) Scheme of recordings from multi-site implanted animals in aIC and pIC, examined for interregional interactions at the habituation and recall stage. STA from the (ii) habituation and (iii) recall stage of 200ms pIC LFP traces centered around the occurrence of 2388 preCS/ 2526 CS (habituation) and 7132 preCS/ 6920 CS (recall) aIC spikes. pIC LFP power-normalized SFC of STAs for habituation (iv) and (v) recall. **c**, (i) Experimental strategy to chemogenetically inhibit the aIC–pIC pathway. (ii) Quantification of behavioral performance in reward and fear domains at recall. $n_{Controls=}12$, $n_{M4(aIC)\text{-}pIC=}9$. Data shown as mean±SEM. Holm post hoc as difference to control, #p<0.05. Full statistical report in Supplementary Table 1. **d**, (i) TE network of incorrect CS (from aiii) with node color illustrating contrast FI between incorrect and correct CS. * depict significantly different FI (Supplementary Fig. 6aii). (ii) TE network (Fig. 2cii) with node color illustrating contrast FI between incorrect and correct behavioral episodes. * depict significantly different FI (Supplementary Fig. 6ai).

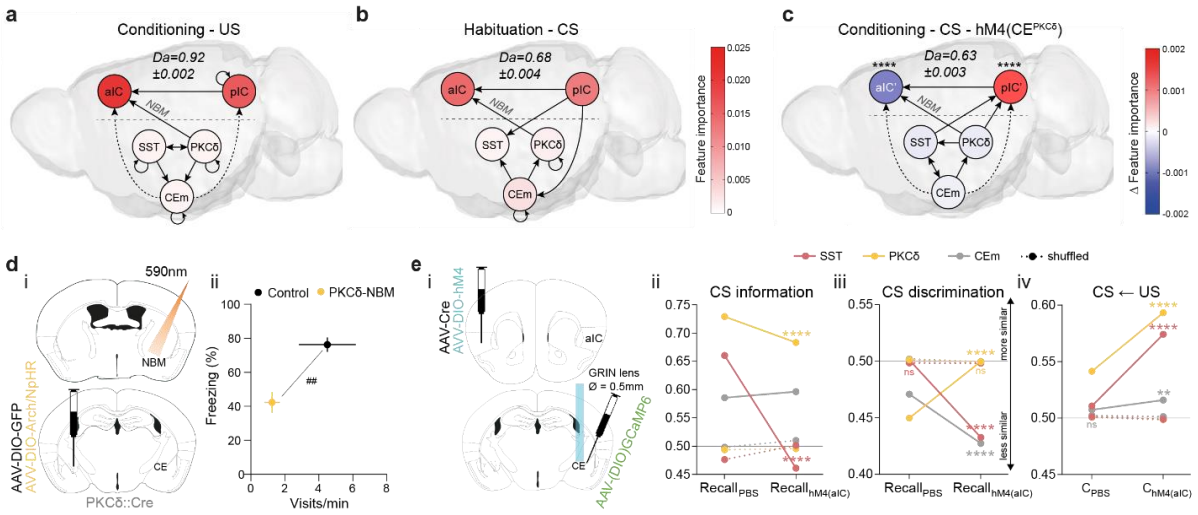

Fig. 5 | The CE–NBM pathway promotes interoceptive top-down models for PL. a, Network depicting significant TE after USs generated from data acquired from RC and FC. Nodes are colored according to the FI ('Control' in Supplementary Fig. 6aiv). **b**, TE network of CSs in the habituation stage. FI as above, ('Control' in Supplementary Fig. 6av). **c**, Network depicting significant TE during CSs generated from data acquired during RC and FC, however aIC/pIC data replaced by a dataset recorded during chemogenetic inhibition of $CE^{PKC\delta}$ in the same animals (aIC', pIC'). FI given as differential to control conditions in Fig. 4ai with * indicating significant differences (Supplementary Fig. 6aiii,vi). **d**, (i) Experimental approach for optogenetic inhibition of the $CE^{PKC\delta}$-NBM pathway during CS presentations at conditioning. (ii) Quantification of approach and avoidance behavior at recall. n_{GFP}=7, $n_{CE\text{-}PKC\delta\text{–}NBM}$=6. Data presented as mean±SEM. Holm post hoc as difference to control, ##p<0.01. **e**, (i) Scheme for chemogenetic inhibition of aIC during CE population recordings. (ii) CS-averaged Da of a MLP trained to detect CS information in activity of 200 random draws of 20 neurons CE^{SST}, 30 $CE^{PKC\delta}$ and 10 CEm neurons per treatment to detect CS information at recall during control conditions (PBS) and chemogenetic inhibition of aIC (hM4(aIC)). (iii) CS-averaged Da of a MLP trained on activity of 20 CE^{SST}, 30 $CE^{PKC\delta}$ and 10 CEm neurons per treatment to detect R(F)-CS applied on F(R)-CS at recall during control conditions (PBS) and chemogenetic inhibition of aIC (hM4(aIC)). (iv) CS-averaged Da of an MLP trained on activity of 200 random draws of 20 CE^{SST}, 30 $CE^{PKC\delta}$ and 10 CEm neurons to detect R-US or F-US applied on R-CS or F-CS in the conditioning stage during control conditions (PBS) and chemogenetic inhibition of aIC (hM4(aIC)).* indicate significant differences between treatments within population, determined by Holm-Sidak post hoc analysis, ****<p0.0001. Only non-significant differences to shuffled data within population and treatment are indicated by 'ns', otherwise omitted. Full statistical report in Supplementary Table 1.

Supplementary Notes

Impact of US responsiveness on learning and task performance

The quality of a task model should impact task performance. Since performance at recall varied within IC/CE groups (Supplementary Fig. 7c/h), we segregated neurons of respective mice into 'performers' and 'non-performers' using a median split on behavioral performance at recall. For IC subregions we found a striking difference in US response magnitude between the two groups, where non-performers population response to R-US in aIC and tonic response to F-US in pIC were largely absent. These data indicate that successful US encoding in IC determines behavioral performance (Supplementary Fig. 7di,iv). This pattern transferred to the CS, where aIC showed population responses to R-CS, whereas pIC showed responses to F-CS at recall (Supplementary Fig. 7ei,iv). Similarly, a median split based on behavioral performance at recall for the CE recording cohort (Supplementary Fig. 7h) revealed significant differences in US response magnitude in the PKCδ^+ population for the fear domain and a trend for the reward domain upon reward delivery (Supplementary Fig. 7v,vi). This suggests that PKCδ^+ neurons may signal necessity to learn, while their level of engagement may determine success.

IC-CE circuit architecture

To address whether IC-CE TE for stimulus-behavior association (Fig. 2c) may emerge from an underlying neural network architecture, we performed retrograde anatomical tracing with fluorescently labelled CTB. We injected CTB into the CE and quantified CTB$^+$ neurons in IC relative to DAPI of the entire IC area and the respective projection field. We found that CE-projecting neurons are more abundant in pIC than aIC relative to its size or projection area (Supplementary Fig. 5ai). TE for stimulus-behavior association could suggest a biased innervation of CE subpopulations by IC subregions. We examined whether TE maps are reflected in the circuit architecture by assaying synaptic connectivity using slice electrophysiology combined with optogenetics. PKCδ::Cre mice received injection of AAVs carrying Cre-dependent GFP into CE to allow for direct identification of SST (approximated by absence of GFP expression) and PKCδ^+ neurons and syn-ChR2 into aIC or pIC for pan-neuronal expression (Supplementary Fig. 5aii). Optogenetic excitation of a/pIC input to CE revealed monosynaptic connections between IC and CEl neurons. Interestingly, we found no difference in synaptic innervation of CEl populations (Fig. 2a, 92% of PKCδ^+ vs 91% of SST for aIC/ 100% of PKCδ^+/SST$^+$ for pIC). These data support an overall functional rostro-

caudal organization of the IC-CE network, reflecting differential US tuning in IC subregions (Supplementary Fig. 7a). Based on these data, we propose that functional differences in subnetworks (Fig. 2c) emerge from distributed ensembles rather than from a pre-determined circuit architecture.

CE–NBM circuit architecture

We assessed the anatomical connectivity between CE and NBM by injecting the retrograde tracer cholera toxin-B (CTB) into the NBM, which showed robust back-labeling in CE. Double-staining for PKCδ revealed this projection is dominated by the PKCδ$^+$ population (~10% of CTB$^+$/DAPI are PKCδ$^+$ vs. ~5% are PKCδ$^-$) (Supplementary Fig. 9a). Backlabeling to CEm was previously reported to be sparse or absent[81].

Since the vast majority of CE neurons are GABAergic[82], we suspected a disinhibitory mechanism to gate (cholinergic) output neurons in the NBM. To examine cell type-specific innervation of NBM by CE, we performed slice electrophysiology combined with optogenetic stimulation of CE fibers in NBM (Supplementary Fig. 9bi). AAV carrying Cre-dependent Channelrhodopsin-2 (DIO-ChR2) was injected into the CE of PKCδ::Cre and SST::Cre mice, and slices containing NBM were obtained after 3 weeks. Patch-clamp was guided by cell morphology, as corticopetal neurons are magnocellular (mc) versus parvocellular (pc) interneurons (IN)[83]. To identify cholinergic cells, neurons were filled with biocytin for labelling with fluorescently tagged streptavidin and stained for choline acetyltransferase (ChAT) post hoc (Supplementary Fig. 9bii). 33% (2/6) of recovered mc neurons were identified as ChAT$^+$ neurons, but no pc neurons stained for ChAT (0/14). Optogenetic stimulation of input from SST$^+$ and PKCδ$^+$ neurons induced inhibitory postsynaptic responses in 82% (9/11 neurons) and 77% (10/13) of ChAT$^-$ IN, respectively. We found 14% (1/7) of mc neurons responsive to CE^{SST} but none to CE^{PKCδ} input (0/7; Fig. 3b), consistent with previous reports showing that CE axons largely avoid ChAT$^+$ neurons[81].

Supplementary Figures

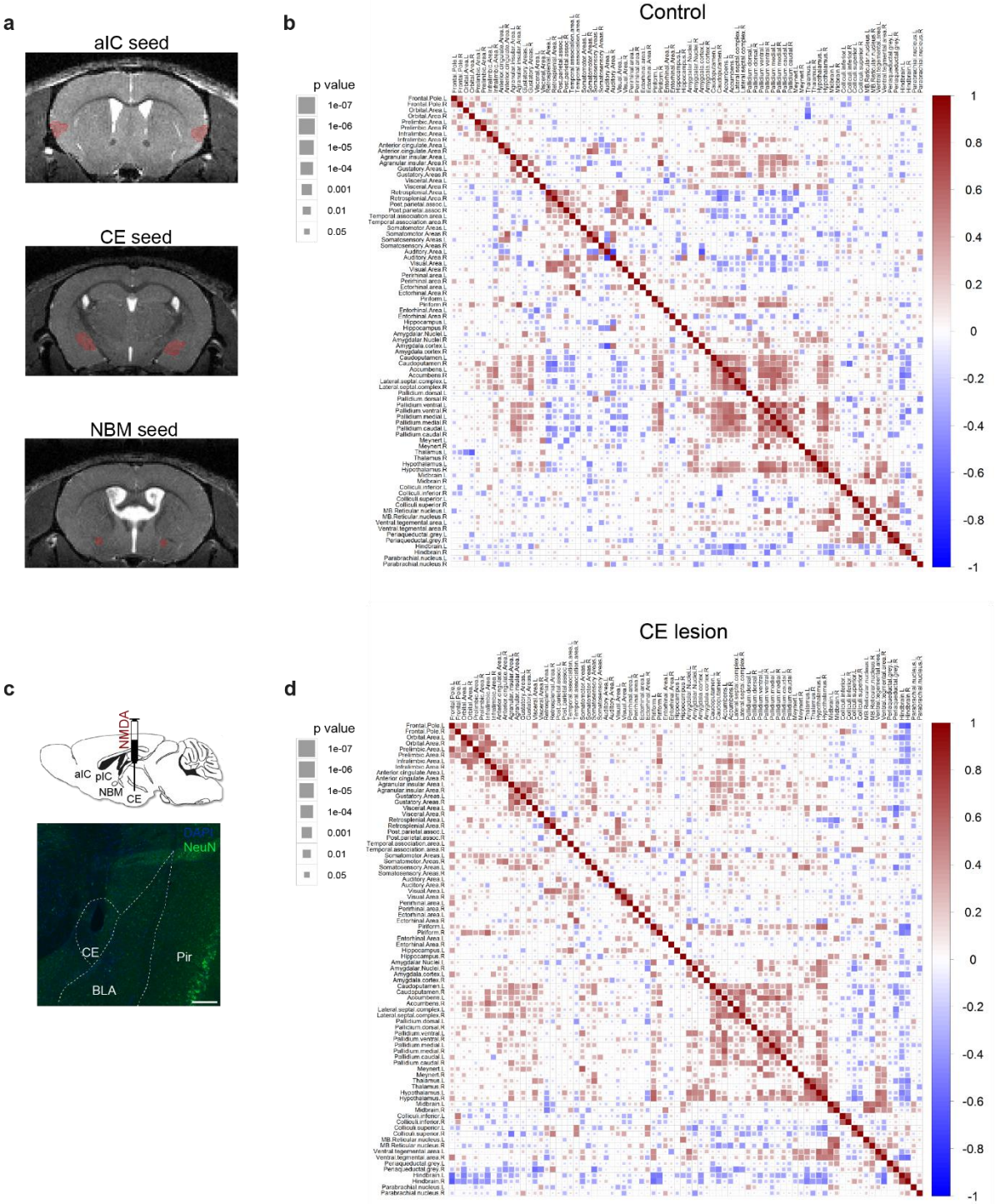

Supplementary Figure 1 | ROI-based functional connectivity of control and CE lesion groups. a, Seed regions masks used for functional connectivity. aIC – anterior insular cortex, CE – central nucleus of amygdala, NBM – Nucleus Basalis of Meynert. **b**, Functional connectivity in the control group with significant (one sample t-test, $p<0.05$) Fisher z-transformed Pearson correlation coefficient between each pair of brain regions (blue-to-red scale) are shown (significance of correlations reflected by the square size). **c**, Mice received injection of NMDA (N-methyl-D-aspartate, lesion group, n=3) or saline (control group, n=4, Fig. 1a) into CE (*top*). Exemplary staining with NeuN in mouse from the lesion group. scalebar=100µm. BLA – basolateral amygdala, Pir – piriform cortex. (*bottom*). **d**, Functional connectivity in the CE lesion group with significant (one sample t-test, $p<0.05$) Fisher z-transformed Pearson correlation coefficient between each pair of brain regions (blue-to-red scale) are shown (significance of correlations reflected by the square size).

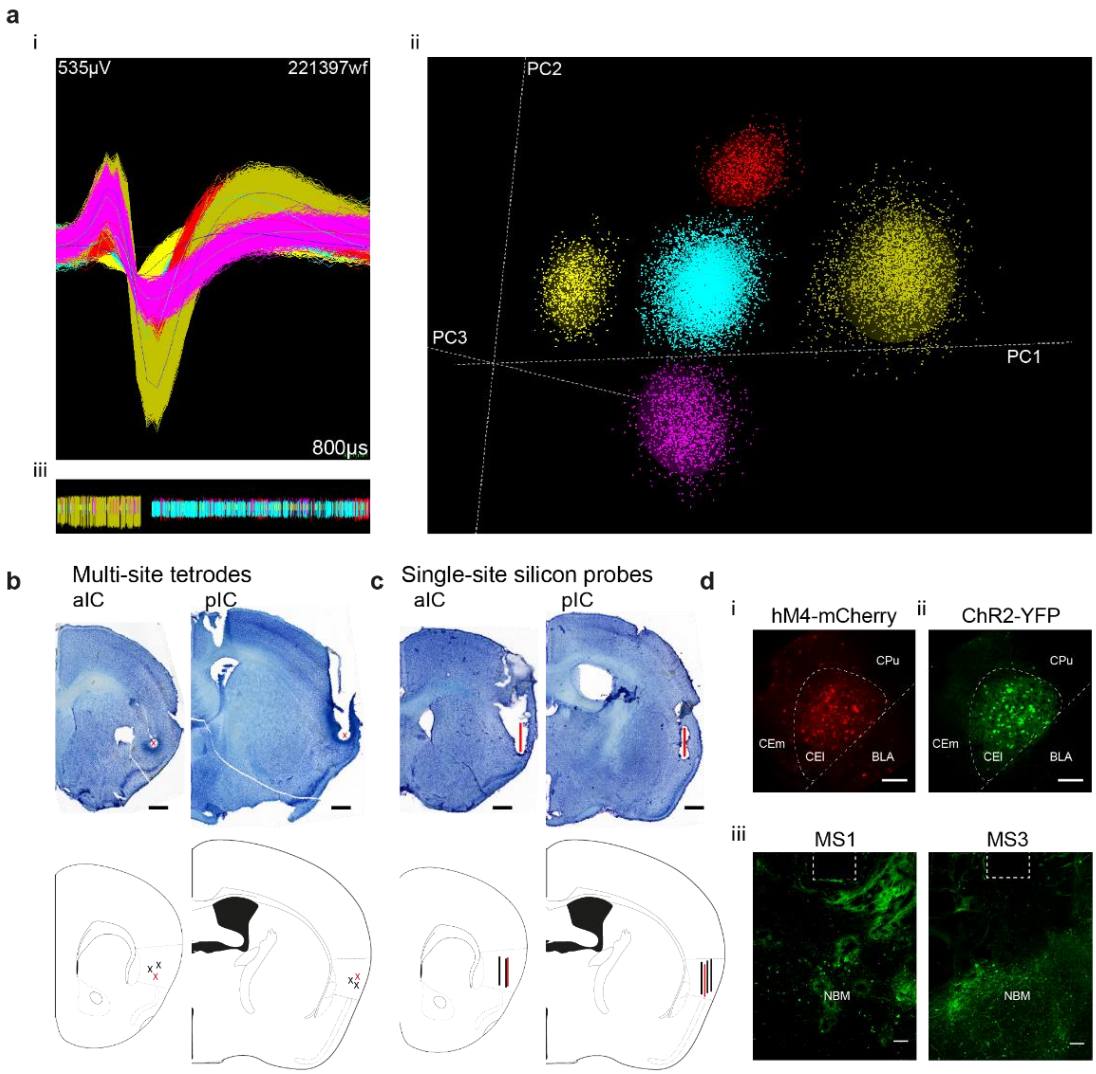

Supplementary Figure 2 | Raw data and histological assessment of IC recordings. a, Example waveforms of 5 single units (i) and their corresponding representation in PC space (ii) from 2 recording sessions on separate days (iii). **b,** Nissl staining on an animal implanted with multi-site tetrodes in aIC (*top, left*) and pIC (*top, right*) and corresponding summary schema of all multi-site implantation sites (*bottom*). Red 'X's indicate electrolytic lesion sites between staining and schema. Scalebar=500µm. **c,** Nissl staining on animals implanted with single-site 16Channel silicon probes in aIC (*top, left*) and pIC (*top, right*) and corresponding summary schema of all single-site implantation sites (*bottom*). Red lines indicate the same electrolytic lesion sites between staining and schema. Scalebar=500µm. **d**, Viral expression of Cre-dependent hM4-mCherry (i) and ChR2-YFP (ii) in the CE and corresponding projection field with optic fiber (400µm) position in NBM (iii) in a multi-site recorded PKCδ::Cre animal. Scalebar =100µm.

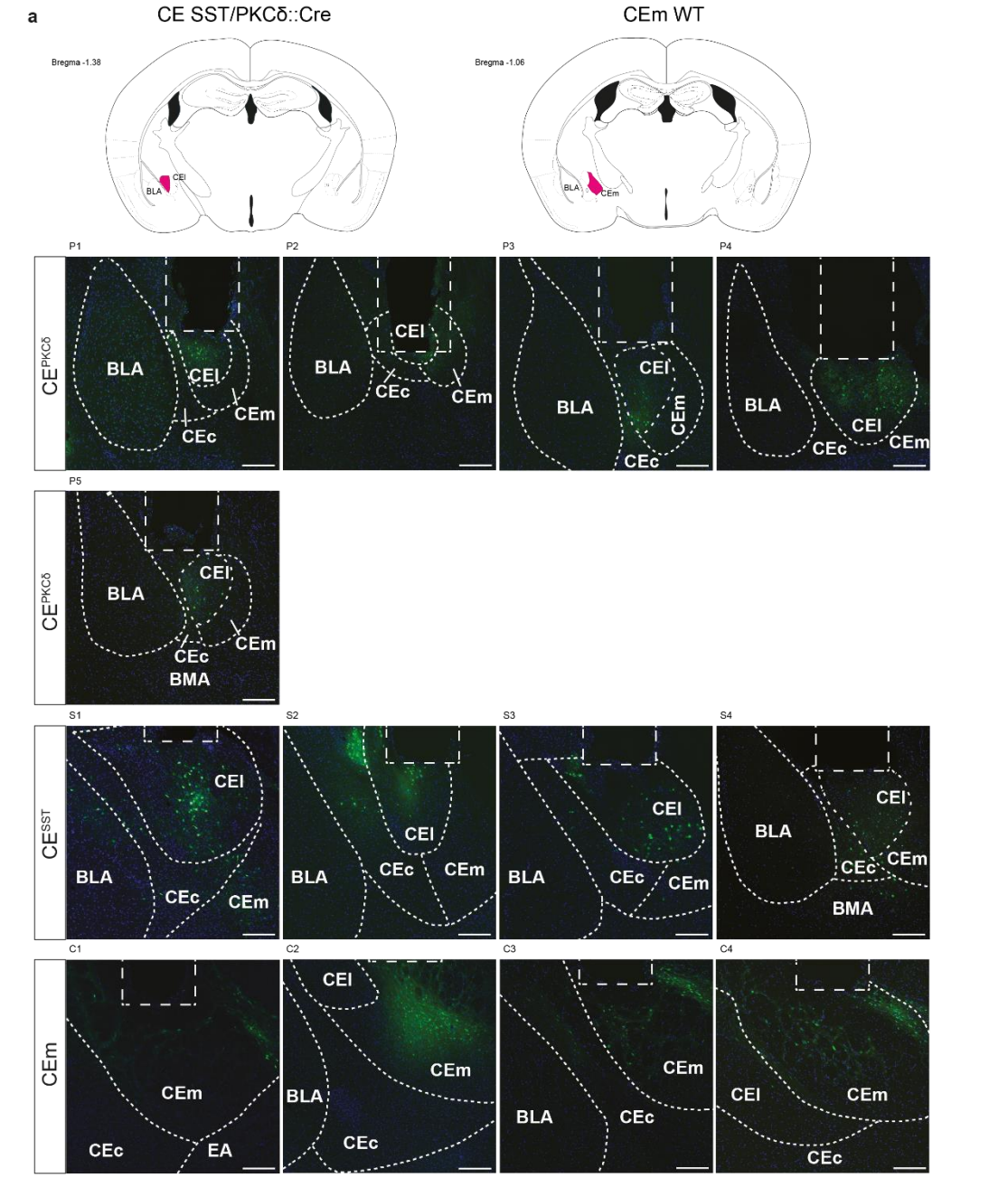
a
CE SST/PKCδ::Cre
CEm WT
Bregma -1.38
Bregma -1.06
BLA
CEl
CEm
P1
P2
P3
P4
P5
S1
S2
S3
S4
C1
C2
C3
C4
CE PKCδ
CE SST
CEm
CEc
BMA
EA

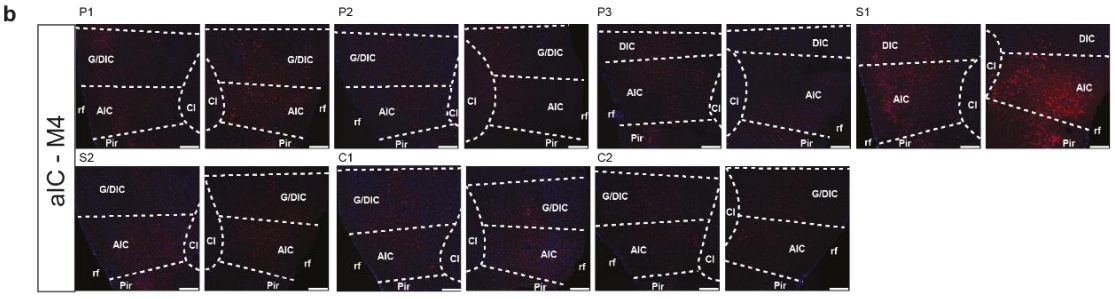
b
aIC - M4
P1
P2
P3
S1
S2
C1
C2
G/DIC
DIC
AIC
Cl
rf
Pir

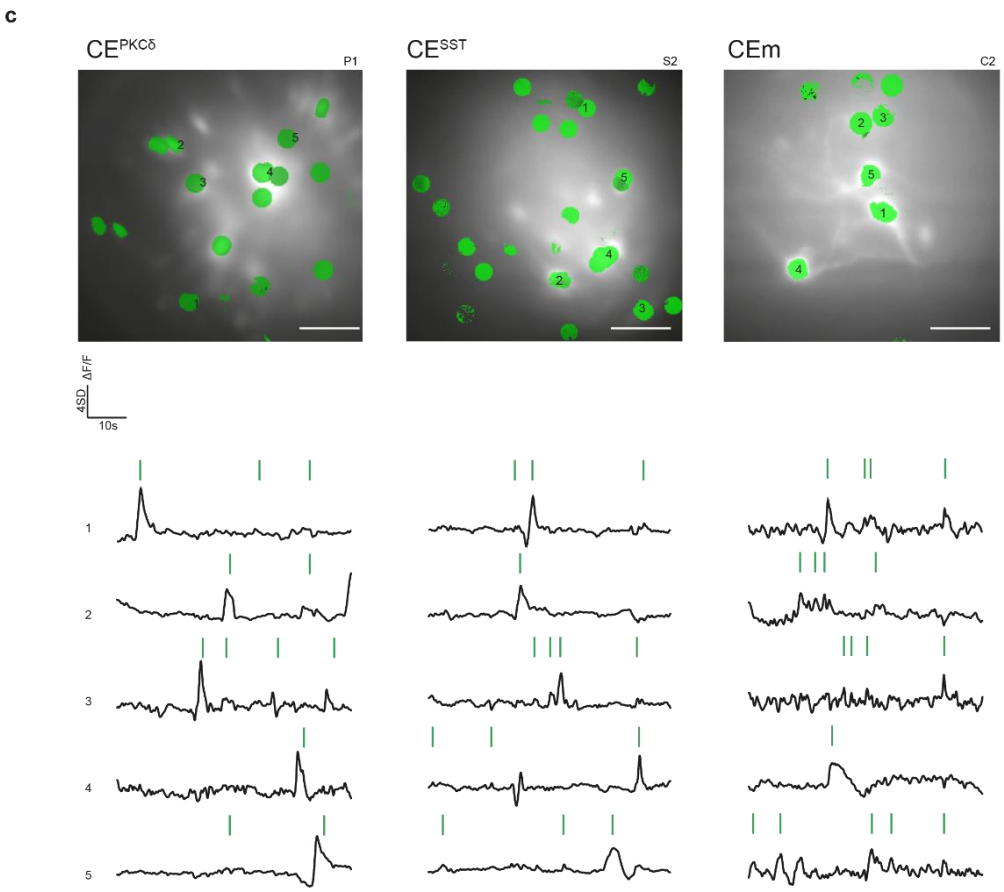

Supplementary Figure 3 | Histology and neural activity in calcium imaging. a, Schematic coronal sections of targeted areas and from all calcium recording groups. PKCδ::Cre and SST::Cre mice were injected with AAV-hSyn-DIO-GCaMP6f in the right lateral division of central amygdalar nucleus (CEl). WT mice were injected with AAV-hSyn-GCaMP6m in the right medial division of central amygdala (CEm). Rectangular dashed shape indicates GRIN lens placement (Ø=500µm); scalebar=200µm. BLA – basolateral amygdala, BMA – basomedial amygdala, CEc, capsular part of central amygdala. **b**, Injection site of AAV-hSyn-DIO-hM4 and AAV::Cre into aIC. Scalebar=200µm. AIC – agranular insula, Cl – claustrum, G/DIC – granular/dysgranular insula, Pir – piriform cortex, rf – rhinal fissure. **c**, Exemplary FOVs from each cellular population recordings. Green overlay corresponds to automatically detected and manually selected units for lack of artifacts. Scalebar=100µm (*top*). Five exemplary traces from each FOV with detected calcium events in green. Vertical scalebar corresponds to 4 standard deviations of ΔF/F calcium signal, horizontal scalebar corresponds to 10s (*bottom*).

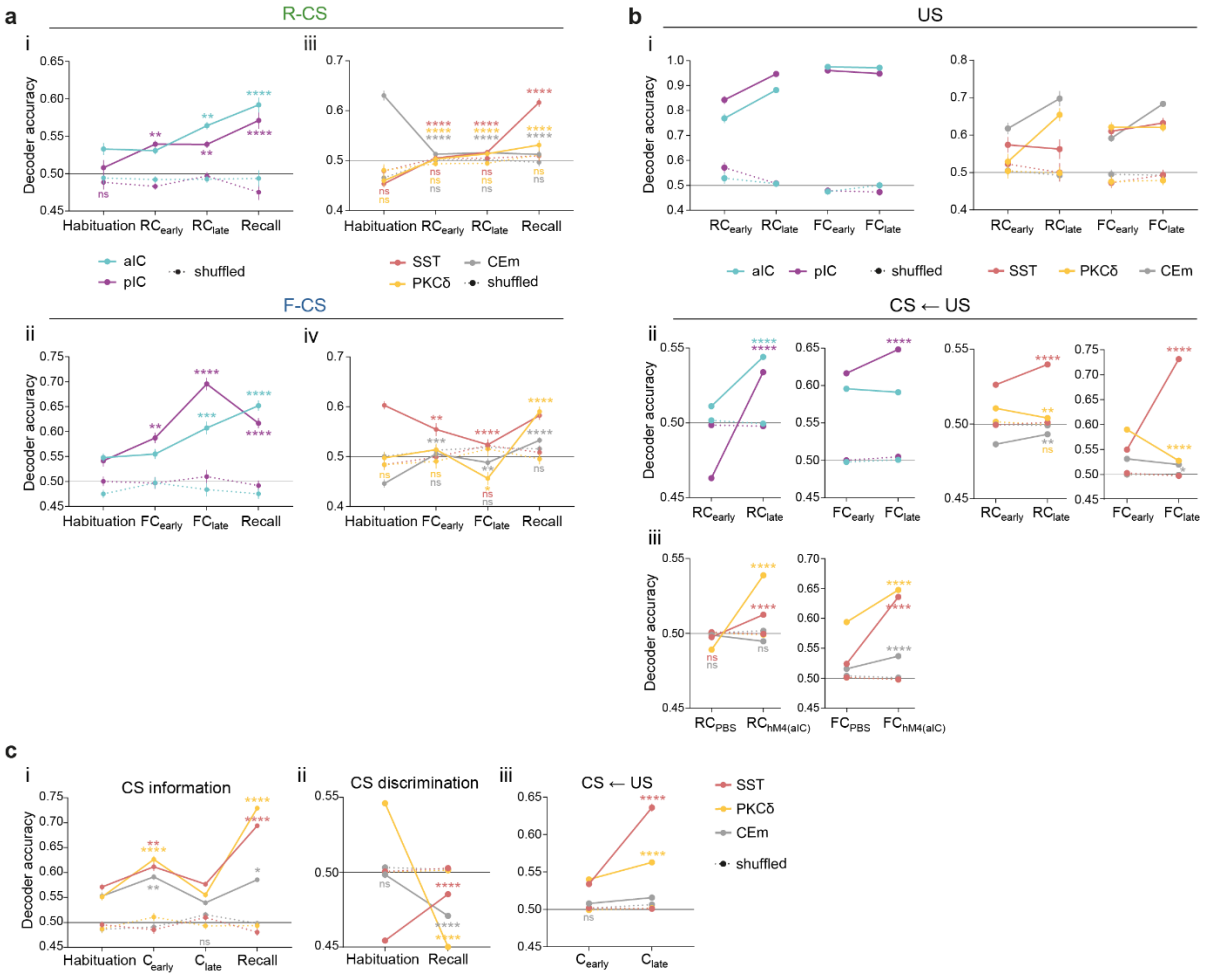

Supplementary Figure 4 | Valence-specific mapping of CS and US features in IC–CE circuitry. a, Da of a MLP trained to detect CS information in activity of 200 random draws of 40 neurons per IC subregions for R-CS (i) and F-CS (ii) and 200 random draws of 30 neurons per for $CE^{PKC\delta}$ and CE^{SST} and 10 neurons for CEm and stage upon R-CS (iii) and F-CS (iv). * indicate significant differences to the respective habituation stage within subregion by a designated post hoc test. Only non-significant differences to shuffled data within subregion and stage are indicated by 'ns', otherwise omitted. **b**, (i) Da of a MLP trained to detect US information in activity of 200 random draws of 40 neurons per IC subregion, 30 for $CE^{PKC\delta}$ and CE^{SST} and 10 neurons for CEm for R-US and F-US, used to for the CS←US task. (ii) Projection of US properties by application of the MLP in (i) applied on the respective the CS. (iii) Projection of US properties by application of a MLP trained to detect US information in control conditions (PBS) and aIC inhibition (hM4(aIC)) applied on the respective the CS. **c**, Equivalent decoding approach as Fig. 1d, using best neurons (see 'Single-region decoding' in Methods) for CS information (i), CS discrimination (ii) and the CS←US task (iii). * indicate significant differences between stages, within subregion/population. Holm-Sidak post hoc for all analyses, *p<0.05, **p<0.01, ***p<0.001, ****/####p<0.0001. All data presented as mean±SEM. Full statistical report in Supplementary Table 1.

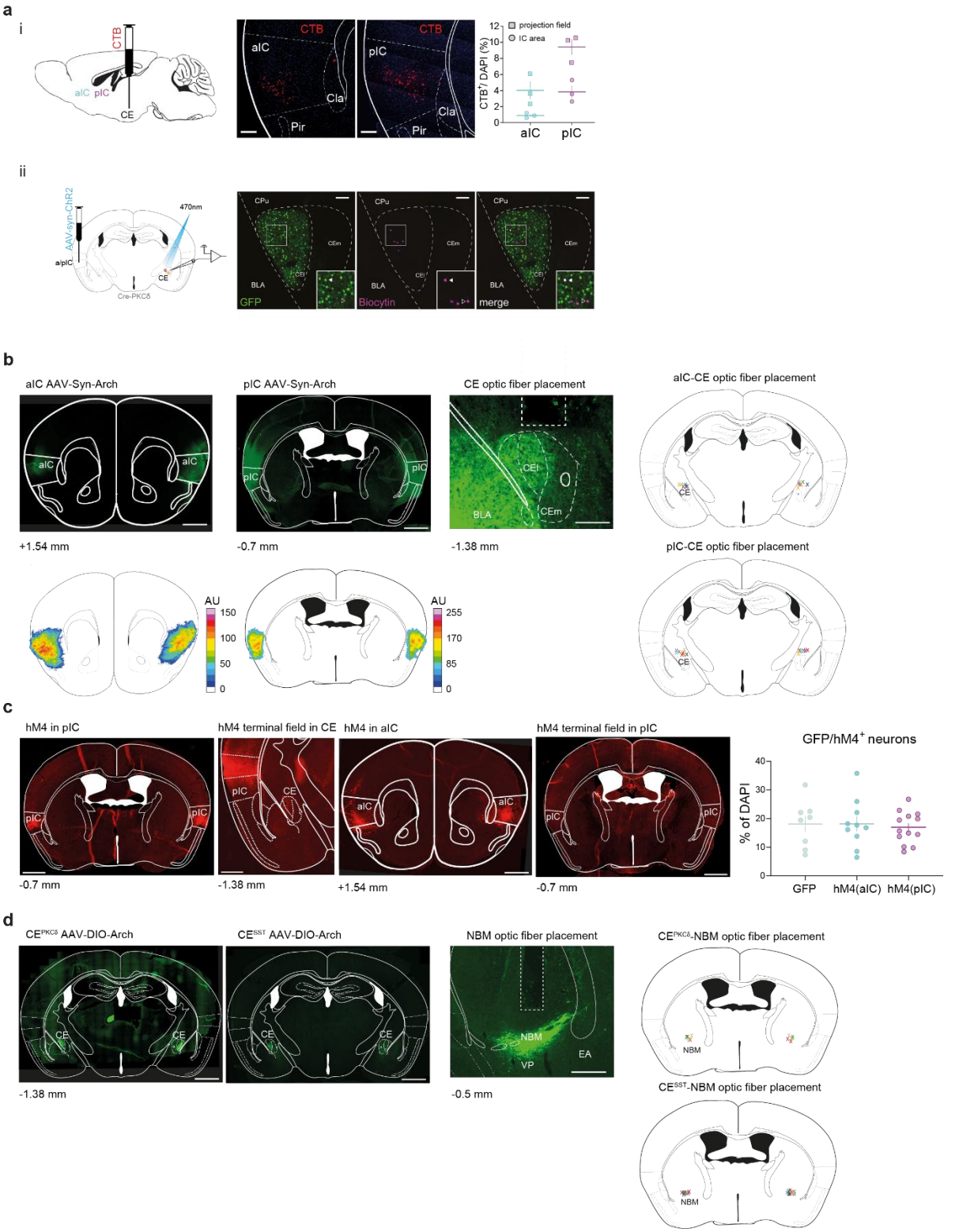

Supplementary Figure 5 | Histological assessment of IC↔CE/NBM connectivity. a, (i) Stereotactic injection of fluorescently labelled cholera toxin-B (CTB) into CE (*left*) with exemplary backlabelling in aIC and pIC (*middle*) and quantification (*right*). Each data point represents a single animal. (ii) For assessing synaptic connectivity between IC subregions and CE subpopulations in Fig. 2a, PKCδ::Cre mice received injection of AAVs carrying Cre-dependent GFP into CE and syn-ChR2 into aIC or pIC (*left*). Exemplary slice showing GFP expression in $CE^{PKC\delta}$ (green), biocytin-filled fluorescently labelled streptavidin-stained patched neurons (magenta) (*right*). **b**, Exemplary pictures of aIC and pIC AAV-Syn-Arch injection sites (scalebar=900µm) and the optic fiber placement above CE (scalebar=100µm) (*top*). Representation of the injection spread in aIC and pIC (*bottom, left*); heatmap corresponds to the fluorescence intensity. Schematic placement of the optic fiber tip above CE marked with 'x' (*bottom, right*). **c**, Exemplary aIC and pIC AAV-DIO-hM4 injection site and terminal

hM4 field in pIC and CE; scalebar=900 (full sections) and 100 µm (*left*). Quantification of GFP and hM4 infection rate in aIC and pIC presented as % of GFP/hM4 positive neurons over DAPI (data shown as mean±SEM) (*right*). **d,** $CE^{PKC\delta}$ and CE^{SST} injection sites of AAV-DIO-Arch/NpHR3.0 (scalebar=900µm). Optic fiber placement in NBM (scalebar=100µm) (*top*). Schematic placement of the optic fiber above terminal field in NBM marked with 'x' (*right*). NBM – nucleus basalis of Meynert.

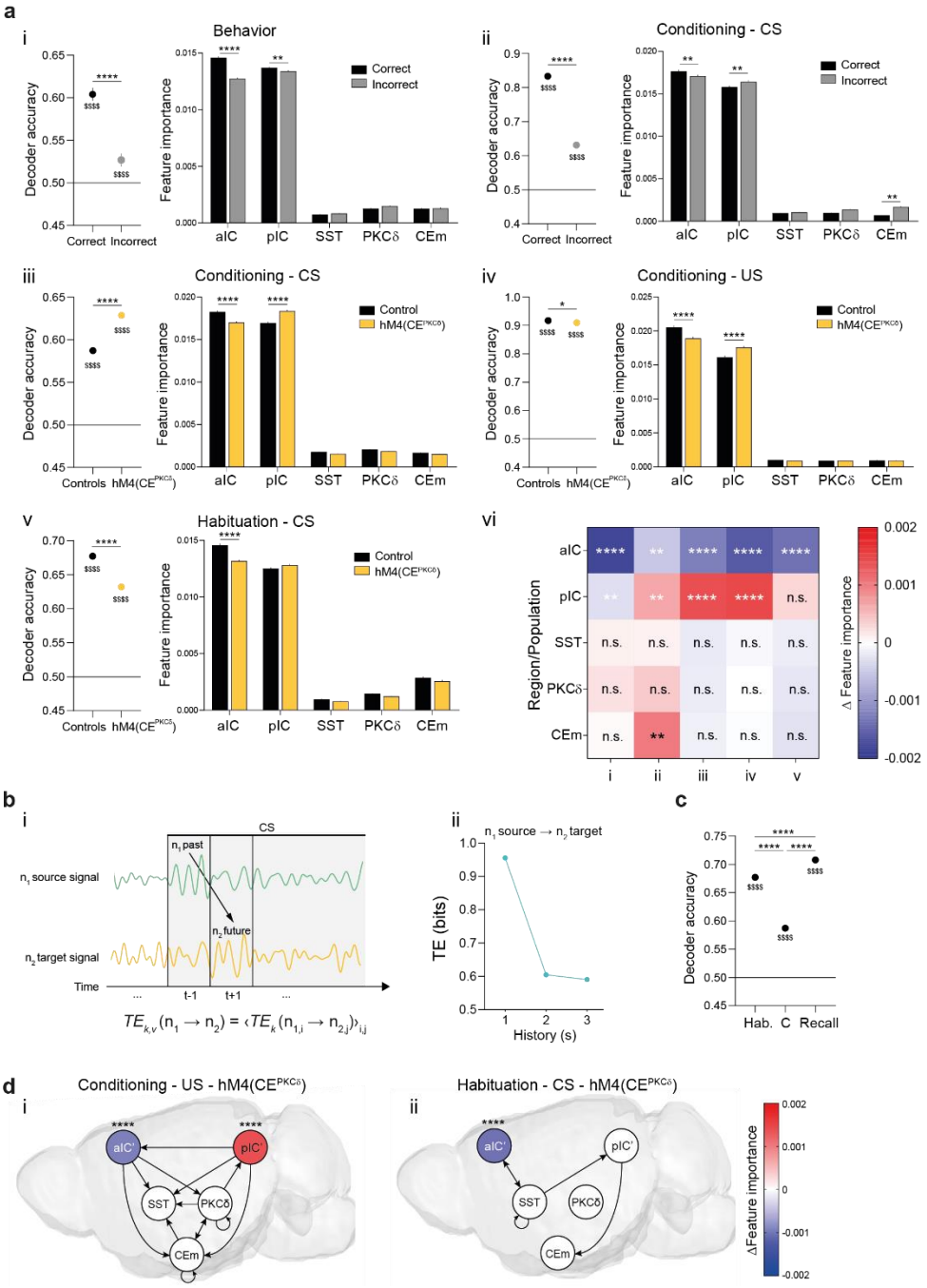

Supplementary Figure 6 | PL task parameter distributions in the IC–CE network are reshaped by performance and CE$^{PKC\delta}$. **a**, RF Da (*left*) and associated FI distribution (*right*) for correct/incorrect behavior (i), correct/incorrect CS in conditioning (ii), CS in conditioning (iii), US in conditioning (iv) and CS in habituation for control and hM4(CE$^{PKC\delta}$) conditions. (vi) Summary of differential FI between conditions. Colors were used for all TE network projections. **b**, (i) Illustration of the principle for quantifying transfer entropy (TE) between source neuron n_1 and target neuron n_2, where *k* refers to past states and *i* and *j* label the sample subset of $n_{1,i}$ and $n_{2,j}$ of size *v* in each region. n_2 future signal (time=t+1) can be predicted from past activity pattern (time=t-1) in n_1. (ii) Averaged TE between pairs of all neurons within CS-type and stage (RC, FC, recall), calculated for the entire network for 1s binned data with history windows of 1, 2 or 3s. **c**, RF Da of all stages under control conditions. ****/$$$$ p<0.0001, * indicates significant difference as determined by two-sample test, $ indicates significant difference as determined by one-sample test to random (0.5). Full statistical report in Supplementary Table 1. **d**, TE networks for US in conditioning (i) and CS in habituation (ii) under the hM4(CE$^{PKC\delta}$) condition.

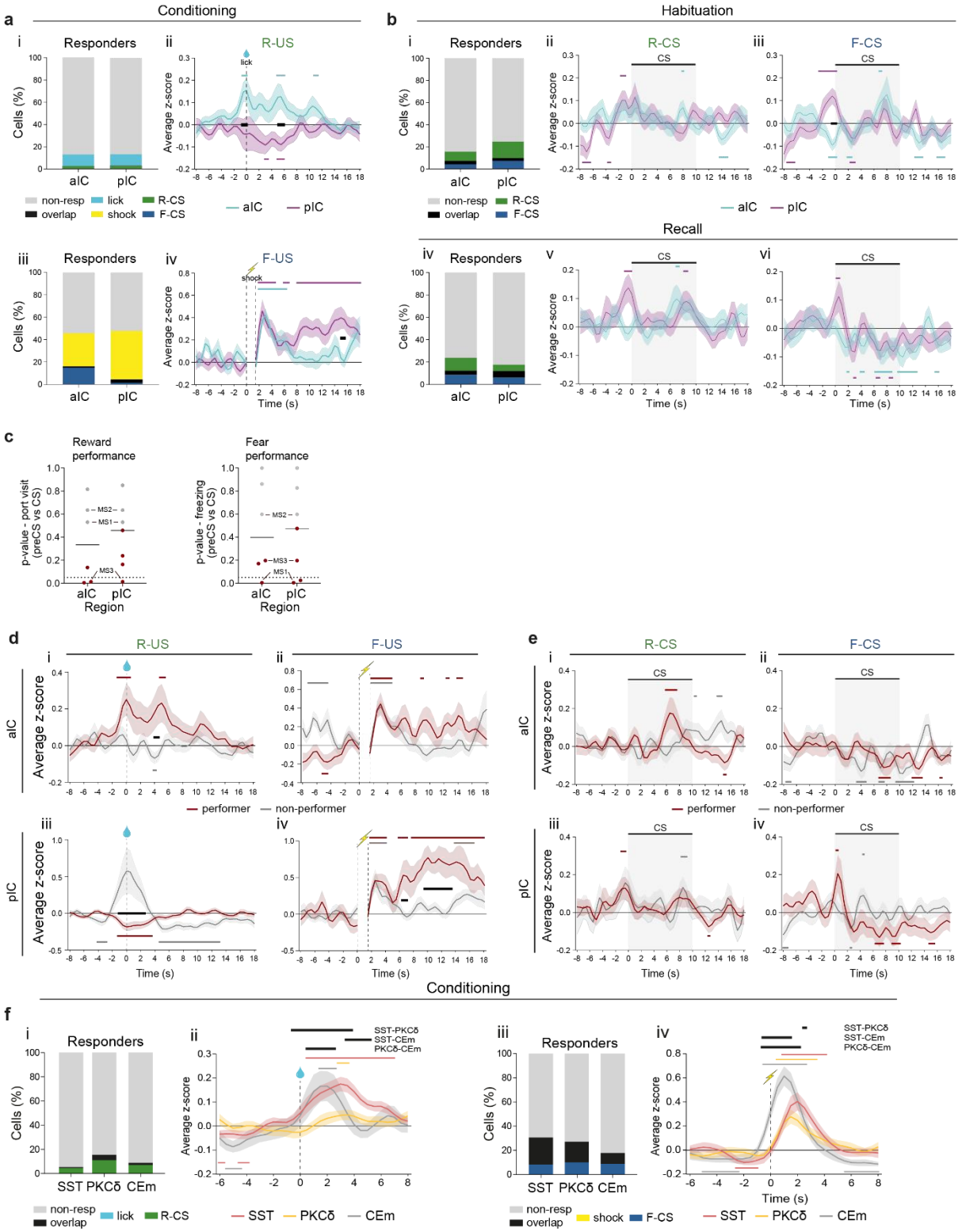
a
Conditioning
i
Responders
Cells (%)
aIC
pIC
non-resp
lick
R-CS
overlap
shock
F-CS
ii
R-US
lick
Average z-score
aIC
pIC
iii
Responders
iv
F-US
shock
Time (s)
b
Habituation
i
Responders
ii
R-CS
CS
iii
F-CS
Recall
iv
Responders
v
vi
c
Reward performance
Fear performance
p-value - port visit (preCS vs CS)
p-value - freezing (preCS vs CS)
MS1
MS2
MS3
Region
d
R-US
F-US
aIC
pIC
performer
non-performer
e
R-CS
F-CS
f
Conditioning
SST
PKCδ
CEm
SST-PKCδ
SST-CEm
PKCδ-CEm

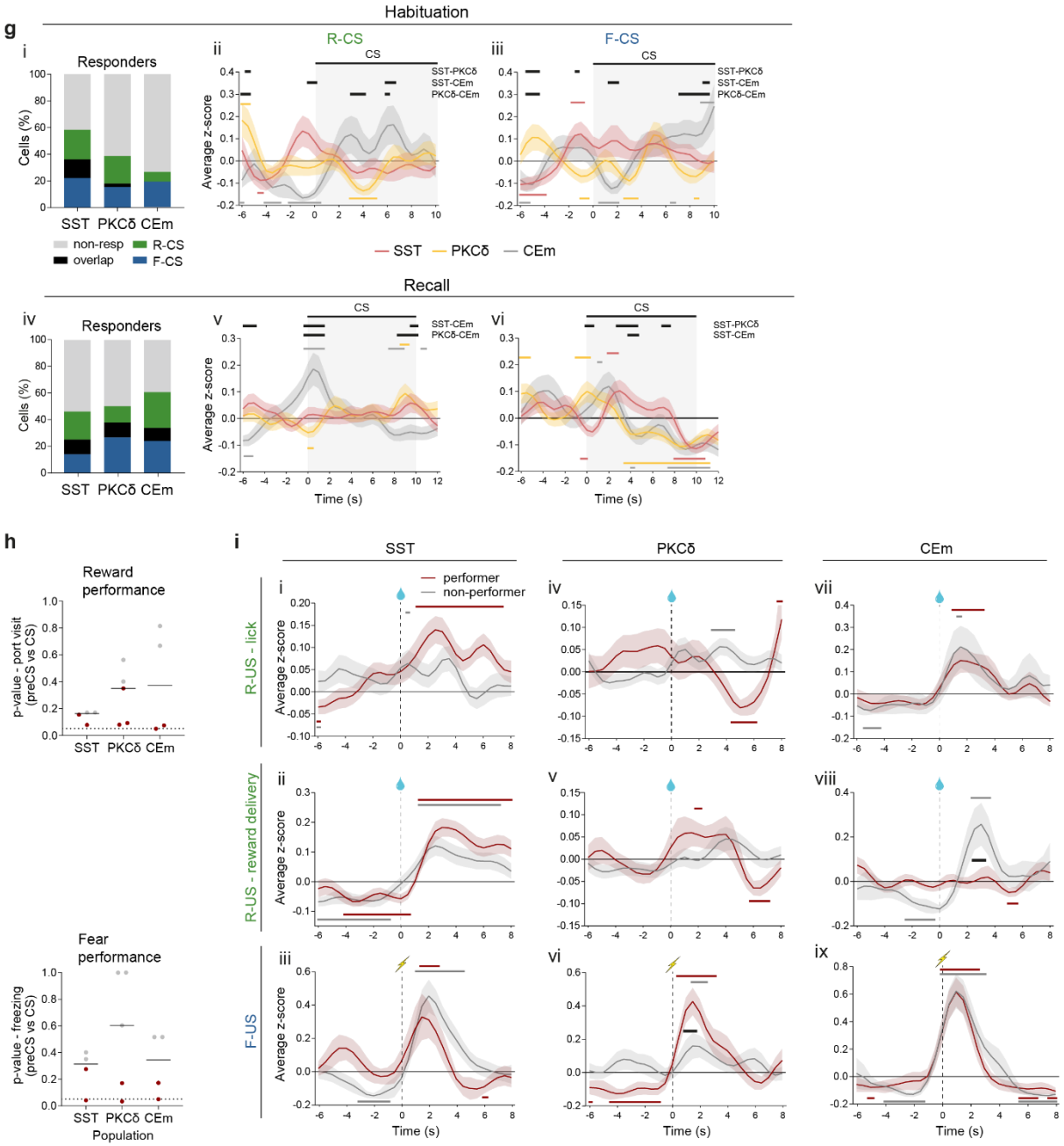

Supplementary Figure 7 | PL task parameters in IC and CE relate to performance. a, (i) Percentage of responsive neurons to task-relevant stimuli, determined by trial-averaged responses above 1.65 in RC. (ii) Average z-scored population responses of IC subregions as PETH upon R-US. Black lines indicate significant differences ($p<0.05$) between subregions as determined by post hoc analysis, Colored lines indicate significant differences ($p<0.05$) to zero per subregion, as determined by one-sample t-tests. (iii) Percentage of responsive neurons to task-relevant stimuli, determined by trial-averaged responses above 1.65 in FC. (iv) Average z-scored population responses as PETH of IC subregions upon F-US. Depiction of significant differences as for R-US (ii). **b**, (i) Percentage of responsive neurons to task-relevant stimuli, determined by trial-averaged responses above 1.65 at habituation. PETH of CS-evoked responses of IC subregions for R-CS (ii) and F-CS (iii) at habituation. Depiction of significant differences as in (aii). (iv) Percentage of responsive neurons to task-relevant stimuli, determined by trial-averaged responses above 1.65 at recall. PETH of CS-evoked responses at recall of IC subregions for R-CS (v) and F-CS (vi). Depiction of significant differences as in (aii). **c,** Performance of individual mice in the reward (*left*) and fear domain (*right*), as determined by the p-value from t-tests comparing the number of port visits (reward) and freezing episode onsets (fear) before versus during CS presentation. Color assignment of individual points according to a median split of p-values (red – performer, grey – non-performer). The median performer was assigned to the 'performer' group if its p-value is ≤0.5. **d**, PETH of US population responses according to performance for aIC upon R-US (i) and F-US (ii), and of pIC upon R-US (iii) and F-US (iv). Depiction of significant differences as in (aii). **e**, PETH of population responses

according to performance for aIC upon R-CS (i) and F-CS (ii) and for pIC upon R-CS (iii) and F-CS (iv). Depiction of significant differences as in (aii). **f**, (i) Percentage of responsive neurons to task-relevant stimuli, determined by trial-averaged responses above 1.65 in RC. (ii) Average z-scored population responses of CE subpopulations as PETH upon R-US. Depiction of significant differences as in (aii). (iii) Percentage of responsive neurons to task-relevant stimuli, determined by trial-averaged responses above 1.65 in FC. (iv) Average z-scored population responses as PETH of CE subpopulations upon F-US. Depiction of significant differences as in (aii). **g**, (i) Percentage of responsive neurons to task-relevant stimuli, determined by trial-averaged responses above 1.65 at habituation. PETH of CS-evoked responses of CE subpopulations for R-CS (ii) and F-CS (iii) at habituation. Depiction of significant differences as in (aii). (iv) Percentage of responsive neurons to task-relevant stimuli, determined by trial-averaged responses above 1.65 at recall. PETH of CS-evoked responses at recall of CE subpopulations for R-CS (v) and F-CS (vi). Depiction of significant differences as in (aii). **h,** Performance of individual mice in the reward (*top*) and fear domain (*bottom).* Group assignment as in c. **i**, (i-ix) PETH of US population responses according to performance for CE subpopulations upon R-US (*top* and *middle*) and F-US (*bottom*). Depiction of significant differences as in (aii). Full statistical report in Supplementary Table 1.

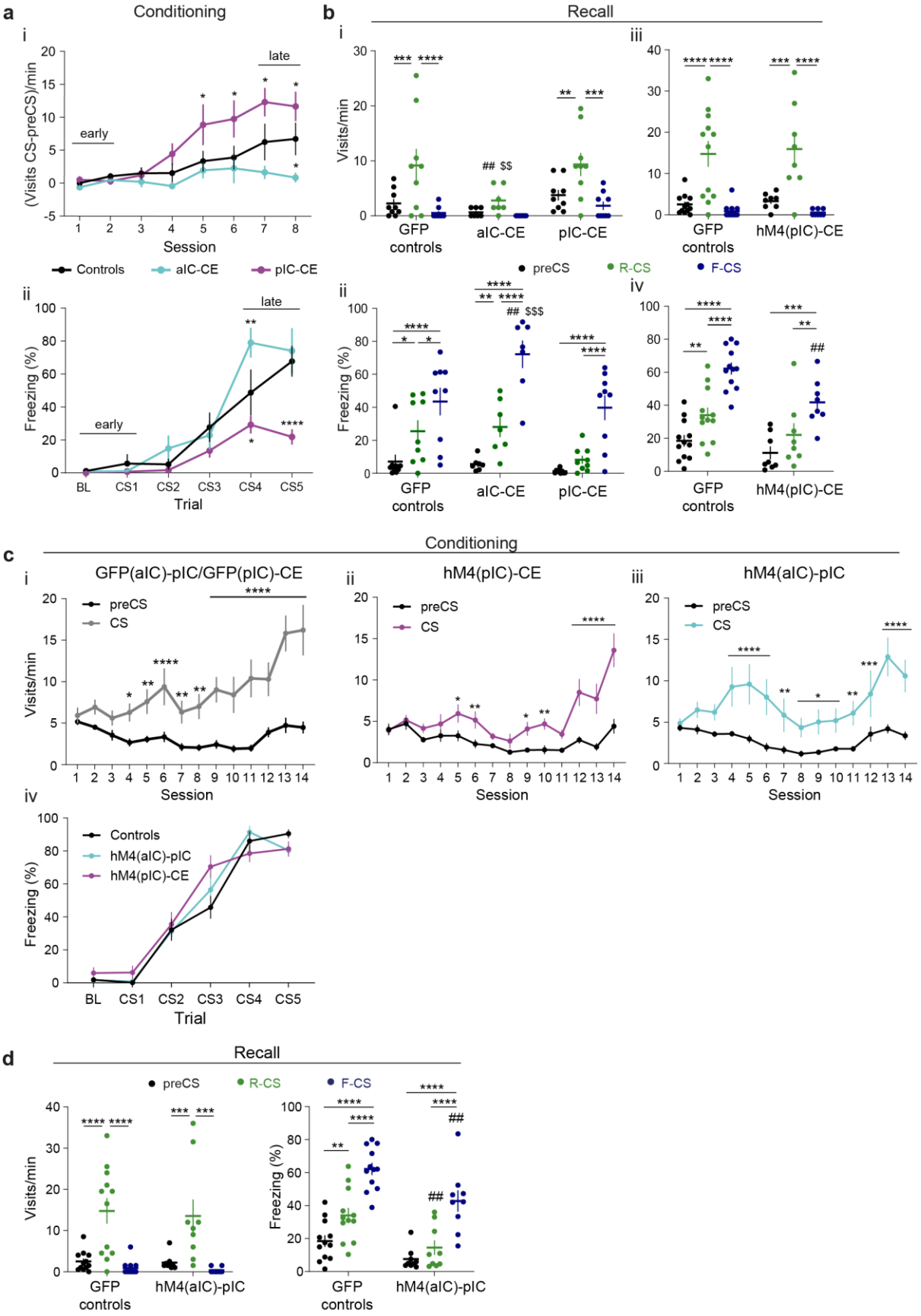

Supplementary Figure 8 | Valence-specific responses of IC–CE optogenetic/chemogenetic cohorts. a, (i) Approach behavior quantified as differential rate of port visits per minute (port visits/min during CS – port visits/min before CS onset). (ii) Avoidance behavior quantified as percent time freezing during baseline (1min)

and each CS presentation (10s). **b**, Quantification of CS-specific approach (visits/min) (i) and avoidance behavior (percent time freezing) (ii) during a single recall session with 4 presentations per R-CS and F-CS without optogenetic manipulation of aIC/pIC–CE pathways. Quantification of CS-specific approach (iii) and avoidance behavior (iv) at recall of a separate cohort receiving chemogenetic inhibition during conditioning of the pIC–CE pathway. Note that control animals are shared with the hM4(aIC)-pIC cohort (Fig. 4c/Supplementary Fig. 8ci,iv/d), as they were trained in parallel. $n_{GFP=}9/12$ $n_{aIC–CE=}7$, $n_{pIC–CE=}9/8$. **c**, Learning curves of the aIC–pIC and pIC–CE cohorts for approach behavior of the control group (i), the hM4(pIC)-CE group (ii) and the hM4(aIC)-pIC group (iii). (iv) Learning curves of avoidance behavior of control and treatment groups during the FC session. **d**, Quantification of CS-specific approach (*left*) and avoidance behavior (*right*) at drug-free recall of mice that underwent chemogenetic aIC–pIC inhibition during conditioning. Holm-Sidak post hoc was used for all analyses. */#/$p<0.05, **/##/$$p<0.01, ***/###/$$$p<0.001, ****/####/$$$$p<0.0001, where '#' indicates comparison to the control and '$' to the respective other treatment group; $n_{Controls=}12$, $n_{M4(aIC)-pIC=}9$. All data presented as mean±SEM. Full statistical report in Supplementary Table 1.

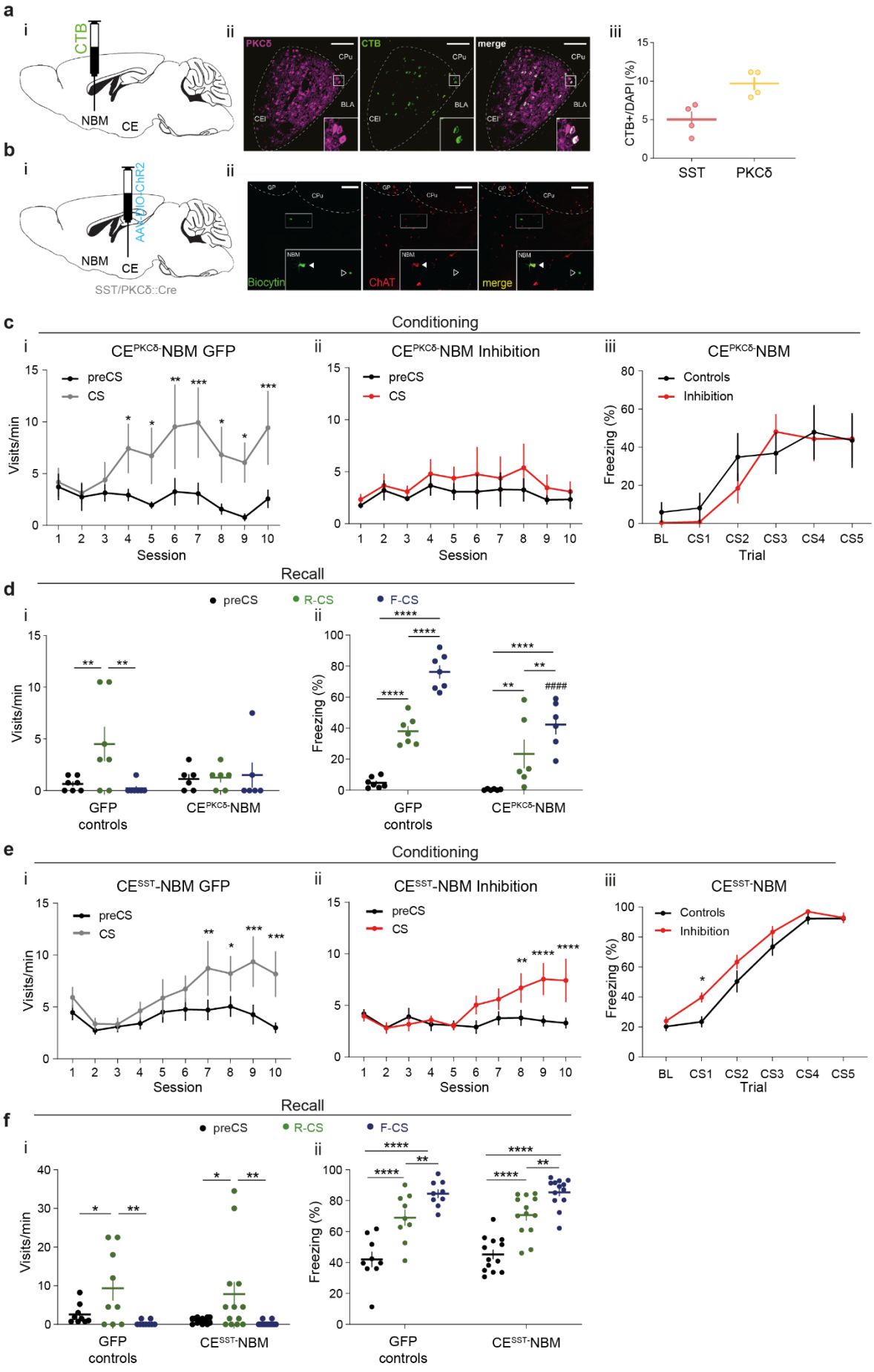
a
i
CTB
NBM
CE
ii
PKCδ
CTB
merge
CPu
BLA
CEl
iii
CTB+/DAPI (%)
SST
PKCδ
b
i
AAV-DIO-ChR2
NBM
CE
SST/PKCδ::Cre
ii
Biocytin
ChAT
merge
c
Conditioning
i
CE^PKCδ-NBM GFP
preCS
CS
Visits/min
Session
ii
CE^PKCδ-NBM Inhibition
preCS
CS
Session
iii
CE^PKCδ-NBM
Controls
Inhibition
Freezing (%)
BL
CS1
CS2
CS3
CS4
CS5
Trial
d
Recall
preCS
R-CS
F-CS
i
Visits/min
GFP controls
CE^PKCδ-NBM
ii
Freezing (%)
GFP controls
CE^PKCδ-NBM
e
Conditioning
i
CE^SST-NBM GFP
preCS
CS
Visits/min
Session
ii
CE^SST-NBM Inhibition
preCS
CS
Session
iii
CE^SST-NBM
Controls
Inhibition
Freezing (%)
BL
CS1
CS2
CS3
CS4
CS5
Trial
f
Recall
preCS
R-CS
F-CS
i
Visits/min
GFP controls
CE^SST-NBM
ii
Freezing (%)
GFP controls
CE^SST-NBM

Supplementary Figure 9 | A cell type-specific CE–NBM pathway is required for PL under uncertainty. a, (i) Stereotactic injection of CTB into NBM with exemplary backlabelling in CE (red) and PKCδ counterstain (magenta) (ii) and quantification according to identified CEl populations (iii). Each data point represents a single animal. **b**, (i) For assessing synaptic connectivity between CEl subpopulations and NBM in Fig. 3b, PKCδ::Cre and SST::Cre mice received injection of AAVs carrying Cre-dependent DIO-ChR2 into CE. (ii) Exemplary slice showing biocytin-filled and fluorescently labelled streptavidin-stained patched neurons (green) and choline acetyl-transferase^{+} (ChAT^{+}) neurons in NBM. Arrows indicate an exemplary magnocellular (mc, filled) and parvocellular neuron (pv, hollow). **c**, Learning curves of the CE$^{PKC\delta}$-NBM cohort for approach behavior of controls (i) and the CE$^{PKC\delta}$-NBM inhibition group (ii). (iii) Learning curves of avoidance behavior of control and the CE$^{PKC\delta}$-NBM inhibition group during the FC session. **d**, Quantification of CS-specific approach (visits/min) (i) and avoidance behavior (% time freezing) (ii) at the recall session. ##p<0.01 (compared to control group), **/##p<0.01, ****p<0.0001; n_{GFP}=7, $n_{CE\text{-}PKC\delta\text{–}NBM}$=6, Data presented as mean±SEM. **e**, Learning curves of the CE^{SST}-NBM cohort for approach behavior of controls (i) and the CE^{SST}-NBM inhibition group (ii). Learning curves for avoidance behavior of control and the CE^{SST}-NBM inhibition group during the FC session (iii). **f**, Quantification of CS-specific approach (i) and avoidance behavior (ii) at recall for the CE^{SST}-NBM cohort. Holm-Sidak post hoc for all analyses, *p<0.05, **p<0.01, ***p<0.001, ****p<0.0001. All data presented as mean±SEM. Full statistical report in Supplementary Table 1.

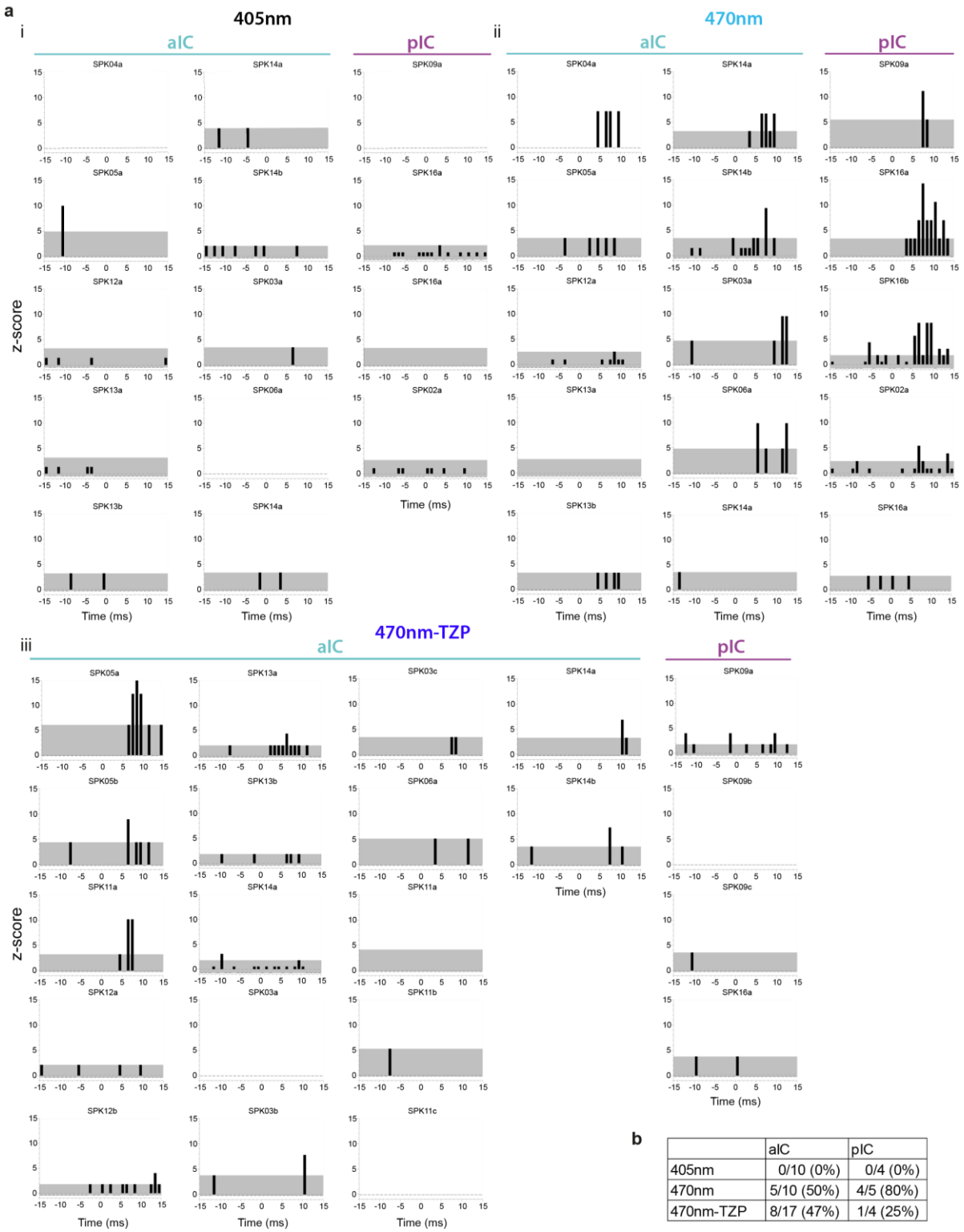

b

	aIC	pIC
405nm	0/10 (0%)	0/4 (0%)
470nm	5/10 (50%)	4/5 (80%)
470nm-TZP	8/17 (47%)	1/4 (25%)

Supplementary Figure 10 | Optogenetic CE–NBM stimulation increases spiking in single neurons in aIC and pIC. a, Peri-laser stimulus time histogram of single unit activity in aIC and pIC upon the control stimulus (405nm, 60 5ms pulses) (i), $CE^{PKC\delta}$-NBM stimulation (470nm, 60 5ms pulses) (ii) and $CE^{PKC\delta}$-NBM stimulation after systemic administration of TZP (470nm-TZP, 40 5ms pulses) (iii). Grey area depicts 95% CI. **b**, Summary table of responding neurons above 95% CI after laser stimulation.

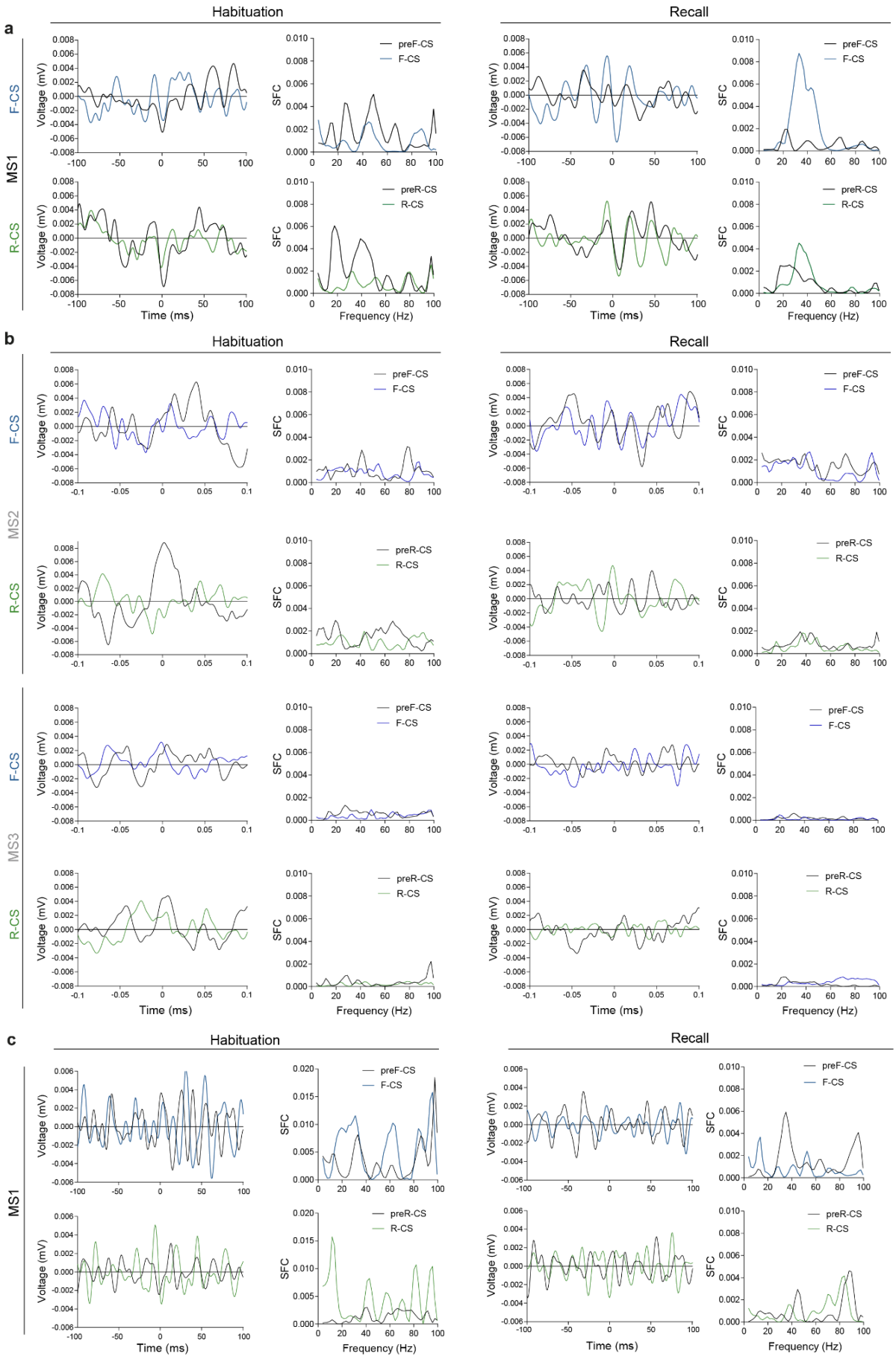
a
Habituation
Recall
MS1
F-CS
R-CS
Voltage (mV)
SFC
preF-CS
F-CS
preR-CS
R-CS
Time (ms)
Frequency (Hz)
b
MS2
MS3

Supplementary Figure 11 | aIC–pIC hierarchy is direction- and valence-asymmetric and performance-dependent. a, Valence-resolved **S**TA of 200ms pIC LFP traces centered around the occurrence of spikes from aIC and respective pIC LFP power-normalized SFC thereof for habituation and recall for animal MS1 (as in Fig. 4b). **b**, Valence-resolved **S**TA of 200ms pIC LFP traces centered around the occurrence of spikes from aIC and respective pIC LFP power-normalized SFC thereof for habituation and recall for worse performers MS2 and MS3. **c**, Valence-resolved **S**TA of 200ms aIC LFP periods centered around the occurrence of spikes from pIC and respective aIC LFP power-normalized SFC thereof for habituation and recall for animal MS1 (as in Fig. 4b).

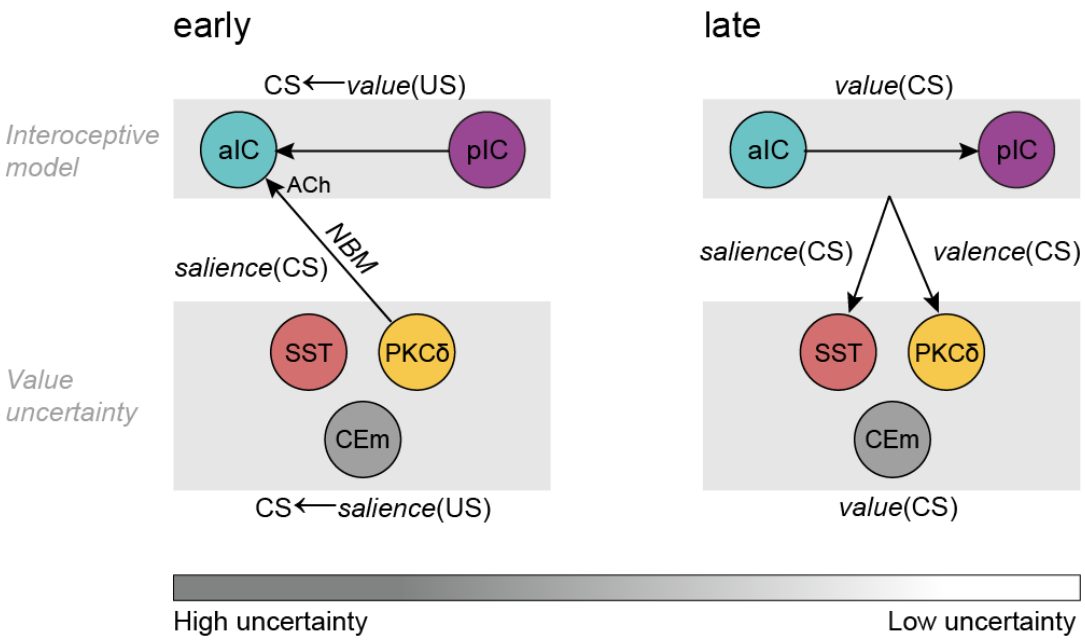

Supplementary Figure 12 | Hierarchical interactions in IC↔CE/NBM circuitry. Left, Stimulus salience at the lower hierarchical level in the amygdala promotes interoceptive models from the IC via $CE^{PKC\delta}$ when uncertain about value. In the absence of interoceptive value in CE CS salience engages NBM-aIC interaction to update intra-insular models. **Right,** Insular interoceptive models about stimulus values is recruited by CE and segregates into salience and valence dimensions, differentially projected onto CE microcircuitry.

Supplementary Tables

Supplementary Table 1. (in Supplementary Information)
Supplementary Table 1 - Detailed statistical report for MANOVA/ANOVA

Supplementary Table 2.

Supplementary Table 2 - ROIs from fMRI.xlsx
ROIs considered in the FC correlation matrix in Supplementary Fig. 1.

Supplementary Table 3.

Supplementary Table 3 – CE single neuron decoding accuracy.xlsx
Decoding accuracy of an MLP classifier on single neuron activity of CE populations. Bold rows indicate neurons used as 'best neurons' in Fig. 5e, Supplementary Fig. 4c.

Supplementary Table 1. Statistics summary of ANOVA analyses.

Dataset	Statistical test	p-values	F ratio (DFn, DFd)
Fig. 1c i CS IC	Two-way ANOVA		
Time x Subregion		p<0.0001	$F_{9,6384}$=13.69
Time		p<0.0001	$F_{3,6384}$=29.11
Subregion		p<0.0001	$F_{3,6384}$=203.31
Fig. 1c ii CS discrimination IC	Two-way ANOVA		
Stage x Subregion			
Stage		p<0.0001	$F_{3,6392}$= 42.10
Subregion		p<0.0001	$F_{1, 6392}$=116.62
		p<0.0001	$F_{3, 6392}$=42.69
Fig. 1c iii CS←US transfer IC	Two-way ANOVA		
Stage x Subregion			
Stage		p<0.0001	$F_{3,6392}$=50.14
Subregion		p<0.0001	$F_{1,6392}$=102.10
		p<0.0001	$F_{3,6392}$=469.13
Fig. 1d i CS CE	Two-way ANOVA		
Stage x Population		p<0.0001	$F_{15,9576}$=9.30
Stage		p<0.0001	$F_{3,9576}$=30.92
Population		p<0.0001	$F_{5,9576}$=28.20
Fig. 1d ii	Two-way ANOVA		
CS discrimination CE			
Stage x Population		p<0.0001	$F_{5,9588}$=30.40
Stage		p<0.0001	$F_{1,9588}$=25.90
Population		p<0.0001	$F_{5,9588}$=33.87
Fig. 1d iii	Two-way ANOVA		
CS←US transfer CE			
Stage x Population		p<0.0001	$F_{5,9588}$=339.60
Stage		p<0.0001	$F_{1,9588}$=88.70
Population		p<0.0001	$F_{5,9588}$=798.90
Fig. 2d ii Conditioning early	MANOVA	p=0.0126	$F_{2,44}$= 3.60
Fig. 2d ii Conditioning late	MANOVA	p= 0.0004	$F_{2,44}$= 6.43
Fig. 2d iii, left Recall opto	MANOVA	p= 0.0069	$F_{2,44}$= 4.06
Fig. 2d iii, right Recall chemo	MANOVA	p= 0.0067	$F_{1,17}$= 6.81
Fig. 3c ii	One-way RM ANOVA		
aIC-pIC		p<0.0001	$F_{1,116,11,16}$=153.00
		p<0.0001	$F_{1,340,14,74}$=23.60
Fig. 3c iii	One-way ANOVA		
PKCδ-NBM stimulation		p<0.0001	$F_{2,32}$=209.40
Fig. 4c ii Recall aIC-pIC	MANOVA	p= 0.0471	$F_{1,18}$= 3.64
Fig. 5d ii Recall PKCδ-NBM	MANOVA	p= 0.0045	$F_{1,10}$= 9.76
Fig. 5e ii CS CE	Two-way ANOVA		
Treatment x Population		p<0.0001	$F_{5,4788}$=117.50
Treatment		p<0.0001	$F_{1,4788}$=102.80
Population		p<0.0001	$F_{5,4788}$=449.30

Fig. 5e iii CS discrimination CE	Two-way ANOVA		
Treatment x Population		p<0.0001	$F_{5,9588}$=306.50
Treatment		p<0.0001	$F_{1,9588}$=134.80
Population		p<0.0001	$F_{5,9588}$=340.70
Fig. 5e iv CS←US transfer CE	Two-way ANOVA		
Treatment x Population			
Treatment		p<0.0001	$F_{5,9588}$=163.90
Population		p<0.0001	$F_{1,9588}$=432.50
		p<0.0001	$F_{5,9588}$=584.50
Supplementary Fig. 4a i R-CS IC	Two-way ANOVA		
Stage x Subregion		p<0.0001	$F_{9,3184}$=5.68
Stage		p<0.0001	$F_{3,3184}$=9.99
Subregion		p<0.0001	$F_{3,3184}$=78.65
Supplementary Fig. 4a ii F-CS IC	Two-way ANOVA		
Stage x Subregion		p<0.0001	$F_{9,3184}$=11.50
Stage		p<0.0001	$F_{3,3184}$=22.38
Subregion		p<0.0001	$F_{3,3184}$=137.80
Supplementary Fig. 4a iii R-CS CE	Two-way ANOVA		
Stage x Population		p<0.0001	$F_{15,4776}$=29.17
Stage		p<0.0001	$F_{3,4776}$=23.21
Population		p<0.0001	$F_{5,4776}$=28.00
Supplementary Fig. 4a iv F-CS CE	Two-way ANOVA		
Stage x Population		p<0.0001	$F_{15,4776}$=7.93
Stage		p<0.0001	$F_{3,4776}$=13.56
Population		p<0.0001	$F_{5,4776}$=24.62
Supplementary Fig. 4b i R-US IC	Two-way ANOVA		
Stage x Subregion		p<0.0001	$F_{3,1592}$=16.06
Stage		p=0.0030	$F_{1,1592}$=8.85
Subregion		p<0.0001	$F_{3,1592}$=302.70
Supplementary Fig. 4b i F-US IC	Two-way ANOVA		
Stage x Subregion		p=0.2300	$F_{3,1592}$=1.44
Stage		p=0.8792	$F_{1,1592}$=0.02
Subregion		p<0.0001	$F_{3,1592}$=1619.00
Supplementary Fig. 4b i R-US CE	Two-way ANOVA		
Stage x Subregion		p<0.0001	$F_{5,2228}$=5.40
Stage		p=0.0213	$F_{1,2228}$=5.31
Subregion		p<0.0001	$F_{5,2228}$=23.34
Supplementary Fig. 4b i F-US CE	Two-way ANOVA		
Stage x Subregion		p=0.0013	$F_{5,2388}$=4.01
Stage		p=0.0020	$F_{1,2388}$=9.53
Subregion		p<0.0001	$F_{5,2388}$=76.81
Supplementary Fig. 4b ii RC CS←US transfer IC	Two-way ANOVA		
Stage x Subregion		p<0.0001	$F_{9,3192}$=242.50
Stage		p<0.0001	$F_{3,3192}$=521.60
Subregion		p<0.0001	$F_{3,3192}$=167.50
Supplementary Fig. 4b ii FC CS←US transfer IC	Two-way ANOVA		
Stage x Subregion		p<0.0001	$F_{9,3192}$=9.97
Stage		p<0.0001	$F_{3,3192}$=11.62
Subregion		p<0.0001	$F_{3,3192}$=688.50

Supplementary Fig. 4b ii RC CS←US transfer CE	Two-way ANOVA		
Stage x Population		p<0.0001	$F_{5,4788}$=18.39
Stage		p=0.0013	$F_{1,4788}$=10.42
Population		p<0.0001	$F_{5,4788}$=326.10
Supplementary Fig. 4b ii FC CS←US transfer CE	Two-way ANOVA		
Stage x Population		p<0.0001	$F_{5,4788}$=603.30
Stage		p<0.0001	$F_{1,4788}$=142.20
Population		p<0.0001	$F_{5,4788}$=1057.40
Supplementary Fig. 4b iii RC CS←US transfer CE+CNO	Two-way ANOVA		
Stage x Population		p<0.0001	$F_{5,4788}$=186.13
Stage		p<0.0001	$F_{1,4788}$=259.70
Population		p<0.0001	$F_{5,4788}$=64.77
Supplementary Fig. 4b iii FC CS←US transfer CE+CNO	Two-way ANOVA		
Stage x Population		p<0.0001	$F_{5,4788}$=195.10
Stage		p<0.0001	$F_{1,4788}$=481.90
Population		p<0.0001	$F_{5,4788}$=948.20
Supplementary Fig. 4c i CS CE	Two-way ANOVA		
Stage x Population		p<0.0001	$F_{15,9576}$=34.91
Stage		p<0.0001	$F_{3,9576}$=89.24
Population		p<0.0001	$F_{5,9576}$=328.04
Supplementary Fig. 4c ii CS discrimination CE	Two-way ANOVA		
Stage x Population		p<0.0001	$F_{5,9588}$=311.70
Stage		p<0.0001	$F_{1,9588}$=221.90
Population		p<0.0001	$F_{5,9588}$=110.60
Supplementary Fig. 4c iii CS←US transfer CE	Two-way ANOVA		
Stage x Population		p<0.0001	$F_{5,9588}$=163.90
Stage		p<0.0001	$F_{1,9588}$=432.50
Population		p<0.0001	$F_{5,9588}$=584.50
Supplementary Fig. 6a i FI behavior performance	One-way ANOVA	p<0.0001	$F_{9,156190}$=5184.00
Supplementary Fig. 6a ii FI CS performance	One-way ANOVA	p<0.0001	$F_{9,73454}$=2437.00
Supplementary Fig. 6a iii FI CS hM4 CE$^{PKC\delta}$	One-way ANOVA	p<0.0001	$F_{9,77790}$=5185.00
Supplementary Fig. 6a iv FI US hM4 CE$^{PKC\delta}$	One-way ANOVA	p<0.0001	$F_{9,77821}$=2126.00
Supplementary Fig. 6a v FI habituation CS hM4 CE$^{PKC\delta}$	One-way ANOVA	p<0.0001	$F_{9,77619}$=1766.00
Supplementary Fig. 6c Da Control	One-way ANOVA	p<0.0001	$F_{2,5997}$=271.60
Supplementary Fig. 7a ii R-US Time x Subregion	Two-way RM ANOVA		
Time		p=0.0002	$F_{52,14248}$=1.87
Subregion		p=0.9740	$F_{52,14248}$=0.66
		p=0.0021	$F_{1,274}$=9.62

Supplementary Fig. 7a iv F-US	Two-way RM ANOVA		
Time x Subregion		p<0.0001	$F_{50,7100}$=2.29
Time		p<0.0001	$F_{50,7100}$=5.03
Subregion		p=0.0587	$F_{1,142}$=3.63
Supplementary Fig. 7b ii Habituation R-CS	Two-way RM ANOVA		
Time x Subregion		p=0.1764	$F_{52,11180}$=1.18
Time		p=0.0037	$F_{52,11180}$=1.61
Subregion		p=0.7836	$F_{1,215}$=0.08
Supplementary Fig. 7b iii Habituation F-CS	Two-way RM ANOVA		
Time x Subregion		p<0.0001	$F_{52,11076}$=2.23
Time		p<0.0001	$F_{52,11076}$=2.17
Subregion		p=0.9293	$F_{1,213}$=0.008
Supplementary Fig. 7b v Recall R-CS	Two-way RM ANOVA		
Time x Subregion		p=0.0537	$F_{52,14560}$=1.34
Time		p=0.1030	$F_{52,14560}$=1.26
Subregion		p=0.79	$F_{1,280}$=0.07
Supplementary Fig. 7b vi Recall F-CS	Two-way RM ANOVA		
Time x Subregion		p=0.5919	$F_{52,14560}$=0.94
Time		p<0.0001	$F_{52,14560}$=2.42
Subregion		p=0.3279	$F_{1,280}$=0.961
Supplementary Fig. 7d i aIC R-US	Two-way RM ANOVA		
Time x Performance		p=0.0029	$F_{52,7592}$=1.63
Time		p=0.0034	$F_{52,7592}$=1.62
Performance		p=0.0388	$F_{1,146}$=4.35
Supplementary Fig. 7d ii aIC F-US	Two-way RM ANOVA		
Time x Performance		p<0.0001	$F_{50,3950}$=2.47
Time		p<0.0001	$F_{50,3950}$=2.50
Performance		p=0.9474	$F_{1,79}$=0.004
Supplementary Fig. 7d iii pIC R-US	Two-way RM ANOVA		
Time x Performance		p<0.0001	$F_{52,6552}$=9.86
Time		p<0.0001	$F_{52,6552}$=3.55
Performance		p=0.6200	$F_{1,126}$=0.247
Supplementary Fig. 7d iv pIC F-US	Two-way RM ANOVA		
Time x Performance		p<0.0001	$F_{50,3050}$=3.27
Time		p<0.0001	$F_{50,3050}$=5.93
Performance		p<0.0001	$F_{1,61}$=17.59
Supplementary Fig. 7e i aIC R-CS	Two-way RM ANOVA		
Time x Performance		p<0.0001	$F_{52,8268}$=2.09
Time		p=0.6431	$F_{52,8268}$=0.917
Performance		p=0.5547	$F_{1,159}$=0.350
Supplementary Fig. 7e ii aIC F-CS	Two-way RM ANOVA		
Time x Performance		p=0.0434	$F_{52,8268}$=1.36
Time		p=0.0002	$F_{52,8268}$=1.84
Performance		p=0.8521	$F_{1,159}$=0.0349
Supplementary Fig. 7e iii pIC R-CS	Two-way RM ANOVA		
Time x Performance		p>0.9999	$F_{52,6188}$=0.353
Time		p=0.1204	$F_{52,6188}$=1.24
Performance		p=0.8266	$F_{1,119}$=0.05

Supplementary Fig. 7e iv pIC F-CS	Two-way RM ANOVA		
Time x Performance		p=0.0003	$F_{52,6188}$=1.81
Time		p=0.0063	$F_{52,6188}$=1.56
Performance		p=0.3331	$F_{1,119}$=0.944
Supplementary Fig. 7f ii R-US	Two-way RM ANOVA		
Time x Population			
Time		p<0.0001	$F_{56,3976}$=2.45
Population		p<0.0001	$F_{28,3976}$=9.61
		p<0.0001	$F_{2,142}$=11.18
Supplementary Fig. 7f iv F-US	Two-way RM ANOVA		
Time x Population			
Time		p<0.0001	$F_{56,4480}$=4.22
Population		p<0.0001	$F_{28,4480}$=31.28
		p=0.6376	$F_{2,160}$=0.451
Supplementary Fig. 7g ii Habituation R-CS	Two-way RM ANOVA		
Time x Population		p<0.0001	$F_{64,3232}$=2.76
Time		p=0.1186	$F_{32,3232}$=1.30
Population		p=0.9656	$F_{2,101}$=0.036
Supplementary Fig. 7g iii Habituation F-CS	Two-way RM ANOVA		
Stage x Population		p<0.0001	$F_{64,4032}$=2.43
Stage		p=0.0104	$F_{32,4032}$=1.67
Population		p=0.1205	$F_{2,126}$=2.15
Supplementary Fig. 7g v Recall R-CS	Two-way RM ANOVA		
Time x Population		p<0.0001	$F_{72,9684}$=2.81
Time		p=0.5507	$F_{36,9684}$=0.952
Population		p=0.8385	$F_{2,269}$=0.176
Supplementary Fig. 7g vi Recall F-CS	Two-way RM ANOVA		
Time x Population		p<0.0001	$F_{72,9072}$=2.01
Time		p<0.0001	$F_{36,9072}$=9.42
Population		p=0.2932	$F_{2,252}$=1.23
Supplementary Fig. 7i i SST R-US	Two-way RM ANOVA		
Time x Performance		p<0.0001	$F_{28,3052}$= 2.33
Time		p<0.0001	$F_{28,3052}$=2.49
Performance		p=0.0607	$F_{1,109}$=3.59
Supplementary Fig. 7i ii SST water	Two-way RM ANOVA		
Time x Performance		p=0.1217	$F_{28,3052}$=1.32
Time		p<0.0001	$F_{28,3052}$=20.42
Performance		p=0.0187	$F_{1,109}$=5.70
Supplementary Fig. 7i iii SST F-US	Two-way RM ANOVA		
Time x Performance		p=0.0003	$F_{28,1344}$=2.22
Time		p<0.0001	$F_{28,1344}$=8.10
Performance		p=0.9986	$F_{1,48}$=3.012e-006
Supplementary Fig. 7i iv PKCδ R-US	Two-way RM ANOVA		
Time x Performance		p<0.0001	$F_{28,3192}$=3.07
Time		p=0.0342	$F_{28,3192}$=1.54
Performance		p=0.7613	$F_{1,114}$=0.09
Supplementary Fig. 7i v PKCδ water	Two-way RM ANOVA		
Time x Performance		p=0.0262	$F_{28,3220}$=1.56
Time		p<0.0001	$F_{28,3220}$=2.67
Performance		p=0.6868	$F_{1,115}$=0.16

Supplementary Fig. 7i vi PKCδ F-US	Two-way RM ANOVA		
Time x Performance		p<0.0001	$F_{28,1848}$=2.96
Time		p<0.0001	$F_{28,1848}$=6.32
Performance		p=0.3513	$F_{1,66}$=0.88
Supplementary Fig. 7i vii CEm R-US	Two-way RM ANOVA		
Time x Performance		p>0.999	$F_{28,1512}$=0.18
Time		p<0.0001	$F_{28,1512}$=3.95
Performance		p=0.7647	$F_{1,54}$=0.09
Supplementary Fig. 7i viii CEm water	Two-way RM ANOVA		
Time x Performance		p<0.0001	$F_{28,1512}$=2.92
Time		p<0.0001	$F_{28,1512}$=3.53
Performance		p=0.5895	$F_{1,54}$=0.30
Supplementary Fig. 7i ix CEm F-US	Two-way RM ANOVA		
Time x Performance		p=0.9646	$F_{28,1204}$=0.57
Time		p<0.0001	$F_{28,1204}$=22.73
Performance		p=0.6271	$F_{1,43}$=0.24
Supplementary Fig. 8a i RC port visits opto	Two-way RM ANOVA		
Session x Treatment		p<0.0001	$F_{14,154}$=3.40
Session		p<0.0001	$F_{7,154}$=15.39
Treatment		p=0.0271	$F_{2,22}$=4.27
Supplementary Fig. 8a ii FC freezing opto	Two-way RM ANOVA		
Treatment x Trial		p<0.0001	$F_{10,110}$=4.71
Treatment		p<0.0001	$F_{5,110}$=50.67
Trial		p=0.0054	$F_{2,22}$=6.69
Supplementary Fig. 8b i Recall port visits opto	Two-way RM ANOVA		
CS x Treatment		p=0.2605	$F_{4,44}$=1.37
CS		p<0.0001	$F_{2,44}$=17.90
Treatment		p=0.0343	$F_{2,22}$=3.95
Supplementary Fig. 8b ii Recall freezing opto	Two-way RM ANOVA		
CS x Treatment		p=0.0225	$F_{4,44}$=3.17
CS		p<0.0001	$F_{2,44}$=66.66
Treatment		p=0.0154	$F_{2,22}$=5.07
Supplementary Fig. 8b iii Recall port visits chemo	Two-way RM ANOVA		
CS x Treatment		p=0.9251	$F_{2,36}$=0.08
CS		p<0.0001	$F_{2,36}$=31.88
Treatment		p=0.7647	$F_{1,18}$=0.09
Supplementary Fig. 8b iv Recall freezing chemo	Two-way RM ANOVA		
CS x Treatment		p=0.2970	$F_{2,36}$=1.26
CS		p<0.0001	$F_{2,36}$=40.47
Treatment		p=0.0087	$F_{1,18}$=8.65
Supplementary Fig. 8c i RC GFP	Two-way RM ANOVA		
CS x Session		p<0.0001	$F_{13,130}$=5.97
CS		p=0.0001	$F_{1,10}$=38.23
Session		p<0.0001	$F_{13,130}$=4.64
Supplementary Fig. 8c ii RC pIC-CE	Two-way RM ANOVA		
CS x Session		p<0.0001	$F_{13,91}$=9.07
CS		p=0.0027	$F_{1,7}$=20.62
Session		p<0.0001	$F_{13,91}$=8.09

Supplementary Fig. 8c iii RC aIC-pIC	Two-way RM ANOVA		
CS x Session		p=0.0003	$F_{13,104}$=3.30
CS		p=0.0053	$F_{1,8}$=14.36
Session		p<0.0001	$F_{13,104}$=4.86
Supplementary Fig. 8c iv FC	Two-way RM ANOVA		
Treatment x Trial		p=0.0537	$F_{10,125}$=1.88
Treatment		p=0.56	$F_{2,25}$=0.59
Trial		p<0.0001	$F_{5,125}$=174.70
Supplementary Fig. 8d freezing aIC-pIC	Two-way RM ANOVA		
CS x Treatment		p=0.4522	$F_{2,38}$=0.81
CS		p<0.0001	$F_{2,38}$=54.69
Treatment		p=0.0008	$F_{1,19}$=15.80
Supplementary Fig. 8d port visits aIC-pIC	Two-way RM ANOVA		
CS x Treatment		p=0.9652	$F_{2,38}$=0.04
CS		p<0.0001	$F_{2,38}$=30.32
Treatment		p=0.7341	$F_{1,19}$=0.19
Supplementary Fig. 9c i Control	Two-way RM ANOVA		
CS x Session		p=0.0163	$F_{9,54}$= 2.54
CS		p=0.0745	$F_{1,6}$= 4.65
Session		p=0.1830	$F_{9,54}$=1.47
Supplementary Fig. 9c ii CE$^{PKC\delta}$-NBM	Two-way RM ANOVA		
CS x Session		p=0.9163	$F_{9,45}$=0.42
CS		p=0.1080	$F_{1,5}$=3.82
Session		p=0.5668	$F_{9,45}$=0.86
Supplementary Fig. 9c iii	Two-way RM ANOVA		
Trial x Treatment		p=0.5363	$F_{5,60}$=0.83
Trial		p<0.0001	$F_{5,60}$=15.37
Treatment		p=0.7568	$F_{1,12}$=0.10
Supplementary Fig. 9d i port visits CE$^{PKC\delta}$-NBM	Two-way RM ANOVA		
CS x Treatment		p=0.0338	$F_{2,22}$=3.97
CS		p=0.0434	$F_{2,22}$=3.63
Treatment		p=0.5666	$F_{1,11}$=0.35
Supplementary Fig. 9d ii freezing CE$^{PKC\delta}$-NBM	Two-way RM ANOVA		
CS x Treatment		p=0.0095	$F_{2,22}$=3.11
CS		p<0.0001	$F_{2,22}$=81.45
Treatment		p=0.0029	$F_{1,11}$=8.72
Supplementary Fig. 9e i Control	Two-way RM ANOVA		
CS x Session		p=0.0109	$F_{9,72}$=2.63
CS		p=0.0104	$F_{1,8}$=11.08
Session		p=0.0048	$F_{9,72}$=2.96
Supplementary Fig. 9e ii CE^{SST}-NBM	Two-way RM ANOVA		
CS x Session		p<0.0001	$F_{9,108}$=4.75
CS		p=0.0062	$F_{1,12}$=10.99
Session		p=0.0008	$F_{9,108}$=3.48
Supplementary Fig. 9e iii	Two-way RM ANOVA		
Trial x Treatment		p=0.3490	$F_{5,100}$=1.13
Trial		p<0.0001	$F_{5,100}$=119.10
Treatment		p=0.0038	$F_{1,20}$=10.70
Supplementary Fig. 9f i port visits CE^{SST}-NBM	Two-way RM ANOVA		
CS x Treatment		p=0.9034	$F_{2,40}$=0.10

CS	p=0.0001	$F_{2,40}$=11.59
Treatment	p=0.5441	$F_{1,20}$=0.38
Supplementary Fig. 9f ii Two-way RM ANOVA **freezing CE^{SST}-NBM**		
CS x Treatment	p=0.9419	$F_{2,40}$=0.06
CS	p<0.0001	$F_{2,40}$=77.68
Treatment	p=0.5966	$F_{1,20}$=0.29

DFn=degrees of freedom for numerator, DFd=degrees of freedom for denominator

Supplementary Table 2. ROIs from fMRI.

Nr	Region
1	Frontal_Pole_L
2	Frontal_Pole_R
3	Orbital_Area_L
4	Orbital_Area_R
5	Prelimbic_Area_L
6	Prelimbic_Area_R
7	Infralimbic_Area_L
8	Infralimbic_Area_R
9	Anterior_cingulate_Area_L
10	Anterior_cingulate_Area_R
11	Agranular_insular_Area_L
12	Agranular_insular_Area_R
13	Gustatory_Areas_L
14	Gustatory_Areas_R
15	Visceral_Area_L
16	Visceral_Area_R
17	Retrosplenial_Area_L
18	Retrosplenial_Area_R
19	Post_parietal_association_L
20	Post_parietal_association_R
21	Temporal_association_area_L
22	Temporal_association_area_R
23	Somatomotor_Areas_L
24	Somatomotor_Areas_R
25	Somatosensory_Areas_L
26	Somatosensory_Areas_R
27	Auditory_Area_L
28	Auditory_Area_R
29	Visual_Area_L
30	Visual_Area_R
31	Perirhinal_area_L
32	Perirhinal_area_R
33	Ectorhinal_area_L
34	Ectorhinal_Area_R
35	Piriform_area_L
36	Piriform_area_R
37	Entorhinal_Area_L
38	Entorhinal_Area_R
39	Hippocampus_L
40	Hippocampus_R
41	Amygdala_Striatum_L
42	Amygdala_Striatum_R
43	Amygdala_cortex_L
44	Amygdala_cortex_R
45	Caudoputamen_L
46	Caudoputamen_R
47	Accumbens_L
48	Accumbens_R

49	Lateral_septal_complex_L
50	Lateral_septal_complex_R
51	Pallidium_dorsal_L
52	Pallidium_dorsal_R
53	Pallidium_ventral_L
54	Pallidium_ventral_R
55	Pallidium_medial_L
56	Pallidium_medial_R
57	Pallidium_caudal_L
58	Pallidium_caudal_R
59	Nucleus Basalis of Meynert_L
60	Nucleus Basalis of Meynert_R
61	Thalamus_L
62	Thalamus_R
63	Hypothalamus_L
64	Hypothalamus_R
65	Midbrain_L
66	Midbrain_R
67	Colliculi_inferior_L
68	Colliculi_inferior_R
69	Colliculi_superior_L
70	Colliculi_superior_R
71	MB_Reticular_nucleus_L
72	MB_Reticular_nucleus_R
73	Ventral_tegemental_area_L
74	Ventral_tegmental_area_R
75	Periaqueductal_grey_L
76	Periaqueductal_grey_R
77	Hindbrain_L
78	Hindbrain_R
79	Parabrachial_nucleus_L
80	Parabrachial_nucleus_R

Supplementary Table 3. CE single neuron decoding accuracy.

Population	Stage	Treatment/ Time point	Task	CS	MouseID	NeuronID	Accuracy	SEM	N(iterations)
SST	**habituation**	**PBS**	**CS**	**R-CS**	**S4**	**ictrace2**	**0.566488095**	**0.003762053**	**200**
SST	**habituation**	**PBS**	**CS**	**R-CS**	**S2**	**ictrace8**	**0.522559524**	**0.002651848**	**200**
SST	**habituation**	**PBS**	**CS**	**R-CS**	**S4**	**ictrace4**	**0.518571429**	**0.002381905**	**200**
SST	**habituation**	**PBS**	**CS**	**R-CS**	**S4**	**ictrace3**	**0.506130952**	**0.001930587**	**200**
SST	**habituation**	**PBS**	**CS**	**R-CS**	**S2**	**ictrace1**	**0.505892857**	**0.002072245**	**200**
SST	**habituation**	**PBS**	**CS**	**R-CS**	**S2**	**ictrace4**	**0.504166667**	**0.001932004**	**200**
SST	**habituation**	**PBS**	**CS**	**R-CS**	**S4**	**ictrace5**	**0.504166667**	**0.001932004**	**200**
SST	**habituation**	**PBS**	**CS**	**R-CS**	**S2**	**ictrace16**	**0.5025**	**0.003814719**	**200**
SST	**habituation**	**PBS**	**CS**	**R-CS**	**S2**	**ictrace2**	**0.501428571**	**0.001424996**	**200**
SST	**habituation**	**PBS**	**CS**	**R-CS**	**S2**	**ictrace18**	**0.50125**	**0.001814056**	**200**
SST	**habituation**	**PBS**	**CS**	**R-CS**	**S2**	**ictrace24**	**0.501071429**	**0.001554905**	**200**
SST	**habituation**	**PBS**	**CS**	**R-CS**	**S2**	**ictrace6**	**0.501071429**	**0.001182084**	**200**
SST	**habituation**	**PBS**	**CS**	**R-CS**	**S4**	**ictrace10**	**0.501071429**	**0.001554905**	**200**
SST	**habituation**	**PBS**	**CS**	**R-CS**	**S2**	**ictrace15**	**0.500833333**	**0.002123774**	**200**
SST	**habituation**	**PBS**	**CS**	**R-CS**	**S2**	**ictrace13**	**0.500416667**	**0.001717708**	**200**
SST	**habituation**	**PBS**	**CS**	**R-CS**	**S2**	**ictrace3**	**0.5**	**0**	**200**
SST	**habituation**	**PBS**	**CS**	**R-CS**	**S4**	**ictrace9**	**0.5**	**0**	**200**
SST	**habituation**	**PBS**	**CS**	**R-CS**	**S2**	**ictrace21**	**0.499583333**	**0.001613474**	**200**
SST	**habituation**	**PBS**	**CS**	**R-CS**	**S2**	**ictrace7**	**0.498333333**	**0.001859659**	**200**
SST	**habituation**	**PBS**	**CS**	**R-CS**	**S2**	**ictrace22**	**0.497916667**	**0.001810224**	**200**
SST	**habituation**	**PBS**	**CS**	**R-CS**	**S2**	**ictrace12**	**0.4975**	**0.001371866**	**200**
SST	**habituation**	**PBS**	**CS**	**R-CS**	**S4**	**ictrace6**	**0.495059524**	**0.00273457**	**200**
SST	**habituation**	**PBS**	**CS**	**R-CS**	**S4**	**ictrace14**	**0.492738095**	**0.001840027**	**200**
SST	**habituation**	**PBS**	**CS**	**R-CS**	**S4**	**ictrace8**	**0.492261905**	**0.003358483**	**200**
SST	**habituation**	**PBS**	**CS**	**R-CS**	**S2**	**ictrace17**	**0.486607143**	**0.003117977**	**200**
SST	**habituation**	**PBS**	**CS**	**R-CS**	**S4**	**ictrace7**	**0.486369048**	**0.002378567**	**200**
SST	**habituation**	**PBS**	**CS**	**R-CS**	**S2**	**ictrace9**	**0.485833333**	**0.003589626**	**200**
SST	**habituation**	**PBS**	**CS**	**R-CS**	**S2**	**ictrace5**	**0.485**	**0.002552232**	**200**
SST	**habituation**	**PBS**	**CS**	**R-CS**	**S2**	**ictrace11**	**0.479940476**	**0.002898483**	**200**
SST	**habituation**	**PBS**	**CS**	**R-CS**	**S2**	**ictrace29**	**0.477857143**	**0.002389924**	**200**
SST	habituation	PBS	CS	R-CS	S4	ictrace1	0.477142857	0.00240959	200
SST	habituation	PBS	CS	R-CS	S2	ictrace14	0.472916667	0.002759925	200
SST	habituation	PBS	CS	R-CS	S4	ictrace12	0.466964286	0.003585723	200
SST	habituation	PBS	CS	R-CS	S2	ictrace19	0.44797619	0.004434672	200
SST	**habituation**	**PBS**	**CS**	**F-CS**	**S4**	**ictrace6**	**0.590357143**	**0.005630078**	**200**
SST	**habituation**	**PBS**	**CS**	**F-CS**	**S2**	**ictrace22**	**0.549821429**	**0.003521554**	**200**
SST	**habituation**	**PBS**	**CS**	**F-CS**	**S2**	**ictrace11**	**0.542857143**	**0.00404061**	**200**
SST	**habituation**	**PBS**	**CS**	**F-CS**	**S2**	**ictrace15**	**0.539761905**	**0.004178928**	**200**
SST	**habituation**	**PBS**	**CS**	**F-CS**	**S2**	**ictrace13**	**0.535654762**	**0.00290571**	**200**
SST	**habituation**	**PBS**	**CS**	**F-CS**	**S2**	**ictrace7**	**0.535119048**	**0.002724799**	**200**
SST	**habituation**	**PBS**	**CS**	**F-CS**	**S2**	**ictrace29**	**0.530952381**	**0.00269374**	**200**
SST	**habituation**	**PBS**	**CS**	**F-CS**	**S2**	**ictrace10**	**0.523630952**	**0.003419877**	**200**
SST	**habituation**	**PBS**	**CS**	**F-CS**	**S2**	**ictrace25**	**0.517857143**	**0.002663316**	**200**
SST	**habituation**	**PBS**	**CS**	**F-CS**	**S4**	**ictrace7**	**0.516607143**	**0.002757305**	**200**
SST	**habituation**	**PBS**	**CS**	**F-CS**	**S2**	**ictrace9**	**0.515714286**	**0.002323351**	**200**
SST	**habituation**	**PBS**	**CS**	**F-CS**	**S2**	**ictrace18**	**0.510595238**	**0.004073612**	**200**
SST	**habituation**	**PBS**	**CS**	**F-CS**	**S2**	**ictrace2**	**0.505654762**	**0.003840958**	**200**
SST	**habituation**	**PBS**	**CS**	**F-CS**	**S4**	**ictrace8**	**0.505**	**0.002176261**	**200**
SST	**habituation**	**PBS**	**CS**	**F-CS**	**S4**	**ictrace3**	**0.501071429**	**0.001554905**	**200**
SST	**habituation**	**PBS**	**CS**	**F-CS**	**S2**	**ictrace8**	**0.500714286**	**0.001128255**	**200**
SST	**habituation**	**PBS**	**CS**	**F-CS**	**S4**	**ictrace5**	**0.500297619**	**0.000968749**	**200**
SST	**habituation**	**PBS**	**CS**	**F-CS**	**S2**	**ictrace16**	**0.5**	**0**	**200**
SST	**habituation**	**PBS**	**CS**	**F-CS**	**S4**	**ictrace10**	**0.499642857**	**0.000618074**	**200**
SST	**habituation**	**PBS**	**CS**	**F-CS**	**S2**	**ictrace21**	**0.49952381**	**0.001599054**	**200**
SST	**habituation**	**PBS**	**CS**	**F-CS**	**S2**	**ictrace19**	**0.499345238**	**0.001628381**	**200**
SST	**habituation**	**PBS**	**CS**	**F-CS**	**S4**	**ictrace4**	**0.499285714**	**0.001008889**	**200**
SST	**habituation**	**PBS**	**CS**	**F-CS**	**S2**	**ictrace4**	**0.498333333**	**0.001554563**	**200**

SST	**habituation**	**PBS**	**CS**	**F-CS**	**S4**	**ictrace12**	**0.497678571**	**0.004140819**	**200**
SST	**habituation**	**PBS**	**CS**	**F-CS**	**S2**	**ictrace1**	**0.492857143**	**0.003392335**	**200**
SST	**habituation**	**PBS**	**CS**	**F-CS**	**S2**	**ictrace12**	**0.492202381**	**0.00233982**	**200**
SST	**habituation**	**PBS**	**CS**	**F-CS**	**S4**	**ictrace1**	**0.49125**	**0.003077418**	**200**
SST	**habituation**	**PBS**	**CS**	**F-CS**	**S2**	**ictrace17**	**0.480714286**	**0.002969707**	**200**
SST	**habituation**	**PBS**	**CS**	**F-CS**	**S4**	**ictrace14**	**0.479464286**	**0.00295341**	**200**
SST	**habituation**	**PBS**	**CS**	**F-CS**	**S2**	**ictrace5**	**0.478511905**	**0.003074216**	**200**
SST	habituation	PBS	CS	F-CS	S2	ictrace3	0.477321429	0.002856644	200
SST	habituation	PBS	CS	F-CS	S2	ictrace6	0.474464286	0.002769486	200
SST	habituation	PBS	CS	F-CS	S2	ictrace24	0.473333333	0.00265831	200
SST	habituation	PBS	CS	F-CS	S4	ictrace9	0.470297619	0.004094613	200
SST	habituation	PBS	CS	F-CS	S2	ictrace14	0.4675	0.003462332	200
SST	habituation	PBS	CS	F-CS	S4	ictrace2	0.456011905	0.004445753	200
SST	**habituation**	**aIC inhibition**	**CS**	**R-CS**	**S2**	**ictrace15**	**0.545**	**0.003937004**	**200**
SST	**habituation**	**aIC inhibition**	**CS**	**R-CS**	**S2**	**ictrace6**	**0.5265**	**0.003277003**	**200**
SST	**habituation**	**aIC inhibition**	**CS**	**R-CS**	**S2**	**ictrace14**	**0.5235**	**0.003080381**	**200**
SST	**habituation**	**aIC inhibition**	**CS**	**R-CS**	**S2**	**ictrace18**	**0.5205**	**0.003106244**	**200**
SST	**habituation**	**aIC inhibition**	**CS**	**R-CS**	**S2**	**ictrace5**	**0.5015**	**0.002288832**	**200**
SST	**habituation**	**aIC inhibition**	**CS**	**R-CS**	**S2**	**ictrace8**	**0.50125**	**0.002793687**	**200**
SST	**habituation**	**aIC inhibition**	**CS**	**R-CS**	**S2**	**ictrace4**	**0.501**	**0.002120142**	**200**
SST	**habituation**	**aIC inhibition**	**CS**	**R-CS**	**S2**	**ictrace10**	**0.5**	**0**	**200**
SST	**habituation**	**aIC inhibition**	**CS**	**R-CS**	**S2**	**ictrace11**	**0.5**	**0**	**200**
SST	**habituation**	**aIC inhibition**	**CS**	**R-CS**	**S2**	**ictrace22**	**0.5**	**0**	**200**
SST	**habituation**	**aIC inhibition**	**CS**	**R-CS**	**S2**	**ictrace3**	**0.5**	**0**	**200**
SST	**habituation**	**aIC inhibition**	**CS**	**R-CS**	**S2**	**ictrace9**	**0.5**	**0**	**200**
SST	**habituation**	**aIC inhibition**	**CS**	**R-CS**	**S2**	**ictrace16**	**0.49875**	**0.002498437**	**200**
SST	**habituation**	**aIC inhibition**	**CS**	**R-CS**	**S2**	**ictrace1**	**0.4985**	**0.002058822**	**200**
SST	**habituation**	**aIC inhibition**	**CS**	**R-CS**	**S2**	**ictrace12**	**0.4975**	**0.001968502**	**200**
SST	habituation	aIC inhibition	CS	R-CS	S2	ictrace19	0.485625	0.004645016	200
SST	habituation	aIC inhibition	CS	R-CS	S2	ictrace17	0.473875	0.003985511	200
SST	habituation	aIC inhibition	CS	R-CS	S2	ictrace7	0.464875	0.003746238	200
SST	habituation	aIC inhibition	CS	R-CS	S2	ictrace20	0.458875	0.00387257	200
SST	**habituation**	**aIC inhibition**	**CS**	**F-CS**	**S2**	**ictrace20**	**0.566666667**	**0.005773503**	**200**
SST	**habituation**	**aIC inhibition**	**CS**	**F-CS**	**S2**	**ictrace12**	**0.536458333**	**0.005195296**	**200**
SST	**habituation**	**aIC inhibition**	**CS**	**F-CS**	**S2**	**ictrace1**	**0.514166667**	**0.005954398**	**200**
SST	**habituation**	**aIC inhibition**	**CS**	**F-CS**	**S2**	**ictrace16**	**0.503333333**	**0.003109126**	**200**
SST	**habituation**	**aIC inhibition**	**CS**	**F-CS**	**S2**	**ictrace6**	**0.503333333**	**0.003527668**	**200**
SST	**habituation**	**aIC inhibition**	**CS**	**F-CS**	**S2**	**ictrace7**	**0.500833333**	**0.003435416**	**200**
SST	**habituation**	**aIC inhibition**	**CS**	**F-CS**	**S2**	**ictrace13**	**0.5**	**0**	**200**
SST	**habituation**	**aIC inhibition**	**CS**	**F-CS**	**S2**	**ictrace18**	**0.5**	**0**	**200**
SST	**habituation**	**aIC inhibition**	**CS**	**F-CS**	**S2**	**ictrace2**	**0.5**	**0**	**200**
SST	**habituation**	**aIC inhibition**	**CS**	**F-CS**	**S2**	**ictrace22**	**0.5**	**0.003333333**	**200**
SST	**habituation**	**aIC inhibition**	**CS**	**F-CS**	**S2**	**ictrace4**	**0.5**	**0**	**200**
SST	**habituation**	**aIC inhibition**	**CS**	**F-CS**	**S2**	**ictrace10**	**0.4975**	**0.003222641**	**200**
SST	**habituation**	**aIC inhibition**	**CS**	**F-CS**	**S2**	**ictrace19**	**0.4975**	**0.004162915**	**200**
SST	**habituation**	**aIC inhibition**	**CS**	**F-CS**	**S2**	**ictrace8**	**0.495**	**0.002910112**	**200**
SST	**habituation**	**aIC inhibition**	**CS**	**F-CS**	**S2**	**ictrace3**	**0.4925**	**0.004132779**	**200**
SST	habituation	aIC inhibition	CS	F-CS	S2	ictrace9	0.460208333	0.006182254	200
SST	habituation	aIC inhibition	CS	F-CS	S2	ictrace17	0.450208333	0.004979973	200
SST	habituation	aIC inhibition	CS	F-CS	S2	ictrace14	0.426666667	0.006629061	200
SST	**RC**	**early**	**CS**	**R-CS**	**S3**	**ictrace7**	**0.530019737**	**0.001704775**	**200**
SST	**RC**	**early**	**CS**	**R-CS**	**S2**	**ictrace10**	**0.524868421**	**0.001481622**	**200**
SST	**RC**	**early**	**CS**	**R-CS**	**S3**	**ictrace10**	**0.522631579**	**0.002138229**	**200**
SST	**RC**	**early**	**CS**	**R-CS**	**S4**	**ictrace8**	**0.520789474**	**0.001388018**	**200**
SST	**RC**	**early**	**CS**	**R-CS**	**S3**	**ictrace9**	**0.520526316**	**0.001333564**	**200**
SST	**RC**	**early**	**CS**	**R-CS**	**S4**	**ictrace16**	**0.518828947**	**0.001974767**	**200**
SST	**RC**	**early**	**CS**	**R-CS**	**S2**	**ictrace13**	**0.517519737**	**0.001630904**	**200**
SST	**RC**	**early**	**CS**	**R-CS**	**S3**	**ictrace1**	**0.517105263**	**0.001692721**	**200**
SST	**RC**	**early**	**CS**	**R-CS**	**S2**	**ictrace9**	**0.514828947**	**0.002477735**	**200**
SST	**RC**	**early**	**CS**	**R-CS**	**S1**	**ictrace4**	**0.512763158**	**0.001019673**	**200**

SST	**RC**	**early**	**CS**	**R-CS**	**S2**	**ictrace7**	**0.511842105**	**0.00092574**	**200**
SST	**RC**	**early**	**CS**	**R-CS**	**S4**	**ictrace2**	**0.510723684**	**0.001968716**	**200**
SST	**RC**	**early**	**CS**	**R-CS**	**S1**	**ictrace3**	**0.510638158**	**0.00247347**	**200**
SST	**RC**	**early**	**CS**	**R-CS**	**S3**	**ictrace14**	**0.510263158**	**0.001326143**	**200**
SST	**RC**	**early**	**CS**	**R-CS**	**S2**	**ictrace8**	**0.507947368**	**0.001253383**	**200**
SST	**RC**	**early**	**CS**	**R-CS**	**S2**	**ictrace11**	**0.506921053**	**0.000846986**	**200**
SST	**RC**	**early**	**CS**	**R-CS**	**S4**	**ictrace15**	**0.506796053**	**0.000842813**	**200**
SST	**RC**	**early**	**CS**	**R-CS**	**S4**	**ictrace11**	**0.505651316**	**0.001664221**	**200**
SST	**RC**	**early**	**CS**	**R-CS**	**S2**	**ictrace17**	**0.503684211**	**0.001611936**	**200**
SST	**RC**	**early**	**CS**	**R-CS**	**S2**	**ictrace14**	**0.503039474**	**0.001239896**	**200**
SST	**RC**	**early**	**CS**	**R-CS**	**S2**	**ictrace15**	**0.503026316**	**0.001686855**	**200**
SST	**RC**	**early**	**CS**	**R-CS**	**S3**	**ictrace3**	**0.502690789**	**0.002078162**	**200**
SST	**RC**	**early**	**CS**	**R-CS**	**S3**	**ictrace4**	**0.502578947**	**0.002593305**	**200**
SST	**RC**	**early**	**CS**	**R-CS**	**S3**	**ictrace8**	**0.502105263**	**0.002058359**	**200**
SST	**RC**	**early**	**CS**	**R-CS**	**S4**	**ictrace1**	**0.501434211**	**0.001846194**	**200**
SST	**RC**	**early**	**CS**	**R-CS**	**S1**	**ictrace5**	**0.500263158**	**0.000455423**	**200**
SST	**RC**	**early**	**CS**	**R-CS**	**S1**	**ictrace6**	**0.5**	**0**	**200**
SST	**RC**	**early**	**CS**	**R-CS**	**S3**	**ictrace2**	**0.499605263**	**0.000347004**	**200**
SST	**RC**	**early**	**CS**	**R-CS**	**S3**	**ictrace12**	**0.499539474**	**0.00155694**	**200**
SST	**RC**	**early**	**CS**	**R-CS**	**S4**	**ictrace7**	**0.499210526**	**0.000555444**	**200**
SST	RC	early	CS	R-CS	S2	ictrace6	0.499092105	0.000631126	200
SST	RC	early	CS	R-CS	S3	ictrace18	0.498684211	0.000550434	200
SST	RC	early	CS	R-CS	S4	ictrace4	0.497947368	0.001585776	200
SST	RC	early	CS	R-CS	S4	ictrace18	0.496842105	0.00143608	200
SST	RC	early	CS	R-CS	S4	ictrace10	0.496519737	0.001112441	200
SST	RC	early	CS	R-CS	S3	ictrace5	0.495131579	0.001524017	200
SST	RC	early	CS	R-CS	S3	ictrace17	0.494855263	0.000997365	200
SST	RC	early	CS	R-CS	S4	ictrace14	0.493947368	0.000924992	200
SST	RC	early	CS	R-CS	S1	ictrace2	0.493730263	0.001546066	200
SST	RC	early	CS	R-CS	S3	ictrace20	0.492236842	0.000926628	200
SST	RC	early	CS	R-CS	S4	ictrace5	0.492105263	0.000930404	200
SST	RC	early	CS	R-CS	S4	ictrace3	0.491539474	0.000911725	200
SST	RC	early	CS	R-CS	S3	ictrace19	0.490348684	0.001594666	200
SST	RC	early	CS	R-CS	S2	ictrace2	0.489875	0.001308605	200
SST	RC	early	CS	R-CS	S4	ictrace13	0.486835526	0.001290195	200
SST	RC	early	CS	R-CS	S4	ictrace6	0.486578947	0.001508259	200
SST	RC	early	CS	R-CS	S1	ictrace7	0.485967105	0.001654348	200
SST	RC	early	CS	R-CS	S3	ictrace11	0.485625	0.001835018	200
SST	RC	early	CS	R-CS	S4	ictrace9	0.484605263	0.001444704	200
SST	RC	early	CS	R-CS	S1	ictrace1	0.483289474	0.002246226	200
SST	RC	early	CS	R-CS	S3	ictrace16	0.481914474	0.002737411	200
SST	RC	early	CS	R-CS	S3	ictrace15	0.481447368	0.002894871	200
SST	RC	early	CS	R-CS	S3	ictrace6	0.469460526	0.002490678	200
SST	**RC**	**early**	**US**	**R-CS**	**S3**	**ictrace6**	**0.6475**	**0.015430287**	**200**
SST	**RC**	**early**	**US**	**R-CS**	**S3**	**ictrace11**	**0.62**	**0.014573092**	**200**
SST	**RC**	**early**	**US**	**R-CS**	**S3**	**ictrace15**	**0.535**	**0.008299096**	**200**
SST	**RC**	**early**	**US**	**R-CS**	**S1**	**ictrace2**	**0.51**	**0.007673005**	**200**
SST	**RC**	**early**	**US**	**R-CS**	**S3**	**ictrace10**	**0.51**	**0.006082763**	**200**
SST	**RC**	**early**	**US**	**R-CS**	**S4**	**ictrace6**	**0.51**	**0.00633443**	**200**
SST	**RC**	**early**	**US**	**R-CS**	**S1**	**ictrace3**	**0.50875**	**0.004099352**	**200**
SST	**RC**	**early**	**US**	**R-CS**	**S4**	**ictrace3**	**0.50875**	**0.00480153**	**200**
SST	**RC**	**early**	**US**	**R-CS**	**S1**	**ictrace5**	**0.5075**	**0.004297528**	**200**
SST	**RC**	**early**	**US**	**R-CS**	**S2**	**ictrace6**	**0.5075**	**0.003495533**	**200**
SST	**RC**	**early**	**US**	**R-CS**	**S3**	**ictrace1**	**0.5075**	**0.004646908**	**200**
SST	**RC**	**early**	**US**	**R-CS**	**S4**	**ictrace8**	**0.5075**	**0.004297528**	**200**
SST	**RC**	**early**	**US**	**R-CS**	**S2**	**ictrace15**	**0.50625**	**0.002759925**	**200**
SST	**RC**	**early**	**US**	**R-CS**	**S4**	**ictrace15**	**0.50625**	**0.006234355**	**200**
SST	**RC**	**early**	**US**	**R-CS**	**S1**	**ictrace1**	**0.505**	**0.00585235**	**200**
SST	**RC**	**early**	**US**	**R-CS**	**S2**	**ictrace10**	**0.505**	**0.00466369**	**200**
SST	**RC**	**early**	**US**	**R-CS**	**S3**	**ictrace3**	**0.505**	**0.00611351**	**200**

SST	**RC**	**early**	**US**	**R-CS**	**S4**	**ictrace11**	**0.505**	**0.004987484**	**200**
SST	**RC**	**early**	**US**	**R-CS**	**S4**	**ictrace4**	**0.505**	**0.003517812**	**200**
SST	**RC**	**early**	**US**	**R-CS**	**S2**	**ictrace17**	**0.50375**	**0.002782479**	**200**
SST	**RC**	**early**	**US**	**R-CS**	**S3**	**ictrace14**	**0.50375**	**0.002782479**	**200**
SST	**RC**	**early**	**US**	**R-CS**	**S3**	**ictrace16**	**0.50375**	**0.002782479**	**200**
SST	**RC**	**early**	**US**	**R-CS**	**S1**	**ictrace7**	**0.5025**	**0.003056755**	**200**
SST	**RC**	**early**	**US**	**R-CS**	**S2**	**ictrace2**	**0.5025**	**0.003056755**	**200**
SST	**RC**	**early**	**US**	**R-CS**	**S3**	**ictrace4**	**0.5025**	**0.005300354**	**200**
SST	**RC**	**early**	**US**	**R-CS**	**S4**	**ictrace16**	**0.5025**	**0.001758906**	**200**
SST	**RC**	**early**	**US**	**R-CS**	**S4**	**ictrace5**	**0.5025**	**0.003948892**	**200**
SST	**RC**	**early**	**US**	**R-CS**	**S4**	**ictrace9**	**0.5025**	**0.001758906**	**200**
SST	**RC**	**early**	**US**	**R-CS**	**S3**	**ictrace17**	**0.50125**	**0.001246871**	**200**
SST	**RC**	**early**	**US**	**R-CS**	**S3**	**ictrace9**	**0.50125**	**0.001246871**	**200**
SST	RC	early	US	R-CS	S4	ictrace2	0.50125	0.002163259	200
SST	RC	early	US	R-CS	S1	ictrace6	0.5	0.003535534	200
SST	RC	early	US	R-CS	S2	ictrace14	0.5	0.001767767	200
SST	RC	early	US	R-CS	S3	ictrace18	0.5	0	200
SST	RC	early	US	R-CS	S3	ictrace20	0.5	0.003535534	200
SST	RC	early	US	R-CS	S4	ictrace10	0.5	0	200
SST	RC	early	US	R-CS	S4	ictrace18	0.5	0.003535534	200
SST	RC	early	US	R-CS	S2	ictrace7	0.49875	0.002793687	200
SST	RC	early	US	R-CS	S4	ictrace13	0.49875	0.001246871	200
SST	RC	early	US	R-CS	S1	ictrace4	0.4975	0.011857224	200
SST	RC	early	US	R-CS	S2	ictrace13	0.4975	0.004326517	200
SST	RC	early	US	R-CS	S4	ictrace14	0.4975	0.004326517	200
SST	RC	early	US	R-CS	S4	ictrace7	0.4975	0.002493742	200
SST	RC	early	US	R-CS	S4	ictrace1	0.49625	0.005147056	200
SST	RC	early	US	R-CS	S2	ictrace8	0.495	0.003517812	200
SST	RC	early	US	R-CS	S3	ictrace2	0.495	0.003041381	200
SST	RC	early	US	R-CS	S3	ictrace8	0.495	0.003517812	200
SST	RC	early	US	R-CS	S2	ictrace11	0.49375	0.005430671	200
SST	RC	early	US	R-CS	S3	ictrace12	0.4775	0.00813749	200
SST	RC	early	US	R-CS	S2	ictrace9	0.4725	0.007024511	200
SST	RC	early	US	R-CS	S3	ictrace19	0.45875	0.009316903	200
SST	RC	early	US	R-CS	S3	ictrace7	0.45375	0.011736362	200
SST	RC	early	US	R-CS	S3	ictrace5	0.4475	0.014207172	200
SST	**RC**	**late**	**CS**	**R-CS**	**S4**	**ictrace6**	**0.527236842**	**0.002520192**	**200**
SST	**RC**	**late**	**CS**	**R-CS**	**S2**	**ictrace29**	**0.524078947**	**0.00217625**	**200**
SST	**RC**	**late**	**CS**	**R-CS**	**S3**	**ictrace2**	**0.521572368**	**0.001148319**	**200**
SST	**RC**	**late**	**CS**	**R-CS**	**S2**	**ictrace7**	**0.521052632**	**0.001392501**	**200**
SST	**RC**	**late**	**CS**	**R-CS**	**S2**	**ictrace3**	**0.520526316**	**0.001333564**	**200**
SST	**RC**	**late**	**CS**	**R-CS**	**S2**	**ictrace23**	**0.517177632**	**0.001778804**	**200**
SST	**RC**	**late**	**CS**	**R-CS**	**S2**	**ictrace35**	**0.517164474**	**0.000881102**	**200**
SST	**RC**	**late**	**CS**	**R-CS**	**S4**	**ictrace8**	**0.51625**	**0.002985317**	**200**
SST	**RC**	**late**	**CS**	**R-CS**	**S1**	**ictrace3**	**0.516052632**	**0.001272852**	**200**
SST	**RC**	**late**	**CS**	**R-CS**	**S2**	**ictrace27**	**0.513756579**	**0.00176786**	**200**
SST	**RC**	**late**	**CS**	**R-CS**	**S2**	**ictrace2**	**0.513460526**	**0.001856562**	**200**
SST	**RC**	**late**	**CS**	**R-CS**	**S2**	**ictrace19**	**0.510526316**	**0.000911606**	**200**
SST	**RC**	**late**	**CS**	**R-CS**	**S4**	**ictrace2**	**0.509967105**	**0.002631158**	**200**
SST	**RC**	**late**	**CS**	**R-CS**	**S3**	**ictrace1**	**0.508026316**	**0.000896235**	**200**
SST	**RC**	**late**	**CS**	**R-CS**	**S4**	**ictrace3**	**0.507210526**	**0.001106318**	**200**
SST	**RC**	**late**	**CS**	**R-CS**	**S2**	**ictrace22**	**0.506842105**	**0.000877544**	**200**
SST	**RC**	**late**	**CS**	**R-CS**	**S2**	**ictrace5**	**0.506789474**	**0.000862391**	**200**
SST	**RC**	**late**	**CS**	**R-CS**	**S2**	**ictrace33**	**0.506631579**	**0.001902939**	**200**
SST	**RC**	**late**	**CS**	**R-CS**	**S2**	**ictrace14**	**0.506315789**	**0.000916152**	**200**
SST	**RC**	**late**	**CS**	**R-CS**	**S2**	**ictrace6**	**0.506105263**	**0.00202082**	**200**
SST	**RC**	**late**	**CS**	**R-CS**	**S2**	**ictrace25**	**0.505973684**	**0.001416624**	**200**
SST	**RC**	**late**	**CS**	**R-CS**	**S2**	**ictrace12**	**0.505355263**	**0.001844019**	**200**
SST	**RC**	**late**	**CS**	**R-CS**	**S4**	**ictrace17**	**0.505243421**	**0.001479619**	**200**
SST	**RC**	**late**	**CS**	**R-CS**	**S2**	**ictrace4**	**0.504842105**	**0.001342549**	**200**

SST	**RC**	**late**	**CS**	**R-CS**	**S1**	**ictrace2**	**0.504743421**	**0.001369682**	**200**
SST	**RC**	**late**	**CS**	**R-CS**	**S2**	**ictrace10**	**0.502756579**	**0.001284954**	**200**
SST	**RC**	**late**	**CS**	**R-CS**	**S2**	**ictrace21**	**0.502309211**	**0.000742314**	**200**
SST	**RC**	**late**	**CS**	**R-CS**	**S4**	**ictrace4**	**0.502105263**	**0.001657686**	**200**
SST	**RC**	**late**	**CS**	**R-CS**	**S2**	**ictrace17**	**0.501585526**	**0.001290725**	**200**
SST	**RC**	**late**	**CS**	**R-CS**	**S4**	**ictrace14**	**0.5015**	**0.001112991**	**200**
SST	RC	late	CS	R-CS	S4	ictrace9	0.500394737	0.001154263	200
SST	RC	late	CS	R-CS	S2	ictrace11	0.50025	0.000467373	200
SST	RC	late	CS	R-CS	S1	ictrace1	0.500131579	0.000436299	200
SST	RC	late	CS	R-CS	S2	ictrace1	0.5	0.000467707	200
SST	RC	late	CS	R-CS	S4	ictrace7	0.5	0.000353553	200
SST	RC	late	CS	R-CS	S2	ictrace16	0.499605263	0.000435504	200
SST	RC	late	CS	R-CS	S2	ictrace8	0.49925	0.000583899	200
SST	RC	late	CS	R-CS	S4	ictrace11	0.496144737	0.00168792	200
SST	RC	late	CS	R-CS	S1	ictrace6	0.496013158	0.000749648	200
SST	RC	late	CS	R-CS	S2	ictrace31	0.494105263	0.00104632	200
SST	RC	late	CS	R-CS	S2	ictrace15	0.493717105	0.000915228	200
SST	RC	late	CS	R-CS	S2	ictrace34	0.492434211	0.000907263	200
SST	RC	late	CS	R-CS	S4	ictrace12	0.492368421	0.000959534	200
SST	RC	late	CS	R-CS	S2	ictrace32	0.491769737	0.001113262	200
SST	RC	late	CS	R-CS	S4	ictrace5	0.490921053	0.000941456	200
SST	RC	late	CS	R-CS	S2	ictrace20	0.489986842	0.001092374	200
SST	RC	late	CS	R-CS	S2	ictrace30	0.489335526	0.001258434	200
SST	RC	late	CS	R-CS	S4	ictrace10	0.488730263	0.001226637	200
SST	RC	late	CS	R-CS	S2	ictrace28	0.487894737	0.001016485	200
SST	RC	late	CS	R-CS	S4	ictrace18	0.486578947	0.00170561	200
SST	RC	late	CS	R-CS	S2	ictrace18	0.486532895	0.001601483	200
SST	RC	late	CS	R-CS	S4	ictrace15	0.485789474	0.001439452	200
SST	RC	late	CS	R-CS	S2	ictrace13	0.485453947	0.001348386	200
SST	RC	late	CS	R-CS	S2	ictrace9	0.482578947	0.001717729	200
SST	RC	late	CS	R-CS	S4	ictrace13	0.481973684	0.001847525	200
SST	RC	late	CS	R-CS	S4	ictrace16	0.481934211	0.001952334	200
SST	RC	late	CS	R-CS	S4	ictrace1	0.478401316	0.001702925	200
SST	RC	late	CS	R-CS	S2	ictrace26	0.471434211	0.002470596	200
SST	**RC**	**late**	**US**	**R-CS**	**S2**	**ictrace26**	**0.733333333**	**0.021858128**	**200**
SST	**RC**	**late**	**US**	**R-CS**	**S2**	**ictrace34**	**0.520833333**	**0.013990944**	**200**
SST	**RC**	**late**	**US**	**R-CS**	**S4**	**ictrace8**	**0.520833333**	**0.007064927**	**200**
SST	**RC**	**late**	**US**	**R-CS**	**S4**	**ictrace9**	**0.520833333**	**0.008411096**	**200**
SST	**RC**	**late**	**US**	**R-CS**	**S4**	**ictrace1**	**0.516666667**	**0.00781736**	**200**
SST	**RC**	**late**	**US**	**R-CS**	**S4**	**ictrace6**	**0.516666667**	**0.006346478**	**200**
SST	**RC**	**late**	**US**	**R-CS**	**S2**	**ictrace22**	**0.5125**	**0.007162547**	**200**
SST	**RC**	**late**	**US**	**R-CS**	**S2**	**ictrace25**	**0.5125**	**0.016113206**	**200**
SST	**RC**	**late**	**US**	**R-CS**	**S4**	**ictrace13**	**0.5125**	**0.005519851**	**200**
SST	**RC**	**late**	**US**	**R-CS**	**S2**	**ictrace19**	**0.508333333**	**0.015800404**	**200**
SST	**RC**	**late**	**US**	**R-CS**	**S2**	**ictrace21**	**0.508333333**	**0.004526159**	**200**
SST	**RC**	**late**	**US**	**R-CS**	**S2**	**ictrace23**	**0.508333333**	**0.004526159**	**200**
SST	**RC**	**late**	**US**	**R-CS**	**S2**	**ictrace28**	**0.508333333**	**0.013680379**	**200**
SST	**RC**	**late**	**US**	**R-CS**	**S2**	**ictrace35**	**0.508333333**	**0.011164801**	**200**
SST	**RC**	**late**	**US**	**R-CS**	**S2**	**ictrace4**	**0.508333333**	**0.004526159**	**200**
SST	**RC**	**late**	**US**	**R-CS**	**S2**	**ictrace9**	**0.508333333**	**0.00642802**	**200**
SST	**RC**	**late**	**US**	**R-CS**	**S3**	**ictrace1**	**0.508333333**	**0.00642802**	**200**
SST	**RC**	**late**	**US**	**R-CS**	**S4**	**ictrace11**	**0.508333333**	**0.015800404**	**200**
SST	**RC**	**late**	**US**	**R-CS**	**S4**	**ictrace2**	**0.508333333**	**0.00642802**	**200**
SST	**RC**	**late**	**US**	**R-CS**	**S2**	**ictrace12**	**0.504166667**	**0.015475675**	**200**
SST	**RC**	**late**	**US**	**R-CS**	**S2**	**ictrace14**	**0.504166667**	**0.013304004**	**200**
SST	**RC**	**late**	**US**	**R-CS**	**S2**	**ictrace15**	**0.504166667**	**0.00321401**	**200**
SST	**RC**	**late**	**US**	**R-CS**	**S3**	**ictrace2**	**0.504166667**	**0.00321401**	**200**
SST	**RC**	**late**	**US**	**R-CS**	**S4**	**ictrace16**	**0.504166667**	**0.007210862**	**200**
SST	**RC**	**late**	**US**	**R-CS**	**S1**	**ictrace1**	**0.5**	**0**	**200**
SST	**RC**	**late**	**US**	**R-CS**	**S1**	**ictrace2**	**0.5**	**0**	**200**

SST	**RC**	**late**	**US**	**R-CS**	**S1**	**ictrace3**	**0.5**	**0**	**200**
SST	**RC**	**late**	**US**	**R-CS**	**S2**	**ictrace13**	**0.5**	**0**	**200**
SST	**RC**	**late**	**US**	**R-CS**	**S2**	**ictrace16**	**0.5**	**0**	**200**
SST	**RC**	**late**	**US**	**R-CS**	**S2**	**ictrace27**	**0.5**	**0.006454972**	**200**
SST	RC	late	US	R-CS	S2	ictrace29	0.5	0.006454972	200
SST	RC	late	US	R-CS	S2	ictrace32	0.5	0.007905694	200
SST	RC	late	US	R-CS	S2	ictrace5	0.5	0.007905694	200
SST	RC	late	US	R-CS	S2	ictrace8	0.5	0.004564355	200
SST	RC	late	US	R-CS	S4	ictrace12	0.5	0.012909944	200
SST	RC	late	US	R-CS	S4	ictrace4	0.5	0	200
SST	RC	late	US	R-CS	S4	ictrace5	0.5	0	200
SST	RC	late	US	R-CS	S4	ictrace7	0.5	0.004564355	200
SST	RC	late	US	R-CS	S2	ictrace1	0.495833333	0.00321401	200
SST	RC	late	US	R-CS	S2	ictrace11	0.495833333	0.00321401	200
SST	RC	late	US	R-CS	S2	ictrace17	0.495833333	0.00321401	200
SST	RC	late	US	R-CS	S2	ictrace30	0.495833333	0.0055824	200
SST	RC	late	US	R-CS	S2	ictrace7	0.495833333	0.00321401	200
SST	RC	late	US	R-CS	S4	ictrace14	0.495833333	0.00321401	200
SST	RC	late	US	R-CS	S4	ictrace17	0.495833333	0.0140652	200
SST	RC	late	US	R-CS	S1	ictrace6	0.491666667	0.00642802	200
SST	RC	late	US	R-CS	S2	ictrace20	0.491666667	0.007883703	200
SST	RC	late	US	R-CS	S2	ictrace31	0.491666667	0.004526159	200
SST	RC	late	US	R-CS	S2	ictrace33	0.491666667	0.00642802	200
SST	RC	late	US	R-CS	S4	ictrace18	0.491666667	0.004526159	200
SST	RC	late	US	R-CS	S4	ictrace3	0.491666667	0.00642802	200
SST	RC	late	US	R-CS	S2	ictrace3	0.4875	0.005519851	200
SST	RC	late	US	R-CS	S4	ictrace15	0.4875	0.014763765	200
SST	RC	late	US	R-CS	S2	ictrace2	0.479166667	0.014716653	200
SST	RC	late	US	R-CS	S4	ictrace10	0.458333333	0.01553446	200
SST	RC	late	US	R-CS	S2	ictrace10	0.454166667	0.016454377	200
SST	RC	late	US	R-CS	S2	ictrace6	0.445833333	0.016327274	200
SST	RC	late	US	R-CS	S2	ictrace18	0.433333333	0.018219343	200
SST	**FC**	**early**	**CS**	**F-CS**	**S2**	**ictrace32**	**0.597916667**	**0.006460013**	**200**
SST	**FC**	**early**	**CS**	**F-CS**	**S2**	**ictrace3**	**0.576875**	**0.006187868**	**200**
SST	**FC**	**early**	**CS**	**F-CS**	**S2**	**ictrace26**	**0.575416667**	**0.005708409**	**200**
SST	**FC**	**early**	**CS**	**F-CS**	**S2**	**ictrace9**	**0.575**	**0.006095308**	**200**
SST	**FC**	**early**	**CS**	**F-CS**	**S2**	**ictrace19**	**0.566666667**	**0.005773503**	**200**
SST	**FC**	**early**	**CS**	**F-CS**	**S2**	**ictrace22**	**0.566666667**	**0.005773503**	**200**
SST	**FC**	**early**	**CS**	**F-CS**	**S1**	**ictrace4**	**0.564583333**	**0.00637888**	**200**
SST	**FC**	**early**	**CS**	**F-CS**	**S2**	**ictrace20**	**0.561666667**	**0.005795712**	**200**
SST	**FC**	**early**	**CS**	**F-CS**	**S4**	**ictrace8**	**0.545**	**0.005491155**	**200**
SST	**FC**	**early**	**CS**	**F-CS**	**S2**	**ictrace10**	**0.54125**	**0.005128471**	**200**
SST	**FC**	**early**	**CS**	**F-CS**	**S2**	**ictrace13**	**0.536666667**	**0.005532103**	**200**
SST	**FC**	**early**	**CS**	**F-CS**	**S2**	**ictrace18**	**0.533958333**	**0.004921938**	**200**
SST	**FC**	**early**	**CS**	**F-CS**	**S4**	**ictrace3**	**0.525625**	**0.005398025**	**200**
SST	**FC**	**early**	**CS**	**F-CS**	**S4**	**ictrace6**	**0.5075**	**0.0082114**	**200**
SST	**FC**	**early**	**CS**	**F-CS**	**S2**	**ictrace8**	**0.505**	**0.003097938**	**200**
SST	**FC**	**early**	**CS**	**F-CS**	**S2**	**ictrace6**	**0.5025**	**0.002758195**	**200**
SST	**FC**	**early**	**CS**	**F-CS**	**S4**	**ictrace12**	**0.5025**	**0.003628112**	**200**
SST	**FC**	**early**	**CS**	**F-CS**	**S4**	**ictrace4**	**0.5025**	**0.003431371**	**200**
SST	**FC**	**early**	**CS**	**F-CS**	**S4**	**ictrace7**	**0.501875**	**0.002416981**	**200**
SST	**FC**	**early**	**CS**	**F-CS**	**S2**	**ictrace16**	**0.501666667**	**0.00311582**	**200**
SST	**FC**	**early**	**CS**	**F-CS**	**S4**	**ictrace2**	**0.501666667**	**0.003906903**	**200**
SST	**FC**	**early**	**CS**	**F-CS**	**S1**	**ictrace6**	**0.501666667**	**0.003331249**	**200**
SST	**FC**	**early**	**CS**	**F-CS**	**S3**	**ictrace8**	**0.501041667**	**0.003206405**	**200**
SST	**FC**	**early**	**CS**	**F-CS**	**S3**	**ictrace5**	**0.500833333**	**0.003996092**	**200**
SST	**FC**	**early**	**CS**	**F-CS**	**S2**	**ictrace17**	**0.500208333**	**0.002724272**	**200**
SST	**FC**	**early**	**CS**	**F-CS**	**S2**	**ictrace28**	**0.5**	**0**	**200**
SST	**FC**	**early**	**CS**	**F-CS**	**S2**	**ictrace5**	**0.5**	**0**	**200**
SST	**FC**	**early**	**CS**	**F-CS**	**S2**	**ictrace7**	**0.5**	**0**	**200**

SST	**FC**	**early**	**CS**	**F-CS**	**S4**	**ictrace15**	**0.5**	**0**	**200**
SST	**FC**	**early**	**CS**	**F-CS**	**S1**	**ictrace5**	**0.5**	**0.002795085**	**200**
SST	FC	early	CS	F-CS	S3	ictrace2	0.5	0	200
SST	FC	early	CS	F-CS	S3	ictrace3	0.5	0	200
SST	FC	early	CS	F-CS	S3	ictrace4	0.5	0	200
SST	FC	early	CS	F-CS	S3	ictrace6	0.5	0	200
SST	FC	early	CS	F-CS	S3	ictrace7	0.5	0	200
SST	FC	early	CS	F-CS	S2	ictrace21	0.499375	0.002253036	200
SST	FC	early	CS	F-CS	S4	ictrace1	0.499166667	0.003004048	200
SST	FC	early	CS	F-CS	S2	ictrace12	0.498333333	0.00311582	200
SST	FC	early	CS	F-CS	S2	ictrace15	0.4975	0.003431371	200
SST	FC	early	CS	F-CS	S4	ictrace9	0.496666667	0.003719319	200
SST	FC	early	CS	F-CS	S1	ictrace2	0.496666667	0.00332499	200
SST	FC	early	CS	F-CS	S3	ictrace1	0.495833333	0.002990146	200
SST	FC	early	CS	F-CS	S2	ictrace11	0.493541667	0.002932953	200
SST	FC	early	CS	F-CS	S1	ictrace7	0.491666667	0.008312474	200
SST	FC	early	CS	F-CS	S2	ictrace1	0.49	0.003659083	200
SST	FC	early	CS	F-CS	S2	ictrace2	0.455208333	0.004990768	200
SST	FC	early	CS	F-CS	S2	ictrace33	0.455208333	0.005965304	200
SST	FC	early	CS	F-CS	S4	ictrace5	0.454166667	0.00576598	200
SST	FC	early	CS	F-CS	S2	ictrace14	0.453541667	0.005699183	200
SST	FC	early	CS	F-CS	S2	ictrace31	0.447083333	0.005587918	200
SST	FC	early	CS	F-CS	S4	ictrace11	0.441666667	0.005743354	200
SST	FC	early	CS	F-CS	S2	ictrace25	0.439583333	0.011187131	200
SST	FC	early	CS	F-CS	S2	ictrace4	0.417916667	0.007659814	200
SST	**FC**	**early**	**US**	**F-CS**	**S2**	**ictrace7**	**0.6**	**0.00942809**	**200**
SST	**FC**	**early**	**US**	**F-CS**	**S3**	**ictrace6**	**0.6**	**0.00942809**	**200**
SST	**FC**	**early**	**US**	**F-CS**	**S2**	**ictrace15**	**0.591666667**	**0.005400617**	**200**
SST	**FC**	**early**	**US**	**F-CS**	**S2**	**ictrace18**	**0.591666667**	**0.005400617**	**200**
SST	**FC**	**early**	**US**	**F-CS**	**S2**	**ictrace21**	**0.591666667**	**0.005400617**	**200**
SST	**FC**	**early**	**US**	**F-CS**	**S3**	**ictrace7**	**0.591666667**	**0.009204468**	**200**
SST	**FC**	**early**	**US**	**F-CS**	**S2**	**ictrace33**	**0.583333333**	**0.010540926**	**200**
SST	**FC**	**early**	**US**	**F-CS**	**S2**	**ictrace13**	**0.566666667**	**0.005773503**	**200**
SST	**FC**	**early**	**US**	**F-CS**	**S2**	**ictrace9**	**0.566666667**	**0.005773503**	**200**
SST	**FC**	**early**	**US**	**F-CS**	**S2**	**ictrace1**	**0.558333333**	**0.005137012**	**200**
SST	**FC**	**early**	**US**	**F-CS**	**S2**	**ictrace11**	**0.558333333**	**0.005137012**	**200**
SST	**FC**	**early**	**US**	**F-CS**	**S2**	**ictrace5**	**0.558333333**	**0.005137012**	**200**
SST	**FC**	**early**	**US**	**F-CS**	**S2**	**ictrace8**	**0.558333333**	**0.005137012**	**200**
SST	**FC**	**early**	**US**	**F-CS**	**S4**	**ictrace12**	**0.558333333**	**0.005137012**	**200**
SST	**FC**	**early**	**US**	**F-CS**	**S4**	**ictrace8**	**0.558333333**	**0.005137012**	**200**
SST	**FC**	**early**	**US**	**F-CS**	**S3**	**ictrace8**	**0.558333333**	**0.005137012**	**200**
SST	**FC**	**early**	**US**	**F-CS**	**S4**	**ictrace2**	**0.508333333**	**0.003486083**	**200**
SST	**FC**	**early**	**US**	**F-CS**	**S2**	**ictrace32**	**0.504166667**	**0.003807431**	**200**
SST	**FC**	**early**	**US**	**F-CS**	**S4**	**ictrace6**	**0.504166667**	**0.00321401**	**200**
SST	**FC**	**early**	**US**	**F-CS**	**S1**	**ictrace6**	**0.504166667**	**0.003807431**	**200**
SST	**FC**	**early**	**US**	**F-CS**	**S2**	**ictrace16**	**0.503333333**	**0.003527668**	**200**
SST	**FC**	**early**	**US**	**F-CS**	**S2**	**ictrace20**	**0.501875**	**0.002416981**	**200**
SST	**FC**	**early**	**US**	**F-CS**	**S1**	**ictrace5**	**0.501875**	**0.002861039**	**200**
SST	**FC**	**early**	**US**	**F-CS**	**S1**	**ictrace7**	**0.501666667**	**0.004080782**	**200**
SST	**FC**	**early**	**US**	**F-CS**	**S2**	**ictrace3**	**0.500833333**	**0.003631938**	**200**
SST	**FC**	**early**	**US**	**F-CS**	**S4**	**ictrace1**	**0.500625**	**0.002253036**	**200**
SST	**FC**	**early**	**US**	**F-CS**	**S4**	**ictrace15**	**0.500625**	**0.002863769**	**200**
SST	**FC**	**early**	**US**	**F-CS**	**S1**	**ictrace4**	**0.500625**	**0.002997069**	**200**
SST	**FC**	**early**	**US**	**F-CS**	**S2**	**ictrace10**	**0.5**	**0.002165064**	**200**
SST	**FC**	**early**	**US**	**F-CS**	**S2**	**ictrace12**	**0.5**	**0.00390868**	**200**
SST	FC	early	US	F-CS	S2	ictrace14	0.5	0	200
SST	FC	early	US	F-CS	S2	ictrace31	0.5	0	200
SST	FC	early	US	F-CS	S2	ictrace6	0.5	0	200
SST	FC	early	US	F-CS	S4	ictrace7	0.5	0	200
SST	FC	early	US	F-CS	S1	ictrace2	0.5	0	200

SST	FC	early	US	F-CS	S3	ictrace2	0.5	0	200
SST	FC	early	US	F-CS	S3	ictrace3	0.5	0	200
SST	FC	early	US	F-CS	S2	ictrace28	0.499166667	0.003226948	200
SST	FC	early	US	F-CS	S4	ictrace4	0.499166667	0.003631938	200
SST	FC	early	US	F-CS	S2	ictrace17	0.49875	0.002793687	200
SST	FC	early	US	F-CS	S3	ictrace1	0.498333333	0.003724916	200
SST	FC	early	US	F-CS	S3	ictrace4	0.498333333	0.003533569	200
SST	FC	early	US	F-CS	S2	ictrace4	0.498125	0.002573528	200
SST	FC	early	US	F-CS	S4	ictrace5	0.495	0.009366014	200
SST	FC	early	US	F-CS	S2	ictrace25	0.479166667	0.006030881	200
SST	FC	early	US	F-CS	S2	ictrace19	0.474166667	0.00581515	200
SST	FC	early	US	F-CS	S2	ictrace22	0.471666667	0.006781306	200
SST	FC	early	US	F-CS	S2	ictrace26	0.453333333	0.006363961	200
SST	FC	early	US	F-CS	S4	ictrace11	0.441666667	0.005137012	200
SST	FC	early	US	F-CS	S4	ictrace3	0.441666667	0.005137012	200
SST	FC	early	US	F-CS	S4	ictrace9	0.441666667	0.005137012	200
SST	FC	early	US	F-CS	S2	ictrace2	0.433333333	0.005773503	200
SST	FC	early	US	F-CS	S3	ictrace5	0.4	0.00942809	200
SST	**FC**	**late**	**CS**	**F-CS**	**S2**	**ictrace32**	**0.591666667**	**0.005400617**	**200**
SST	**FC**	**late**	**CS**	**F-CS**	**S4**	**ictrace3**	**0.566666667**	**0.005773503**	**200**
SST	**FC**	**late**	**CS**	**F-CS**	**S2**	**ictrace22**	**0.558333333**	**0.005137012**	**200**
SST	**FC**	**late**	**CS**	**F-CS**	**S2**	**ictrace6**	**0.512291667**	**0.006365581**	**200**
SST	**FC**	**late**	**CS**	**F-CS**	**S2**	**ictrace4**	**0.505833333**	**0.002465737**	**200**
SST	**FC**	**late**	**CS**	**F-CS**	**S2**	**ictrace31**	**0.5025**	**0.003814719**	**200**
SST	**FC**	**late**	**CS**	**F-CS**	**S2**	**ictrace2**	**0.501666667**	**0.003533569**	**200**
SST	**FC**	**late**	**CS**	**F-CS**	**S2**	**ictrace15**	**0.50125**	**0.001765556**	**200**
SST	**FC**	**late**	**CS**	**F-CS**	**S2**	**ictrace1**	**0.5**	**0**	**200**
SST	**FC**	**late**	**CS**	**F-CS**	**S2**	**ictrace12**	**0.5**	**0.003535534**	**200**
SST	**FC**	**late**	**CS**	**F-CS**	**S2**	**ictrace18**	**0.5**	**0**	**200**
SST	**FC**	**late**	**CS**	**F-CS**	**S2**	**ictrace23**	**0.5**	**0.001530931**	**200**
SST	**FC**	**late**	**CS**	**F-CS**	**S2**	**ictrace29**	**0.5**	**0**	**200**
SST	**FC**	**late**	**CS**	**F-CS**	**S2**	**ictrace3**	**0.5**	**0**	**200**
SST	**FC**	**late**	**CS**	**F-CS**	**S2**	**ictrace35**	**0.5**	**0.001976424**	**200**
SST	**FC**	**late**	**CS**	**F-CS**	**S4**	**ictrace10**	**0.5**	**0**	**200**
SST	**FC**	**late**	**CS**	**F-CS**	**S4**	**ictrace15**	**0.5**	**0**	**200**
SST	**FC**	**late**	**CS**	**F-CS**	**S2**	**ictrace14**	**0.49875**	**0.002163259**	**200**
SST	**FC**	**late**	**CS**	**F-CS**	**S4**	**ictrace9**	**0.49875**	**0.002930177**	**200**
SST	**FC**	**late**	**CS**	**F-CS**	**S4**	**ictrace2**	**0.498333333**	**0.003533569**	**200**
SST	**FC**	**late**	**CS**	**F-CS**	**S2**	**ictrace21**	**0.4975**	**0.002999421**	**200**
SST	**FC**	**late**	**CS**	**F-CS**	**S2**	**ictrace7**	**0.4975**	**0.003628112**	**200**
SST	**FC**	**late**	**CS**	**F-CS**	**S4**	**ictrace8**	**0.495833333**	**0.00321401**	**200**
SST	**FC**	**late**	**CS**	**F-CS**	**S4**	**ictrace4**	**0.495625**	**0.006662743**	**200**
SST	**FC**	**late**	**CS**	**F-CS**	**S2**	**ictrace10**	**0.494166667**	**0.003796471**	**200**
SST	**FC**	**late**	**CS**	**F-CS**	**S2**	**ictrace5**	**0.493958333**	**0.00529017**	**200**
SST	**FC**	**late**	**CS**	**F-CS**	**S2**	**ictrace20**	**0.4925**	**0.004919138**	**200**
SST	**FC**	**late**	**CS**	**F-CS**	**S2**	**ictrace8**	**0.488333333**	**0.002963317**	**200**
SST	**FC**	**late**	**CS**	**F-CS**	**S4**	**ictrace6**	**0.481666667**	**0.006049851**	**200**
SST	**FC**	**late**	**CS**	**F-CS**	**S2**	**ictrace11**	**0.479166667**	**0.004279716**	**200**
SST	FC	late	CS	F-CS	S2	ictrace9	0.472291667	0.004576486	200
SST	FC	late	CS	F-CS	S4	ictrace11	0.452916667	0.005346582	200
SST	FC	late	CS	F-CS	S4	ictrace1	0.450416667	0.004959821	200
SST	FC	late	CS	F-CS	S4	ictrace5	0.449583333	0.005065457	200
SST	FC	late	CS	F-CS	S2	ictrace13	0.445833333	0.005644257	200
SST	**FC**	**late**	**US**	**F-CS**	**S2**	**ictrace31**	**0.625**	**0.004564355**	**200**
SST	**FC**	**late**	**US**	**F-CS**	**S2**	**ictrace29**	**0.616666667**	**0.007071068**	**200**
SST	**FC**	**late**	**US**	**F-CS**	**S2**	**ictrace1**	**0.591666667**	**0.005400617**	**200**
SST	**FC**	**late**	**US**	**F-CS**	**S2**	**ictrace12**	**0.591666667**	**0.005400617**	**200**
SST	**FC**	**late**	**US**	**F-CS**	**S4**	**ictrace11**	**0.583333333**	**0.010540926**	**200**
SST	**FC**	**late**	**US**	**F-CS**	**S2**	**ictrace35**	**0.566666667**	**0.005773503**	**200**
SST	**FC**	**late**	**US**	**F-CS**	**S4**	**ictrace15**	**0.566666667**	**0.005773503**	**200**

SST	**FC**	**late**	**US**	**F-CS**	**S4**	**ictrace3**	**0.566666667**	**0.005773503**	**200**
SST	**FC**	**late**	**US**	**F-CS**	**S2**	**ictrace11**	**0.558333333**	**0.005137012**	**200**
SST	**FC**	**late**	**US**	**F-CS**	**S2**	**ictrace5**	**0.558333333**	**0.005137012**	**200**
SST	**FC**	**late**	**US**	**F-CS**	**S2**	**ictrace8**	**0.558333333**	**0.005137012**	**200**
SST	**FC**	**late**	**US**	**F-CS**	**S4**	**ictrace10**	**0.558333333**	**0.005137012**	**200**
SST	**FC**	**late**	**US**	**F-CS**	**S2**	**ictrace22**	**0.505833333**	**0.003411073**	**200**
SST	**FC**	**late**	**US**	**F-CS**	**S2**	**ictrace13**	**0.5025**	**0.009481524**	**200**
SST	**FC**	**late**	**US**	**F-CS**	**S2**	**ictrace15**	**0.501666667**	**0.003331249**	**200**
SST	**FC**	**late**	**US**	**F-CS**	**S2**	**ictrace14**	**0.50125**	**0.002650177**	**200**
SST	**FC**	**late**	**US**	**F-CS**	**S2**	**ictrace10**	**0.5**	**0**	**200**
SST	**FC**	**late**	**US**	**F-CS**	**S2**	**ictrace23**	**0.5**	**0.002338536**	**200**
SST	**FC**	**late**	**US**	**F-CS**	**S4**	**ictrace8**	**0.5**	**0**	**200**
SST	**FC**	**late**	**US**	**F-CS**	**S4**	**ictrace9**	**0.5**	**0.002635231**	**200**
SST	**FC**	**late**	**US**	**F-CS**	**S4**	**ictrace2**	**0.499375**	**0.002723953**	**200**
SST	**FC**	**late**	**US**	**F-CS**	**S2**	**ictrace3**	**0.49875**	**0.002650177**	**200**
SST	**FC**	**late**	**US**	**F-CS**	**S2**	**ictrace18**	**0.498333333**	**0.003533569**	**200**
SST	**FC**	**late**	**US**	**F-CS**	**S2**	**ictrace21**	**0.4975**	**0.002331845**	**200**
SST	**FC**	**late**	**US**	**F-CS**	**S2**	**ictrace4**	**0.495**	**0.003517812**	**200**
SST	**FC**	**late**	**US**	**F-CS**	**S2**	**ictrace7**	**0.495**	**0.003097938**	**200**
SST	**FC**	**late**	**US**	**F-CS**	**S4**	**ictrace1**	**0.475**	**0.005651942**	**200**
SST	**FC**	**late**	**US**	**F-CS**	**S2**	**ictrace20**	**0.474166667**	**0.006163006**	**200**
SST	**FC**	**late**	**US**	**F-CS**	**S2**	**ictrace32**	**0.470208333**	**0.006410288**	**200**
SST	**FC**	**late**	**US**	**F-CS**	**S2**	**ictrace2**	**0.460833333**	**0.006559292**	**200**
SST	FC	late	US	F-CS	S4	ictrace4	0.441666667	0.005137012	200
SST	FC	late	US	F-CS	S4	ictrace5	0.441666667	0.005137012	200
SST	FC	late	US	F-CS	S2	ictrace6	0.44125	0.010454888	200
SST	FC	late	US	F-CS	S2	ictrace9	0.433333333	0.005773503	200
SST	FC	late	US	F-CS	S4	ictrace6	0.375	0.004564355	200
SST	**recall**	**PBS**	**CS**	**R-CS**	**S4**	**ictrace9**	**0.611904762**	**0.006153737**	**200**
SST	**recall**	**PBS**	**CS**	**R-CS**	**S3**	**ictrace5**	**0.575**	**0.003819741**	**200**
SST	**recall**	**PBS**	**CS**	**R-CS**	**S4**	**ictrace15t2**	**0.569**	**0.007949528**	**200**
SST	**recall**	**PBS**	**CS**	**R-CS**	**S4**	**ictrace18t2**	**0.565**	**0.003807887**	**200**
SST	**recall**	**PBS**	**CS**	**R-CS**	**S2**	**ictrace2t2**	**0.56**	**0.003464102**	**200**
SST	**recall**	**PBS**	**CS**	**R-CS**	**S4**	**ictrace10**	**0.556071429**	**0.004939106**	**200**
SST	**recall**	**PBS**	**CS**	**R-CS**	**S2**	**ictrace20t2**	**0.550875**	**0.003862389**	**200**
SST	**recall**	**PBS**	**CS**	**R-CS**	**S3**	**ictrace3**	**0.550178571**	**0.009729504**	**200**
SST	**recall**	**PBS**	**CS**	**R-CS**	**S2**	**ictrace18**	**0.55**	**0.002886751**	**200**
SST	**recall**	**PBS**	**CS**	**R-CS**	**S2**	**ictrace24**	**0.549821429**	**0.004105053**	**200**
SST	**recall**	**PBS**	**CS**	**R-CS**	**S2**	**ictrace10**	**0.545238095**	**0.004137654**	**200**
SST	**recall**	**PBS**	**CS**	**R-CS**	**S2**	**ictrace12**	**0.545238095**	**0.002629848**	**200**
SST	**recall**	**PBS**	**CS**	**R-CS**	**S4**	**ictrace9t2**	**0.545**	**0.003937004**	**200**
SST	**recall**	**PBS**	**CS**	**R-CS**	**S1**	**ictrace10**	**0.533452381**	**0.002737306**	**200**
SST	**recall**	**PBS**	**CS**	**R-CS**	**S3**	**ictrace1**	**0.533214286**	**0.004542248**	**200**
SST	**recall**	**PBS**	**CS**	**R-CS**	**S2**	**ictrace5**	**0.530952381**	**0.00269374**	**200**
SST	**recall**	**PBS**	**CS**	**R-CS**	**S4**	**ictrace23t2**	**0.5285**	**0.003191982**	**200**
SST	**recall**	**PBS**	**CS**	**R-CS**	**S2**	**ictrace15**	**0.528035714**	**0.002775237**	**200**
SST	**recall**	**PBS**	**CS**	**R-CS**	**S2**	**ictrace4t2**	**0.526375**	**0.003889881**	**200**
SST	**recall**	**PBS**	**CS**	**R-CS**	**S2**	**ictrace9t2**	**0.524**	**0.003258834**	**200**
SST	**recall**	**PBS**	**CS**	**R-CS**	**S2**	**ictrace3t2**	**0.524**	**0.003181195**	**200**
SST	**recall**	**PBS**	**CS**	**R-CS**	**S2**	**ictrace21**	**0.518928571**	**0.00260166**	**200**
SST	**recall**	**PBS**	**CS**	**R-CS**	**S4**	**ictrace7t2**	**0.5125**	**0.003803781**	**200**
SST	**recall**	**PBS**	**CS**	**R-CS**	**S2**	**ictrace4**	**0.506428571**	**0.003241551**	**200**
SST	**recall**	**PBS**	**CS**	**R-CS**	**S2**	**ictrace1**	**0.506071429**	**0.003264587**	**200**
SST	**recall**	**PBS**	**CS**	**R-CS**	**S4**	**ictrace6t2**	**0.50475**	**0.002280282**	**200**
SST	**recall**	**PBS**	**CS**	**R-CS**	**S4**	**ictrace20t2**	**0.503125**	**0.002567449**	**200**
SST	**recall**	**PBS**	**CS**	**R-CS**	**S2**	**ictrace6**	**0.502857143**	**0.001414214**	**200**
SST	**recall**	**PBS**	**CS**	**R-CS**	**S2**	**ictrace7t2**	**0.501875**	**0.002068646**	**200**
SST	**recall**	**PBS**	**CS**	**R-CS**	**S2**	**ictrace12t2**	**0.5015**	**0.001933585**	**200**
SST	recall	PBS	CS	R-CS	S4	ictrace16t2	0.5015	0.002176867	200
SST	recall	PBS	CS	R-CS	S2	ictrace15t2	0.501	0.001412445	200

SST	recall	PBS	CS	R-CS	S4	ictrace8	0.500892857	0.001924999	200
SST	recall	PBS	CS	R-CS	S4	ictrace1	0.500833333	0.002123774	200
SST	recall	PBS	CS	R-CS	S2	ictrace13	0.500714286	0.001596393	200
SST	recall	PBS	CS	R-CS	S1	ictrace4t2	0.5005	0.002397655	200
SST	recall	PBS	CS	R-CS	S2	ictrace16	0.500357143	0.001556545	200
SST	recall	PBS	CS	R-CS	S4	ictrace3	0.500357143	0.001287449	200
SST	recall	PBS	CS	R-CS	S1	ictrace3	0.500357143	0.001636439	200
SST	recall	PBS	CS	R-CS	S2	ictrace10t2	0.50025	0.007409854	200
SST	recall	PBS	CS	R-CS	S2	ictrace9	0.5	0	200
SST	recall	PBS	CS	R-CS	S4	ictrace15	0.5	0.001749636	200
SST	recall	PBS	CS	R-CS	S4	ictrace4	0.5	0	200
SST	recall	PBS	CS	R-CS	S1	ictrace2	0.5	0	200
SST	recall	PBS	CS	R-CS	S3	ictrace7	0.5	0	200
SST	recall	PBS	CS	R-CS	S2	ictrace23t2	0.5	0.000707107	200
SST	recall	PBS	CS	R-CS	S2	ictrace26t2	0.5	0	200
SST	recall	PBS	CS	R-CS	S4	ictrace19t2	0.5	0.002236068	200
SST	recall	PBS	CS	R-CS	S4	ictrace2t2	0.5	0.0025	200
SST	recall	PBS	CS	R-CS	S4	ictrace8t2	0.5	0.001870829	200
SST	recall	PBS	CS	R-CS	S3	ictrace2t2	0.5	0	200
SST	recall	PBS	CS	R-CS	S2	ictrace16t2	0.4995	0.000865303	200
SST	recall	PBS	CS	R-CS	S4	ictrace5t2	0.4995	0.001657935	200
SST	recall	PBS	CS	R-CS	S1	ictrace4t2	0.499166667	0.001766785	200
SST	recall	PBS	CS	R-CS	S4	ictrace14t2	0.499	0.00223495	200
SST	recall	PBS	CS	R-CS	S4	ictrace21t2	0.499	0.001869492	200
SST	recall	PBS	CS	R-CS	S4	ictrace4t2	0.499	0.00458203	200
SST	recall	PBS	CS	R-CS	S4	ictrace17t2	0.4985	0.001737815	200
SST	recall	PBS	CS	R-CS	S3	ictrace3t2	0.498	0.002327552	200
SST	recall	PBS	CS	R-CS	S2	ictrace8	0.497559524	0.001586725	200
SST	recall	PBS	CS	R-CS	S2	ictrace25	0.497142857	0.001584362	200
SST	recall	PBS	CS	R-CS	S2	ictrace2	0.496785714	0.001620776	200
SST	recall	PBS	CS	R-CS	S2	ictrace28t2	0.496	0.002433105	200
SST	recall	PBS	CS	R-CS	S4	ictrace5	0.495416667	0.001881701	200
SST	recall	PBS	CS	R-CS	S4	ictrace7	0.492619048	0.001905803	200
SST	recall	PBS	CS	R-CS	S2	ictrace27t2	0.49	0.004394599	200
SST	recall	PBS	CS	R-CS	S2	ictrace21t2	0.487875	0.004680336	200
SST	recall	PBS	CS	R-CS	S2	ictrace8t2	0.48725	0.0031074	200
SST	recall	PBS	CS	R-CS	S2	ictrace11t2	0.480375	0.003325458	200
SST	recall	PBS	CS	R-CS	S4	ictrace2	0.479047619	0.002599003	200
SST	recall	PBS	CS	R-CS	S2	ictrace20	0.478452381	0.002538521	200
SST	recall	PBS	CS	R-CS	S4	ictrace6	0.476607143	0.002683695	200
SST	recall	PBS	CS	R-CS	S2	ictrace28	0.476369048	0.002679864	200
SST	recall	PBS	CS	R-CS	S2	ictrace14	0.475178571	0.002636277	200
SST	recall	PBS	CS	R-CS	S2	ictrace22t2	0.4745	0.003807722	200
SST	recall	PBS	CS	R-CS	S4	ictrace12t2	0.474	0.003757659	200
SST	recall	PBS	CS	R-CS	S3	ictrace4	0.47375	0.002791022	200
SST	recall	PBS	CS	R-CS	S2	ictrace17t2	0.473	0.004105484	200
SST	recall	PBS	CS	R-CS	S2	ictrace19	0.472083333	0.00278123	200
SST	recall	PBS	CS	R-CS	S2	ictrace7	0.471785714	0.002708575	200
SST	recall	PBS	CS	R-CS	S2	ictrace22	0.470119048	0.003622639	200
SST	recall	PBS	CS	R-CS	S2	ictrace5t2	0.469125	0.003652814	200
SST	recall	PBS	CS	R-CS	S2	ictrace14t2	0.469	0.003419795	200
SST	recall	PBS	CS	R-CS	S2	ictrace24t2	0.469	0.003492134	200
SST	recall	PBS	CS	R-CS	S4	ictrace1t2	0.46725	0.004024884	200
SST	recall	PBS	CS	R-CS	S1	ictrace3t2	0.466	0.003423449	200
SST	recall	PBS	CS	R-CS	S4	ictrace13t2	0.4655	0.003846914	200
SST	recall	PBS	CS	R-CS	S4	ictrace3t2	0.4645	0.003938432	200
SST	recall	PBS	CS	R-CS	S4	ictrace25t2	0.464	0.003847239	200
SST	recall	PBS	CS	R-CS	S2	ictrace6t2	0.46225	0.00392504	200
SST	recall	PBS	CS	R-CS	S4	ictrace10t2	0.46125	0.003876008	200
SST	recall	PBS	CS	R-CS	S2	ictrace1t2	0.4605	0.00463128	200

SST	recall	PBS	CS	R-CS	S2	ictrace13t2	0.4595	0.003919343	200
SST	recall	PBS	CS	R-CS	S2	ictrace19t2	0.45075	0.004831246	200
SST	recall	PBS	CS	R-CS	S4	ictrace11t2	0.4275	0.005654091	200
SST	**recall**	**PBS**	**CS**	**F-CS**	**S4**	**ictrace2**	**0.566428571**	**0.00430416**	**200**
SST	**recall**	**PBS**	**CS**	**F-CS**	**S3**	**ictrace7**	**0.564285714**	**0.004377328**	**200**
SST	**recall**	**PBS**	**CS**	**F-CS**	**S3**	**ictrace4**	**0.561904762**	**0.004338302**	**200**
SST	**recall**	**PBS**	**CS**	**F-CS**	**S2**	**ictrace22t2**	**0.548690476**	**0.002952513**	**200**
SST	**recall**	**PBS**	**CS**	**F-CS**	**S2**	**ictrace21**	**0.548333333**	**0.002732448**	**200**
SST	**recall**	**PBS**	**CS**	**F-CS**	**S3**	**ictrace5**	**0.547619048**	**0.002766417**	**200**
SST	**recall**	**PBS**	**CS**	**F-CS**	**S4**	**ictrace15t2**	**0.547619048**	**0.002766417**	**200**
SST	**recall**	**PBS**	**CS**	**F-CS**	**S3**	**ictrace3t2**	**0.547619048**	**0.002766417**	**200**
SST	**recall**	**PBS**	**CS**	**F-CS**	**S4**	**ictrace11t2**	**0.54702381**	**0.003010222**	**200**
SST	**recall**	**PBS**	**CS**	**F-CS**	**S2**	**ictrace19t2**	**0.54577381**	**0.004669564**	**200**
SST	**recall**	**PBS**	**CS**	**F-CS**	**S4**	**ictrace2t2**	**0.541964286**	**0.003378664**	**200**
SST	**recall**	**PBS**	**CS**	**F-CS**	**S2**	**ictrace15**	**0.537321429**	**0.002727305**	**200**
SST	**recall**	**PBS**	**CS**	**F-CS**	**S4**	**ictrace9t2**	**0.536785714**	**0.004241831**	**200**
SST	**recall**	**PBS**	**CS**	**F-CS**	**S2**	**ictrace23t2**	**0.536488095**	**0.002808461**	**200**
SST	**recall**	**PBS**	**CS**	**F-CS**	**S2**	**ictrace16t2**	**0.53577381**	**0.002808991**	**200**
SST	**recall**	**PBS**	**CS**	**F-CS**	**S4**	**ictrace19t2**	**0.535595238**	**0.003886855**	**200**
SST	**recall**	**PBS**	**CS**	**F-CS**	**S4**	**ictrace3t2**	**0.535119048**	**0.004157942**	**200**
SST	**recall**	**PBS**	**CS**	**F-CS**	**S4**	**ictrace13t2**	**0.533869048**	**0.002743392**	**200**
SST	**recall**	**PBS**	**CS**	**F-CS**	**S4**	**ictrace8**	**0.530952381**	**0.00269374**	**200**
SST	**recall**	**PBS**	**CS**	**F-CS**	**S2**	**ictrace17t2**	**0.530952381**	**0.00269374**	**200**
SST	**recall**	**PBS**	**CS**	**F-CS**	**S2**	**ictrace20t2**	**0.530952381**	**0.00269374**	**200**
SST	**recall**	**PBS**	**CS**	**F-CS**	**S2**	**ictrace21t2**	**0.530952381**	**0.00269374**	**200**
SST	**recall**	**PBS**	**CS**	**F-CS**	**S2**	**ictrace16**	**0.52375**	**0.002787466**	**200**
SST	**recall**	**PBS**	**CS**	**F-CS**	**S2**	**ictrace17**	**0.52125**	**0.002763697**	**200**
SST	**recall**	**PBS**	**CS**	**F-CS**	**S4**	**ictrace14t2**	**0.520119048**	**0.004544431**	**200**
SST	**recall**	**PBS**	**CS**	**F-CS**	**S2**	**ictrace22**	**0.518511905**	**0.00246388**	**200**
SST	**recall**	**PBS**	**CS**	**F-CS**	**S2**	**ictrace9**	**0.517440476**	**0.002582095**	**200**
SST	**recall**	**PBS**	**CS**	**F-CS**	**S4**	**ictrace5**	**0.517321429**	**0.002599763**	**200**
SST	**recall**	**PBS**	**CS**	**F-CS**	**S2**	**ictrace10**	**0.516666667**	**0.002442653**	**200**
SST	**recall**	**PBS**	**CS**	**F-CS**	**S2**	**ictrace12t2**	**0.516309524**	**0.002599099**	**200**
SST	recall	PBS	CS	F-CS	S4	ictrace6	0.513392857	0.002532299	200
SST	recall	PBS	CS	F-CS	S2	ictrace5	0.509821429	0.003562924	200
SST	recall	PBS	CS	F-CS	S2	ictrace28	0.50952381	0.003198816	200
SST	recall	PBS	CS	F-CS	S4	ictrace1t2	0.507559524	0.003783559	200
SST	recall	PBS	CS	F-CS	S2	ictrace13	0.503809524	0.003244741	200
SST	recall	PBS	CS	F-CS	S3	ictrace3	0.503214286	0.001454891	200
SST	recall	PBS	CS	F-CS	S3	ictrace1	0.502916667	0.001705536	200
SST	recall	PBS	CS	F-CS	S2	ictrace24t2	0.502916667	0.00180446	200
SST	recall	PBS	CS	F-CS	S2	ictrace13t2	0.5025	0.001758906	200
SST	recall	PBS	CS	F-CS	S2	ictrace3	0.502083333	0.001495073	200
SST	recall	PBS	CS	F-CS	S4	ictrace8t2	0.501666667	0.001662495	200
SST	recall	PBS	CS	F-CS	S2	ictrace5t2	0.50125	0.001715685	200
SST	recall	PBS	CS	F-CS	S4	ictrace24t2	0.50125	0.001611321	200
SST	recall	PBS	CS	F-CS	S2	ictrace4t2	0.500833333	0.001316297	200
SST	recall	PBS	CS	F-CS	S2	ictrace18	0.500357143	0.001556545	200
SST	recall	PBS	CS	F-CS	S2	ictrace12	0.500297619	0.003795022	200
SST	recall	PBS	CS	F-CS	S2	ictrace2	0.5	0.001767767	200
SST	recall	PBS	CS	F-CS	S2	ictrace8	0.5	0	200
SST	recall	PBS	CS	F-CS	S2	ictrace2t2	0.5	0	200
SST	recall	PBS	CS	F-CS	S2	ictrace6t2	0.5	0	200
SST	recall	PBS	CS	F-CS	S4	ictrace6t2	0.5	0	200
SST	recall	PBS	CS	F-CS	S4	ictrace7t2	0.5	0	200
SST	recall	PBS	CS	F-CS	S4	ictrace5t2	0.499642857	0.001287449	200
SST	recall	PBS	CS	F-CS	S2	ictrace6	0.499583333	0.001502024	200
SST	recall	PBS	CS	F-CS	S4	ictrace7	0.499583333	0.000931229	200
SST	recall	PBS	CS	F-CS	S4	ictrace18t2	0.499583333	0.001613474	200
SST	recall	PBS	CS	F-CS	S2	ictrace14t2	0.499166667	0.001862458	200

SST	recall	PBS	CS	F-CS	S1	ictrace2	0.49875	0.001499711	200
SST	recall	PBS	CS	F-CS	S4	ictrace16t2	0.498630952	0.003145401	200
SST	recall	PBS	CS	F-CS	S4	ictrace12t2	0.498333333	0.004313764	200
SST	recall	PBS	CS	F-CS	S2	ictrace25	0.497916667	0.001810224	200
SST	recall	PBS	CS	F-CS	S2	ictrace10t2	0.497738095	0.001707389	200
SST	recall	PBS	CS	F-CS	S4	ictrace9	0.496607143	0.001912887	200
SST	recall	PBS	CS	F-CS	S2	ictrace11	0.496488095	0.003037228	200
SST	recall	PBS	CS	F-CS	S2	ictrace7t2	0.493154762	0.002181265	200
SST	recall	PBS	CS	F-CS	S2	ictrace7	0.49202381	0.002172595	200
SST	recall	PBS	CS	F-CS	S2	ictrace20	0.490833333	0.002554272	200
SST	recall	PBS	CS	F-CS	S2	ictrace19	0.487738095	0.004544837	200
SST	recall	PBS	CS	F-CS	S2	ictrace26	0.48625	0.003083882	200
SST	recall	PBS	CS	F-CS	S4	ictrace23t2	0.486190476	0.002151833	200
SST	recall	PBS	CS	F-CS	S4	ictrace17t2	0.481904762	0.002665923	200
SST	recall	PBS	CS	F-CS	S2	ictrace26t2	0.480238095	0.003022778	200
SST	recall	PBS	CS	F-CS	S2	ictrace9t2	0.479285714	0.002453132	200
SST	recall	PBS	CS	F-CS	S4	ictrace22t2	0.47922619	0.002822204	200
SST	recall	PBS	CS	F-CS	S2	ictrace27t2	0.477559524	0.004334361	200
SST	recall	PBS	CS	F-CS	S2	ictrace8t2	0.476428571	0.003144029	200
SST	recall	PBS	CS	F-CS	S2	ictrace14	0.47625	0.002909366	200
SST	recall	PBS	CS	F-CS	S4	ictrace21t2	0.476071429	0.002584992	200
SST	recall	PBS	CS	F-CS	S2	ictrace15t2	0.476011905	0.002979138	200
SST	recall	PBS	CS	F-CS	S2	ictrace28t2	0.475714286	0.002547508	200
SST	recall	PBS	CS	F-CS	S4	ictrace4t2	0.475595238	0.002688144	200
SST	recall	PBS	CS	F-CS	S2	ictrace3t2	0.475297619	0.00255736	200
SST	recall	PBS	CS	F-CS	S4	ictrace20t2	0.475178571	0.002701329	200
SST	recall	PBS	CS	F-CS	S4	ictrace3	0.474166667	0.002788244	200
SST	recall	PBS	CS	F-CS	S2	ictrace24	0.473809524	0.002808363	200
SST	recall	PBS	CS	F-CS	S4	ictrace10t2	0.46577381	0.00360199	200
SST	recall	PBS	CS	F-CS	S4	ictrace15	0.465714286	0.004239633	200
SST	recall	PBS	CS	F-CS	S4	ictrace1	0.458333333	0.00417601	200
SST	recall	PBS	CS	F-CS	S4	ictrace10	0.438630952	0.006484598	200
SST	**recall**	**aIC inhibition**	**CS**	**R-CS**	**S2**	**ictrace12**	**0.547619048**	**0.004641331**	**200**
SST	**recall**	**aIC inhibition**	**CS**	**R-CS**	**S2**	**ictrace12t2**	**0.545**	**0.003937004**	**200**
SST	**recall**	**aIC inhibition**	**CS**	**R-CS**	**S2**	**ictrace1t2**	**0.54**	**0.003464102**	**200**
SST	**recall**	**aIC inhibition**	**CS**	**R-CS**	**S2**	**ictrace15t2**	**0.54**	**0.003464102**	**200**
SST	**recall**	**aIC inhibition**	**CS**	**R-CS**	**S2**	**ictrace18t2**	**0.54**	**0.003464102**	**200**
SST	**recall**	**aIC inhibition**	**CS**	**R-CS**	**S2**	**ictrace20t2**	**0.54**	**0.003464102**	**200**
SST	**recall**	**aIC inhibition**	**CS**	**R-CS**	**S2**	**ictrace21t2**	**0.54**	**0.003464102**	**200**
SST	**recall**	**aIC inhibition**	**CS**	**R-CS**	**S2**	**ictrace3t2**	**0.54**	**0.003464102**	**200**
SST	**recall**	**aIC inhibition**	**CS**	**R-CS**	**S2**	**ictrace17**	**0.537380952**	**0.002908809**	**200**
SST	**recall**	**aIC inhibition**	**CS**	**R-CS**	**S2**	**ictrace9t2**	**0.531375**	**0.004190754**	**200**
SST	**recall**	**aIC inhibition**	**CS**	**R-CS**	**S2**	**ictrace22t2**	**0.5295**	**0.003719711**	**200**
SST	**recall**	**aIC inhibition**	**CS**	**R-CS**	**S2**	**ictrace29t2**	**0.518625**	**0.005684402**	**200**
SST	**recall**	**aIC inhibition**	**CS**	**R-CS**	**S2**	**ictrace9**	**0.509047619**	**0.004819767**	**200**
SST	**recall**	**aIC inhibition**	**CS**	**R-CS**	**S2**	**ictrace13**	**0.503333333**	**0.001848423**	**200**
SST	**recall**	**aIC inhibition**	**CS**	**R-CS**	**S2**	**ictrace15**	**0.503214286**	**0.0027801**	**200**
SST	recall	aIC inhibition	CS	R-CS	S1	ictrace5	0.502083333	0.001810224	200
SST	recall	aIC inhibition	CS	R-CS	S2	ictrace16t2	0.502	0.002231591	200
SST	recall	aIC inhibition	CS	R-CS	S2	ictrace6t2	0.502	0.002231591	200
SST	recall	aIC inhibition	CS	R-CS	S1	ictrace3t2	0.501875	0.002721084	200
SST	recall	aIC inhibition	CS	R-CS	S2	ictrace2	0.501666667	0.001950783	200
SST	recall	aIC inhibition	CS	R-CS	S1	ictrace9t2	0.5015	0.002058822	200
SST	recall	aIC inhibition	CS	R-CS	S2	ictrace14t2	0.501	0.00199875	200
SST	recall	aIC inhibition	CS	R-CS	S2	ictrace17t2	0.5005	0.00206125	200
SST	recall	aIC inhibition	CS	R-CS	S2	ictrace19	0.50047619	0.001649229	200
SST	recall	aIC inhibition	CS	R-CS	S2	ictrace5	0.500416667	0.002083125	200
SST	recall	aIC inhibition	CS	R-CS	S2	ictrace8	0.5	0	200
SST	recall	aIC inhibition	CS	R-CS	S2	ictrace10t2	0.5	0.001732051	200
SST	recall	aIC inhibition	CS	R-CS	S2	ictrace11t2	0.5	0	200

SST	recall	aIC inhibition	CS	R-CS	S2	ictrace2t2	0.5	0	200
SST	recall	aIC inhibition	CS	R-CS	S2	ictrace1	0.499940476	0.001291811	200
SST	recall	aIC inhibition	CS	R-CS	S1	ictrace7t2	0.4995	0.001802429	200
SST	recall	aIC inhibition	CS	R-CS	S1	ictrace2	0.498928571	0.001470587	200
SST	recall	aIC inhibition	CS	R-CS	S2	ictrace23t2	0.497	0.002225983	200
SST	recall	aIC inhibition	CS	R-CS	S2	ictrace7	0.496904762	0.003255076	200
SST	recall	aIC inhibition	CS	R-CS	S2	ictrace25t2	0.4965	0.00238511	200
SST	recall	aIC inhibition	CS	R-CS	S2	ictrace4	0.495595238	0.003264934	200
SST	recall	aIC inhibition	CS	R-CS	S2	ictrace14	0.494345238	0.00325039	200
SST	recall	aIC inhibition	CS	R-CS	S2	ictrace10	0.4875	0.002109109	200
SST	recall	aIC inhibition	CS	R-CS	S2	ictrace26t2	0.482	0.003965318	200
SST	recall	aIC inhibition	CS	R-CS	S2	ictrace19t2	0.480875	0.003561853	200
SST	recall	aIC inhibition	CS	R-CS	S2	ictrace6	0.480238095	0.002606083	200
SST	recall	aIC inhibition	CS	R-CS	S2	ictrace11	0.477857143	0.002602818	200
SST	recall	aIC inhibition	CS	R-CS	S1	ictrace3	0.475952381	0.00274063	200
SST	recall	aIC inhibition	CS	R-CS	S2	ictrace18	0.475416667	0.002574124	200
SST	recall	aIC inhibition	CS	R-CS	S2	ictrace3	0.47297619	0.004547798	200
SST	recall	aIC inhibition	CS	R-CS	S2	ictrace13t2	0.4705	0.003376203	200
SST	recall	aIC inhibition	CS	R-CS	S2	ictrace16	0.468452381	0.00501892	200
SST	recall	aIC inhibition	CS	R-CS	S2	ictrace27t2	0.46225	0.003897074	200
SST	recall	aIC inhibition	CS	R-CS	S2	ictrace7t2	0.459	0.004713809	200
SST	recall	aIC inhibition	CS	R-CS	S2	ictrace4t2	0.449625	0.004248079	200
SST	**recall**	**aIC inhibition**	**CS**	**F-CS**	**S2**	**ictrace12**	**0.547440476**	**0.002702247**	**200**
SST	**recall**	**aIC inhibition**	**CS**	**F-CS**	**S2**	**ictrace8**	**0.533333333**	**0.002886751**	**200**
SST	**recall**	**aIC inhibition**	**CS**	**F-CS**	**S2**	**ictrace4**	**0.53172619**	**0.003185806**	**200**
SST	**recall**	**aIC inhibition**	**CS**	**F-CS**	**S2**	**ictrace14t2**	**0.525**	**0.003535534**	**200**
SST	**recall**	**aIC inhibition**	**CS**	**F-CS**	**S2**	**ictrace17**	**0.518452381**	**0.002475432**	**200**
SST	**recall**	**aIC inhibition**	**CS**	**F-CS**	**S2**	**ictrace19t2**	**0.511375**	**0.00287118**	**200**
SST	**recall**	**aIC inhibition**	**CS**	**F-CS**	**S2**	**ictrace25t2**	**0.50975**	**0.005522086**	**200**
SST	**recall**	**aIC inhibition**	**CS**	**F-CS**	**S2**	**ictrace14**	**0.508333333**	**0.002282177**	**200**
SST	**recall**	**aIC inhibition**	**CS**	**F-CS**	**S2**	**ictrace2**	**0.503928571**	**0.002634035**	**200**
SST	**recall**	**aIC inhibition**	**CS**	**F-CS**	**S2**	**ictrace8t2**	**0.502**	**0.001865476**	**200**
SST	**recall**	**aIC inhibition**	**CS**	**F-CS**	**S2**	**ictrace29t2**	**0.5015**	**0.001933585**	**200**
SST	**recall**	**aIC inhibition**	**CS**	**F-CS**	**S2**	**ictrace4t2**	**0.5015**	**0.00421174**	**200**
SST	**recall**	**aIC inhibition**	**CS**	**F-CS**	**S1**	**ictrace1t2**	**0.5015**	**0.002395569**	**200**
SST	**recall**	**aIC inhibition**	**CS**	**F-CS**	**S2**	**ictrace21t2**	**0.50125**	**0.002336865**	**200**
SST	**recall**	**aIC inhibition**	**CS**	**F-CS**	**S1**	**ictrace3t2**	**0.501**	**0.002344142**	**200**
SST	**recall**	**aIC inhibition**	**CS**	**F-CS**	**S2**	**ictrace9t2**	**0.501**	**0.002448469**	**200**
SST	**recall**	**aIC inhibition**	**CS**	**F-CS**	**S2**	**ictrace11t2**	**0.5005**	**0.002179163**	**200**
SST	**recall**	**aIC inhibition**	**CS**	**F-CS**	**S1**	**ictrace3**	**0.5**	**0**	**200**
SST	**recall**	**aIC inhibition**	**CS**	**F-CS**	**S2**	**ictrace10t2**	**0.5**	**0**	**200**
SST	**recall**	**aIC inhibition**	**CS**	**F-CS**	**S2**	**ictrace27t2**	**0.5**	**0**	**200**
SST	recall	aIC inhibition	CS	F-CS	S2	ictrace3t2	0.5	0.001	200
SST	recall	aIC inhibition	CS	F-CS	S2	ictrace5t2	0.5	0	200
SST	recall	aIC inhibition	CS	F-CS	S2	ictrace13t2	0.499875	0.001463061	200
SST	recall	aIC inhibition	CS	F-CS	S2	ictrace1t2	0.4995	0.00206125	200
SST	recall	aIC inhibition	CS	F-CS	S2	ictrace16t2	0.4995	0.000865303	200
SST	recall	aIC inhibition	CS	F-CS	S2	ictrace17t2	0.4995	0.002179163	200
SST	recall	aIC inhibition	CS	F-CS	S1	ictrace7t2	0.4995	0.00206125	200
SST	recall	aIC inhibition	CS	F-CS	S2	ictrace15	0.499285714	0.001674387	200
SST	recall	aIC inhibition	CS	F-CS	S2	ictrace6	0.499166667	0.001766785	200
SST	recall	aIC inhibition	CS	F-CS	S2	ictrace6t2	0.4985	0.002176867	200
SST	recall	aIC inhibition	CS	F-CS	S2	ictrace22t2	0.498	0.001407125	200
SST	recall	aIC inhibition	CS	F-CS	S2	ictrace23t2	0.498	0.001726268	200
SST	recall	aIC inhibition	CS	F-CS	S1	ictrace8	0.4975	0.003566057	200
SST	recall	aIC inhibition	CS	F-CS	S2	ictrace3	0.497321429	0.003331672	200
SST	recall	aIC inhibition	CS	F-CS	S2	ictrace7	0.496785714	0.001841798	200
SST	recall	aIC inhibition	CS	F-CS	S2	ictrace13	0.4875	0.002618709	200
SST	recall	aIC inhibition	CS	F-CS	S2	ictrace18	0.48625	0.002501555	200
SST	recall	aIC inhibition	CS	F-CS	S2	ictrace5	0.481785714	0.003036193	200

SST	recall	aIC inhibition	CS	F-CS	S2	ictrace16	0.480357143	0.002887672	200
SST	recall	aIC inhibition	CS	F-CS	S2	ictrace26t2	0.47775	0.00393617	200
SST	recall	aIC inhibition	CS	F-CS	S2	ictrace11	0.477202381	0.00263762	200
SST	recall	aIC inhibition	CS	F-CS	S2	ictrace20t2	0.476875	0.003321039	200
SST	recall	aIC inhibition	CS	F-CS	S2	ictrace10	0.476428571	0.002725073	200
SST	recall	aIC inhibition	CS	F-CS	S1	ictrace5t2	0.476	0.003481379	200
SST	recall	aIC inhibition	CS	F-CS	S2	ictrace1	0.475238095	0.002759184	200
SST	recall	aIC inhibition	CS	F-CS	S2	ictrace18t2	0.4705	0.003449456	200
SST	recall	aIC inhibition	CS	F-CS	S2	ictrace15t2	0.46825	0.004219412	200
SST	recall	aIC inhibition	CS	F-CS	S2	ictrace12t2	0.468	0.004472695	200
SST	recall	aIC inhibition	CS	F-CS	S2	ictrace7t2	0.468	0.003925716	200
SST	recall	aIC inhibition	CS	F-CS	S2	ictrace9	0.459821429	0.003163664	200
PKCd	**habituation**	**PBS**	**CS**	**R-CS**	**P3**	**ictrace4**	**0.58**	**0.005291503**	**200**
PKCd	**habituation**	**PBS**	**CS**	**R-CS**	**P2**	**ictrace6**	**0.545**	**0.003937004**	**200**
PKCd	**habituation**	**PBS**	**CS**	**R-CS**	**P3**	**ictrace5**	**0.545**	**0.003937004**	**200**
PKCd	**habituation**	**PBS**	**CS**	**R-CS**	**P4**	**ictrace1**	**0.5445**	**0.005199639**	**200**
PKCd	**habituation**	**PBS**	**CS**	**R-CS**	**P1**	**ictrace7**	**0.520875**	**0.00331086**	**200**
PKCd	**habituation**	**PBS**	**CS**	**R-CS**	**P4**	**ictrace5**	**0.5115**	**0.005358521**	**200**
PKCd	**habituation**	**PBS**	**CS**	**R-CS**	**P3**	**ictrace8**	**0.504375**	**0.002400765**	**200**
PKCd	**habituation**	**PBS**	**CS**	**R-CS**	**P1**	**ictrace9**	**0.504**	**0.002218107**	**200**
PKCd	**habituation**	**PBS**	**CS**	**R-CS**	**P1**	**ictrace4**	**0.5015**	**0.002288832**	**200**
PKCd	**habituation**	**PBS**	**CS**	**R-CS**	**P3**	**ictrace3**	**0.5015**	**0.006873045**	**200**
PKCd	**habituation**	**PBS**	**CS**	**R-CS**	**P2**	**ictrace11**	**0.501**	**0.001869492**	**200**
PKCd	**habituation**	**PBS**	**CS**	**R-CS**	**P4**	**ictrace4**	**0.501**	**0.00223495**	**200**
PKCd	**habituation**	**PBS**	**CS**	**R-CS**	**P2**	**ictrace5**	**0.5005**	**0.005717189**	**200**
PKCd	**habituation**	**PBS**	**CS**	**R-CS**	**P1**	**ictrace5**	**0.5**	**0**	**200**
PKCd	**habituation**	**PBS**	**CS**	**R-CS**	**P2**	**ictrace4**	**0.5**	**0**	**200**
PKCd	**habituation**	**PBS**	**CS**	**R-CS**	**P3**	**ictrace17**	**0.5**	**0.0025**	**200**
PKCd	**habituation**	**PBS**	**CS**	**R-CS**	**P3**	**ictrace27**	**0.5**	**0**	**200**
PKCd	**habituation**	**PBS**	**CS**	**R-CS**	**P4**	**ictrace10**	**0.5**	**0**	**200**
PKCd	**habituation**	**PBS**	**CS**	**R-CS**	**P2**	**ictrace1**	**0.4995**	**0.00206125**	**200**
PKCd	**habituation**	**PBS**	**CS**	**R-CS**	**P2**	**ictrace8**	**0.498**	**0.002116601**	**200**
PKCd	**habituation**	**PBS**	**CS**	**R-CS**	**P3**	**ictrace29**	**0.498**	**0.001865476**	**200**
PKCd	**habituation**	**PBS**	**CS**	**R-CS**	**P2**	**ictrace7**	**0.4975**	**0.001311011**	**200**
PKCd	**habituation**	**PBS**	**CS**	**R-CS**	**P3**	**ictrace9**	**0.4975**	**0.001928406**	**200**
PKCd	**habituation**	**PBS**	**CS**	**R-CS**	**P1**	**ictrace1**	**0.495**	**0.002524876**	**200**
PKCd	**habituation**	**PBS**	**CS**	**R-CS**	**P1**	**ictrace14**	**0.492**	**0.002275961**	**200**
PKCd	**habituation**	**PBS**	**CS**	**R-CS**	**P2**	**ictrace3**	**0.4875**	**0.002543374**	**200**
PKCd	**habituation**	**PBS**	**CS**	**R-CS**	**P1**	**ictrace2**	**0.483875**	**0.004046208**	**200**
PKCd	**habituation**	**PBS**	**CS**	**R-CS**	**P4**	**ictrace2**	**0.4805**	**0.003853408**	**200**
PKCd	**habituation**	**PBS**	**CS**	**R-CS**	**P1**	**ictrace6**	**0.475125**	**0.004166449**	**200**
PKCd	**habituation**	**PBS**	**CS**	**R-CS**	**P1**	**ictrace12**	**0.4735**	**0.003352424**	**200**
PKCd	habituation	PBS	CS	R-CS	P1	ictrace3	0.4705	0.003301325	200
PKCd	habituation	PBS	CS	R-CS	P4	ictrace6	0.469	0.00365821	200
PKCd	habituation	PBS	CS	R-CS	P1	ictrace15	0.467625	0.004148786	200
PKCd	habituation	PBS	CS	R-CS	P4	ictrace3	0.467	0.003399265	200
PKCd	habituation	PBS	CS	R-CS	P4	ictrace7	0.464	0.003538361	200
PKCd	habituation	PBS	CS	R-CS	P3	ictrace2	0.46275	0.003889047	200
PKCd	habituation	PBS	CS	R-CS	P4	ictrace8	0.462	0.004447471	200
PKCd	habituation	PBS	CS	R-CS	P1	ictrace8	0.4565	0.004312917	200
PKCd	**habituation**	**PBS**	**CS**	**F-CS**	**P2**	**ictrace6**	**0.58**	**0.008246211**	**200**
PKCd	**habituation**	**PBS**	**CS**	**F-CS**	**P4**	**ictrace2**	**0.58**	**0.005291503**	**200**
PKCd	**habituation**	**PBS**	**CS**	**F-CS**	**P4**	**ictrace7**	**0.55075**	**0.003916751**	**200**
PKCd	**habituation**	**PBS**	**CS**	**F-CS**	**P1**	**ictrace3**	**0.549375**	**0.004944813**	**200**
PKCd	**habituation**	**PBS**	**CS**	**F-CS**	**P3**	**ictrace29**	**0.5475**	**0.004965506**	**200**
PKCd	**habituation**	**PBS**	**CS**	**F-CS**	**P2**	**ictrace3**	**0.547**	**0.004577663**	**200**
PKCd	**habituation**	**PBS**	**CS**	**F-CS**	**P4**	**ictrace5**	**0.546875**	**0.004776039**	**200**
PKCd	**habituation**	**PBS**	**CS**	**F-CS**	**P1**	**ictrace5**	**0.5305**	**0.006185063**	**200**
PKCd	**habituation**	**PBS**	**CS**	**F-CS**	**P1**	**ictrace6**	**0.529**	**0.006396874**	**200**
PKCd	**habituation**	**PBS**	**CS**	**F-CS**	**P2**	**ictrace5**	**0.5265**	**0.006343402**	**200**

PKCd	**habituation**	**PBS**	**CS**	**F-CS**	**P4**	**ictrace1**	**0.5115**	**0.003014755**	**200**
PKCd	**habituation**	**PBS**	**CS**	**F-CS**	**P1**	**ictrace12**	**0.504**	**0.002901724**	**200**
PKCd	**habituation**	**PBS**	**CS**	**F-CS**	**P3**	**ictrace3**	**0.504**	**0.002433105**	**200**
PKCd	**habituation**	**PBS**	**CS**	**F-CS**	**P4**	**ictrace4**	**0.50375**	**0.002638359**	**200**
PKCd	**habituation**	**PBS**	**CS**	**F-CS**	**P3**	**ictrace27**	**0.5035**	**0.001785707**	**200**
PKCd	**habituation**	**PBS**	**CS**	**F-CS**	**P3**	**ictrace11**	**0.5005**	**0.001936169**	**200**
PKCd	**habituation**	**PBS**	**CS**	**F-CS**	**P1**	**ictrace9**	**0.5**	**0**	**200**
PKCd	**habituation**	**PBS**	**CS**	**F-CS**	**P2**	**ictrace1**	**0.5**	**0**	**200**
PKCd	**habituation**	**PBS**	**CS**	**F-CS**	**P2**	**ictrace4**	**0.5**	**0.00212132**	**200**
PKCd	**habituation**	**PBS**	**CS**	**F-CS**	**P3**	**ictrace5**	**0.5**	**0**	**200**
PKCd	**habituation**	**PBS**	**CS**	**F-CS**	**P3**	**ictrace9**	**0.5**	**0**	**200**
PKCd	**habituation**	**PBS**	**CS**	**F-CS**	**P1**	**ictrace4**	**0.4985**	**0.002288832**	**200**
PKCd	**habituation**	**PBS**	**CS**	**F-CS**	**P3**	**ictrace2**	**0.498**	**0.002231591**	**200**
PKCd	**habituation**	**PBS**	**CS**	**F-CS**	**P4**	**ictrace10**	**0.497**	**0.001988718**	**200**
PKCd	**habituation**	**PBS**	**CS**	**F-CS**	**P2**	**ictrace7**	**0.4965**	**0.002165352**	**200**
PKCd	**habituation**	**PBS**	**CS**	**F-CS**	**P1**	**ictrace8**	**0.488**	**0.002505993**	**200**
PKCd	**habituation**	**PBS**	**CS**	**F-CS**	**P4**	**ictrace8**	**0.484375**	**0.005938322**	**200**
PKCd	**habituation**	**PBS**	**CS**	**F-CS**	**P2**	**ictrace11**	**0.4805**	**0.003567037**	**200**
PKCd	**habituation**	**PBS**	**CS**	**F-CS**	**P1**	**ictrace2**	**0.4755**	**0.003791273**	**200**
PKCd	**habituation**	**PBS**	**CS**	**F-CS**	**P4**	**ictrace6**	**0.4735**	**0.003426186**	**200**
PKCd	habituation	PBS	CS	F-CS	P3	ictrace17	0.47325	0.003954863	200
PKCd	habituation	PBS	CS	F-CS	P3	ictrace8	0.471	0.003974292	200
PKCd	habituation	PBS	CS	F-CS	P3	ictrace4	0.46575	0.003523626	200
PKCd	habituation	PBS	CS	F-CS	P1	ictrace7	0.4625	0.003495533	200
PKCd	habituation	PBS	CS	F-CS	P1	ictrace15	0.462	0.00477284	200
PKCd	habituation	PBS	CS	F-CS	P1	ictrace14	0.447375	0.004477016	200
PKCd	habituation	PBS	CS	F-CS	P4	ictrace3	0.419	0.006457167	200
PKCd	habituation	PBS	CS	F-CS	P2	ictrace8	0.41375	0.006568747	200
PKCd	**habituation**	**aIC inhibition**	**CS**	**R-CS**	**P3**	**ictrace22**	**0.64625**	**0.013176124**	**200**
PKCd	**habituation**	**aIC inhibition**	**CS**	**R-CS**	**P1**	**ictrace13**	**0.6175**	**0.006645539**	**200**
PKCd	**habituation**	**aIC inhibition**	**CS**	**R-CS**	**P2**	**ictrace5**	**0.61**	**0.009009255**	**200**
PKCd	**habituation**	**aIC inhibition**	**CS**	**R-CS**	**P1**	**ictrace1**	**0.607916667**	**0.011373512**	**200**
PKCd	**habituation**	**aIC inhibition**	**CS**	**R-CS**	**P2**	**ictrace3**	**0.570625**	**0.005699335**	**200**
PKCd	**habituation**	**aIC inhibition**	**CS**	**R-CS**	**P1**	**ictrace2**	**0.566666667**	**0.005773503**	**200**
PKCd	**habituation**	**aIC inhibition**	**CS**	**R-CS**	**P1**	**ictrace3**	**0.566666667**	**0.005773503**	**200**
PKCd	**habituation**	**aIC inhibition**	**CS**	**R-CS**	**P2**	**ictrace1**	**0.545833333**	**0.005519851**	**200**
PKCd	**habituation**	**aIC inhibition**	**CS**	**R-CS**	**P3**	**ictrace12**	**0.545416667**	**0.006706845**	**200**
PKCd	**habituation**	**aIC inhibition**	**CS**	**R-CS**	**P1**	**ictrace10**	**0.5325**	**0.010065584**	**200**
PKCd	**habituation**	**aIC inhibition**	**CS**	**R-CS**	**P3**	**ictrace6**	**0.525625**	**0.008383585**	**200**
PKCd	**habituation**	**aIC inhibition**	**CS**	**R-CS**	**P1**	**ictrace8**	**0.520833333**	**0.008814248**	**200**
PKCd	**habituation**	**aIC inhibition**	**CS**	**R-CS**	**P1**	**ictrace4**	**0.509791667**	**0.00937721**	**200**
PKCd	**habituation**	**aIC inhibition**	**CS**	**R-CS**	**P2**	**ictrace7**	**0.5**	**0**	**200**
PKCd	**habituation**	**aIC inhibition**	**CS**	**R-CS**	**P3**	**ictrace2**	**0.499166667**	**0.002855915**	**200**
PKCd	**habituation**	**aIC inhibition**	**CS**	**R-CS**	**P3**	**ictrace21**	**0.49875**	**0.002793687**	**200**
PKCd	**habituation**	**aIC inhibition**	**CS**	**R-CS**	**P3**	**ictrace7**	**0.498333333**	**0.001172604**	**200**
PKCd	**habituation**	**aIC inhibition**	**CS**	**R-CS**	**P3**	**ictrace3**	**0.496875**	**0.003117178**	**200**
PKCd	**habituation**	**aIC inhibition**	**CS**	**R-CS**	**P2**	**ictrace2**	**0.496666667**	**0.003109126**	**200**
PKCd	**habituation**	**aIC inhibition**	**CS**	**R-CS**	**P2**	**ictrace4**	**0.486875**	**0.006748055**	**200**
PKCd	**habituation**	**aIC inhibition**	**CS**	**R-CS**	**P1**	**ictrace16**	**0.463958333**	**0.013481203**	**200**
PKCd	**habituation**	**aIC inhibition**	**CS**	**R-CS**	**P1**	**ictrace20**	**0.461041667**	**0.005129212**	**200**
PKCd	**habituation**	**aIC inhibition**	**CS**	**R-CS**	**P1**	**ictrace5**	**0.46**	**0.006794606**	**200**
PKCd	**habituation**	**aIC inhibition**	**CS**	**R-CS**	**P3**	**ictrace11**	**0.457916667**	**0.005810894**	**200**
PKCd	**habituation**	**aIC inhibition**	**CS**	**R-CS**	**P3**	**ictrace9**	**0.449791667**	**0.010338446**	**200**
PKCd	**habituation**	**aIC inhibition**	**CS**	**R-CS**	**P3**	**ictrace20**	**0.448541667**	**0.006501719**	**200**
PKCd	**habituation**	**aIC inhibition**	**CS**	**R-CS**	**P1**	**ictrace12**	**0.44375**	**0.005703541**	**200**
PKCd	**habituation**	**aIC inhibition**	**CS**	**R-CS**	**P3**	**ictrace8**	**0.443125**	**0.006582658**	**200**
PKCd	**habituation**	**aIC inhibition**	**CS**	**R-CS**	**P3**	**ictrace1**	**0.4425**	**0.007031427**	**200**
PKCd	**habituation**	**aIC inhibition**	**CS**	**R-CS**	**P3**	**ictrace4**	**0.439791667**	**0.007555911**	**200**
PKCd	habituation	aIC inhibition	CS	R-CS	P3	ictrace18	0.4375	0.006915914	200
PKCd	habituation	aIC inhibition	CS	R-CS	P3	ictrace15	0.430833333	0.007385938	200

PKCd	habituation	aIC inhibition	CS	R-CS	P1	ictrace11	0.418541667	0.007109617	200
PKCd	**habituation**	**aIC inhibition**	**CS**	**F-CS**	**P3**	**ictrace21**	**0.6**	**0.00942809**	**200**
PKCd	**habituation**	**aIC inhibition**	**CS**	**F-CS**	**P3**	**ictrace12**	**0.5975**	**0.009035232**	**200**
PKCd	**habituation**	**aIC inhibition**	**CS**	**F-CS**	**P2**	**ictrace4**	**0.591666667**	**0.005400617**	**200**
PKCd	**habituation**	**aIC inhibition**	**CS**	**F-CS**	**P1**	**ictrace1**	**0.566666667**	**0.005773503**	**200**
PKCd	**habituation**	**aIC inhibition**	**CS**	**F-CS**	**P3**	**ictrace15**	**0.566666667**	**0.005773503**	**200**
PKCd	**habituation**	**aIC inhibition**	**CS**	**F-CS**	**P3**	**ictrace22**	**0.566666667**	**0.005773503**	**200**
PKCd	**habituation**	**aIC inhibition**	**CS**	**F-CS**	**P3**	**ictrace4**	**0.549583333**	**0.013055005**	**200**
PKCd	**habituation**	**aIC inhibition**	**CS**	**F-CS**	**P1**	**ictrace13**	**0.54625**	**0.005462864**	**200**
PKCd	**habituation**	**aIC inhibition**	**CS**	**F-CS**	**P1**	**ictrace12**	**0.54**	**0.004848754**	**200**
PKCd	**habituation**	**aIC inhibition**	**CS**	**F-CS**	**P3**	**ictrace9**	**0.51625**	**0.006079551**	**200**
PKCd	**habituation**	**aIC inhibition**	**CS**	**F-CS**	**P1**	**ictrace5**	**0.506875**	**0.003044484**	**200**
PKCd	**habituation**	**aIC inhibition**	**CS**	**F-CS**	**P1**	**ictrace2**	**0.506666667**	**0.003880149**	**200**
PKCd	**habituation**	**aIC inhibition**	**CS**	**F-CS**	**P1**	**ictrace8**	**0.503541667**	**0.002898418**	**200**
PKCd	**habituation**	**aIC inhibition**	**CS**	**F-CS**	**P1**	**ictrace4**	**0.5025**	**0.002758195**	**200**
PKCd	**habituation**	**aIC inhibition**	**CS**	**F-CS**	**P1**	**ictrace10**	**0.5**	**0**	**200**
PKCd	**habituation**	**aIC inhibition**	**CS**	**F-CS**	**P3**	**ictrace2**	**0.5**	**0**	**200**
PKCd	**habituation**	**aIC inhibition**	**CS**	**F-CS**	**P3**	**ictrace18**	**0.499583333**	**0.007424329**	**200**
PKCd	**habituation**	**aIC inhibition**	**CS**	**F-CS**	**P2**	**ictrace1**	**0.498333333**	**0.00311582**	**200**
PKCd	**habituation**	**aIC inhibition**	**CS**	**F-CS**	**P2**	**ictrace3**	**0.488333333**	**0.006509608**	**200**
PKCd	**habituation**	**aIC inhibition**	**CS**	**F-CS**	**P3**	**ictrace7**	**0.479166667**	**0.006731456**	**200**
PKCd	**habituation**	**aIC inhibition**	**CS**	**F-CS**	**P1**	**ictrace3**	**0.46625**	**0.004942288**	**200**
PKCd	**habituation**	**aIC inhibition**	**CS**	**F-CS**	**P1**	**ictrace11**	**0.463541667**	**0.005220299**	**200**
PKCd	**habituation**	**aIC inhibition**	**CS**	**F-CS**	**P1**	**ictrace16**	**0.4575**	**0.005773202**	**200**
PKCd	**habituation**	**aIC inhibition**	**CS**	**F-CS**	**P3**	**ictrace11**	**0.455**	**0.005975645**	**200**
PKCd	**habituation**	**aIC inhibition**	**CS**	**F-CS**	**P2**	**ictrace7**	**0.4525**	**0.005052159**	**200**
PKCd	**habituation**	**aIC inhibition**	**CS**	**F-CS**	**P2**	**ictrace2**	**0.44875**	**0.005014822**	**200**
PKCd	**habituation**	**aIC inhibition**	**CS**	**F-CS**	**P3**	**ictrace8**	**0.448333333**	**0.006707169**	**200**
PKCd	**habituation**	**aIC inhibition**	**CS**	**F-CS**	**P3**	**ictrace6**	**0.445833333**	**0.005644257**	**200**
PKCd	**habituation**	**aIC inhibition**	**CS**	**F-CS**	**P3**	**ictrace3**	**0.428125**	**0.008684964**	**200**
PKCd	**habituation**	**aIC inhibition**	**CS**	**F-CS**	**P3**	**ictrace20**	**0.407291667**	**0.011162614**	**200**
PKCd	**RC**	**early**	**CS**	**R-CS**	**P4**	**ictrace3**	**0.538394737**	**0.003283491**	**200**
PKCd	**RC**	**early**	**CS**	**R-CS**	**P2**	**ictrace6**	**0.537809211**	**0.002183685**	**200**
PKCd	**RC**	**early**	**CS**	**R-CS**	**P1**	**ictrace11**	**0.535914474**	**0.002663569**	**200**
PKCd	**RC**	**early**	**CS**	**R-CS**	**P2**	**ictrace4**	**0.532513158**	**0.001188683**	**200**
PKCd	**RC**	**early**	**CS**	**R-CS**	**P1**	**ictrace15**	**0.528026316**	**0.001526287**	**200**
PKCd	**RC**	**early**	**CS**	**R-CS**	**P3**	**ictrace15**	**0.522059211**	**0.003095141**	**200**
PKCd	**RC**	**early**	**CS**	**R-CS**	**P2**	**ictrace1**	**0.521052632**	**0.002170056**	**200**
PKCd	**RC**	**early**	**CS**	**R-CS**	**P5**	**ictrace10**	**0.520868421**	**0.002712139**	**200**
PKCd	**RC**	**early**	**CS**	**R-CS**	**P5**	**ictrace2**	**0.518802632**	**0.001680779**	**200**
PKCd	**RC**	**early**	**CS**	**R-CS**	**P1**	**ictrace16**	**0.51875**	**0.001432603**	**200**
PKCd	**RC**	**early**	**CS**	**R-CS**	**P3**	**ictrace14**	**0.5175**	**0.002899547**	**200**
PKCd	**RC**	**early**	**CS**	**R-CS**	**P1**	**ictrace6**	**0.515526316**	**0.000897056**	**200**
PKCd	**RC**	**early**	**CS**	**R-CS**	**P3**	**ictrace6**	**0.515526316**	**0.000897056**	**200**
PKCd	**RC**	**early**	**CS**	**R-CS**	**P1**	**ictrace9**	**0.510769737**	**0.001414889**	**200**
PKCd	**RC**	**early**	**CS**	**R-CS**	**P5**	**ictrace11**	**0.510315789**	**0.001775571**	**200**
PKCd	**RC**	**early**	**CS**	**R-CS**	**P3**	**ictrace4**	**0.508657895**	**0.002319121**	**200**
PKCd	**RC**	**early**	**CS**	**R-CS**	**P1**	**ictrace2**	**0.507835526**	**0.001875849**	**200**
PKCd	**RC**	**early**	**CS**	**R-CS**	**P1**	**ictrace8**	**0.504828947**	**0.001540517**	**200**
PKCd	**RC**	**early**	**CS**	**R-CS**	**P2**	**ictrace2**	**0.504605263**	**0.000861566**	**200**
PKCd	**RC**	**early**	**CS**	**R-CS**	**P1**	**ictrace5**	**0.501230263**	**0.000969545**	**200**
PKCd	**RC**	**early**	**CS**	**R-CS**	**P2**	**ictrace3**	**0.500375**	**0.000214876**	**200**
PKCd	**RC**	**early**	**CS**	**R-CS**	**P3**	**ictrace11**	**0.5**	**0.000526316**	**200**
PKCd	**RC**	**early**	**CS**	**R-CS**	**P3**	**ictrace16**	**0.499638158**	**0.001165604**	**200**
PKCd	**RC**	**early**	**CS**	**R-CS**	**P3**	**ictrace13**	**0.498572368**	**0.001270053**	**200**
PKCd	**RC**	**early**	**CS**	**R-CS**	**P3**	**ictrace18**	**0.498552632**	**0.000701144**	**200**
PKCd	**RC**	**early**	**CS**	**R-CS**	**P5**	**ictrace12**	**0.498217105**	**0.00147374**	**200**
PKCd	**RC**	**early**	**CS**	**R-CS**	**P3**	**ictrace19**	**0.497269737**	**0.002312122**	**200**
PKCd	**RC**	**early**	**CS**	**R-CS**	**P1**	**ictrace14**	**0.495513158**	**0.001327878**	**200**
PKCd	**RC**	**early**	**CS**	**R-CS**	**P1**	**ictrace13**	**0.495263158**	**0.000962597**	**200**

PKCd	**RC**	**early**	**CS**	**R-CS**	**P5**	**ictrace6**	**0.495125**	**0.001369521**	**200**
PKCd	RC	early	CS	R-CS	P5	ictrace8	0.494342105	0.001415651	200
PKCd	RC	early	CS	R-CS	P1	ictrace12	0.494	0.001182039	200
PKCd	RC	early	CS	R-CS	P1	ictrace4	0.493289474	0.001036012	200
PKCd	RC	early	CS	R-CS	P3	ictrace12	0.492934211	0.001749686	200
PKCd	RC	early	CS	R-CS	P3	ictrace3	0.492894737	0.001449878	200
PKCd	RC	early	CS	R-CS	P5	ictrace3	0.492302632	0.000850378	200
PKCd	RC	early	CS	R-CS	P3	ictrace8	0.492289474	0.001543406	200
PKCd	RC	early	CS	R-CS	P5	ictrace9	0.491973684	0.000876705	200
PKCd	RC	early	CS	R-CS	P3	ictrace2	0.491875	0.00098857	200
PKCd	RC	early	CS	R-CS	P3	ictrace9	0.491328947	0.001347936	200
PKCd	RC	early	CS	R-CS	P5	ictrace4	0.491276316	0.001636593	200
PKCd	RC	early	CS	R-CS	P2	ictrace5	0.491138158	0.002346766	200
PKCd	RC	early	CS	R-CS	P1	ictrace10	0.490921053	0.000884569	200
PKCd	RC	early	CS	R-CS	P5	ictrace5	0.489098684	0.002472028	200
PKCd	RC	early	CS	R-CS	P5	ictrace7	0.488967105	0.002107907	200
PKCd	RC	early	CS	R-CS	P3	ictrace1	0.487006579	0.001338713	200
PKCd	RC	early	CS	R-CS	P1	ictrace1	0.480092105	0.00163172	200
PKCd	RC	early	CS	R-CS	P3	ictrace10	0.480006579	0.00190264	200
PKCd	RC	early	CS	R-CS	P1	ictrace3	0.475875	0.002211608	200
PKCd	RC	early	CS	R-CS	P1	ictrace7	0.475592105	0.001918454	200
PKCd	RC	early	CS	R-CS	P2	ictrace7	0.473401316	0.001606257	200
PKCd	RC	early	CS	R-CS	P3	ictrace5	0.470263158	0.002445812	200
PKCd	RC	early	CS	R-CS	P3	ictrace7	0.464052632	0.002153875	200
PKCd	RC	early	CS	R-CS	P4	ictrace1	0.451973684	0.003655208	200
PKCd	**RC**	**early**	**US**	**R-CS**	**P1**	**ictrace14**	**0.61375**	**0.011699025**	**200**
PKCd	**RC**	**early**	**US**	**R-CS**	**P3**	**ictrace9**	**0.61375**	**0.015082844**	**200**
PKCd	**RC**	**early**	**US**	**R-CS**	**P2**	**ictrace6**	**0.52625**	**0.010061918**	**200**
PKCd	**RC**	**early**	**US**	**R-CS**	**P5**	**ictrace11**	**0.52**	**0.007778175**	**200**
PKCd	**RC**	**early**	**US**	**R-CS**	**P3**	**ictrace4**	**0.51875**	**0.006107756**	**200**
PKCd	**RC**	**early**	**US**	**R-CS**	**P3**	**ictrace14**	**0.51625**	**0.007305285**	**200**
PKCd	**RC**	**early**	**US**	**R-CS**	**P1**	**ictrace3**	**0.51375**	**0.005915419**	**200**
PKCd	**RC**	**early**	**US**	**R-CS**	**P3**	**ictrace7**	**0.5125**	**0.007015608**	**200**
PKCd	**RC**	**early**	**US**	**R-CS**	**P5**	**ictrace5**	**0.5125**	**0.004592793**	**200**
PKCd	**RC**	**early**	**US**	**R-CS**	**P1**	**ictrace15**	**0.51125**	**0.004775425**	**200**
PKCd	**RC**	**early**	**US**	**R-CS**	**P2**	**ictrace1**	**0.51125**	**0.00509212**	**200**
PKCd	**RC**	**early**	**US**	**R-CS**	**P1**	**ictrace12**	**0.5075**	**0.005276718**	**200**
PKCd	**RC**	**early**	**US**	**R-CS**	**P2**	**ictrace2**	**0.5075**	**0.005276718**	**200**
PKCd	**RC**	**early**	**US**	**R-CS**	**P1**	**ictrace11**	**0.50625**	**0.005134899**	**200**
PKCd	**RC**	**early**	**US**	**R-CS**	**P2**	**ictrace4**	**0.50625**	**0.003723867**	**200**
PKCd	**RC**	**early**	**US**	**R-CS**	**P2**	**ictrace5**	**0.50625**	**0.004485219**	**200**
PKCd	**RC**	**early**	**US**	**R-CS**	**P5**	**ictrace12**	**0.50625**	**0.004821015**	**200**
PKCd	**RC**	**early**	**US**	**R-CS**	**P1**	**ictrace4**	**0.505**	**0.003517812**	**200**
PKCd	**RC**	**early**	**US**	**R-CS**	**P3**	**ictrace19**	**0.505**	**0.004315669**	**200**
PKCd	**RC**	**early**	**US**	**R-CS**	**P1**	**ictrace13**	**0.50375**	**0.004137292**	**200**
PKCd	**RC**	**early**	**US**	**R-CS**	**P1**	**ictrace5**	**0.50375**	**0.004499132**	**200**
PKCd	**RC**	**early**	**US**	**R-CS**	**P2**	**ictrace7**	**0.50375**	**0.003740613**	**200**
PKCd	**RC**	**early**	**US**	**R-CS**	**P5**	**ictrace10**	**0.50375**	**0.005722079**	**200**
PKCd	**RC**	**early**	**US**	**R-CS**	**P5**	**ictrace6**	**0.50375**	**0.002782479**	**200**
PKCd	**RC**	**early**	**US**	**R-CS**	**P5**	**ictrace7**	**0.50375**	**0.003740613**	**200**
PKCd	**RC**	**early**	**US**	**R-CS**	**P3**	**ictrace1**	**0.5025**	**0.002493742**	**200**
PKCd	**RC**	**early**	**US**	**R-CS**	**P5**	**ictrace4**	**0.5025**	**0.003056755**	**200**
PKCd	**RC**	**early**	**US**	**R-CS**	**P5**	**ictrace8**	**0.5025**	**0.003948892**	**200**
PKCd	**RC**	**early**	**US**	**R-CS**	**P3**	**ictrace11**	**0.50125**	**0.001246871**	**200**
PKCd	**RC**	**early**	**US**	**R-CS**	**P1**	**ictrace10**	**0.5**	**0**	**200**
PKCd	RC	early	US	R-CS	P1	ictrace9	0.5	0.00559017	200
PKCd	RC	early	US	R-CS	P5	ictrace3	0.5	0.001767767	200
PKCd	RC	early	US	R-CS	P5	ictrace9	0.5	0	200
PKCd	RC	early	US	R-CS	P1	ictrace7	0.49875	0.004840422	200
PKCd	RC	early	US	R-CS	P3	ictrace5	0.49875	0.003748958	200

PKCd	RC	early	US	R-CS	P3	ictrace8	0.49875	0.001246871	200
PKCd	RC	early	US	R-CS	P1	ictrace6	0.4975	0.001758906	200
PKCd	RC	early	US	R-CS	P3	ictrace12	0.4975	0.003056755	200
PKCd	RC	early	US	R-CS	P3	ictrace16	0.4975	0.006371322	200
PKCd	RC	early	US	R-CS	P3	ictrace18	0.4975	0.001758906	200
PKCd	RC	early	US	R-CS	P2	ictrace3	0.49625	0.002148764	200
PKCd	RC	early	US	R-CS	P3	ictrace15	0.49625	0.004833962	200
PKCd	RC	early	US	R-CS	P3	ictrace6	0.49375	0.003723867	200
PKCd	RC	early	US	R-CS	P1	ictrace8	0.48625	0.007330906	200
PKCd	RC	early	US	R-CS	P3	ictrace10	0.48625	0.006173912	200
PKCd	RC	early	US	R-CS	P5	ictrace2	0.48375	0.006632661	200
PKCd	RC	early	US	R-CS	P1	ictrace1	0.48125	0.007486968	200
PKCd	RC	early	US	R-CS	P3	ictrace13	0.48	0.005958188	200
PKCd	RC	early	US	R-CS	P1	ictrace2	0.4775	0.012523727	200
PKCd	RC	early	US	R-CS	P4	ictrace1	0.475	0.011726039	200
PKCd	RC	early	US	R-CS	P3	ictrace2	0.4725	0.008060319	200
PKCd	RC	early	US	R-CS	P1	ictrace16	0.4675	0.012662691	200
PKCd	RC	early	US	R-CS	P4	ictrace3	0.4675	0.010354649	200
PKCd	RC	early	US	R-CS	P3	ictrace3	0.44375	0.012429489	200
PKCd	**RC**	**late**	**CS**	**R-CS**	**P4**	**ictrace5**	**0.542763158**	**0.0013786**	**200**
PKCd	**RC**	**late**	**CS**	**R-CS**	**P3**	**ictrace3**	**0.540309211**	**0.002709459**	**200**
PKCd	**RC**	**late**	**CS**	**R-CS**	**P1**	**ictrace10**	**0.537763158**	**0.001048966**	**200**
PKCd	**RC**	**late**	**CS**	**R-CS**	**P5**	**ictrace4**	**0.533519737**	**0.003034627**	**200**
PKCd	**RC**	**late**	**CS**	**R-CS**	**P3**	**ictrace10**	**0.526118421**	**0.002297998**	**200**
PKCd	**RC**	**late**	**CS**	**R-CS**	**P2**	**ictrace9**	**0.525717105**	**0.001723302**	**200**
PKCd	**RC**	**late**	**CS**	**R-CS**	**P2**	**ictrace8**	**0.524203947**	**0.00213764**	**200**
PKCd	**RC**	**late**	**CS**	**R-CS**	**P3**	**ictrace15**	**0.523763158**	**0.002528536**	**200**
PKCd	**RC**	**late**	**CS**	**R-CS**	**P1**	**ictrace14**	**0.518993421**	**0.00204095**	**200**
PKCd	**RC**	**late**	**CS**	**R-CS**	**P1**	**ictrace6**	**0.516842105**	**0.001824066**	**200**
PKCd	**RC**	**late**	**CS**	**R-CS**	**P3**	**ictrace2**	**0.514888158**	**0.001354291**	**200**
PKCd	**RC**	**late**	**CS**	**R-CS**	**P2**	**ictrace4**	**0.512105263**	**0.000927422**	**200**
PKCd	**RC**	**late**	**CS**	**R-CS**	**P3**	**ictrace19**	**0.512052632**	**0.00096974**	**200**
PKCd	**RC**	**late**	**CS**	**R-CS**	**P5**	**ictrace5**	**0.511671053**	**0.001773812**	**200**
PKCd	**RC**	**late**	**CS**	**R-CS**	**P3**	**ictrace23**	**0.511368421**	**0.001184906**	**200**
PKCd	**RC**	**late**	**CS**	**R-CS**	**P3**	**ictrace24**	**0.511263158**	**0.001028702**	**200**
PKCd	**RC**	**late**	**CS**	**R-CS**	**P1**	**ictrace11**	**0.509578947**	**0.00112094**	**200**
PKCd	**RC**	**late**	**CS**	**R-CS**	**P2**	**ictrace1**	**0.509171053**	**0.001639964**	**200**
PKCd	**RC**	**late**	**CS**	**R-CS**	**P4**	**ictrace2**	**0.507592105**	**0.001878395**	**200**
PKCd	**RC**	**late**	**CS**	**R-CS**	**P2**	**ictrace6**	**0.507565789**	**0.002082707**	**200**
PKCd	**RC**	**late**	**CS**	**R-CS**	**P2**	**ictrace5**	**0.50625**	**0.001621113**	**200**
PKCd	**RC**	**late**	**CS**	**R-CS**	**P2**	**ictrace2**	**0.506078947**	**0.001359586**	**200**
PKCd	**RC**	**late**	**CS**	**R-CS**	**P2**	**ictrace12**	**0.505592105**	**0.001978038**	**200**
PKCd	**RC**	**late**	**CS**	**R-CS**	**P1**	**ictrace4**	**0.505065789**	**0.002365052**	**200**
PKCd	**RC**	**late**	**CS**	**R-CS**	**P1**	**ictrace16**	**0.504868421**	**0.000854301**	**200**
PKCd	**RC**	**late**	**CS**	**R-CS**	**P3**	**ictrace18**	**0.503592105**	**0.001398137**	**200**
PKCd	**RC**	**late**	**CS**	**R-CS**	**P1**	**ictrace13**	**0.502953947**	**0.001431779**	**200**
PKCd	**RC**	**late**	**CS**	**R-CS**	**P5**	**ictrace10**	**0.501447368**	**0.000952426**	**200**
PKCd	**RC**	**late**	**CS**	**R-CS**	**P1**	**ictrace12**	**0.501315789**	**0.001338618**	**200**
PKCd	**RC**	**late**	**CS**	**R-CS**	**P3**	**ictrace17**	**0.500967105**	**0.001053021**	**200**
PKCd	RC	late	CS	R-CS	P5	ictrace9	0.500611842	0.001217901	200
PKCd	RC	late	CS	R-CS	P3	ictrace22	0.500263158	0.000767005	200
PKCd	RC	late	CS	R-CS	P3	ictrace9	0.500131579	0.001348893	200
PKCd	RC	late	CS	R-CS	P3	ictrace12	0.5	0	200
PKCd	RC	late	CS	R-CS	P1	ictrace1	0.49975	0.000530035	200
PKCd	RC	late	CS	R-CS	P3	ictrace16	0.499736842	0.001191353	200
PKCd	RC	late	CS	R-CS	P3	ictrace7	0.499342105	0.00057165	200
PKCd	RC	late	CS	R-CS	P1	ictrace3	0.499217105	0.00150133	200
PKCd	RC	late	CS	R-CS	P3	ictrace5	0.497631579	0.001164901	200
PKCd	RC	late	CS	R-CS	P3	ictrace6	0.4975	0.001062413	200
PKCd	RC	late	CS	R-CS	P5	ictrace7	0.496572368	0.00118278	200

PKCd	RC	late	CS	R-CS	P1	ictrace18	0.496447368	0.001496504	200
PKCd	RC	late	CS	R-CS	P1	ictrace17	0.495657895	0.001821097	200
PKCd	RC	late	CS	R-CS	P3	ictrace13	0.495638158	0.000704321	200
PKCd	RC	late	CS	R-CS	P1	ictrace15	0.492230263	0.000960373	200
PKCd	RC	late	CS	R-CS	P5	ictrace6	0.491539474	0.000852856	200
PKCd	RC	late	CS	R-CS	P1	ictrace7	0.491203947	0.001194132	200
PKCd	RC	late	CS	R-CS	P3	ictrace20	0.490993421	0.002192085	200
PKCd	RC	late	CS	R-CS	P4	ictrace3	0.490552632	0.001677277	200
PKCd	RC	late	CS	R-CS	P1	ictrace5	0.490289474	0.001534392	200
PKCd	RC	late	CS	R-CS	P1	ictrace19	0.490263158	0.001571363	200
PKCd	RC	late	CS	R-CS	P4	ictrace4	0.489565789	0.001784375	200
PKCd	RC	late	CS	R-CS	P3	ictrace11	0.489434211	0.001459931	200
PKCd	RC	late	CS	R-CS	P1	ictrace9	0.48725	0.001358019	200
PKCd	RC	late	CS	R-CS	P3	ictrace25	0.486973684	0.00132885	200
PKCd	RC	late	CS	R-CS	P3	ictrace1	0.485361842	0.001171826	200
PKCd	RC	late	CS	R-CS	P3	ictrace14	0.482986842	0.001739693	200
PKCd	RC	late	CS	R-CS	P3	ictrace8	0.482388158	0.001991926	200
PKCd	RC	late	CS	R-CS	P3	ictrace21	0.476296053	0.002340802	200
PKCd	RC	late	CS	R-CS	P3	ictrace4	0.472105263	0.002097766	200
PKCd	RC	late	CS	R-CS	P2	ictrace7	0.472085526	0.002331286	200
PKCd	RC	late	CS	R-CS	P2	ictrace3	0.470230263	0.003158709	200
PKCd	RC	late	CS	R-CS	P1	ictrace20	0.468263158	0.002506787	200
PKCd	**RC**	**late**	**US**	**R-CS**	**P5**	**ictrace4**	**0.65125**	**0.014434689**	**200**
PKCd	**RC**	**late**	**US**	**R-CS**	**P4**	**ictrace2**	**0.604583333**	**0.010408288**	**200**
PKCd	**RC**	**late**	**US**	**R-CS**	**P3**	**ictrace9**	**0.590833333**	**0.008358088**	**200**
PKCd	**RC**	**late**	**US**	**R-CS**	**P3**	**ictrace22**	**0.575416667**	**0.008591774**	**200**
PKCd	**RC**	**late**	**US**	**R-CS**	**P3**	**ictrace19**	**0.570833333**	**0.007922147**	**200**
PKCd	**RC**	**late**	**US**	**R-CS**	**P3**	**ictrace12**	**0.563333333**	**0.008191289**	**200**
PKCd	**RC**	**late**	**US**	**R-CS**	**P3**	**ictrace25**	**0.547083333**	**0.008303645**	**200**
PKCd	**RC**	**late**	**US**	**R-CS**	**P1**	**ictrace9**	**0.544583333**	**0.008577213**	**200**
PKCd	**RC**	**late**	**US**	**R-CS**	**P3**	**ictrace16**	**0.526666667**	**0.009785193**	**200**
PKCd	**RC**	**late**	**US**	**R-CS**	**P1**	**ictrace17**	**0.525**	**0.005137012**	**200**
PKCd	**RC**	**late**	**US**	**R-CS**	**P2**	**ictrace3**	**0.524166667**	**0.005968377**	**200**
PKCd	**RC**	**late**	**US**	**R-CS**	**P4**	**ictrace5**	**0.524166667**	**0.005054907**	**200**
PKCd	**RC**	**late**	**US**	**R-CS**	**P1**	**ictrace14**	**0.523333333**	**0.005748188**	**200**
PKCd	**RC**	**late**	**US**	**R-CS**	**P2**	**ictrace1**	**0.523333333**	**0.00580828**	**200**
PKCd	**RC**	**late**	**US**	**R-CS**	**P3**	**ictrace18**	**0.520833333**	**0.005128556**	**200**
PKCd	**RC**	**late**	**US**	**R-CS**	**P2**	**ictrace8**	**0.52**	**0.005008326**	**200**
PKCd	**RC**	**late**	**US**	**R-CS**	**P3**	**ictrace7**	**0.51625**	**0.008891661**	**200**
PKCd	**RC**	**late**	**US**	**R-CS**	**P1**	**ictrace4**	**0.512916667**	**0.004212148**	**200**
PKCd	**RC**	**late**	**US**	**R-CS**	**P2**	**ictrace6**	**0.512916667**	**0.004491408**	**200**
PKCd	**RC**	**late**	**US**	**R-CS**	**P1**	**ictrace7**	**0.51125**	**0.004953867**	**200**
PKCd	**RC**	**late**	**US**	**R-CS**	**P2**	**ictrace4**	**0.509583333**	**0.003394107**	**200**
PKCd	**RC**	**late**	**US**	**R-CS**	**P2**	**ictrace7**	**0.509583333**	**0.005341709**	**200**
PKCd	**RC**	**late**	**US**	**R-CS**	**P1**	**ictrace10**	**0.508333333**	**0.003173239**	**200**
PKCd	**RC**	**late**	**US**	**R-CS**	**P1**	**ictrace12**	**0.508333333**	**0.004714045**	**200**
PKCd	**RC**	**late**	**US**	**R-CS**	**P3**	**ictrace20**	**0.505416667**	**0.004252348**	**200**
PKCd	**RC**	**late**	**US**	**R-CS**	**P1**	**ictrace6**	**0.505**	**0.003980857**	**200**
PKCd	**RC**	**late**	**US**	**R-CS**	**P4**	**ictrace3**	**0.505**	**0.004550641**	**200**
PKCd	**RC**	**late**	**US**	**R-CS**	**P2**	**ictrace9**	**0.504583333**	**0.003495905**	**200**
PKCd	**RC**	**late**	**US**	**R-CS**	**P3**	**ictrace17**	**0.504583333**	**0.002712977**	**200**
PKCd	**RC**	**late**	**US**	**R-CS**	**P4**	**ictrace4**	**0.50375**	**0.003740613**	**200**
PKCd	RC	late	US	R-CS	P1	ictrace3	0.503333333	0.002816124	200
PKCd	RC	late	US	R-CS	P1	ictrace18	0.502916667	0.003504833	200
PKCd	RC	late	US	R-CS	P5	ictrace9	0.502916667	0.002968439	200
PKCd	RC	late	US	R-CS	P2	ictrace5	0.5025	0.003056755	200
PKCd	RC	late	US	R-CS	P3	ictrace21	0.5025	0.004162915	200
PKCd	RC	late	US	R-CS	P3	ictrace24	0.502083333	0.002597909	200
PKCd	RC	late	US	R-CS	P5	ictrace6	0.501666667	0.002426703	200
PKCd	RC	late	US	R-CS	P1	ictrace1	0.500833333	0.000831247	200

PKCd	RC	late	US	R-CS	P3	ictrace11	0.500833333	0.001442172	200
PKCd	RC	late	US	R-CS	P3	ictrace13	0.500833333	0.002499305	200
PKCd	RC	late	US	R-CS	P1	ictrace13	0.500416667	0.002243625	200
PKCd	RC	late	US	R-CS	P3	ictrace14	0.500416667	0.001717708	200
PKCd	RC	late	US	R-CS	P5	ictrace5	0.500416667	0.001909179	200
PKCd	RC	late	US	R-CS	P1	ictrace11	0.5	0	200
PKCd	RC	late	US	R-CS	P1	ictrace16	0.5	0	200
PKCd	RC	late	US	R-CS	P5	ictrace10	0.5	0.003061862	200
PKCd	RC	late	US	R-CS	P1	ictrace20	0.499583333	0.002534313	200
PKCd	RC	late	US	R-CS	P3	ictrace4	0.499166667	0.003004048	200
PKCd	RC	late	US	R-CS	P3	ictrace6	0.49875	0.001246871	200
PKCd	RC	late	US	R-CS	P2	ictrace12	0.498333333	0.00212132	200
PKCd	RC	late	US	R-CS	P3	ictrace1	0.497916667	0.001495073	200
PKCd	RC	late	US	R-CS	P3	ictrace23	0.4975	0.005300354	200
PKCd	RC	late	US	R-CS	P1	ictrace15	0.497083333	0.004385008	200
PKCd	RC	late	US	R-CS	P5	ictrace7	0.497083333	0.002593896	200
PKCd	RC	late	US	R-CS	P3	ictrace5	0.493333333	0.003138028	200
PKCd	RC	late	US	R-CS	P3	ictrace15	0.492916667	0.004742593	200
PKCd	RC	late	US	R-CS	P1	ictrace19	0.49125	0.004305903	200
PKCd	RC	late	US	R-CS	P2	ictrace2	0.487916667	0.006163217	200
PKCd	RC	late	US	R-CS	P1	ictrace5	0.4875	0.006712085	200
PKCd	RC	late	US	R-CS	P3	ictrace10	0.485833333	0.006183255	200
PKCd	RC	late	US	R-CS	P3	ictrace2	0.475416667	0.006790452	200
PKCd	RC	late	US	R-CS	P3	ictrace3	0.470416667	0.006063824	200
PKCd	RC	late	US	R-CS	P3	ictrace8	0.469583333	0.007387525	200
PKCd	**FC**	**early**	**CS**	**F-CS**	**P4**	**ictrace8**	**0.6**	**0.005773503**	**200**
PKCd	**FC**	**early**	**CS**	**F-CS**	**P3**	**ictrace22**	**0.5775**	**0.006222439**	**200**
PKCd	**FC**	**early**	**CS**	**F-CS**	**P5**	**ictrace10**	**0.566666667**	**0.005773503**	**200**
PKCd	**FC**	**early**	**CS**	**F-CS**	**P3**	**ictrace12**	**0.558333333**	**0.005137012**	**200**
PKCd	**FC**	**early**	**CS**	**F-CS**	**P3**	**ictrace20**	**0.558333333**	**0.005137012**	**200**
PKCd	**FC**	**early**	**CS**	**F-CS**	**P3**	**ictrace7**	**0.558333333**	**0.005137012**	**200**
PKCd	**FC**	**early**	**CS**	**F-CS**	**P4**	**ictrace6**	**0.546666667**	**0.005547772**	**200**
PKCd	**FC**	**early**	**CS**	**F-CS**	**P1**	**ictrace7**	**0.525833333**	**0.005150175**	**200**
PKCd	**FC**	**early**	**CS**	**F-CS**	**P1**	**ictrace12**	**0.521458333**	**0.005574445**	**200**
PKCd	**FC**	**early**	**CS**	**F-CS**	**P3**	**ictrace1**	**0.518541667**	**0.008289978**	**200**
PKCd	**FC**	**early**	**CS**	**F-CS**	**P3**	**ictrace11**	**0.516875**	**0.004420375**	**200**
PKCd	**FC**	**early**	**CS**	**F-CS**	**P1**	**ictrace9**	**0.505**	**0.002865019**	**200**
PKCd	**FC**	**early**	**CS**	**F-CS**	**P3**	**ictrace5**	**0.505**	**0.00611351**	**200**
PKCd	**FC**	**early**	**CS**	**F-CS**	**P3**	**ictrace8**	**0.503333333**	**0.003719319**	**200**
PKCd	**FC**	**early**	**CS**	**F-CS**	**P3**	**ictrace3**	**0.503125**	**0.002061079**	**200**
PKCd	**FC**	**early**	**CS**	**F-CS**	**P1**	**ictrace2**	**0.5025**	**0.003992615**	**200**
PKCd	**FC**	**early**	**CS**	**F-CS**	**P2**	**ictrace9**	**0.5025**	**0.003431371**	**200**
PKCd	**FC**	**early**	**CS**	**F-CS**	**P3**	**ictrace15**	**0.500833333**	**0.00416625**	**200**
PKCd	**FC**	**early**	**CS**	**F-CS**	**P2**	**ictrace6**	**0.500625**	**0.002723953**	**200**
PKCd	**FC**	**early**	**CS**	**F-CS**	**P1**	**ictrace14**	**0.5**	**0**	**200**
PKCd	**FC**	**early**	**CS**	**F-CS**	**P1**	**ictrace4**	**0.5**	**0**	**200**
PKCd	**FC**	**early**	**CS**	**F-CS**	**P2**	**ictrace2**	**0.5**	**0**	**200**
PKCd	**FC**	**early**	**CS**	**F-CS**	**P2**	**ictrace3**	**0.5**	**0.002338536**	**200**
PKCd	**FC**	**early**	**CS**	**F-CS**	**P2**	**ictrace4**	**0.5**	**0.001530931**	**200**
PKCd	**FC**	**early**	**CS**	**F-CS**	**P2**	**ictrace5**	**0.5**	**0**	**200**
PKCd	**FC**	**early**	**CS**	**F-CS**	**P2**	**ictrace7**	**0.5**	**0**	**200**
PKCd	**FC**	**early**	**CS**	**F-CS**	**P3**	**ictrace10**	**0.5**	**0**	**200**
PKCd	**FC**	**early**	**CS**	**F-CS**	**P3**	**ictrace4**	**0.5**	**0**	**200**
PKCd	**FC**	**early**	**CS**	**F-CS**	**P4**	**ictrace4**	**0.5**	**0.006373774**	**200**
PKCd	**FC**	**early**	**CS**	**F-CS**	**P5**	**ictrace12**	**0.5**	**0**	**200**
PKCd	FC	early	CS	F-CS	P5	ictrace13	0.5	0	200
PKCd	FC	early	CS	F-CS	P5	ictrace2	0.5	0	200
PKCd	FC	early	CS	F-CS	P5	ictrace6	0.5	0	200
PKCd	FC	early	CS	F-CS	P5	ictrace8	0.5	0	200
PKCd	FC	early	CS	F-CS	P5	ictrace9	0.5	0	200

PKCd	FC	early	CS	F-CS	P4	ictrace7	0.499166667	0.003631938	200
PKCd	FC	early	CS	F-CS	P4	ictrace5	0.49875	0.002336865	200
PKCd	FC	early	CS	F-CS	P3	ictrace25	0.498125	0.002573528	200
PKCd	FC	early	CS	F-CS	P1	ictrace6	0.4975	0.001968502	200
PKCd	FC	early	CS	F-CS	P1	ictrace8	0.4975	0.003431371	200
PKCd	FC	early	CS	F-CS	P3	ictrace9	0.496041667	0.003379851	200
PKCd	FC	early	CS	F-CS	P2	ictrace8	0.495833333	0.003620447	200
PKCd	FC	early	CS	F-CS	P1	ictrace10	0.495	0.002865019	200
PKCd	FC	early	CS	F-CS	P1	ictrace13	0.495	0.003709972	200
PKCd	FC	early	CS	F-CS	P1	ictrace11	0.493333333	0.003299832	200
PKCd	FC	early	CS	F-CS	P3	ictrace17	0.479375	0.004448758	200
PKCd	FC	early	CS	F-CS	P3	ictrace23	0.479166667	0.006660153	200
PKCd	FC	early	CS	F-CS	P1	ictrace3	0.473958333	0.005298695	200
PKCd	FC	early	CS	F-CS	P2	ictrace1	0.458333333	0.006640574	200
PKCd	FC	early	CS	F-CS	P1	ictrace1	0.456666667	0.005920773	200
PKCd	FC	early	CS	F-CS	P3	ictrace2	0.450833333	0.005502209	200
PKCd	FC	early	CS	F-CS	P3	ictrace6	0.444166667	0.005685935	200
PKCd	FC	early	CS	F-CS	P3	ictrace13	0.419791667	0.006242617	200
PKCd	FC	early	CS	F-CS	P4	ictrace2	0.417916667	0.007453036	200
PKCd	FC	early	CS	F-CS	P5	ictrace7	0.413958333	0.007016087	200
PKCd	FC	early	CS	F-CS	P1	ictrace5	0.41125	0.006090393	200
PKCd	**FC**	**early**	**US**	**F-CS**	**P3**	**ictrace10**	**0.666666667**	**0.00745356**	**200**
PKCd	**FC**	**early**	**US**	**F-CS**	**P2**	**ictrace7**	**0.616666667**	**0.010274023**	**200**
PKCd	**FC**	**early**	**US**	**F-CS**	**P4**	**ictrace8**	**0.6**	**0.005773503**	**200**
PKCd	**FC**	**early**	**US**	**F-CS**	**P5**	**ictrace2**	**0.6**	**0.00942809**	**200**
PKCd	**FC**	**early**	**US**	**F-CS**	**P3**	**ictrace4**	**0.591666667**	**0.005400617**	**200**
PKCd	**FC**	**early**	**US**	**F-CS**	**P3**	**ictrace9**	**0.591666667**	**0.005400617**	**200**
PKCd	**FC**	**early**	**US**	**F-CS**	**P5**	**ictrace9**	**0.591666667**	**0.009204468**	**200**
PKCd	**FC**	**early**	**US**	**F-CS**	**P3**	**ictrace3**	**0.583333333**	**0.00745356**	**200**
PKCd	**FC**	**early**	**US**	**F-CS**	**P1**	**ictrace5**	**0.566666667**	**0.005773503**	**200**
PKCd	**FC**	**early**	**US**	**F-CS**	**P1**	**ictrace6**	**0.566666667**	**0.005773503**	**200**
PKCd	**FC**	**early**	**US**	**F-CS**	**P3**	**ictrace23**	**0.566666667**	**0.005773503**	**200**
PKCd	**FC**	**early**	**US**	**F-CS**	**P1**	**ictrace9**	**0.558333333**	**0.005137012**	**200**
PKCd	**FC**	**early**	**US**	**F-CS**	**P2**	**ictrace2**	**0.558333333**	**0.005137012**	**200**
PKCd	**FC**	**early**	**US**	**F-CS**	**P2**	**ictrace5**	**0.558333333**	**0.005137012**	**200**
PKCd	**FC**	**early**	**US**	**F-CS**	**P2**	**ictrace6**	**0.558333333**	**0.005137012**	**200**
PKCd	**FC**	**early**	**US**	**F-CS**	**P2**	**ictrace8**	**0.558333333**	**0.005137012**	**200**
PKCd	**FC**	**early**	**US**	**F-CS**	**P2**	**ictrace9**	**0.558333333**	**0.005137012**	**200**
PKCd	**FC**	**early**	**US**	**F-CS**	**P3**	**ictrace2**	**0.558333333**	**0.009052317**	**200**
PKCd	**FC**	**early**	**US**	**F-CS**	**P3**	**ictrace7**	**0.558333333**	**0.005137012**	**200**
PKCd	**FC**	**early**	**US**	**F-CS**	**P4**	**ictrace7**	**0.558333333**	**0.005137012**	**200**
PKCd	**FC**	**early**	**US**	**F-CS**	**P5**	**ictrace12**	**0.558333333**	**0.005137012**	**200**
PKCd	**FC**	**early**	**US**	**F-CS**	**P5**	**ictrace13**	**0.558333333**	**0.005137012**	**200**
PKCd	**FC**	**early**	**US**	**F-CS**	**P5**	**ictrace6**	**0.558333333**	**0.005137012**	**200**
PKCd	**FC**	**early**	**US**	**F-CS**	**P1**	**ictrace2**	**0.504166667**	**0.00321401**	**200**
PKCd	**FC**	**early**	**US**	**F-CS**	**P2**	**ictrace4**	**0.5025**	**0.003222641**	**200**
PKCd	**FC**	**early**	**US**	**F-CS**	**P3**	**ictrace25**	**0.5025**	**0.003222641**	**200**
PKCd	**FC**	**early**	**US**	**F-CS**	**P1**	**ictrace4**	**0.501875**	**0.002721084**	**200**
PKCd	**FC**	**early**	**US**	**F-CS**	**P1**	**ictrace8**	**0.500833333**	**0.003226948**	**200**
PKCd	**FC**	**early**	**US**	**F-CS**	**P1**	**ictrace12**	**0.5**	**0**	**200**
PKCd	**FC**	**early**	**US**	**F-CS**	**P3**	**ictrace5**	**0.5**	**0.004330127**	**200**
PKCd	FC	early	US	F-CS	P4	ictrace6	0.5	0	200
PKCd	FC	early	US	F-CS	P5	ictrace8	0.5	0	200
PKCd	FC	early	US	F-CS	P1	ictrace14	0.49875	0.003185661	200
PKCd	FC	early	US	F-CS	P2	ictrace3	0.49875	0.002650177	200
PKCd	FC	early	US	F-CS	P1	ictrace11	0.4975	0.003431371	200
PKCd	FC	early	US	F-CS	P1	ictrace10	0.495	0.003892657	200
PKCd	FC	early	US	F-CS	P1	ictrace3	0.494375	0.00254606	200
PKCd	FC	early	US	F-CS	P3	ictrace12	0.494166667	0.00360892	200
PKCd	FC	early	US	F-CS	P3	ictrace22	0.490833333	0.003574116	200

PKCd	FC	early	US	F-CS	P5	ictrace10	0.4725	0.006349486	200
PKCd	FC	early	US	F-CS	P5	ictrace7	0.471666667	0.006573305	200
PKCd	FC	early	US	F-CS	P3	ictrace8	0.4675	0.006124858	200
PKCd	FC	early	US	F-CS	P3	ictrace11	0.466666667	0.006461693	200
PKCd	FC	early	US	F-CS	P3	ictrace13	0.4625	0.006394171	200
PKCd	FC	early	US	F-CS	P1	ictrace13	0.441666667	0.005137012	200
PKCd	FC	early	US	F-CS	P3	ictrace15	0.441666667	0.005137012	200
PKCd	FC	early	US	F-CS	P3	ictrace17	0.441666667	0.005137012	200
PKCd	FC	early	US	F-CS	P3	ictrace6	0.441666667	0.005137012	200
PKCd	FC	early	US	F-CS	P4	ictrace5	0.441666667	0.005137012	200
PKCd	FC	early	US	F-CS	P1	ictrace7	0.433333333	0.005773503	200
PKCd	FC	early	US	F-CS	P2	ictrace1	0.433333333	0.005773503	200
PKCd	FC	early	US	F-CS	P3	ictrace20	0.433333333	0.005773503	200
PKCd	FC	early	US	F-CS	P4	ictrace4	0.416666667	0.00745356	200
PKCd	FC	early	US	F-CS	P1	ictrace1	0.375	0.004564355	200
PKCd	FC	early	US	F-CS	P4	ictrace2	0.367291667	0.009233081	200
PKCd	FC	early	US	F-CS	P3	ictrace1	0.366666667	0.004714045	200
PKCd	**FC**	**late**	**CS**	**F-CS**	**P2**	**ictrace1**	**0.558333333**	**0.005137012**	**200**
PKCd	**FC**	**late**	**CS**	**F-CS**	**P3**	**ictrace7**	**0.558333333**	**0.005137012**	**200**
PKCd	**FC**	**late**	**CS**	**F-CS**	**P1**	**ictrace9**	**0.546458333**	**0.005529102**	**200**
PKCd	**FC**	**late**	**CS**	**F-CS**	**P1**	**ictrace17**	**0.545833333**	**0.005644257**	**200**
PKCd	**FC**	**late**	**CS**	**F-CS**	**P4**	**ictrace10**	**0.545208333**	**0.005235575**	**200**
PKCd	**FC**	**late**	**CS**	**F-CS**	**P1**	**ictrace8**	**0.540833333**	**0.005060056**	**200**
PKCd	**FC**	**late**	**CS**	**F-CS**	**P1**	**ictrace18**	**0.534375**	**0.004763846**	**200**
PKCd	**FC**	**late**	**CS**	**F-CS**	**P3**	**ictrace17**	**0.534166667**	**0.004803066**	**200**
PKCd	**FC**	**late**	**CS**	**F-CS**	**P3**	**ictrace8**	**0.517916667**	**0.005859391**	**200**
PKCd	**FC**	**late**	**CS**	**F-CS**	**P4**	**ictrace4**	**0.516458333**	**0.006481126**	**200**
PKCd	**FC**	**late**	**CS**	**F-CS**	**P1**	**ictrace2**	**0.505833333**	**0.00320102**	**200**
PKCd	**FC**	**late**	**CS**	**F-CS**	**P2**	**ictrace8**	**0.503333333**	**0.004242641**	**200**
PKCd	**FC**	**late**	**CS**	**F-CS**	**P1**	**ictrace13**	**0.503125**	**0.002410508**	**200**
PKCd	**FC**	**late**	**CS**	**F-CS**	**P3**	**ictrace9**	**0.503125**	**0.002715335**	**200**
PKCd	**FC**	**late**	**CS**	**F-CS**	**P1**	**ictrace7**	**0.5025**	**0.003431371**	**200**
PKCd	**FC**	**late**	**CS**	**F-CS**	**P2**	**ictrace12**	**0.501875**	**0.001074382**	**200**
PKCd	**FC**	**late**	**CS**	**F-CS**	**P3**	**ictrace4**	**0.501875**	**0.002799701**	**200**
PKCd	**FC**	**late**	**CS**	**F-CS**	**P3**	**ictrace13**	**0.50125**	**0.002930177**	**200**
PKCd	**FC**	**late**	**CS**	**F-CS**	**P1**	**ictrace16**	**0.5**	**0**	**200**
PKCd	**FC**	**late**	**CS**	**F-CS**	**P1**	**ictrace5**	**0.5**	**0**	**200**
PKCd	**FC**	**late**	**CS**	**F-CS**	**P2**	**ictrace11**	**0.5**	**0**	**200**
PKCd	**FC**	**late**	**CS**	**F-CS**	**P2**	**ictrace13**	**0.5**	**0**	**200**
PKCd	**FC**	**late**	**CS**	**F-CS**	**P2**	**ictrace2**	**0.5**	**0**	**200**
PKCd	**FC**	**late**	**CS**	**F-CS**	**P2**	**ictrace4**	**0.5**	**0.002338536**	**200**
PKCd	**FC**	**late**	**CS**	**F-CS**	**P2**	**ictrace9**	**0.5**	**0**	**200**
PKCd	**FC**	**late**	**CS**	**F-CS**	**P3**	**ictrace1**	**0.5**	**0**	**200**
PKCd	**FC**	**late**	**CS**	**F-CS**	**P3**	**ictrace10**	**0.5**	**0**	**200**
PKCd	**FC**	**late**	**CS**	**F-CS**	**P3**	**ictrace12**	**0.5**	**0**	**200**
PKCd	**FC**	**late**	**CS**	**F-CS**	**P3**	**ictrace14**	**0.5**	**0**	**200**
PKCd	**FC**	**late**	**CS**	**F-CS**	**P3**	**ictrace2**	**0.5**	**0**	**200**
PKCd	FC	late	CS	F-CS	P3	ictrace3	0.5	0	200
PKCd	FC	late	CS	F-CS	P4	ictrace5	0.5	0	200
PKCd	FC	late	CS	F-CS	P2	ictrace3	0.499375	0.002723953	200
PKCd	FC	late	CS	F-CS	P1	ictrace15	0.499166667	0.003435416	200
PKCd	FC	late	CS	F-CS	P1	ictrace6	0.499166667	0.003226948	200
PKCd	FC	late	CS	F-CS	P4	ictrace9	0.499166667	0.003226948	200
PKCd	FC	late	CS	F-CS	P1	ictrace14	0.4975	0.003222641	200
PKCd	FC	late	CS	F-CS	P3	ictrace5	0.4975	0.002493742	200
PKCd	FC	late	CS	F-CS	P1	ictrace3	0.495833333	0.002748105	200
PKCd	FC	late	CS	F-CS	P1	ictrace4	0.495833333	0.00321401	200
PKCd	FC	late	CS	F-CS	P1	ictrace1	0.48	0.007027723	200
PKCd	FC	late	CS	F-CS	P3	ictrace11	0.47875	0.0037959	200
PKCd	FC	late	CS	F-CS	P1	ictrace10	0.471458333	0.006070888	200

PKCd	FC	late	CS	F-CS	P2	ictrace5	0.461041667	0.004974566	200
PKCd	FC	late	CS	F-CS	P2	ictrace10	0.4575	0.004929714	200
PKCd	FC	late	CS	F-CS	P3	ictrace6	0.451041667	0.005106823	200
PKCd	FC	late	CS	F-CS	P4	ictrace11	0.44875	0.005014822	200
PKCd	FC	late	CS	F-CS	P2	ictrace7	0.445625	0.006368307	200
PKCd	FC	late	CS	F-CS	P2	ictrace14	0.444166667	0.005562461	200
PKCd	FC	late	CS	F-CS	P1	ictrace12	0.4425	0.005724885	200
PKCd	FC	late	CS	F-CS	P4	ictrace2	0.44125	0.008765809	200
PKCd	FC	late	CS	F-CS	P2	ictrace6	0.4275	0.006790772	200
PKCd	**FC**	**late**	**US**	**F-CS**	**P2**	**ictrace2**	**0.625**	**0.004564355**	**200**
PKCd	**FC**	**late**	**US**	**F-CS**	**P1**	**ictrace2**	**0.591666667**	**0.005400617**	**200**
PKCd	**FC**	**late**	**US**	**F-CS**	**P2**	**ictrace4**	**0.591666667**	**0.005400617**	**200**
PKCd	**FC**	**late**	**US**	**F-CS**	**P2**	**ictrace9**	**0.591666667**	**0.005400617**	**200**
PKCd	**FC**	**late**	**US**	**F-CS**	**P3**	**ictrace8**	**0.591666667**	**0.005400617**	**200**
PKCd	**FC**	**late**	**US**	**F-CS**	**P2**	**ictrace13**	**0.583333333**	**0.00745356**	**200**
PKCd	**FC**	**late**	**US**	**F-CS**	**P3**	**ictrace3**	**0.583333333**	**0.00745356**	**200**
PKCd	**FC**	**late**	**US**	**F-CS**	**P1**	**ictrace1**	**0.566666667**	**0.005773503**	**200**
PKCd	**FC**	**late**	**US**	**F-CS**	**P1**	**ictrace15**	**0.566666667**	**0.005773503**	**200**
PKCd	**FC**	**late**	**US**	**F-CS**	**P2**	**ictrace10**	**0.566666667**	**0.005773503**	**200**
PKCd	**FC**	**late**	**US**	**F-CS**	**P3**	**ictrace12**	**0.566666667**	**0.005773503**	**200**
PKCd	**FC**	**late**	**US**	**F-CS**	**P3**	**ictrace17**	**0.566666667**	**0.005773503**	**200**
PKCd	**FC**	**late**	**US**	**F-CS**	**P4**	**ictrace9**	**0.566666667**	**0.005773503**	**200**
PKCd	**FC**	**late**	**US**	**F-CS**	**P1**	**ictrace17**	**0.558333333**	**0.005137012**	**200**
PKCd	**FC**	**late**	**US**	**F-CS**	**P2**	**ictrace11**	**0.558333333**	**0.005137012**	**200**
PKCd	**FC**	**late**	**US**	**F-CS**	**P3**	**ictrace10**	**0.558333333**	**0.005137012**	**200**
PKCd	**FC**	**late**	**US**	**F-CS**	**P3**	**ictrace11**	**0.558333333**	**0.005137012**	**200**
PKCd	**FC**	**late**	**US**	**F-CS**	**P3**	**ictrace14**	**0.558333333**	**0.005137012**	**200**
PKCd	**FC**	**late**	**US**	**F-CS**	**P3**	**ictrace4**	**0.558333333**	**0.005137012**	**200**
PKCd	**FC**	**late**	**US**	**F-CS**	**P3**	**ictrace5**	**0.558333333**	**0.005137012**	**200**
PKCd	**FC**	**late**	**US**	**F-CS**	**P2**	**ictrace3**	**0.5075**	**0.002883141**	**200**
PKCd	**FC**	**late**	**US**	**F-CS**	**P1**	**ictrace6**	**0.505**	**0.003097938**	**200**
PKCd	**FC**	**late**	**US**	**F-CS**	**P3**	**ictrace7**	**0.504166667**	**0.003423266**	**200**
PKCd	**FC**	**late**	**US**	**F-CS**	**P3**	**ictrace2**	**0.50375**	**0.002638359**	**200**
PKCd	**FC**	**late**	**US**	**F-CS**	**P1**	**ictrace5**	**0.503333333**	**0.003109126**	**200**
PKCd	**FC**	**late**	**US**	**F-CS**	**P3**	**ictrace9**	**0.503333333**	**0.00332499**	**200**
PKCd	**FC**	**late**	**US**	**F-CS**	**P4**	**ictrace5**	**0.503125**	**0.002410508**	**200**
PKCd	**FC**	**late**	**US**	**F-CS**	**P1**	**ictrace16**	**0.5025**	**0.003814719**	**200**
PKCd	**FC**	**late**	**US**	**F-CS**	**P1**	**ictrace13**	**0.501666667**	**0.003533569**	**200**
PKCd	**FC**	**late**	**US**	**F-CS**	**P2**	**ictrace8**	**0.500833333**	**0.003818358**	**200**
PKCd	FC	late	US	F-CS	P1	ictrace10	0.5	0	200
PKCd	FC	late	US	F-CS	P1	ictrace18	0.5	0	200
PKCd	FC	late	US	F-CS	P1	ictrace3	0.5	0	200
PKCd	FC	late	US	F-CS	P1	ictrace4	0.5	0	200
PKCd	FC	late	US	F-CS	P1	ictrace8	0.5	0	200
PKCd	FC	late	US	F-CS	P1	ictrace9	0.5	0	200
PKCd	FC	late	US	F-CS	P2	ictrace1	0.5	0	200
PKCd	FC	late	US	F-CS	P2	ictrace14	0.5	0	200
PKCd	FC	late	US	F-CS	P2	ictrace5	0.5	0.00372678	200
PKCd	FC	late	US	F-CS	P3	ictrace6	0.5	0	200
PKCd	FC	late	US	F-CS	P4	ictrace10	0.5	0	200
PKCd	FC	late	US	F-CS	P3	ictrace13	0.49875	0.003185661	200
PKCd	FC	late	US	F-CS	P4	ictrace2	0.498333333	0.010137253	200
PKCd	FC	late	US	F-CS	P2	ictrace6	0.49625	0.008790531	200
PKCd	FC	late	US	F-CS	P2	ictrace12	0.495	0.002910112	200
PKCd	FC	late	US	F-CS	P3	ictrace1	0.49375	0.002460627	200
PKCd	FC	late	US	F-CS	P1	ictrace12	0.467916667	0.006378607	200
PKCd	FC	late	US	F-CS	P4	ictrace4	0.467708333	0.006349469	200
PKCd	FC	late	US	F-CS	P4	ictrace11	0.465416667	0.006319818	200
PKCd	FC	late	US	F-CS	P1	ictrace14	0.461666667	0.006423697	200
PKCd	FC	late	US	F-CS	P1	ictrace7	0.433333333	0.005773503	200

PKCd	FC	late	US	F-CS	P2	ictrace7	0.433333333	0.005773503	200
PKCd	**recall**	**PBS**	**CS**	**R-CS**	**P4**	**ictrace3**	**0.578690476**	**0.005654317**	**200**
PKCd	**recall**	**PBS**	**CS**	**R-CS**	**P2**	**ictrace4**	**0.558869048**	**0.004070486**	**200**
PKCd	**recall**	**PBS**	**CS**	**R-CS**	**P3**	**ictrace5t2**	**0.55422619**	**0.005692355**	**200**
PKCd	**recall**	**PBS**	**CS**	**R-CS**	**P3**	**ictrace4**	**0.552440476**	**0.004011655**	**200**
PKCd	**recall**	**PBS**	**CS**	**R-CS**	**P3**	**ictrace10t2**	**0.537083333**	**0.003520648**	**200**
PKCd	**recall**	**PBS**	**CS**	**R-CS**	**P3**	**ictrace6**	**0.535059524**	**0.002672874**	**200**
PKCd	**recall**	**PBS**	**CS**	**R-CS**	**P1**	**ictrace24t2**	**0.53452381**	**0.00282973**	**200**
PKCd	**recall**	**PBS**	**CS**	**R-CS**	**P3**	**ictrace12**	**0.533571429**	**0.004046533**	**200**
PKCd	**recall**	**PBS**	**CS**	**R-CS**	**P3**	**ictrace3t2**	**0.53327381**	**0.00329839**	**200**
PKCd	**recall**	**PBS**	**CS**	**R-CS**	**P1**	**ictrace9t2**	**0.530952381**	**0.00269374**	**200**
PKCd	**recall**	**PBS**	**CS**	**R-CS**	**P1**	**ictrace3**	**0.530297619**	**0.003798158**	**200**
PKCd	**recall**	**PBS**	**CS**	**R-CS**	**P5**	**ictrace3**	**0.526547619**	**0.004154498**	**200**
PKCd	**recall**	**PBS**	**CS**	**R-CS**	**P5**	**ictrace8t2**	**0.5225**	**0.00292914**	**200**
PKCd	**recall**	**PBS**	**CS**	**R-CS**	**P1**	**ictrace1**	**0.522440476**	**0.002561845**	**200**
PKCd	**recall**	**PBS**	**CS**	**R-CS**	**P5**	**ictrace9**	**0.521845238**	**0.00254603**	**200**
PKCd	**recall**	**PBS**	**CS**	**R-CS**	**P2**	**ictrace2**	**0.52172619**	**0.004248714**	**200**
PKCd	**recall**	**PBS**	**CS**	**R-CS**	**P3**	**ictrace5**	**0.521607143**	**0.00399216**	**200**
PKCd	**recall**	**PBS**	**CS**	**R-CS**	**P3**	**ictrace16**	**0.52**	**0.004867694**	**200**
PKCd	**recall**	**PBS**	**CS**	**R-CS**	**P1**	**ictrace13**	**0.519583333**	**0.002698862**	**200**
PKCd	**recall**	**PBS**	**CS**	**R-CS**	**P1**	**ictrace8**	**0.51922619**	**0.002624018**	**200**
PKCd	**recall**	**PBS**	**CS**	**R-CS**	**P1**	**ictrace12t2**	**0.518928571**	**0.002647559**	**200**
PKCd	**recall**	**PBS**	**CS**	**R-CS**	**P3**	**ictrace1t2**	**0.518928571**	**0.002731864**	**200**
PKCd	**recall**	**PBS**	**CS**	**R-CS**	**P5**	**ictrace1**	**0.517142857**	**0.002470977**	**200**
PKCd	**recall**	**PBS**	**CS**	**R-CS**	**P4**	**ictrace12**	**0.516607143**	**0.002513988**	**200**
PKCd	**recall**	**PBS**	**CS**	**R-CS**	**P2**	**ictrace1**	**0.514285714**	**0.002428105**	**200**
PKCd	**recall**	**PBS**	**CS**	**R-CS**	**P1**	**ictrace27t2**	**0.514166667**	**0.003233398**	**200**
PKCd	**recall**	**PBS**	**CS**	**R-CS**	**P3**	**ictrace13t2**	**0.514107143**	**0.004243407**	**200**
PKCd	**recall**	**PBS**	**CS**	**R-CS**	**P1**	**ictrace11**	**0.513928571**	**0.002560368**	**200**
PKCd	**recall**	**PBS**	**CS**	**R-CS**	**P1**	**ictrace18t2**	**0.511785714**	**0.004104114**	**200**
PKCd	**recall**	**PBS**	**CS**	**R-CS**	**P3**	**ictrace3**	**0.51125**	**0.002546614**	**200**
PKCd	recall	PBS	CS	R-CS	P3	ictrace7t2	0.508690476	0.001941079	200
PKCd	recall	PBS	CS	R-CS	P2	ictrace8t2	0.5075	0.002712497	200
PKCd	recall	PBS	CS	R-CS	P3	ictrace18	0.50702381	0.003269142	200
PKCd	recall	PBS	CS	R-CS	P4	ictrace6	0.50547619	0.004169931	200
PKCd	recall	PBS	CS	R-CS	P3	ictrace2	0.505416667	0.00156763	200
PKCd	recall	PBS	CS	R-CS	P3	ictrace12t2	0.50452381	0.003937184	200
PKCd	recall	PBS	CS	R-CS	P2	ictrace3	0.502142857	0.001420513	200
PKCd	recall	PBS	CS	R-CS	P2	ictrace1t2	0.501904762	0.003278071	200
PKCd	recall	PBS	CS	R-CS	P3	ictrace9	0.501428571	0.0016721	200
PKCd	recall	PBS	CS	R-CS	P1	ictrace17t2	0.501428571	0.0016721	200
PKCd	recall	PBS	CS	R-CS	P1	ictrace7	0.50125	0.003088818	200
PKCd	recall	PBS	CS	R-CS	P1	ictrace16t2	0.50125	0.001814056	200
PKCd	recall	PBS	CS	R-CS	P1	ictrace19t2	0.50125	0.001611321	200
PKCd	recall	PBS	CS	R-CS	P3	ictrace10	0.501071429	0.001470587	200
PKCd	recall	PBS	CS	R-CS	P1	ictrace5	0.500833333	0.001766785	200
PKCd	recall	PBS	CS	R-CS	P5	ictrace4	0.500714286	0.001674387	200
PKCd	recall	PBS	CS	R-CS	P1	ictrace12	0.500416667	0.001717708	200
PKCd	recall	PBS	CS	R-CS	P5	ictrace18	0.500416667	0.002863804	200
PKCd	recall	PBS	CS	R-CS	P3	ictrace6t2	0.500357143	0.000356249	200
PKCd	recall	PBS	CS	R-CS	P1	ictrace14	0.5	0	200
PKCd	recall	PBS	CS	R-CS	P1	ictrace17	0.5	0.001767767	200
PKCd	recall	PBS	CS	R-CS	P1	ictrace2	0.5	0.001443376	200
PKCd	recall	PBS	CS	R-CS	P1	ictrace9	0.5	0.00186339	200
PKCd	recall	PBS	CS	R-CS	P3	ictrace19	0.5	0	200
PKCd	recall	PBS	CS	R-CS	P1	ictrace11t2	0.5	0.000589256	200
PKCd	recall	PBS	CS	R-CS	P1	ictrace15t2	0.5	0	200
PKCd	recall	PBS	CS	R-CS	P1	ictrace22t2	0.5	0	200
PKCd	recall	PBS	CS	R-CS	P1	ictrace23t2	0.5	0	200
PKCd	recall	PBS	CS	R-CS	P1	ictrace4t2	0.5	0	200

PKCd	recall	PBS	CS	R-CS	P1	ictrace6t2	0.5	0	200
PKCd	recall	PBS	CS	R-CS	P2	ictrace5t2	0.5	0	200
PKCd	recall	PBS	CS	R-CS	P2	ictrace7t2	0.5	0	200
PKCd	recall	PBS	CS	R-CS	P2	ictrace4t2	0.499642857	0.00118424	200
PKCd	recall	PBS	CS	R-CS	P5	ictrace8	0.499642857	0.001636439	200
PKCd	recall	PBS	CS	R-CS	P1	ictrace15	0.499464286	0.003962961	200
PKCd	recall	PBS	CS	R-CS	P1	ictrace1t2	0.499285714	0.001514387	200
PKCd	recall	PBS	CS	R-CS	P1	ictrace5t2	0.499285714	0.001596393	200
PKCd	recall	PBS	CS	R-CS	P5	ictrace2	0.499166667	0.001862458	200
PKCd	recall	PBS	CS	R-CS	P5	ictrace10t2	0.499166667	0.001665625	200
PKCd	recall	PBS	CS	R-CS	P1	ictrace6	0.497916667	0.001711633	200
PKCd	recall	PBS	CS	R-CS	P1	ictrace20	0.4975	0.001165178	200
PKCd	recall	PBS	CS	R-CS	P5	ictrace11	0.4975	0.001657265	200
PKCd	recall	PBS	CS	R-CS	P3	ictrace15t2	0.497202381	0.001737397	200
PKCd	recall	PBS	CS	R-CS	P1	ictrace21t2	0.496369048	0.002781995	200
PKCd	recall	PBS	CS	R-CS	P3	ictrace17	0.494702381	0.003211747	200
PKCd	recall	PBS	CS	R-CS	P2	ictrace3t2	0.49452381	0.003203067	200
PKCd	recall	PBS	CS	R-CS	P5	ictrace8	0.49422619	0.001963343	200
PKCd	recall	PBS	CS	R-CS	P1	ictrace18	0.493928571	0.001579323	200
PKCd	recall	PBS	CS	R-CS	P1	ictrace7t2	0.493511905	0.001915516	200
PKCd	recall	PBS	CS	R-CS	P4	ictrace7	0.493214286	0.003311482	200
PKCd	recall	PBS	CS	R-CS	P2	ictrace6	0.492678571	0.003309521	200
PKCd	recall	PBS	CS	R-CS	P3	ictrace15	0.492202381	0.004177365	200
PKCd	recall	PBS	CS	R-CS	P3	ictrace4t2	0.491904762	0.003321365	200
PKCd	recall	PBS	CS	R-CS	P5	ictrace6t2	0.488928571	0.004822905	200
PKCd	recall	PBS	CS	R-CS	P2	ictrace6t2	0.488214286	0.003351344	200
PKCd	recall	PBS	CS	R-CS	P5	ictrace6	0.483333333	0.003227486	200
PKCd	recall	PBS	CS	R-CS	P5	ictrace5	0.482619048	0.002944883	200
PKCd	recall	PBS	CS	R-CS	P5	ictrace14	0.478869048	0.002539983	200
PKCd	recall	PBS	CS	R-CS	P1	ictrace3t2	0.478452381	0.003280178	200
PKCd	recall	PBS	CS	R-CS	P3	ictrace20	0.477857143	0.003036344	200
PKCd	recall	PBS	CS	R-CS	P1	ictrace16	0.477559524	0.00262874	200
PKCd	recall	PBS	CS	R-CS	P3	ictrace2t2	0.4775	0.004329137	200
PKCd	recall	PBS	CS	R-CS	P1	ictrace26t2	0.476666667	0.002773886	200
PKCd	recall	PBS	CS	R-CS	P3	ictrace21	0.476011905	0.002738713	200
PKCd	recall	PBS	CS	R-CS	P3	ictrace8	0.475297619	0.004579805	200
PKCd	recall	PBS	CS	R-CS	P1	ictrace13t2	0.474702381	0.002949809	200
PKCd	recall	PBS	CS	R-CS	P1	ictrace2t2	0.47375	0.002597718	200
PKCd	recall	PBS	CS	R-CS	P3	ictrace1	0.472916667	0.002942593	200
PKCd	recall	PBS	CS	R-CS	P1	ictrace10t2	0.472559524	0.002756406	200
PKCd	recall	PBS	CS	R-CS	P3	ictrace23	0.4725	0.002633066	200
PKCd	recall	PBS	CS	R-CS	P1	ictrace10	0.469583333	0.002897407	200
PKCd	recall	PBS	CS	R-CS	P3	ictrace7	0.46952381	0.003431422	200
PKCd	recall	PBS	CS	R-CS	P1	ictrace14t2	0.464880952	0.003905733	200
PKCd	recall	PBS	CS	R-CS	P1	ictrace21	0.463511905	0.00349935	200
PKCd	recall	PBS	CS	R-CS	P5	ictrace4	0.463511905	0.004206508	200
PKCd	recall	PBS	CS	R-CS	P1	ictrace4	0.460535714	0.004038485	200
PKCd	recall	PBS	CS	R-CS	P2	ictrace2t2	0.460297619	0.003469046	200
PKCd	recall	PBS	CS	R-CS	P5	ictrace7	0.459166667	0.004039303	200
PKCd	recall	PBS	CS	R-CS	P5	ictrace7t2	0.454166667	0.00477806	200
PKCd	recall	PBS	CS	R-CS	P1	ictrace8t2	0.452202381	0.004432408	200
PKCd	recall	PBS	CS	R-CS	P2	ictrace5	0.426666667	0.004619477	200
PKCd	**recall**	**PBS**	**CS**	**F-CS**	**P2**	**ictrace2**	**0.597875**	**0.004103267**	**200**
PKCd	**recall**	**PBS**	**CS**	**F-CS**	**P3**	**ictrace5**	**0.565**	**0.003807887**	**200**
PKCd	**recall**	**PBS**	**CS**	**F-CS**	**P2**	**ictrace8t2**	**0.561309524**	**0.003326683**	**200**
PKCd	**recall**	**PBS**	**CS**	**F-CS**	**P1**	**ictrace3**	**0.56**	**0.005656854**	**200**
PKCd	**recall**	**PBS**	**CS**	**F-CS**	**P5**	**ictrace8t2**	**0.547619048**	**0.002766417**	**200**
PKCd	**recall**	**PBS**	**CS**	**F-CS**	**P1**	**ictrace20t2**	**0.545952381**	**0.003734416**	**200**
PKCd	**recall**	**PBS**	**CS**	**F-CS**	**P2**	**ictrace6t2**	**0.545238095**	**0.002629848**	**200**
PKCd	**recall**	**PBS**	**CS**	**F-CS**	**P3**	**ictrace5t2**	**0.545238095**	**0.004137654**	**200**

PKCd	**recall**	**PBS**	**CS**	**F-CS**	**P5**	**ictrace4**	**0.544125**	**0.00473345**	**200**
PKCd	**recall**	**PBS**	**CS**	**F-CS**	**P1**	**ictrace12**	**0.54**	**0.003464102**	**200**
PKCd	**recall**	**PBS**	**CS**	**F-CS**	**P1**	**ictrace9**	**0.54**	**0.003464102**	**200**
PKCd	**recall**	**PBS**	**CS**	**F-CS**	**P2**	**ictrace1**	**0.54**	**0.003464102**	**200**
PKCd	**recall**	**PBS**	**CS**	**F-CS**	**P2**	**ictrace6**	**0.54**	**0.003464102**	**200**
PKCd	**recall**	**PBS**	**CS**	**F-CS**	**P1**	**ictrace14t2**	**0.530952381**	**0.00269374**	**200**
PKCd	**recall**	**PBS**	**CS**	**F-CS**	**P2**	**ictrace2t2**	**0.530952381**	**0.00269374**	**200**
PKCd	**recall**	**PBS**	**CS**	**F-CS**	**P1**	**ictrace11t2**	**0.530952381**	**0.00269374**	**200**
PKCd	**recall**	**PBS**	**CS**	**F-CS**	**P1**	**ictrace23t2**	**0.530952381**	**0.00269374**	**200**
PKCd	**recall**	**PBS**	**CS**	**F-CS**	**P1**	**ictrace3t2**	**0.530952381**	**0.00269374**	**200**
PKCd	**recall**	**PBS**	**CS**	**F-CS**	**P3**	**ictrace2t2**	**0.53077381**	**0.005012935**	**200**
PKCd	**recall**	**PBS**	**CS**	**F-CS**	**P4**	**ictrace12**	**0.5245**	**0.003353916**	**200**
PKCd	**recall**	**PBS**	**CS**	**F-CS**	**P3**	**ictrace9**	**0.5235**	**0.003238634**	**200**
PKCd	**recall**	**PBS**	**CS**	**F-CS**	**P1**	**ictrace25t2**	**0.523214286**	**0.002518005**	**200**
PKCd	**recall**	**PBS**	**CS**	**F-CS**	**P1**	**ictrace17t2**	**0.523035714**	**0.002828574**	**200**
PKCd	**recall**	**PBS**	**CS**	**F-CS**	**P1**	**ictrace6t2**	**0.517857143**	**0.002562982**	**200**
PKCd	**recall**	**PBS**	**CS**	**F-CS**	**P1**	**ictrace19t2**	**0.515833333**	**0.002863473**	**200**
PKCd	**recall**	**PBS**	**CS**	**F-CS**	**P1**	**ictrace11**	**0.51475**	**0.003113429**	**200**
PKCd	**recall**	**PBS**	**CS**	**F-CS**	**P3**	**ictrace2**	**0.5105**	**0.003633008**	**200**
PKCd	**recall**	**PBS**	**CS**	**F-CS**	**P1**	**ictrace1t2**	**0.508690476**	**0.00456413**	**200**
PKCd	**recall**	**PBS**	**CS**	**F-CS**	**P1**	**ictrace2t2**	**0.505416667**	**0.001868702**	**200**
PKCd	**recall**	**PBS**	**CS**	**F-CS**	**P1**	**ictrace2**	**0.5045**	**0.002269086**	**200**
PKCd	recall	PBS	CS	F-CS	P4	ictrace6	0.5045	0.006866495	200
PKCd	recall	PBS	CS	F-CS	P1	ictrace13t2	0.503630952	0.004192266	200
PKCd	recall	PBS	CS	F-CS	P1	ictrace4t2	0.503214286	0.001540069	200
PKCd	recall	PBS	CS	F-CS	P3	ictrace14	0.5025	0.002926175	200
PKCd	recall	PBS	CS	F-CS	P1	ictrace5t2	0.502142857	0.001227865	200
PKCd	recall	PBS	CS	F-CS	P1	ictrace10	0.502	0.001994994	200
PKCd	recall	PBS	CS	F-CS	P1	ictrace19	0.502	0.002116601	200
PKCd	recall	PBS	CS	F-CS	P1	ictrace18t2	0.501785714	0.00155162	200
PKCd	recall	PBS	CS	F-CS	P3	ictrace10t2	0.501666667	0.001554563	200
PKCd	recall	PBS	CS	F-CS	P1	ictrace17	0.5015	0.001933585	200
PKCd	recall	PBS	CS	F-CS	P3	ictrace21	0.5015	0.002176867	200
PKCd	recall	PBS	CS	F-CS	P1	ictrace12t2	0.50125	0.001611321	200
PKCd	recall	PBS	CS	F-CS	P3	ictrace6t2	0.50125	0.001379097	200
PKCd	recall	PBS	CS	F-CS	P1	ictrace21	0.500625	0.002863769	200
PKCd	recall	PBS	CS	F-CS	P1	ictrace7	0.5005	0.00206125	200
PKCd	recall	PBS	CS	F-CS	P1	ictrace13	0.5	0.00212132	200
PKCd	recall	PBS	CS	F-CS	P1	ictrace18	0.5	0	200
PKCd	recall	PBS	CS	F-CS	P1	ictrace4	0.5	0	200
PKCd	recall	PBS	CS	F-CS	P1	ictrace5	0.5	0	200
PKCd	recall	PBS	CS	F-CS	P1	ictrace8	0.5	0	200
PKCd	recall	PBS	CS	F-CS	P3	ictrace10	0.5	0	200
PKCd	recall	PBS	CS	F-CS	P3	ictrace12	0.5	0	200
PKCd	recall	PBS	CS	F-CS	P3	ictrace20	0.5	0	200
PKCd	recall	PBS	CS	F-CS	P3	ictrace7	0.5	0	200
PKCd	recall	PBS	CS	F-CS	P4	ictrace7	0.5	0	200
PKCd	recall	PBS	CS	F-CS	P5	ictrace2	0.5	0.002	200
PKCd	recall	PBS	CS	F-CS	P1	ictrace22t2	0.499642857	0.001382978	200
PKCd	recall	PBS	CS	F-CS	P3	ictrace12t2	0.499642857	0.001382978	200
PKCd	recall	PBS	CS	F-CS	P3	ictrace15t2	0.499583333	0.001613474	200
PKCd	recall	PBS	CS	F-CS	P3	ictrace1	0.499375	0.002420211	200
PKCd	recall	PBS	CS	F-CS	P2	ictrace5t2	0.499166667	0.001862458	200
PKCd	recall	PBS	CS	F-CS	P5	ictrace7t2	0.499107143	0.002947405	200
PKCd	recall	PBS	CS	F-CS	P3	ictrace8	0.498875	0.002245116	200
PKCd	recall	PBS	CS	F-CS	P1	ictrace1	0.4985	0.001654917	200
PKCd	recall	PBS	CS	F-CS	P3	ictrace6	0.4985	0.002288832	200
PKCd	recall	PBS	CS	F-CS	P1	ictrace16t2	0.498333333	0.001763834	200
PKCd	recall	PBS	CS	F-CS	P1	ictrace8t2	0.498214286	0.001281491	200
PKCd	recall	PBS	CS	F-CS	P5	ictrace9	0.498	0.001865476	200

PKCd	recall	PBS	CS	F-CS	P2	ictrace1t2	0.497916667	0.001711633	200
PKCd	recall	PBS	CS	F-CS	P1	ictrace24t2	0.497857143	0.001327688	200
PKCd	recall	PBS	CS	F-CS	P1	ictrace15	0.497125	0.004744001	200
PKCd	recall	PBS	CS	F-CS	P1	ictrace20	0.497	0.002335594	200
PKCd	recall	PBS	CS	F-CS	P3	ictrace15	0.496375	0.004845737	200
PKCd	recall	PBS	CS	F-CS	P2	ictrace4	0.49625	0.005722079	200
PKCd	recall	PBS	CS	F-CS	P3	ictrace17	0.49625	0.002638359	200
PKCd	recall	PBS	CS	F-CS	P3	ictrace4	0.495625	0.004761294	200
PKCd	recall	PBS	CS	F-CS	P1	ictrace10t2	0.494047619	0.001517565	200
PKCd	recall	PBS	CS	F-CS	P1	ictrace15t2	0.493333333	0.003494854	200
PKCd	recall	PBS	CS	F-CS	P4	ictrace3	0.492875	0.006674058	200
PKCd	recall	PBS	CS	F-CS	P3	ictrace13t2	0.491369048	0.002519675	200
PKCd	recall	PBS	CS	F-CS	P3	ictrace4t2	0.487261905	0.00241128	200
PKCd	recall	PBS	CS	F-CS	P3	ictrace3t2	0.484404762	0.004284383	200
PKCd	recall	PBS	CS	F-CS	P1	ictrace21t2	0.482083333	0.003214283	200
PKCd	recall	PBS	CS	F-CS	P1	ictrace9t2	0.480297619	0.003039327	200
PKCd	recall	PBS	CS	F-CS	P3	ictrace7t2	0.479404762	0.00295913	200
PKCd	recall	PBS	CS	F-CS	P5	ictrace6	0.4785	0.003733464	200
PKCd	recall	PBS	CS	F-CS	P5	ictrace6t2	0.477797619	0.003005425	200
PKCd	recall	PBS	CS	F-CS	P2	ictrace4t2	0.477380952	0.00314182	200
PKCd	recall	PBS	CS	F-CS	P1	ictrace26t2	0.477202381	0.004360929	200
PKCd	recall	PBS	CS	F-CS	P5	ictrace14	0.476	0.003888444	200
PKCd	recall	PBS	CS	F-CS	P5	ictrace10t2	0.474464286	0.002715222	200
PKCd	recall	PBS	CS	F-CS	P1	ictrace27t2	0.474107143	0.002591081	200
PKCd	recall	PBS	CS	F-CS	P5	ictrace8	0.4705	0.003376203	200
PKCd	recall	PBS	CS	F-CS	P5	ictrace11	0.47	0.003535534	200
PKCd	recall	PBS	CS	F-CS	P5	ictrace1	0.4695	0.003405694	200
PKCd	recall	PBS	CS	F-CS	P2	ictrace5	0.469375	0.003743484	200
PKCd	recall	PBS	CS	F-CS	P3	ictrace16	0.469	0.003509986	200
PKCd	recall	PBS	CS	F-CS	P5	ictrace5	0.4685	0.003505531	200
PKCd	recall	PBS	CS	F-CS	P3	ictrace11	0.466	0.003423449	200
PKCd	recall	PBS	CS	F-CS	P1	ictrace16	0.466	0.003349627	200
PKCd	recall	PBS	CS	F-CS	P1	ictrace14	0.464	0.003394113	200
PKCd	recall	PBS	CS	F-CS	P2	ictrace7t2	0.463333333	0.003802412	200
PKCd	recall	PBS	CS	F-CS	P3	ictrace18	0.46125	0.004010728	200
PKCd	recall	PBS	CS	F-CS	P1	ictrace7t2	0.449642857	0.00498418	200
PKCd	**recall**	**aIC inhibition**	**CS**	**R-CS**	**P3**	**ictrace5**	**0.578571429**	**0.003749528**	**200**
PKCd	**recall**	**aIC inhibition**	**CS**	**R-CS**	**P1**	**ictrace19**	**0.553511905**	**0.003487097**	**200**
PKCd	**recall**	**aIC inhibition**	**CS**	**R-CS**	**P2**	**ictrace9**	**0.548392857**	**0.005310029**	**200**
PKCd	**recall**	**aIC inhibition**	**CS**	**R-CS**	**P1**	**ictrace9**	**0.547619048**	**0.002766417**	**200**
PKCd	**recall**	**aIC inhibition**	**CS**	**R-CS**	**P2**	**ictrace1**	**0.547619048**	**0.004641331**	**200**
PKCd	**recall**	**aIC inhibition**	**CS**	**R-CS**	**P1**	**ictrace9t2**	**0.547619048**	**0.002766417**	**200**
PKCd	**recall**	**aIC inhibition**	**CS**	**R-CS**	**P1**	**ictrace13t2**	**0.537619048**	**0.002888518**	**200**
PKCd	**recall**	**aIC inhibition**	**CS**	**R-CS**	**P1**	**ictrace20**	**0.537202381**	**0.002807023**	**200**
PKCd	**recall**	**aIC inhibition**	**CS**	**R-CS**	**P2**	**ictrace7**	**0.534940476**	**0.002878242**	**200**
PKCd	**recall**	**aIC inhibition**	**CS**	**R-CS**	**P1**	**ictrace1t2**	**0.533333333**	**0.002886751**	**200**
PKCd	**recall**	**aIC inhibition**	**CS**	**R-CS**	**P1**	**ictrace7**	**0.530952381**	**0.00269374**	**200**
PKCd	**recall**	**aIC inhibition**	**CS**	**R-CS**	**P3**	**ictrace18t2**	**0.523333333**	**0.004698114**	**200**
PKCd	**recall**	**aIC inhibition**	**CS**	**R-CS**	**P2**	**ictrace2t2**	**0.520833333**	**0.002748105**	**200**
PKCd	**recall**	**aIC inhibition**	**CS**	**R-CS**	**P3**	**ictrace24**	**0.519880952**	**0.002675408**	**200**
PKCd	**recall**	**aIC inhibition**	**CS**	**R-CS**	**P2**	**ictrace2**	**0.518154762**	**0.002526696**	**200**
PKCd	**recall**	**aIC inhibition**	**CS**	**R-CS**	**P3**	**ictrace20t2**	**0.517916667**	**0.005722339**	**200**
PKCd	**recall**	**aIC inhibition**	**CS**	**R-CS**	**P1**	**ictrace13**	**0.516785714**	**0.002473198**	**200**
PKCd	**recall**	**aIC inhibition**	**CS**	**R-CS**	**P3**	**ictrace6t2**	**0.516309524**	**0.005358009**	**200**
PKCd	**recall**	**aIC inhibition**	**CS**	**R-CS**	**P2**	**ictrace6**	**0.514285714**	**0.003160933**	**200**
PKCd	**recall**	**aIC inhibition**	**CS**	**R-CS**	**P1**	**ictrace6t2**	**0.514285714**	**0.002585006**	**200**
PKCd	**recall**	**aIC inhibition**	**CS**	**R-CS**	**P3**	**ictrace14**	**0.510714286**	**0.002244608**	**200**
PKCd	**recall**	**aIC inhibition**	**CS**	**R-CS**	**P1**	**ictrace6**	**0.509642857**	**0.002922601**	**200**
PKCd	**recall**	**aIC inhibition**	**CS**	**R-CS**	**P3**	**ictrace11**	**0.50952381**	**0.003500283**	**200**
PKCd	**recall**	**aIC inhibition**	**CS**	**R-CS**	**P2**	**ictrace8**	**0.508630952**	**0.003991148**	**200**

PKCd	**recall**	**aIC inhibition**	**CS**	**R-CS**	**P3**	**ictrace16**	**0.508571429**	**0.002882034**	**200**
PKCd	**recall**	**aIC inhibition**	**CS**	**R-CS**	**P3**	**ictrace7**	**0.50702381**	**0.002222702**	**200**
PKCd	**recall**	**aIC inhibition**	**CS**	**R-CS**	**P3**	**ictrace9**	**0.506428571**	**0.001763432**	**200**
PKCd	**recall**	**aIC inhibition**	**CS**	**R-CS**	**P3**	**ictrace16t2**	**0.505238095**	**0.003838838**	**200**
PKCd	**recall**	**aIC inhibition**	**CS**	**R-CS**	**P3**	**ictrace5t2**	**0.503214286**	**0.002218746**	**200**
PKCd	**recall**	**aIC inhibition**	**CS**	**R-CS**	**P1**	**ictrace14**	**0.502083333**	**0.001374053**	**200**
PKCd	recall	aIC inhibition	CS	R-CS	P1	ictrace11	0.501666667	0.001662495	200
PKCd	recall	aIC inhibition	CS	R-CS	P2	ictrace6t2	0.501071429	0.00163488	200
PKCd	recall	aIC inhibition	CS	R-CS	P3	ictrace12t2	0.500595238	0.001459851	200
PKCd	recall	aIC inhibition	CS	R-CS	P1	ictrace10	0.500416667	0.001502024	200
PKCd	recall	aIC inhibition	CS	R-CS	P2	ictrace3	0.500416667	0.001717708	200
PKCd	recall	aIC inhibition	CS	R-CS	P1	ictrace1	0.500357143	0.001287449	200
PKCd	recall	aIC inhibition	CS	R-CS	P2	ictrace4	0.500357143	0.00388587	200
PKCd	recall	aIC inhibition	CS	R-CS	P3	ictrace21	0.500357143	0.001636439	200
PKCd	recall	aIC inhibition	CS	R-CS	P2	ictrace4t2	0.500357143	0.001712611	200
PKCd	recall	aIC inhibition	CS	R-CS	P1	ictrace2t2	0.5	0	200
PKCd	recall	aIC inhibition	CS	R-CS	P1	ictrace5t2	0.5	0	200
PKCd	recall	aIC inhibition	CS	R-CS	P3	ictrace7t2	0.5	0	200
PKCd	recall	aIC inhibition	CS	R-CS	P3	ictrace19	0.499642857	0.00118424	200
PKCd	recall	aIC inhibition	CS	R-CS	P3	ictrace22t2	0.499642857	0.001472321	200
PKCd	recall	aIC inhibition	CS	R-CS	P1	ictrace15	0.499583333	0.001717708	200
PKCd	recall	aIC inhibition	CS	R-CS	P1	ictrace16	0.499583333	0.001502024	200
PKCd	recall	aIC inhibition	CS	R-CS	P1	ictrace3	0.499583333	0.001909179	200
PKCd	recall	aIC inhibition	CS	R-CS	P1	ictrace10t2	0.499583333	0.001909179	200
PKCd	recall	aIC inhibition	CS	R-CS	P1	ictrace12t2	0.499285714	0.001427678	200
PKCd	recall	aIC inhibition	CS	R-CS	P1	ictrace14t2	0.499166667	0.001442172	200
PKCd	recall	aIC inhibition	CS	R-CS	P1	ictrace12	0.49875	0.001499711	200
PKCd	recall	aIC inhibition	CS	R-CS	P1	ictrace4t2	0.498571429	0.001233048	200
PKCd	recall	aIC inhibition	CS	R-CS	P1	ictrace7t2	0.498571429	0.001593994	200
PKCd	recall	aIC inhibition	CS	R-CS	P3	ictrace8	0.498333333	0.001859659	200
PKCd	recall	aIC inhibition	CS	R-CS	P3	ictrace18	0.498214286	0.001281491	200
PKCd	recall	aIC inhibition	CS	R-CS	P1	ictrace15t2	0.498035714	0.001341011	200
PKCd	recall	aIC inhibition	CS	R-CS	P2	ictrace15t2	0.4975	0.001657265	200
PKCd	recall	aIC inhibition	CS	R-CS	P3	ictrace17	0.497142857	0.001584362	200
PKCd	recall	aIC inhibition	CS	R-CS	P3	ictrace17t2	0.49702381	0.003105238	200
PKCd	recall	aIC inhibition	CS	R-CS	P3	ictrace10	0.496428571	0.001166424	200
PKCd	recall	aIC inhibition	CS	R-CS	P1	ictrace4	0.49625	0.001796747	200
PKCd	recall	aIC inhibition	CS	R-CS	P3	ictrace1t2	0.496071429	0.003854009	200
PKCd	recall	aIC inhibition	CS	R-CS	P3	ictrace13	0.494940476	0.001617991	200
PKCd	recall	aIC inhibition	CS	R-CS	P1	ictrace16t2	0.494940476	0.001483176	200
PKCd	recall	aIC inhibition	CS	R-CS	P3	ictrace4	0.494642857	0.002145749	200
PKCd	recall	aIC inhibition	CS	R-CS	P1	ictrace18	0.491666667	0.00195434	200
PKCd	recall	aIC inhibition	CS	R-CS	P3	ictrace3t2	0.49077381	0.001843197	200
PKCd	recall	aIC inhibition	CS	R-CS	P3	ictrace2t2	0.488214286	0.004436812	200
PKCd	recall	aIC inhibition	CS	R-CS	P2	ictrace7t2	0.48375	0.004390403	200
PKCd	recall	aIC inhibition	CS	R-CS	P3	ictrace12	0.483095238	0.002873663	200
PKCd	recall	aIC inhibition	CS	R-CS	P1	ictrace8t2	0.48077381	0.003091433	200
PKCd	recall	aIC inhibition	CS	R-CS	P1	ictrace17	0.479702381	0.002880359	200
PKCd	recall	aIC inhibition	CS	R-CS	P3	ictrace3	0.479285714	0.002400574	200
PKCd	recall	aIC inhibition	CS	R-CS	P3	ictrace20	0.478333333	0.002603798	200
PKCd	recall	aIC inhibition	CS	R-CS	P2	ictrace3t2	0.478035714	0.002992926	200
PKCd	recall	aIC inhibition	CS	R-CS	P3	ictrace9t2	0.476785714	0.003177423	200
PKCd	recall	aIC inhibition	CS	R-CS	P1	ictrace3t2	0.476071429	0.002668619	200
PKCd	recall	aIC inhibition	CS	R-CS	P2	ictrace5t2	0.476071429	0.002709465	200
PKCd	recall	aIC inhibition	CS	R-CS	P3	ictrace15t2	0.474880952	0.002637637	200
PKCd	recall	aIC inhibition	CS	R-CS	P3	ictrace4t2	0.47452381	0.002627206	200
PKCd	recall	aIC inhibition	CS	R-CS	P1	ictrace11t2	0.474047619	0.002693424	200
PKCd	recall	aIC inhibition	CS	R-CS	P3	ictrace11t2	0.47375	0.002921276	200
PKCd	recall	aIC inhibition	CS	R-CS	P1	ictrace5	0.472559524	0.002827472	200
PKCd	recall	aIC inhibition	CS	R-CS	P3	ictrace1	0.47172619	0.002649227	200

PKCd	recall	aIC inhibition	CS	R-CS	P3	ictrace8t2	0.465654762	0.004705904	200
PKCd	recall	aIC inhibition	CS	R-CS	P3	ictrace2	0.459583333	0.003052472	200
PKCd	recall	aIC inhibition	CS	R-CS	P3	ictrace10t2	0.456071429	0.00429677	200
PKCd	recall	aIC inhibition	CS	R-CS	P2	ictrace5	0.453452381	0.003869679	200
PKCd	**recall**	**aIC inhibition**	**CS**	**F-CS**	**P3**	**ictrace8t2**	**0.592857143**	**0.004137654**	**200**
PKCd	**recall**	**aIC inhibition**	**CS**	**F-CS**	**P3**	**ictrace18**	**0.564285714**	**0.004377328**	**200**
PKCd	**recall**	**aIC inhibition**	**CS**	**F-CS**	**P1**	**ictrace12t2**	**0.561904762**	**0.00538748**	**200**
PKCd	**recall**	**aIC inhibition**	**CS**	**F-CS**	**P2**	**ictrace3**	**0.558869048**	**0.003535732**	**200**
PKCd	**recall**	**aIC inhibition**	**CS**	**F-CS**	**P1**	**ictrace16**	**0.55**	**0.002886751**	**200**
PKCd	**recall**	**aIC inhibition**	**CS**	**F-CS**	**P1**	**ictrace4**	**0.547619048**	**0.004641331**	**200**
PKCd	**recall**	**aIC inhibition**	**CS**	**F-CS**	**P1**	**ictrace14t2**	**0.547619048**	**0.002766417**	**200**
PKCd	**recall**	**aIC inhibition**	**CS**	**F-CS**	**P2**	**ictrace7t2**	**0.54672619**	**0.00273672**	**200**
PKCd	**recall**	**aIC inhibition**	**CS**	**F-CS**	**P2**	**ictrace6**	**0.537261905**	**0.003968332**	**200**
PKCd	**recall**	**aIC inhibition**	**CS**	**F-CS**	**P1**	**ictrace11t2**	**0.537261905**	**0.003968332**	**200**
PKCd	**recall**	**aIC inhibition**	**CS**	**F-CS**	**P3**	**ictrace10t2**	**0.537261905**	**0.00297656**	**200**
PKCd	**recall**	**aIC inhibition**	**CS**	**F-CS**	**P2**	**ictrace4**	**0.536071429**	**0.005758085**	**200**
PKCd	**recall**	**aIC inhibition**	**CS**	**F-CS**	**P1**	**ictrace17**	**0.534285714**	**0.00274915**	**200**
PKCd	**recall**	**aIC inhibition**	**CS**	**F-CS**	**P1**	**ictrace4t2**	**0.533333333**	**0.002886751**	**200**
PKCd	**recall**	**aIC inhibition**	**CS**	**F-CS**	**P3**	**ictrace8**	**0.532440476**	**0.002810807**	**200**
PKCd	**recall**	**aIC inhibition**	**CS**	**F-CS**	**P1**	**ictrace6**	**0.530952381**	**0.00269374**	**200**
PKCd	**recall**	**aIC inhibition**	**CS**	**F-CS**	**P3**	**ictrace4**	**0.530952381**	**0.00269374**	**200**
PKCd	**recall**	**aIC inhibition**	**CS**	**F-CS**	**P1**	**ictrace11**	**0.530952381**	**0.00269374**	**200**
PKCd	**recall**	**aIC inhibition**	**CS**	**F-CS**	**P1**	**ictrace13t2**	**0.530952381**	**0.00269374**	**200**
PKCd	**recall**	**aIC inhibition**	**CS**	**F-CS**	**P2**	**ictrace6t2**	**0.530952381**	**0.00269374**	**200**
PKCd	**recall**	**aIC inhibition**	**CS**	**F-CS**	**P3**	**ictrace15t2**	**0.530952381**	**0.00269374**	**200**
PKCd	**recall**	**aIC inhibition**	**CS**	**F-CS**	**P2**	**ictrace4t2**	**0.530595238**	**0.003026375**	**200**
PKCd	**recall**	**aIC inhibition**	**CS**	**F-CS**	**P2**	**ictrace9**	**0.528214286**	**0.003958499**	**200**
PKCd	**recall**	**aIC inhibition**	**CS**	**F-CS**	**P3**	**ictrace22t2**	**0.523333333**	**0.002773886**	**200**
PKCd	**recall**	**aIC inhibition**	**CS**	**F-CS**	**P3**	**ictrace3t2**	**0.519047619**	**0.002795719**	**200**
PKCd	**recall**	**aIC inhibition**	**CS**	**F-CS**	**P3**	**ictrace1t2**	**0.513154762**	**0.003967518**	**200**
PKCd	**recall**	**aIC inhibition**	**CS**	**F-CS**	**P1**	**ictrace2t2**	**0.511904762**	**0.004315374**	**200**
PKCd	**recall**	**aIC inhibition**	**CS**	**F-CS**	**P3**	**ictrace12**	**0.504166667**	**0.002618709**	**200**
PKCd	**recall**	**aIC inhibition**	**CS**	**F-CS**	**P1**	**ictrace19**	**0.503214286**	**0.001454891**	**200**
PKCd	**recall**	**aIC inhibition**	**CS**	**F-CS**	**P1**	**ictrace9**	**0.502142857**	**0.001589988**	**200**
PKCd	recall	aIC inhibition	CS	F-CS	P1	ictrace17t2	0.502142857	0.001420513	200
PKCd	recall	aIC inhibition	CS	F-CS	P1	ictrace3t2	0.502083333	0.003454882	200
PKCd	recall	aIC inhibition	CS	F-CS	P1	ictrace9t2	0.502083333	0.001903715	200
PKCd	recall	aIC inhibition	CS	F-CS	P3	ictrace17t2	0.501666667	0.001763834	200
PKCd	recall	aIC inhibition	CS	F-CS	P3	ictrace4t2	0.501666667	0.003741051	200
PKCd	recall	aIC inhibition	CS	F-CS	P3	ictrace18t2	0.50125	0.00190736	200
PKCd	recall	aIC inhibition	CS	F-CS	P1	ictrace8t2	0.501011905	0.002107475	200
PKCd	recall	aIC inhibition	CS	F-CS	P3	ictrace7	0.500416667	0.001815969	200
PKCd	recall	aIC inhibition	CS	F-CS	P1	ictrace16t2	0.500416667	0.001909179	200
PKCd	recall	aIC inhibition	CS	F-CS	P1	ictrace1	0.500357143	0.001472321	200
PKCd	recall	aIC inhibition	CS	F-CS	P3	ictrace16	0.500357143	0.001472321	200
PKCd	recall	aIC inhibition	CS	F-CS	P3	ictrace10	0.5	0	200
PKCd	recall	aIC inhibition	CS	F-CS	P3	ictrace11	0.5	0	200
PKCd	recall	aIC inhibition	CS	F-CS	P3	ictrace5	0.5	0	200
PKCd	recall	aIC inhibition	CS	F-CS	P1	ictrace5t2	0.499583333	0.001717708	200
PKCd	recall	aIC inhibition	CS	F-CS	P1	ictrace3	0.499166667	0.001316297	200
PKCd	recall	aIC inhibition	CS	F-CS	P1	ictrace20	0.498928571	0.001554905	200
PKCd	recall	aIC inhibition	CS	F-CS	P2	ictrace1t2	0.498928571	0.001381132	200
PKCd	recall	aIC inhibition	CS	F-CS	P1	ictrace7	0.49875	0.001814056	200
PKCd	recall	aIC inhibition	CS	F-CS	P2	ictrace7	0.498571429	0.001332483	200
PKCd	recall	aIC inhibition	CS	F-CS	P3	ictrace16t2	0.498571429	0.001887121	200
PKCd	recall	aIC inhibition	CS	F-CS	P3	ictrace9	0.497916667	0.001810224	200
PKCd	recall	aIC inhibition	CS	F-CS	P3	ictrace11t2	0.497857143	0.001589988	200
PKCd	recall	aIC inhibition	CS	F-CS	P3	ictrace21	0.497142857	0.0015017	200
PKCd	recall	aIC inhibition	CS	F-CS	P1	ictrace19t2	0.496666667	0.001649916	200
PKCd	recall	aIC inhibition	CS	F-CS	P3	ictrace6	0.496309524	0.001922149	200

PKCd	recall	aIC inhibition	CS	F-CS	P3	ictrace17	0.49625	0.001478726	200
PKCd	recall	aIC inhibition	CS	F-CS	P3	ictrace12t2	0.496011905	0.003606256	200
PKCd	recall	aIC inhibition	CS	F-CS	P1	ictrace10	0.495714286	0.001568178	200
PKCd	recall	aIC inhibition	CS	F-CS	P1	ictrace12	0.495059524	0.003465981	200
PKCd	recall	aIC inhibition	CS	F-CS	P1	ictrace13	0.49375	0.002035919	200
PKCd	recall	aIC inhibition	CS	F-CS	P1	ictrace7t2	0.492678571	0.001900437	200
PKCd	recall	aIC inhibition	CS	F-CS	P2	ictrace5	0.492380952	0.003265726	200
PKCd	recall	aIC inhibition	CS	F-CS	P3	ictrace2	0.492142857	0.003332738	200
PKCd	recall	aIC inhibition	CS	F-CS	P3	ictrace20t2	0.491428571	0.003296093	200
PKCd	recall	aIC inhibition	CS	F-CS	P1	ictrace6t2	0.488809524	0.003250065	200
PKCd	recall	aIC inhibition	CS	F-CS	P2	ictrace8	0.485119048	0.003208493	200
PKCd	recall	aIC inhibition	CS	F-CS	P3	ictrace2t2	0.483392857	0.002780339	200
PKCd	recall	aIC inhibition	CS	F-CS	P1	ictrace2	0.478095238	0.003373945	200
PKCd	recall	aIC inhibition	CS	F-CS	P2	ictrace2t2	0.476071429	0.002732901	200
PKCd	recall	aIC inhibition	CS	F-CS	P1	ictrace10t2	0.475833333	0.002980842	200
PKCd	recall	aIC inhibition	CS	F-CS	P3	ictrace24	0.475595238	0.002617356	200
PKCd	recall	aIC inhibition	CS	F-CS	P2	ictrace5t2	0.475178571	0.002667009	200
PKCd	recall	aIC inhibition	CS	F-CS	P3	ictrace20	0.472916667	0.00288299	200
PKCd	recall	aIC inhibition	CS	F-CS	P3	ictrace7t2	0.4725	0.002770755	200
PKCd	recall	aIC inhibition	CS	F-CS	P1	ictrace18	0.470357143	0.003249357	200
PKCd	recall	aIC inhibition	CS	F-CS	P1	ictrace15	0.461964286	0.004106451	200
PKCd	recall	aIC inhibition	CS	F-CS	P3	ictrace19	0.461547619	0.004108187	200
PKCd	recall	aIC inhibition	CS	F-CS	P1	ictrace14	0.46	0.004857697	200
CEm	**habituation**	**PBS**	**CS**	**R-CS**	**C2**	**ictrace15**	**0.6**	**0.004828302**	**200**
CEm	**habituation**	**PBS**	**CS**	**R-CS**	**C2**	**ictrace10**	**0.585**	**0.006860211**	**200**
CEm	**habituation**	**PBS**	**CS**	**R-CS**	**C2**	**ictrace11**	**0.570875**	**0.006128258**	**200**
CEm	**habituation**	**PBS**	**CS**	**R-CS**	**C2**	**ictrace9**	**0.56625**	**0.003786283**	**200**
CEm	**habituation**	**PBS**	**CS**	**R-CS**	**C2**	**ictrace13**	**0.560375**	**0.007955496**	**200**
CEm	**habituation**	**PBS**	**CS**	**R-CS**	**C2**	**ictrace17**	**0.551375**	**0.003961524**	**200**
CEm	**habituation**	**PBS**	**CS**	**R-CS**	**C2**	**ictrace14**	**0.540125**	**0.006422367**	**200**
CEm	habituation	PBS	CS	R-CS	C2	ictrace2	0.4785	0.00366589	200
CEm	**habituation**	**PBS**	**CS**	**F-CS**	**C2**	**ictrace9**	**0.524166667**	**0.006238601**	**200**
CEm	**habituation**	**PBS**	**CS**	**F-CS**	**C2**	**ictrace10**	**0.500625**	**0.002863769**	**200**
CEm	**habituation**	**PBS**	**CS**	**F-CS**	**C2**	**ictrace13**	**0.499166667**	**0.003435416**	**200**
CEm	**habituation**	**PBS**	**CS**	**F-CS**	**C2**	**ictrace15**	**0.496666667**	**0.002345208**	**200**
CEm	**habituation**	**PBS**	**CS**	**F-CS**	**C2**	**ictrace2**	**0.493333333**	**0.003299832**	**200**
CEm	**habituation**	**PBS**	**CS**	**F-CS**	**C2**	**ictrace11**	**0.462291667**	**0.005747867**	**200**
CEm	**habituation**	**PBS**	**CS**	**F-CS**	**C2**	**ictrace14**	**0.418541667**	**0.007650671**	**200**
CEm	**habituation**	**aIC inhibition**	**CS**	**R-CS**	**C2**	**ictrace6**	**0.516785714**	**0.002473198**	**200**
CEm	**habituation**	**aIC inhibition**	**CS**	**R-CS**	**C2**	**ictrace10**	**0.5**	**0.001666667**	**200**
CEm	**habituation**	**aIC inhibition**	**CS**	**R-CS**	**C2**	**ictrace3**	**0.493809524**	**0.003256948**	**200**
CEm	**habituation**	**aIC inhibition**	**CS**	**R-CS**	**C2**	**ictrace4**	**0.485654762**	**0.004210903**	**200**
CEm	**habituation**	**aIC inhibition**	**CS**	**R-CS**	**C2**	**ictrace1**	**0.484940476**	**0.002325969**	**200**
CEm	**habituation**	**aIC inhibition**	**CS**	**R-CS**	**C2**	**ictrace9**	**0.481071429**	**0.002285575**	**200**
CEm	**habituation**	**aIC inhibition**	**CS**	**R-CS**	**C2**	**ictrace5**	**0.473333333**	**0.002739699**	**200**
CEm	**habituation**	**aIC inhibition**	**CS**	**F-CS**	**C2**	**ictrace6**	**0.542857143**	**0.00404061**	**200**
CEm	**habituation**	**aIC inhibition**	**CS**	**F-CS**	**C2**	**ictrace1**	**0.501666667**	**0.001662495**	**200**
CEm	**habituation**	**aIC inhibition**	**CS**	**F-CS**	**C2**	**ictrace4**	**0.5**	**0**	**200**
CEm	habituation	aIC inhibition	CS	F-CS	C2	ictrace10	0.499583333	0.001613474	200
CEm	habituation	aIC inhibition	CS	F-CS	C2	ictrace5	0.498928571	0.001470587	200
CEm	habituation	aIC inhibition	CS	F-CS	C2	ictrace3	0.497083333	0.002724471	200
CEm	habituation	aIC inhibition	CS	F-CS	C2	ictrace9	0.460892857	0.003696594	200
CEm	**RC**	**early**	**CS**	**R-CS**	**C2**	**ictrace13**	**0.540730263**	**0.001350506**	**200**
CEm	**RC**	**early**	**CS**	**R-CS**	**C2**	**ictrace12**	**0.533631579**	**0.001621751**	**200**
CEm	**RC**	**early**	**CS**	**R-CS**	**C3**	**ictrace4**	**0.519638158**	**0.001474358**	**200**
CEm	**RC**	**early**	**CS**	**R-CS**	**C3**	**ictrace11**	**0.517177632**	**0.002020287**	**200**
CEm	**RC**	**early**	**CS**	**R-CS**	**C2**	**ictrace6**	**0.517059211**	**0.00173568**	**200**
CEm	**RC**	**early**	**CS**	**R-CS**	**C2**	**ictrace10**	**0.516309211**	**0.001218434**	**200**
CEm	**RC**	**early**	**CS**	**R-CS**	**C4**	**ictrace2**	**0.511842105**	**0.000907799**	**200**

CEm	**RC**	**early**	**CS**	**R-CS**	**C2**	**ictrace2**	**0.511315789**	**0.001387019**	**200**
CEm	**RC**	**early**	**CS**	**R-CS**	**C2**	**ictrace8**	**0.507730263**	**0.002090117**	**200**
CEm	**RC**	**early**	**CS**	**R-CS**	**C4**	**ictrace10**	**0.507203947**	**0.001768255**	**200**
CEm	RC	early	CS	R-CS	C4	ictrace7	0.505789474	0.002219047	200
CEm	RC	early	CS	R-CS	C2	ictrace11	0.502592105	0.001173007	200
CEm	RC	early	CS	R-CS	C1	ictrace6	0.502309211	0.000715655	200
CEm	RC	early	CS	R-CS	C1	ictrace1	0.501578947	0.000942238	200
CEm	RC	early	CS	R-CS	C3	ictrace1	0.501	0.000582022	200
CEm	RC	early	CS	R-CS	C1	ictrace2	0.500625	0.000482102	200
CEm	RC	early	CS	R-CS	C3	ictrace5	0.500394737	0.000473593	200
CEm	RC	early	CS	R-CS	C1	ictrace5	0.500131579	0.000227711	200
CEm	RC	early	CS	R-CS	C4	ictrace11	0.500125	0.000544791	200
CEm	RC	early	CS	R-CS	C2	ictrace7	0.5	0	200
CEm	RC	early	CS	R-CS	C3	ictrace9	0.499486842	0.000406278	200
CEm	RC	early	CS	R-CS	C2	ictrace4	0.499375	0.000779373	200
CEm	RC	early	CS	R-CS	C1	ictrace11	0.499078947	0.001225557	200
CEm	RC	early	CS	R-CS	C3	ictrace2	0.499019737	0.001226369	200
CEm	RC	early	CS	R-CS	C3	ictrace8	0.498684211	0.000664441	200
CEm	RC	early	CS	R-CS	C2	ictrace1	0.493802632	0.001158477	200
CEm	RC	early	CS	R-CS	C4	ictrace13	0.492407895	0.000940017	200
CEm	RC	early	CS	R-CS	C3	ictrace6	0.491677632	0.001017759	200
CEm	RC	early	CS	R-CS	C3	ictrace3	0.490927632	0.000883952	200
CEm	RC	early	CS	R-CS	C3	ictrace10	0.490789474	0.000986711	200
CEm	RC	early	CS	R-CS	C3	ictrace7	0.490763158	0.00111361	200
CEm	RC	early	CS	R-CS	C2	ictrace3	0.483269737	0.001521299	200
CEm	**RC**	**early**	**US**	**R-CS**	**C3**	**ictrace3**	**0.64875**	**0.008856054**	**200**
CEm	**RC**	**early**	**US**	**R-CS**	**C1**	**ictrace5**	**0.56875**	**0.009509453**	**200**
CEm	**RC**	**early**	**US**	**R-CS**	**C3**	**ictrace2**	**0.5675**	**0.010110329**	**200**
CEm	**RC**	**early**	**US**	**R-CS**	**C4**	**ictrace11**	**0.56625**	**0.009918023**	**200**
CEm	**RC**	**early**	**US**	**R-CS**	**C3**	**ictrace1**	**0.555**	**0.009708244**	**200**
CEm	**RC**	**early**	**US**	**R-CS**	**C4**	**ictrace2**	**0.54**	**0.010068515**	**200**
CEm	**RC**	**early**	**US**	**R-CS**	**C2**	**ictrace6**	**0.50875**	**0.004099352**	**200**
CEm	**RC**	**early**	**US**	**R-CS**	**C3**	**ictrace6**	**0.5075**	**0.00391711**	**200**
CEm	**RC**	**early**	**US**	**R-CS**	**C3**	**ictrace9**	**0.50625**	**0.003277528**	**200**
CEm	**RC**	**early**	**US**	**R-CS**	**C2**	**ictrace12**	**0.50375**	**0.002782479**	**200**
CEm	RC	early	US	R-CS	C1	ictrace11	0.50125	0.002163259	200
CEm	RC	early	US	R-CS	C1	ictrace2	0.50125	0.001246871	200
CEm	RC	early	US	R-CS	C2	ictrace10	0.50125	0.001246871	200
CEm	RC	early	US	R-CS	C2	ictrace3	0.50125	0.001246871	200
CEm	RC	early	US	R-CS	C1	ictrace6	0.5	0	200
CEm	RC	early	US	R-CS	C2	ictrace13	0.5	0.001767767	200
CEm	RC	early	US	R-CS	C2	ictrace4	0.5	0	200
CEm	RC	early	US	R-CS	C3	ictrace11	0.5	0	200
CEm	RC	early	US	R-CS	C3	ictrace5	0.5	0	200
CEm	RC	early	US	R-CS	C3	ictrace8	0.5	0	200
CEm	RC	early	US	R-CS	C1	ictrace1	0.49875	0.002163259	200
CEm	RC	early	US	R-CS	C2	ictrace11	0.49875	0.004144839	200
CEm	RC	early	US	R-CS	C3	ictrace4	0.49875	0.004840422	200
CEm	RC	early	US	R-CS	C4	ictrace7	0.49875	0.002793687	200
CEm	RC	early	US	R-CS	C2	ictrace2	0.4975	0.003056755	200
CEm	RC	early	US	R-CS	C2	ictrace7	0.4975	0.004996874	200
CEm	RC	early	US	R-CS	C4	ictrace13	0.4975	0.002493742	200
CEm	RC	early	US	R-CS	C2	ictrace1	0.495	0.005578978	200
CEm	RC	early	US	R-CS	C3	ictrace7	0.4925	0.005564957	200
CEm	RC	early	US	R-CS	C2	ictrace8	0.48375	0.005883637	200
CEm	RC	early	US	R-CS	C3	ictrace10	0.48	0.006698881	200
CEm	RC	early	US	R-CS	C4	ictrace10	0.44625	0.008638124	200
CEm	**RC**	**late**	**CS**	**R-CS**	**C3**	**ictrace2**	**0.541907895**	**0.002106019**	**200**
CEm	**RC**	**late**	**CS**	**R-CS**	**C3**	**ictrace7**	**0.541796053**	**0.002362217**	**200**
CEm	**RC**	**late**	**CS**	**R-CS**	**C2**	**ictrace7**	**0.526052632**	**0.002882991**	**200**

CEm	**RC**	**late**	**CS**	**R-CS**	**C2**	**ictrace2**	**0.519111842**	**0.003080605**	**200**
CEm	**RC**	**late**	**CS**	**R-CS**	**C3**	**ictrace4**	**0.506921053**	**0.000867186**	**200**
CEm	**RC**	**late**	**CS**	**R-CS**	**C2**	**ictrace8**	**0.505263158**	**0.000818121**	**200**
CEm	**RC**	**late**	**CS**	**R-CS**	**C3**	**ictrace1**	**0.504480263**	**0.002235489**	**200**
CEm	**RC**	**late**	**CS**	**R-CS**	**C2**	**ictrace11**	**0.503565789**	**0.000896071**	**200**
CEm	**RC**	**late**	**CS**	**R-CS**	**C2**	**ictrace6**	**0.502144737**	**0.001262654**	**200**
CEm	**RC**	**late**	**CS**	**R-CS**	**C1**	**ictrace5**	**0.501914474**	**0.000839676**	**200**
CEm	RC	late	CS	R-CS	C4	ictrace7	0.500967105	0.001046796	200
CEm	RC	late	CS	R-CS	C1	ictrace7	0.5	0	200
CEm	RC	late	CS	R-CS	C4	ictrace3	0.499875	0.000484042	200
CEm	RC	late	CS	R-CS	C2	ictrace5	0.499736842	0.002426125	200
CEm	RC	late	CS	R-CS	C4	ictrace5	0.499552632	0.001166551	200
CEm	RC	late	CS	R-CS	C3	ictrace9	0.499480263	0.000489228	200
CEm	RC	late	CS	R-CS	C4	ictrace1	0.499375	0.000372387	200
CEm	RC	late	CS	R-CS	C2	ictrace16	0.497953947	0.000695174	200
CEm	RC	late	CS	R-CS	C2	ictrace4	0.496592105	0.000832812	200
CEm	RC	late	CS	R-CS	C3	ictrace15	0.495921053	0.000894301	200
CEm	RC	late	CS	R-CS	C2	ictrace9	0.493697368	0.00102575	200
CEm	RC	late	CS	R-CS	C2	ictrace1	0.493026316	0.001627302	200
CEm	RC	late	CS	R-CS	C3	ictrace3	0.486605263	0.001678954	200
CEm	RC	late	CS	R-CS	C2	ictrace3	0.466223684	0.001946926	200
CEm	**RC**	**late**	**US**	**R-CS**	**C1**	**ictrace7**	**0.65**	**0.014142136**	**200**
CEm	**RC**	**late**	**US**	**R-CS**	**C4**	**ictrace3**	**0.65**	**0.014142136**	**200**
CEm	**RC**	**late**	**US**	**R-CS**	**C2**	**ictrace4**	**0.63875**	**0.019501402**	**200**
CEm	**RC**	**late**	**US**	**R-CS**	**C2**	**ictrace3**	**0.5975**	**0.016277861**	**200**
CEm	**RC**	**late**	**US**	**R-CS**	**C2**	**ictrace6**	**0.56625**	**0.014945474**	**200**
CEm	**RC**	**late**	**US**	**R-CS**	**C2**	**ictrace7**	**0.5075**	**0.004297528**	**200**
CEm	**RC**	**late**	**US**	**R-CS**	**C2**	**ictrace5**	**0.50625**	**0.005134899**	**200**
CEm	**RC**	**late**	**US**	**R-CS**	**C3**	**ictrace3**	**0.50625**	**0.004485219**	**200**
CEm	**RC**	**late**	**US**	**R-CS**	**C2**	**ictrace11**	**0.5025**	**0.002493742**	**200**
CEm	**RC**	**late**	**US**	**R-CS**	**C2**	**ictrace1**	**0.50125**	**0.002163259**	**200**
CEm	RC	late	US	R-CS	C3	ictrace4	0.50125	0.001246871	200
CEm	RC	late	US	R-CS	C2	ictrace16	0.5	0.005303301	200
CEm	RC	late	US	R-CS	C2	ictrace8	0.5	0	200
CEm	RC	late	US	R-CS	C2	ictrace9	0.5	0.003061862	200
CEm	RC	late	US	R-CS	C3	ictrace7	0.5	0	200
CEm	RC	late	US	R-CS	C3	ictrace9	0.5	0	200
CEm	RC	late	US	R-CS	C1	ictrace5	0.49875	0.001246871	200
CEm	RC	late	US	R-CS	C4	ictrace5	0.49875	0.005994138	200
CEm	RC	late	US	R-CS	C4	ictrace7	0.49875	0.002793687	200
CEm	RC	late	US	R-CS	C3	ictrace15	0.4975	0.002493742	200
CEm	RC	late	US	R-CS	C3	ictrace2	0.49625	0.003740613	200
CEm	RC	late	US	R-CS	C4	ictrace1	0.495	0.00611351	200
CEm	RC	late	US	R-CS	C3	ictrace1	0.47125	0.009044594	200
CEm	RC	late	US	R-CS	C2	ictrace2	0.455	0.01366565	200
CEm	**FC**	**early**	**CS**	**F-CS**	**C2**	**ictrace5**	**0.6**	**0.005773503**	**200**
CEm	**FC**	**early**	**CS**	**F-CS**	**C2**	**ictrace11**	**0.569791667**	**0.005757977**	**200**
CEm	**FC**	**early**	**CS**	**F-CS**	**C4**	**ictrace11**	**0.558333333**	**0.005137012**	**200**
CEm	**FC**	**early**	**CS**	**F-CS**	**C1**	**ictrace4**	**0.544166667**	**0.005333008**	**200**
CEm	**FC**	**early**	**CS**	**F-CS**	**C4**	**ictrace13**	**0.541666667**	**0.005212498**	**200**
CEm	**FC**	**early**	**CS**	**F-CS**	**C3**	**ictrace2**	**0.535**	**0.005216161**	**200**
CEm	**FC**	**early**	**CS**	**F-CS**	**C2**	**ictrace3**	**0.509375**	**0.00728534**	**200**
CEm	**FC**	**early**	**CS**	**F-CS**	**C3**	**ictrace17**	**0.507708333**	**0.005796592**	**200**
CEm	**FC**	**early**	**CS**	**F-CS**	**C3**	**ictrace9**	**0.504166667**	**0.00321401**	**200**
CEm	**FC**	**early**	**CS**	**F-CS**	**C4**	**ictrace9**	**0.503333333**	**0.00332499**	**200**
CEm	FC	early	CS	F-CS	C2	ictrace13	0.501666667	0.003724916	200
CEm	FC	early	CS	F-CS	C2	ictrace7	0.501666667	0.00311582	200
CEm	FC	early	CS	F-CS	C1	ictrace2	0.50125	0.002498437	200
CEm	FC	early	CS	F-CS	C2	ictrace10	0.500833333	0.003226948	200
CEm	FC	early	CS	F-CS	C1	ictrace3	0.500208333	0.002997359	200

CEm	FC	early	CS	F-CS	C2	ictrace1	0.5	0	200
CEm	FC	early	CS	F-CS	C2	ictrace2	0.5	0	200
CEm	FC	early	CS	F-CS	C2	ictrace4	0.5	0	200
CEm	FC	early	CS	F-CS	C2	ictrace6	0.5	0	200
CEm	FC	early	CS	F-CS	C3	ictrace1	0.5	0	200
CEm	FC	early	CS	F-CS	C3	ictrace11	0.5	0	200
CEm	FC	early	CS	F-CS	C3	ictrace14	0.5	0.00390868	200
CEm	FC	early	CS	F-CS	C3	ictrace19	0.5	0	200
CEm	FC	early	CS	F-CS	C3	ictrace3	0.5	0	200
CEm	FC	early	CS	F-CS	C3	ictrace5	0.5	0	200
CEm	FC	early	CS	F-CS	C3	ictrace6	0.5	0	200
CEm	FC	early	CS	F-CS	C1	ictrace1	0.5	0	200
CEm	FC	early	CS	F-CS	C1	ictrace10	0.5	0	200
CEm	FC	early	CS	F-CS	C1	ictrace12	0.5	0	200
CEm	FC	early	CS	F-CS	C1	ictrace14	0.5	0	200
CEm	FC	early	CS	F-CS	C1	ictrace6	0.5	0	200
CEm	FC	early	CS	F-CS	C4	ictrace5	0.5	0	200
CEm	FC	early	CS	F-CS	C4	ictrace7	0.5	0	200
CEm	FC	early	CS	F-CS	C3	ictrace7	0.499166667	0.00268354	200
CEm	FC	early	CS	F-CS	C3	ictrace8	0.498333333	0.003533569	200
CEm	FC	early	CS	F-CS	C2	ictrace16	0.498125	0.002891221	200
CEm	FC	early	CS	F-CS	C4	ictrace12	0.498125	0.002994461	200
CEm	FC	early	CS	F-CS	C2	ictrace9	0.496666667	0.002345208	200
CEm	FC	early	CS	F-CS	C4	ictrace2	0.478333333	0.007101447	200
CEm	FC	early	CS	F-CS	C4	ictrace4	0.473333333	0.004630815	200
CEm	FC	early	CS	F-CS	C1	ictrace7	0.456875	0.005097806	200
CEm	FC	early	CS	F-CS	C3	ictrace4	0.454375	0.00597737	200
CEm	FC	early	CS	F-CS	C2	ictrace8	0.452291667	0.006708188	200
CEm	FC	early	CS	F-CS	C4	ictrace15	0.452083333	0.005176989	200
CEm	FC	early	CS	F-CS	C3	ictrace10	0.422708333	0.007763862	200
CEm	**FC**	**early**	**US**	**F-CS**	**C2**	**ictrace6**	**0.658333333**	**0.001178511**	**200**
CEm	**FC**	**early**	**US**	**F-CS**	**C2**	**ictrace2**	**0.6**	**0.00942809**	**200**
CEm	**FC**	**early**	**US**	**F-CS**	**C3**	**ictrace10**	**0.6**	**0.005773503**	**200**
CEm	**FC**	**early**	**US**	**F-CS**	**C2**	**ictrace10**	**0.591666667**	**0.005400617**	**200**
CEm	**FC**	**early**	**US**	**F-CS**	**C2**	**ictrace11**	**0.591666667**	**0.005400617**	**200**
CEm	**FC**	**early**	**US**	**F-CS**	**C1**	**ictrace3**	**0.583333333**	**0.00745356**	**200**
CEm	**FC**	**early**	**US**	**F-CS**	**C2**	**ictrace5**	**0.566666667**	**0.005773503**	**200**
CEm	**FC**	**early**	**US**	**F-CS**	**C4**	**ictrace5**	**0.566666667**	**0.005773503**	**200**
CEm	**FC**	**early**	**US**	**F-CS**	**C2**	**ictrace1**	**0.558333333**	**0.005137012**	**200**
CEm	**FC**	**early**	**US**	**F-CS**	**C3**	**ictrace5**	**0.558333333**	**0.005137012**	**200**
CEm	FC	early	US	F-CS	C3	ictrace7	0.558333333	0.005137012	200
CEm	FC	early	US	F-CS	C1	ictrace2	0.558333333	0.005137012	200
CEm	FC	early	US	F-CS	C4	ictrace13	0.558333333	0.005137012	200
CEm	FC	early	US	F-CS	C4	ictrace2	0.558333333	0.009052317	200
CEm	FC	early	US	F-CS	C4	ictrace7	0.558333333	0.005137012	200
CEm	FC	early	US	F-CS	C4	ictrace9	0.558333333	0.005137012	200
CEm	FC	early	US	F-CS	C1	ictrace6	0.505833333	0.003411073	200
CEm	FC	early	US	F-CS	C3	ictrace6	0.505	0.003892657	200
CEm	FC	early	US	F-CS	C1	ictrace7	0.503125	0.002855573	200
CEm	FC	early	US	F-CS	C2	ictrace13	0.5025	0.003628112	200
CEm	FC	early	US	F-CS	C1	ictrace1	0.50125	0.002650177	200
CEm	FC	early	US	F-CS	C2	ictrace4	0.500625	0.002576562	200
CEm	FC	early	US	F-CS	C2	ictrace7	0.5	0	200
CEm	FC	early	US	F-CS	C3	ictrace1	0.5	0.00293151	200
CEm	FC	early	US	F-CS	C3	ictrace14	0.5	0.003535534	200
CEm	FC	early	US	F-CS	C3	ictrace19	0.5	0	200
CEm	FC	early	US	F-CS	C3	ictrace2	0.5	0	200
CEm	FC	early	US	F-CS	C3	ictrace9	0.5	0	200
CEm	FC	early	US	F-CS	C1	ictrace10	0.5	0	200
CEm	FC	early	US	F-CS	C1	ictrace14	0.5	0	200

CEm	FC	early	US	F-CS	C1	ictrace4	0.5	0	200
CEm	FC	early	US	F-CS	C3	ictrace4	0.499166667	0.003996092	200
CEm	FC	early	US	F-CS	C2	ictrace9	0.498125	0.002721084	200
CEm	FC	early	US	F-CS	C4	ictrace12	0.498125	0.002249566	200
CEm	FC	early	US	F-CS	C2	ictrace3	0.4975	0.003814719	200
CEm	FC	early	US	F-CS	C3	ictrace11	0.4975	0.002999421	200
CEm	FC	early	US	F-CS	C3	ictrace8	0.4975	0.002926175	200
CEm	FC	early	US	F-CS	C4	ictrace15	0.495833333	0.003620447	200
CEm	FC	early	US	F-CS	C1	ictrace12	0.495	0.004067145	200
CEm	FC	early	US	F-CS	C3	ictrace3	0.494375	0.00269512	200
CEm	FC	early	US	F-CS	C2	ictrace16	0.493333333	0.003696846	200
CEm	FC	early	US	F-CS	C3	ictrace17	0.48	0.00610214	200
CEm	FC	early	US	F-CS	C2	ictrace8	0.4625	0.006712085	200
CEm	FC	early	US	F-CS	C4	ictrace11	0.443333333	0.007878416	200
CEm	FC	early	US	F-CS	C4	ictrace4	0.441666667	0.005137012	200
CEm	**FC**	**late**	**CS**	**F-CS**	**C2**	**ictrace13**	**0.530833333**	**0.006018202**	**200**
CEm	**FC**	**late**	**CS**	**F-CS**	**C2**	**ictrace6**	**0.504166667**	**0.003423266**	**200**
CEm	**FC**	**late**	**CS**	**F-CS**	**C2**	**ictrace7**	**0.503958333**	**0.003579425**	**200**
CEm	**FC**	**late**	**CS**	**F-CS**	**C2**	**ictrace12**	**0.5025**	**0.002999421**	**200**
CEm	**FC**	**late**	**CS**	**F-CS**	**C2**	**ictrace5**	**0.501666667**	**0.003906903**	**200**
CEm	**FC**	**late**	**CS**	**F-CS**	**C2**	**ictrace1**	**0.5**	**0.003118048**	**200**
CEm	**FC**	**late**	**CS**	**F-CS**	**C2**	**ictrace11**	**0.5**	**0.003535534**	**200**
CEm	**FC**	**late**	**CS**	**F-CS**	**C2**	**ictrace3**	**0.5**	**0**	**200**
CEm	**FC**	**late**	**CS**	**F-CS**	**C2**	**ictrace4**	**0.5**	**0**	**200**
CEm	**FC**	**late**	**CS**	**F-CS**	**C2**	**ictrace8**	**0.5**	**0**	**200**
CEm	**FC**	**late**	**US**	**F-CS**	**C2**	**ictrace8**	**0.625**	**0.004564355**	**200**
CEm	**FC**	**late**	**US**	**F-CS**	**C2**	**ictrace3**	**0.6**	**0.00942809**	**200**
CEm	**FC**	**late**	**US**	**F-CS**	**C2**	**ictrace1**	**0.591666667**	**0.005400617**	**200**
CEm	**FC**	**late**	**US**	**F-CS**	**C2**	**ictrace12**	**0.583333333**	**0.00745356**	**200**
CEm	**FC**	**late**	**US**	**F-CS**	**C2**	**ictrace4**	**0.498333333**	**0.003724916**	**200**
CEm	**FC**	**late**	**US**	**F-CS**	**C2**	**ictrace11**	**0.4975**	**0.002331845**	**200**
CEm	**FC**	**late**	**US**	**F-CS**	**C2**	**ictrace5**	**0.495**	**0.005578978**	**200**
CEm	**FC**	**late**	**US**	**F-CS**	**C2**	**ictrace6**	**0.473541667**	**0.006435966**	**200**
CEm	**FC**	**late**	**US**	**F-CS**	**C2**	**ictrace13**	**0.433333333**	**0.005773503**	**200**
CEm	**FC**	**late**	**US**	**F-CS**	**C2**	**ictrace7**	**0.4**	**0.00942809**	**200**
CEm	**recall**	**PBS**	**CS**	**R-CS**	**C3**	**ictrace10**	**0.573214286**	**0.004593565**	**200**
CEm	**recall**	**PBS**	**CS**	**R-CS**	**C4**	**ictrace10t2**	**0.561904762**	**0.002220805**	**200**
CEm	**recall**	**PBS**	**CS**	**R-CS**	**C2**	**ictrace1**	**0.553571429**	**0.007573805**	**200**
CEm	**recall**	**PBS**	**CS**	**R-CS**	**C3**	**ictrace1t2**	**0.547619048**	**0.004641331**	**200**
CEm	**recall**	**PBS**	**CS**	**R-CS**	**C1**	**ictrace1**	**0.546547619**	**0.003635526**	**200**
CEm	**recall**	**PBS**	**CS**	**R-CS**	**C4**	**ictrace3**	**0.544166667**	**0.003905588**	**200**
CEm	**recall**	**PBS**	**CS**	**R-CS**	**C1**	**ictrace4t2**	**0.5425**	**0.00398366**	**200**
CEm	**recall**	**PBS**	**CS**	**R-CS**	**C2**	**ictrace3t2**	**0.54125**	**0.00504787**	**200**
CEm	**recall**	**PBS**	**CS**	**R-CS**	**C3**	**ictrace6t2**	**0.534107143**	**0.003751112**	**200**
CEm	**recall**	**PBS**	**CS**	**R-CS**	**C4**	**ictrace12**	**0.530952381**	**0.00269374**	**200**
CEm	recall	PBS	CS	R-CS	C3	ictrace12	0.530952381	0.00269374	200
CEm	recall	PBS	CS	R-CS	C2	ictrace7t2	0.504166667	0.002068399	200
CEm	recall	PBS	CS	R-CS	C1	ictrace14	0.501785714	0.001377433	200
CEm	recall	PBS	CS	R-CS	C2	ictrace9t2	0.501666667	0.001763834	200
CEm	recall	PBS	CS	R-CS	C3	ictrace9	0.501428571	0.001424996	200
CEm	recall	PBS	CS	R-CS	C1	ictrace10	0.50125	0.000716255	200
CEm	recall	PBS	CS	R-CS	C1	ictrace6t2	0.501071429	0.001470587	200
CEm	recall	PBS	CS	R-CS	C3	ictrace11t2	0.500714286	0.000712498	200
CEm	recall	PBS	CS	R-CS	C2	ictrace4	0.500416667	0.001815969	200
CEm	recall	PBS	CS	R-CS	C2	ictrace6	0.500416667	0.001998046	200
CEm	recall	PBS	CS	R-CS	C2	ictrace6t2	0.500357143	0.001472321	200
CEm	recall	PBS	CS	R-CS	C3	ictrace3	0.500059524	0.001476136	200
CEm	recall	PBS	CS	R-CS	C4	ictrace1	0.5	0	200
CEm	recall	PBS	CS	R-CS	C4	ictrace7	0.5	0	200
CEm	recall	PBS	CS	R-CS	C3	ictrace10t2	0.5	0	200

CEm	recall	PBS	CS	R-CS	C1	ictrace10t2	0.5	0	200
CEm	recall	PBS	CS	R-CS	C4	ictrace12t2	0.5	0	200
CEm	recall	PBS	CS	R-CS	C4	ictrace4t2	0.5	0.003030458	200
CEm	recall	PBS	CS	R-CS	C4	ictrace8t2	0.5	0	200
CEm	recall	PBS	CS	R-CS	C2	ictrace2	0.499642857	0.001472321	200
CEm	recall	PBS	CS	R-CS	C2	ictrace8t2	0.49952381	0.001897008	200
CEm	recall	PBS	CS	R-CS	C3	ictrace1	0.499285714	0.001335351	200
CEm	recall	PBS	CS	R-CS	C3	ictrace13	0.499285714	0.001335351	200
CEm	recall	PBS	CS	R-CS	C2	ictrace10t2	0.499166667	0.001442172	200
CEm	recall	PBS	CS	R-CS	C3	ictrace7	0.499047619	0.004384897	200
CEm	recall	PBS	CS	R-CS	C3	ictrace15	0.498928571	0.002549385	200
CEm	recall	PBS	CS	R-CS	C4	ictrace11	0.498928571	0.000613933	200
CEm	recall	PBS	CS	R-CS	C2	ictrace2t2	0.498571429	0.001424996	200
CEm	recall	PBS	CS	R-CS	C4	ictrace6t2	0.498571429	0.003028774	200
CEm	recall	PBS	CS	R-CS	C3	ictrace7t2	0.498214286	0.001177759	200
CEm	recall	PBS	CS	R-CS	C2	ictrace5t2	0.4975	0.001461888	200
CEm	recall	PBS	CS	R-CS	C1	ictrace1t2	0.496785714	0.001454891	200
CEm	recall	PBS	CS	R-CS	C2	ictrace10	0.495714286	0.003098716	200
CEm	recall	PBS	CS	R-CS	C3	ictrace4t2	0.492857143	0.001889822	200
CEm	recall	PBS	CS	R-CS	C1	ictrace3t2	0.492797619	0.003315105	200
CEm	recall	PBS	CS	R-CS	C2	ictrace5	0.492559524	0.003218073	200
CEm	recall	PBS	CS	R-CS	C2	ictrace3	0.490833333	0.002686773	200
CEm	recall	PBS	CS	R-CS	C1	ictrace2	0.485654762	0.00287605	200
CEm	recall	PBS	CS	R-CS	C3	ictrace5	0.484583333	0.004032533	200
CEm	recall	PBS	CS	R-CS	C3	ictrace4	0.481904762	0.002874402	200
CEm	recall	PBS	CS	R-CS	C4	ictrace3t2	0.481845238	0.002987997	200
CEm	recall	PBS	CS	R-CS	C4	ictrace6	0.48125	0.002751568	200
CEm	recall	PBS	CS	R-CS	C2	ictrace7	0.480714286	0.002964931	200
CEm	recall	PBS	CS	R-CS	C1	ictrace12	0.480654762	0.003119681	200
CEm	recall	PBS	CS	R-CS	C1	ictrace2t2	0.47952381	0.002473155	200
CEm	recall	PBS	CS	R-CS	C1	ictrace12t2	0.47922619	0.002477217	200
CEm	recall	PBS	CS	R-CS	C4	ictrace5t2	0.47875	0.003165276	200
CEm	recall	PBS	CS	R-CS	C2	ictrace11	0.47672619	0.002719004	200
CEm	recall	PBS	CS	R-CS	C2	ictrace4t2	0.47327381	0.002663978	200
CEm	recall	PBS	CS	R-CS	C4	ictrace2t2	0.470416667	0.002819667	200
CEm	recall	PBS	CS	R-CS	C3	ictrace8	0.468571429	0.003678013	200
CEm	recall	PBS	CS	R-CS	C3	ictrace2t2	0.463928571	0.003457416	200
CEm	recall	PBS	CS	R-CS	C2	ictrace13	0.459583333	0.004710961	200
CEm	recall	PBS	CS	R-CS	C2	ictrace2	0.44922619	0.005089531	200
CEm	recall	PBS	CS	R-CS	C4	ictrace7t2	0.441190476	0.005222949	200
CEm	**recall**	**PBS**	**CS**	**F-CS**	**C2**	**ictrace8t2**	**0.5955**	**0.00402632**	**200**
CEm	**recall**	**PBS**	**CS**	**F-CS**	**C2**	**ictrace1t2**	**0.5665**	**0.0066437**	**200**
CEm	**recall**	**PBS**	**CS**	**F-CS**	**C2**	**ictrace2t2**	**0.56325**	**0.004220153**	**200**
CEm	**recall**	**PBS**	**CS**	**F-CS**	**C2**	**ictrace13**	**0.548571429**	**0.002596439**	**200**
CEm	**recall**	**PBS**	**CS**	**F-CS**	**C2**	**ictrace7t2**	**0.546125**	**0.003937391**	**200**
CEm	**recall**	**PBS**	**CS**	**F-CS**	**C2**	**ictrace3t2**	**0.532**	**0.003298485**	**200**
CEm	**recall**	**PBS**	**CS**	**F-CS**	**C4**	**ictrace7**	**0.530952381**	**0.00269374**	**200**
CEm	**recall**	**PBS**	**CS**	**F-CS**	**C2**	**ictrace5**	**0.528571429**	**0.002474358**	**200**
CEm	**recall**	**PBS**	**CS**	**F-CS**	**C1**	**ictrace3t2**	**0.52**	**0.003391165**	**200**
CEm	**recall**	**PBS**	**CS**	**F-CS**	**C2**	**ictrace4**	**0.518869048**	**0.002651687**	**200**
CEm	recall	PBS	CS	F-CS	C3	ictrace1	0.51827381	0.003894948	200
CEm	recall	PBS	CS	F-CS	C3	ictrace5	0.51452381	0.002422495	200
CEm	recall	PBS	CS	F-CS	C1	ictrace6t2	0.503	0.002335594	200
CEm	recall	PBS	CS	F-CS	C2	ictrace11	0.50202381	0.0033164	200
CEm	recall	PBS	CS	F-CS	C1	ictrace10	0.50125	0.001611321	200
CEm	recall	PBS	CS	F-CS	C3	ictrace9	0.501071429	0.00163488	200
CEm	recall	PBS	CS	F-CS	C4	ictrace6	0.500714286	0.000873359	200
CEm	recall	PBS	CS	F-CS	C1	ictrace1	0.500416667	0.001998046	200
CEm	recall	PBS	CS	F-CS	C1	ictrace14	0.500416667	0.001717708	200
CEm	recall	PBS	CS	F-CS	C2	ictrace6	0.500357143	0.002648522	200

CEm	recall	PBS	CS	F-CS	C2	ictrace2	0.500357143	0.000798196	200
CEm	recall	PBS	CS	F-CS	C2	ictrace1	0.5	0	200
CEm	recall	PBS	CS	F-CS	C1	ictrace6	0.5	0	200
CEm	recall	PBS	CS	F-CS	C4	ictrace1	0.5	0.003194383	200
CEm	recall	PBS	CS	F-CS	C2	ictrace10t2	0.5	0	200
CEm	recall	PBS	CS	F-CS	C2	ictrace9t2	0.5	0	200
CEm	recall	PBS	CS	F-CS	C3	ictrace1t2	0.5	0	200
CEm	recall	PBS	CS	F-CS	C1	ictrace4t2	0.5	0	200
CEm	recall	PBS	CS	F-CS	C4	ictrace8t2	0.5	0	200
CEm	recall	PBS	CS	F-CS	C3	ictrace4t2	0.4995	0.001936169	200
CEm	recall	PBS	CS	F-CS	C4	ictrace4t2	0.4995	0.001936169	200
CEm	recall	PBS	CS	F-CS	C1	ictrace1t2	0.499	0.002344142	200
CEm	recall	PBS	CS	F-CS	C4	ictrace3t2	0.499	0.002120142	200
CEm	recall	PBS	CS	F-CS	C4	ictrace3	0.498928571	0.00163488	200
CEm	recall	PBS	CS	F-CS	C3	ictrace10	0.498571429	0.001424996	200
CEm	recall	PBS	CS	F-CS	C3	ictrace3	0.498571429	0.002855357	200
CEm	recall	PBS	CS	F-CS	C1	ictrace12	0.498571429	0.001332483	200
CEm	recall	PBS	CS	F-CS	C3	ictrace11t2	0.4985	0.002058822	200
CEm	recall	PBS	CS	F-CS	C3	ictrace5t2	0.4985	0.001933585	200
CEm	recall	PBS	CS	F-CS	C3	ictrace3t2	0.498	0.001726268	200
CEm	recall	PBS	CS	F-CS	C4	ictrace12t2	0.498	0.002545584	200
CEm	recall	PBS	CS	F-CS	C3	ictrace13	0.49625	0.001980592	200
CEm	recall	PBS	CS	F-CS	C2	ictrace4t2	0.4845	0.003247884	200
CEm	recall	PBS	CS	F-CS	C3	ictrace15	0.480357143	0.002723499	200
CEm	recall	PBS	CS	F-CS	C1	ictrace2	0.478571429	0.002422261	200
CEm	recall	PBS	CS	F-CS	C2	ictrace7	0.478214286	0.002878282	200
CEm	recall	PBS	CS	F-CS	C4	ictrace5t2	0.476	0.003552464	200
CEm	recall	PBS	CS	F-CS	C2	ictrace5t2	0.4745	0.003390981	200
CEm	recall	PBS	CS	F-CS	C3	ictrace7	0.473333333	0.002811188	200
CEm	recall	PBS	CS	F-CS	C3	ictrace6t2	0.472	0.003328663	200
CEm	recall	PBS	CS	F-CS	C1	ictrace2t2	0.468	0.003446738	200
CEm	recall	PBS	CS	F-CS	C3	ictrace10t2	0.466	0.003423449	200
CEm	recall	PBS	CS	F-CS	C3	ictrace8	0.460833333	0.00456093	200
CEm	recall	PBS	CS	F-CS	C4	ictrace7t2	0.409	0.006630988	200
CEm	**recall**	**aIC inhibition**	**CS**	**R-CS**	**C2**	**ictrace2**	**0.577797619**	**0.005888272**	**200**
CEm	**recall**	**aIC inhibition**	**CS**	**R-CS**	**C2**	**ictrace2t2**	**0.558392857**	**0.006652087**	**200**
CEm	**recall**	**aIC inhibition**	**CS**	**R-CS**	**C2**	**ictrace4t2**	**0.547619048**	**0.002766417**	**200**
CEm	**recall**	**aIC inhibition**	**CS**	**R-CS**	**C2**	**ictrace1t2**	**0.541547619**	**0.003626549**	**200**
CEm	**recall**	**aIC inhibition**	**CS**	**R-CS**	**C2**	**ictrace1**	**0.532619048**	**0.00581462**	**200**
CEm	**recall**	**aIC inhibition**	**CS**	**R-CS**	**C2**	**ictrace4**	**0.531071429**	**0.002968788**	**200**
CEm	**recall**	**aIC inhibition**	**CS**	**R-CS**	**C2**	**ictrace7t2**	**0.530952381**	**0.00269374**	**200**
CEm	**recall**	**aIC inhibition**	**CS**	**R-CS**	**C1**	**ictrace1t2**	**0.517559524**	**0.00270547**	**200**
CEm	**recall**	**aIC inhibition**	**CS**	**R-CS**	**C2**	**ictrace12t2**	**0.516785714**	**0.002559095**	**200**
CEm	**recall**	**aIC inhibition**	**CS**	**R-CS**	**C1**	**ictrace11**	**0.516071429**	**0.004208758**	**200**
CEm	recall	aIC inhibition	CS	R-CS	C1	ictrace18t2	0.515892857	0.002709841	200
CEm	recall	aIC inhibition	CS	R-CS	C1	ictrace3t2	0.503690476	0.002262516	200
CEm	recall	aIC inhibition	CS	R-CS	C2	ictrace11t2	0.501071429	0.00163488	200
CEm	recall	aIC inhibition	CS	R-CS	C2	ictrace3t2	0.500357143	0.001636439	200
CEm	recall	aIC inhibition	CS	R-CS	C2	ictrace13	0.500297619	0.001495073	200
CEm	recall	aIC inhibition	CS	R-CS	C2	ictrace6	0.5	0	200
CEm	recall	aIC inhibition	CS	R-CS	C1	ictrace2t2	0.5	0.001443376	200
CEm	recall	aIC inhibition	CS	R-CS	C1	ictrace6	0.499642857	0.001287449	200
CEm	recall	aIC inhibition	CS	R-CS	C2	ictrace7	0.499166667	0.002040391	200
CEm	recall	aIC inhibition	CS	R-CS	C1	ictrace5t2	0.495416667	0.001933704	200
CEm	recall	aIC inhibition	CS	R-CS	C2	ictrace8	0.493571429	0.002095779	200
CEm	recall	aIC inhibition	CS	R-CS	C1	ictrace7	0.490595238	0.003135713	200
CEm	recall	aIC inhibition	CS	R-CS	C2	ictrace5	0.488214286	0.00206881	200
CEm	recall	aIC inhibition	CS	R-CS	C2	ictrace6t2	0.487559524	0.002364972	200
CEm	recall	aIC inhibition	CS	R-CS	C1	ictrace1	0.468154762	0.003240564	200
CEm	recall	aIC inhibition	CS	R-CS	C2	ictrace3	0.465178571	0.003705746	200

CEm	**recall**	**aIC inhibition**	**CS**	**F-CS**	**C2**	**ictrace4**	**0.5475**	**0.004382173**	**200**
CEm	**recall**	**aIC inhibition**	**CS**	**F-CS**	**C2**	**ictrace1**	**0.545238095**	**0.004137654**	**200**
CEm	**recall**	**aIC inhibition**	**CS**	**F-CS**	**C2**	**ictrace4t2**	**0.542797619**	**0.003782547**	**200**
CEm	**recall**	**aIC inhibition**	**CS**	**F-CS**	**C1**	**ictrace1**	**0.533809524**	**0.003064684**	**200**
CEm	**recall**	**aIC inhibition**	**CS**	**F-CS**	**C2**	**ictrace10t2**	**0.53297619**	**0.003001924**	**200**
CEm	**recall**	**aIC inhibition**	**CS**	**F-CS**	**C1**	**ictrace6**	**0.530952381**	**0.00269374**	**200**
CEm	**recall**	**aIC inhibition**	**CS**	**F-CS**	**C1**	**ictrace2t2**	**0.530952381**	**0.00269374**	**200**
CEm	**recall**	**aIC inhibition**	**CS**	**F-CS**	**C2**	**ictrace3t2**	**0.512083333**	**0.005445357**	**200**
CEm	**recall**	**aIC inhibition**	**CS**	**F-CS**	**C2**	**ictrace8**	**0.5075**	**0.004250275**	**200**
CEm	**recall**	**aIC inhibition**	**CS**	**F-CS**	**C2**	**ictrace6t2**	**0.5025**	**0.001432509**	**200**
CEm	recall	aIC inhibition	CS	F-CS	C2	ictrace2	0.501666667	0.001859659	200
CEm	recall	aIC inhibition	CS	F-CS	C2	ictrace5	0.500357143	0.001556545	200
CEm	recall	aIC inhibition	CS	F-CS	C2	ictrace12	0.5	0	200
CEm	recall	aIC inhibition	CS	F-CS	C2	ictrace13t2	0.5	0.001559024	200
CEm	recall	aIC inhibition	CS	F-CS	C1	ictrace3t2	0.5	0	200
CEm	recall	aIC inhibition	CS	F-CS	C1	ictrace5t2	0.5	0	200
CEm	recall	aIC inhibition	CS	F-CS	C1	ictrace1t2	0.499583333	0.001815969	200
CEm	recall	aIC inhibition	CS	F-CS	C2	ictrace3	0.499166667	0.001442172	200
CEm	recall	aIC inhibition	CS	F-CS	C2	ictrace11t2	0.496666667	0.001751983	200
CEm	recall	aIC inhibition	CS	F-CS	C1	ictrace7	0.4925	0.002159837	200
CEm	recall	aIC inhibition	CS	F-CS	C2	ictrace2t2	0.476011905	0.00267457	200
CEm	recall	aIC inhibition	CS	F-CS	C1	ictrace11	0.473928571	0.002845201	200
CEm	recall	aIC inhibition	CS	F-CS	C2	ictrace7	0.472559524	0.002692684	200
CEm	recall	aIC inhibition	CS	F-CS	C2	**ictrace6**	0.461130952	0.004232036	200
CEm	recall	aIC inhibition	CS	F-CS	C2	ictrace1t2	0.459880952	0.004210072	200
CEm	recall	aIC inhibition	CS	F-CS	C2	ictrace12t2	0.454821429	0.003931544	200

Supplementary References

66. Yan. DPARSF: a MATLAB toolbox for "pipeline" data analysis of resting-state fMRI. *Front. Syst. Neurosci.* (2010). doi:10.3389/fnsys.2010.00013
67. Friston, K. J., Williams, S., Howard, R., Frackowiak, R. S. J. & Turner, R. Movement-related effects in fMRI time-series. *Magn. Reson. Med.* (1996). doi:10.1002/mrm.1910350312
68. Margulies, D. S. *et al.* Mapping the functional connectivity of anterior cingulate cortex. *Neuroimage* (2007). doi:10.1016/j.neuroimage.2007.05.019
69. Saad, Z. S. *et al.* Trouble at Rest: How Correlation Patterns and Group Differences Become Distorted After Global Signal Regression. *Brain Connect.* (2012). doi:10.1089/brain.2012.0080
70. Murphy, K., Birn, R. M., Handwerker, D. A., Jones, T. B. & Bandettini, P. A. The impact of global signal regression on resting state correlations: Are anti-correlated networks introduced? *Neuroimage* (2009). doi:10.1016/j.neuroimage.2008.09.036
71. Murphy, K. & Fox, M. D. Towards a consensus regarding global signal regression for resting state functional connectivity MRI. *Neuroimage* (2017). doi:10.1016/j.neuroimage.2016.11.052
72. Wee, C. Y. *et al.* Resting-state multi-spectrum functional connectivity networks for identification of MCI patients. *PLoS One* (2012). doi:10.1371/journal.pone.0037828
73. Song, X. W. *et al.* REST: A Toolkit for resting-state functional magnetic resonance imaging data processing. *PLoS One* (2011). doi:10.1371/journal.pone.0025031
74. R Development Core Team, R. *R: A Language and Environment for Statistical Computing*. *R Foundation for Statistical Computing* (2011). doi:10.1007/978-3-540-74686-7
75. Behzadi, Y., Restom, K., Liau, J. & Liu, T. T. A component based noise correction method (CompCor) for BOLD and perfusion based fMRI. *Neuroimage* (2007). doi:10.1016/j.neuroimage.2007.04.042
76. Fox, M. D., Zhang, D., Snyder, A. Z. & Raichle, M. E. The global signal and observed anticorrelated resting state brain networks. *J. Neurophysiol.* (2009). doi:10.1152/jn.90777.2008
77. Weissenbacher, A. *et al.* Correlations and anticorrelations in resting-state functional connectivity MRI: A quantitative comparison of preprocessing strategies. *Neuroimage* (2009). doi:10.1016/j.neuroimage.2009.05.005
78. Boes, A. D. *et al.* Network localization of neurological symptoms from focal brain lesions. *Brain* (2015). doi:10.1093/brain/awv228
79. Pedregosa Fabian *et al.* Scikit-learn: Machine Learning in Python. *J. Mach. Learn. Res.* (2011). doi:10.1007/s13398-014-0173-7.2
80. Timme, N. M. & Lapish, C. A tutorial for information theory in neuroscience. *eNeuro* (2018). doi:10.1523/ENEURO.0052-18.2018
81. Jolkkonen, E., Miettinen, R., Pikkarainen, M. & Pitkänen, A. Projections from the amygdaloid complex to the magnocellular cholinergic basal forebrain in rat. *Neuroscience* **111**, 133–49 (2002).
82. Cassell, M. D., Freedman, L. J. & Shi, C. The intrinsic organization of the central extended amygdala. in *Annals of the New York Academy of Sciences* (1999). doi:10.1111/j.1749-6632.1999.tb09270.x
83. Gritti, I., Mainville, L., Mancia, M. & Jones, B. E. GABAergic and other noncholinergic basal forebrain neurons, together with cholinergic neurons, project to the mesocortex and isocortex in the rat. *J. Comp. Neurol.* **383**, 163–177 (1997).

Manuscript 2

(Groessl et al., 2018)
https://dx.doi.org/10.1038/s41593-018-0174-5

Title: Dorsal tegmental dopamine neurons gate associative learning of fear

Authors: Florian Grössl[1], Thomas Munsch[2#], Susanne Meis[2#], Johannes Griessner[1,3], Joanna Kaczanowska[1], Pinelopi Pliota[1], Dominic Kargl[1], Sylvia Badurek[4], Klaus Kraitsy[4], Arash Rassoulpour[5], Johannes Zuber[1], Volkmar Lessmann[2] and Wulf Haubensak[1*]

Affiliations:

[1]Research Institute of Molecular Pathology (IMP), Vienna Biocenter (VBC), Campus-Vienna-Biocenter 1, 1030 Vienna, Austria

[2]Institute of Physiology (Medical Faculty), and Center for Behavioral Brain Sciences (CBBS), Otto-von-Guericke University, Leipziger Str. 44, 39120 Magdeburg, Germany

[3]Medical University of Vienna, Spitalgasse 23, 1090 Vienna, Austria

[4]Preclinical Phenotyping Facility, Vienna Biocenter Core Facilities (VBCF), Vienna Biocenter (VBC), Dr. Bohr Gasse 3, 1030 Vienna, Austria

[5]Brains On-Line, Charles River Laboratories), San Francisco, USA

[#]These authors contributed equally

*To whom correspondence should be addressed.

Abstract: Functional neuroanatomy of Pavlovian fear has identified neuronal circuits and synapses associating conditioned stimuli with aversive events. Hebbian plasticity within these networks requires additional reinforcement to store particularly salient experiences into long-term memory. Here, we have identified a circuit reciprocally connecting the ventral periaqueductal grey (vPAG)/dorsal raphe (DR) region and the central amygdala (CE) that gates fear learning. We found that vPAG/DR dopaminergic (vPdRD) neurons encode a positive prediction error in response to unpredicted shocks, strengthen a dopamine-dependent form of long-term potentiation (LTP) in the CE, and contribute to the establishment of learned fear. Negative feedback from the CE to vPdRD neurons might limit reinforcement to events that have not been predicted. These findings add a new module to the midbrain DA circuit architecture underlying associative reinforcement learning and identify vPdRD neurons as critical component of Pavlovian fear conditioning. We propose that dysregulation of vPdRD neuronal activity may contribute to fear-related psychiatric disorders.

Introduction

The brain uses predictors of important events to optimize future behavioral responses. Pavlovian learning pairs a stimulus with an emotionally salient experience to form emotional memories that can be stored for life[1]. Deconstructing the neuronal basis of storage and recall of such associative memories and the underlying learning models promises insight into fundamental and biomedically relevant brain functions.

The primary neuronal representation of associations between conditioned stimulus (CS) and unconditioned stimulus (US)(CS-US pairing) is stored as synaptic memory traces in neuronal circuitry[2]. While Hebbian plasticity (coinciding pre- and postsynaptic activity) accounts for the primary CS-US pairing, additional processes are required to link associative plasticity to particularly salient events and to the progress in learning itself. Reinforcement signals coupled to prediction errors (PE; a central element in learning models representing the discrepancy between the value of actual and predicted events) can serve that purpose. However, neuronal circuit motifs encoding all necessary components for associative learning, i.e., CS-US integration, PE-coupled reinforcement signals and synaptic memory trace, remain largely uncharted.

In the mammalian brain, Pavlovian fear-related neuronal plasticity in the amygdala is the canonical model for storage of associative memory traces[1]. Within the amygdala, the central amygdala (CE) operates as central hub that re-shapes neural responses[3,4] and synaptic connectivity during learning[5]. In this regard, neurons in the lateral part of the CE (CEl) can be functionally divided into several classes of distinguishable inhibitory neurons, which receive excitatory input from the basolateral amygdala (BLA). Fear learning leads to postsynaptically expressed LTP of the input onto $SST^{+}/PKC\delta^{-}$ neurons[5], whose activity correlates with aversive fear states in various fear-related behavioral assays[3,4,6].

Dopamine (DA) is the canonical link between PE and synaptic reinforcement signals modulating Hebbian plasticity rules of CS-US associations[7]. Foremost identified as key mediator of reward learning[8,9], DA neurons may also drive aversive learning[10-12], suggesting a general role in both negative and positive reinforcement learning. DA modulates neural activity in the CEl via DA1-like and DA2-like receptors (D1R, D2R)[13,14], making it a promising candidate for experience dependent rewiring of amygdala connectivity.

Although evidence for aversive signaling in VTA DA neurons (the midbrain DA neurons for appetitive reinforcement) has been reported[15], the majority of studies observed inhibition[16-18] or no response at all[8,9,19] in response to aversive signals. This raised the obvious question

whether other DAergic neurons outside the VTA reward system might provide DA driven aversive teaching signals for CE fear learning. Interestingly, a relatively neglected group of DA neurons in the ventral PAG/dorsal Raphe (vPdRD neurons)[20-22] represent a particularly promising candidate: although optogenetic stimulation of vPdRD neurons modulates social behavior[21], it does not reinforce operant responses[23], functionally separating these vPdRD from VTA DA neurons[24]. Moreover, the vPAG itself can encode aversive teaching signals[25,26] as it integrates afferent, aversive somatosensory and nociceptive information while being an output structure for various fear-conditioned responses.

Taken together, the CE and the midbrain DA system emerged as promising entry points in our search for circuit motifs integrating Hebbian memory traces and reinforcement signals in associative learning. Synaptic tracing and circuit mapping revealed vPdRD neurons as major source of DAergic projections to the CE. Suppression of vPdRD neuron activity diminished fear learning, accompanied by reduction of experience dependent potentiation of the BLA-CE SST^{+} synapses. Notably, vPdRD neuronal activity shifted from US to CS as learning progressed, linking experience dependent CE rewiring to the animals' PE. We tested this by optogenetically modulating PE signals in vPdRD neurons during associative learning. Reducing PE-related neuronal activity decreased Pavlovian fear learning. Conversely, increasing PE-related neuronal activity interfered with associative blocking. Taken together, these results delineate a learning circuit of reciprocally connected vPdRD and CE neurons, and demonstrate how neural systems integrate reinforcement signals with CS-US associations to write experiences into long-term memory. We assign a defined function to vPdRD neurons and identify them as a critical element for associative learning.

Results

The vPAG/DR provides a major DAergic input to the CE

Tyrosine hydroxylase (TH) immunohistochemistry (IHC) in mice highlight the CE as one of the most densely innervated DA targets in the temporal lobe (Fig. 1a). Although projections to CE from canonical DA-ergic midbrain sources (i.e. substantia nigra (SN) and ventral tegmental area (VTA); compare Fig. 1b), have been reported[27-29], combined CE Cholera toxin B (CTB; retrograde synaptic marker) injections (Fig. 1c) and TH IHC (Fig. 1d), mapped the majority of DA-ergic afferents to a group of vPdRD neurons (Fig. 1e) of largely unknown function (but see[21,22]). Moreover, a large fraction of these neurons throughout the rostral – caudal extension of vPAG/DR (Fig. 1f), projects to the CE, and particularly to CEl, with

surprising specificity (Supplementary Fig. 1), whereas DAergic projections from SN and VTA to the amygdala in general, appear to be rather sparse (Supplementary Fig. 2). Collectively, these data establish a potential link between vPdRD neurons, Pavlovian fear conditioning and DA modulation of CE circuitry.

We therefore investigated the synaptic connectivity of vPdRD neuron projections to SST^+ and $PKC\delta^+$ cells, two major neuronal types in the CEl, in acute brain slices. We injected PKCδ::Cre/TH::Cre double transgenic mice with AAV::DIO-GFP into the CEl and AAV::DIO-ChR2-YFP into the vPAG/DR (Fig. 1g-i). Targeted electrophysiological recordings of postsynaptic CEl GFP^- and GFP^+ cells, considered identical with $SST^+/PKC\delta^-$ and $PKC\delta^+/SST^-$ neurons[5] (Supplementary Fig. 3a), respectively, revealed direct excitatory post-synaptic currents in response to optogenetic presynaptic stimulation of CEl vPdRD neuron terminals (Fig. 1j), blocked by bath-application of CNQX and APV-5. Together with recent reports[28,39], these data suggest that vPdRD neurons innervate, potentially co-release glutamate and DA[21], into the CEl in vivo. While the fraction of responding cells (Fig. 1k) and the signal amplitude in responding neurons (Fig. 1l) was similar between cell types, the overall location of responding neurons was spatially biased to the medial part of the CEl at the CEl/m transition boundary (Fig. 1m), congruent with the vPdRD neuron innervation pattern (Fig. 1a and 1i).

The vPdRD neuron - CE axis features characteristics of a learning circuit

We reasoned that this specific innervation from the vPAG/DR, a multimodal brain region involved in pain processing, might directly reinforce fear learning in the CE circuitry through Glu/DA co-release in response to aversive experiences. Indeed, fiber-endomicroscopic Ca^{2+} imaging in freely moving animals, injected with AAV-expressing GCaMP6m in the vPAG/DR (Fig. 2a, Supplementary Fig. 4a), showed strong bulk Ca^{2+} responses to the Pavlovian shock US (Fig. 2b) in this region, with neuronal subsets directly responding to the US (Fig. 2c).

These responses were accompanied by a shock-US specific rise in intra-amygdalar DA levels as observed through targeted microdialysis in freely moving animals during Pavlovian fear conditioning (Fig. 2d, Supplementary Fig. 5a). Note that for better feasibility the microdialysis was performed in rats, assuming a (gross) fear neuroanatomy similar to mice. These experiments must be interpreted with caution with respect to the stereo specificity of sampling site (CEl vs. BLA) and source (VTA vs. vPdRD neurons). First, the method samples amygdala DA across CEl and BLA. However, given the steep gradients in amygdala

DA innervation (Fig. 1a, Supplementary Fig. 2), we believe that the majority of the sampled DA originates from CEl. Second, these experiments will also sample CE DA from VTA. However, most of CE (and amygdala) DAergic innervation stems from vPdRD neurons and not from VTA (Fig. 1e, Supplementary Fig. 2). Jointly with the fact that vPdRD neurons are active during shock (Fig. 2c) and have been shown to increase CE DA[21] it seems likely that a large part of shock induced DA observed (Fig. 2d) originates from vPdRD neurons and CE. Notably, the increase in amygdalar DA was absent during re-exposure to the shock-context (CS) 24 h later (Fig. 2d), consistent with a role for CE DA in aversive reinforcement learning.

To determine whether DA re-shapes CE synaptic connectivity, we examined DA-ergic modulation of BLA to CE synapses, which potentiate during Pavlovian fear conditioning[5]. We first probed glutamaterigc synapses onto CEl neurons for activity-dependent plasticity in response to high-frequency stimulation (HFS) of BLA inputs using acute slice electrophysiology (Fig. 2e). HFS induced synaptic plasticity of evoked local field potentials (LFPs) in the CEl increased in the presence of DA[30]. To assess the cell-type specificity of this potentiation, we performed single cell whole cell patch-clamp recordings and filled recorded neurons with biocytin for post-hoc classification of neuronal subtypes (Supplementary Fig. 3a). Under basal conditions, the major ($SST^+/PKC\delta^-$ and $PKC\delta^+/SST^-$) CEl cell types failed to undergo LTP after HFS stimulation of BLA inputs (Supplementary Fig. 3b). However, application of DA specifically gated LTP of excitatory BLA inputs onto CEl $SST^+/PKC\delta^-$ cells (Fig. 2f), but not $PKC\delta^+/SST^-$ neurons. This effect was blocked by the D1R antagonist SCH 23390 (Fig. 2g). Population specific transcriptional profiling of FACS-sorted neurons from Cre-dependent td-Tomato reporter mouse lines crossed to either SST::Cre or PKCδ::Cre animals revealed higher expression of D1Rs in $SST^+/PKC\delta^-$ neurons (Supplementary Fig. 6). These data suggest that cell-type specific DA dependent LTP (Fig. 2f) may be mediated by post-synaptic D1R signaling. The asymmetric distribution of D1Rs could specifically sensitize $SST^+/PKC\delta^-$ neurons for fear-related associations and map aversive states asymmetrically on genetically and functionally pre-defined $SST^+/PKC\delta^-$ neurons. These data might explain how fear conditioning could teach $SST^+/PKC\delta^-$ neurons to respond to tone-CSs[4,31], selectively strengthen their responses to BLA input[5] and ultimately link them to aversive states[31].

Taken together, DA, likely released from vPdRD neuron afferents, contributes to cell type specific potentiation of a BLA-to-CE fear synapse to gate associative learning of Pavlovian fear. Therefore, we examined if successful acquisition, storage and/or expression of fearful experiences of animals may require vPdRD neuronal activity.

vPdRD neurons control associative learning of fear

We injected Cre-dependent AAV into the vPAG/DR of TH::Cre animals for selective expression of Clozapine N-Oxide (CNO) activatable receptors exclusively activated by designer drugs (M4-DREADD, AAV::DIO-M4) in vPdRD neurons (*M4-cohort* in Supplementary Fig. 7a). These animals received intra-peritoneal CNO injections 30 min prior the conditioning phase. This treatment, expected to hyperpolarize and electrically silence vPdRD neurons, resulted in decreased freezing responses to the CS during training (Fig. 3a-b). Notably, this cohort showed significantly less freezing than controls during (drug-free) recall the next day. These results establish a critical role for vPdRD neurons in fear learning. Silencing vPdRD neurons with M4 did not lead to overt differences in the elevated plus maze or light/dark transition test (Supplementary Fig. 8a-b), indicating that these cells do not directly modulate anxiety states.

We next tested whether input from vPdRD neurons is required for experience dependent rewiring of CE circuitry. To this end, we ablated vPdRD neurons with stereotactic injections of the neurotoxin 6-hydroxydopamine (6-OHDA) into the vPAG/DR (Supplementary Fig. 7b), and post hoc determined synaptic weights of BLA-CEl connectivity (Fig. 3c; compare next paragraph), after fear conditioning (FC). As expected, ablating vPdRD neurons impacted fear learning and recall, similarly to the effects observed in our DREADD cohort earlier (Fig. 3d). Note that 6-OHDA neurotoxicity towards vPdRD neurons, which lack dopamine-β-hydroxylase[32], provides direct evidence that these cells are indeed DAergic.

Next, we isolated acute slices from these lesioned animals and recorded excitatory postsynaptic currents (EPSCs) in neighboring SST^+ and PKC-δ^+ neuronal pairs after electrical stimulation of BLA inputs. Interestingly, EPSC amplitudes were increased selectively in SST^+ neurons after fear conditioning, resulting in a shift of synaptic weights from BLA-to-PKC-δ^+/SST^- towards BLA-to-SST^+/PKC-δ^- synaptic connectivity (Fig. 3e-f, FC vs. home cage (HC) cohorts). These results are in line with previous studies[5] and indicates that fear conditioning rewires BLA-CE circuitry in a cell type specific manner.

In 6-OHDA lesioned animals, in which ablation of vPdRD neurons decreased fear memory formation (Fig. 3c-d), the fear conditioning induced shift of synaptic weights was markedly reduced and not significantly different from the HC cohort (Fig. 3f). Furthermore, the excitatory drive, determined as frequency and amplitude of spontaneous EPSCs recorded in SST^+ and PKC-δ^+ neurons, resembled the HC state in 6-OHDA lesioned animals (Supplementary Fig. 9). Thus, selectively ablating vPdRD neurons and thereby eliminating

their inputs to the CE resulted in fear memory deficits, which were accompanied by failure to rewire BLA-CE connectivity.

Following the observation of D1R dependent cell type specific gating of LTP at BLA-CEl synapses, we next probed if experience-dependent synaptic plasticity in the CE and fear memory were dependent on CEl D1R signaling. Indeed, RNAi-mediated knockdown of CE1 D1R through injection of AAV viruses expressing GFP-linked shRNAs before fear conditioning (Supplementary Fig. 10a-e) resulted in a similar shift in BLA-CE connectivity as observed in 6-OHDA lesioned animals (Fig. 3f) and fear memory deficits at recall (Supplementary Fig. 10f). Together, these results suggest that vPdRD neuronal activity and asymmetric D1R signalling in CE may underlie a fear memory trace in BLA-CE connectivity.

The comparably mild behavioral phenotype of the D1R knock down experiment (Supplementary Fig. 10) in comparison with the noticeable synaptic effects (Fig. 3e) may be attributed to the fact that slice electrophysiology records specifically from neurons infected with D1R knock down virus, whereas D1R knockdown efficiency in the CE might have been too low to strongly affect behavior, also in comparison to the DREADD silencing (Fig. 3b) and 6-OHDA lesions (Fig. 3d). To interfere with D1R signaling in the CEl more efficiently, we cannulated mouse cohorts bilaterally over the CEl for infusion of the D1R antagonist SCH23390 (Fig. 3g, Supplementary Fig. 5b). Similar to the circuit genetic perturbation using M4-DREADDs (Fig. 3a, b) this manipulation did not alter anxiety (Supplementary Fig. 8c-d). In contrast to the M4-DREADD-silenced cohort (Fig. 3b), pre-training SCH23390 infusion did not result in significantly different freezing responses during training. However, drug-free fear memory recall was strongly decreased (Fig. 3h), similarly to our observations in the M4-DREADD cohort (Fig. 3b). Thus, simultaneous blocking of Glu- and D1R-signaling perturbs short- and long-term fear memory, whereas blocking D1Rs selectively prevents long-term fear memory formation and leaves short-term memory intact. Hypothetically, these data may dissociate Glu- and DA-components of vPdRD signaling: Glu could control short-term memory, whereas DA co-release may primarily consolidate long-term associative memory at BLA-to-CEl SST^{+}/$PKC\delta^{-}$ synapses.

Collectively, these data suggest that vPdRD neurons sense aversive USs to gate memory formation in the amygdala circuitry.

vPdRD neurons and the CE form a learning circuit

As components of DAergic reinforcement systems, vPdRD neurons should be most active when important events have not been predicted (large positive PE) and decrease activity with the progress in learning – a notion supported by the fact that the PAG has the capacity to signal aversive PEs in both, rats[25] and humans[33]. The most intuitive implementation of such negative feedback from learning would be direct inhibition of DA neurons by CEl $SST^+/PKC\delta^-$ cells – or CEm (the major CE output), the elements that "learn" with conditioning. Indeed, PAG targeted CTB injections revealed retrogradely labelled neurons in the CEl, originating predominantly from $SST^+/PKC\delta^-$ neurons (Supplementary Fig. 11). This was supported by bilateral AAV::DIO-ChR2 injections in the CE of SST::CRE and PKCδ::CRE mice, showing rather selective vPAG/DR innervation from $SST^+/PKC\delta^-$ neurons (Supplementary Fig. 11). Together with the strong retrograde labeling of the CEm (Supplementary Fig. 11), this indicates that $SST^+/PKC\delta^-$ neurons, but not $PKC\delta^+/SST^-$ neurons, and the CEm are the major CE sources for vPdRD neuron innervation.

To elucidate the inter-connectivity between CE and vPdRD neurons in more depth, we co-injected ChR2-YFP and CTB 555 in the CE for optogenetic manipulation of CE arising fibers connecting to vPdRD neurons (retrogradely labelled by CTB) that project back to the CEl (Fig. 4a). The DA-ergic nature of biocytin labelled recorded neurons was confirmed post hoc by TH IHC (Fig. 4b). Optogenetic stimulation of CE inputs evoked inhibitory PSCs in CEl projecting DA neurons in the PAG, sensitive to application of the $GABA_A$ receptor antagonist bicuculline (50 µM) (Fig. 4c). Thus, CEl $SST^+/PKC\delta^-$ neurons and CEm may inhibit further reinforcement from vPdRD neurons, in particular after BLA-CE circuitry has learned to respond to, and predict, the fear US[4,31].

In search for the proposed modulation of vPdRD neuron activity during learning progress, we compared deep brain Ca^{2+} signals of vPdRD neurons expressing GCaMP6f (Fig. 4d-h, Supplementary Fig. 4b) during a series of two-reinforced (Fig. 4e-i; Cond. 1, Cond 2) and one non-reinforced (Fig. 4e-i; Recall) fear conditioning sessions. Freezing levels of animals confirmed that mice developed robust fear memories during CS-US association trials (Fig. 4e).

Bulk Ca^{2+} population signals from vPdRD neurons showed a strong increase in Ca^{2+} signals during CS-US pairings in the first conditioning (Supplementary Data 1; Supplementary Fig. 12e-f; Fig. 4f-g). As learning progressed to the second conditioning, the population Ca^{2+} signal of vPdRD neurons started to register the previously reinforced CS, whereas the population Ca^{2+} signal to the US, which could be predicted by the animal at this time point,

decreased. During non-reinforced recall 24h later, after consolidation of fear memories, vPdRD neurons showed strong increase in Ca^{2+} signals to the CS, when compared to the conditioning sessions.

A similar picture emerged at the level of single units (Supplementary Videos 1-3; Supplementary Data 1; Supplementary Fig. 12f; Fig. 4h-i). Analysis of single unit Ca^{2+} signals (Fig. 4i) revealed a shift of the dominant response clusters from US- to CS-driven activity over the course of the paradigm. To investigate if this trend reflected discrete, stimulus driven neuronal firing (mirroring actual action potentials), we transformed the Ca^{2+} signals into neuronal activity events, defined as rise in Ca^{2+} signals above 3 median S.D. We then filtered for those units (referred to as responders) whose firing to either CS and/or US exceeded >95% CI of the expected mean activity (Supplementary Fig. 12f). Indeed, the population activity of these responders followed a similar pattern (Fig. 4j, *top*), with the fraction of responder types shifting from US to CS throughout the paradigm (Fig. 4j, *bottom*). Notably, these results are also contained within the vPAG/DR neuronal population as a whole (Supplementary Fig. 12a-d). Thus, vPdRD neurons appear to encode a positive PE in aversive reinforcement learning.

Stimulus associated activity of vPdRD neurons gates learning

If vPdRD neurons encode PE linked reinforcement signals, their activity during associations should critically modulate learning. Thus, we examined whether optogenetic inhibition of vPdRD neurons during the four 20s CS-US pairings, a period that corresponds to the highest neuronal activity during fear conditioning (Fig. 4i), would be sufficient to recapitulate the behavioral consequences of M4-DREADD silencing (Fig. 3a-b). Selective optogenetic inhibition of Arch expressing vPdRD neurons (Fig. 5a, Supplementary Fig. 4), suppressing PE linked reinforcement signals during associative periods, resulted in less freezing behavior to CS during conditioning and impaired fear responses when tested the next day (Fig. 5b, Recall). This establishes a critical role for vPdRD neurons at the time of CS-US pairings, and for the conversion of these pairings into short- and long-term fear memory. Similarly to M4-DREADD inhibition, Arch-mediated silencing of vPdRD neurons did not influence nociception (Supplementary Fig. 8e-h), functionally dissociating these neurons from a general role of vPAG/DR in gating pain.

Hypothetically, activation of vPdRD neurons could be enough to induce plasticity in the CE in the absence of an instructive US (foot shock). To investigate this possibility, we performed Ch2R-driven optogenetic activation of vPdRD neurons during CS-pairings (Fig. 5a, lower

panel, Supplementary Fig. 7d). This optogenetic activation was not sufficient to instruct aversive memories in the absence of real shock-USs (Supplementary Fig. 13). Interestingly, we observed that optogenetic vPdRD neuron activation evoked slow continuous movement (Fig. 5c, Supplementary Video 4). A similar observation has been made recently upon activation of a different neuronal population in the ventral vPAG/DR[34].

Overall, these results are in line with a role of vPdRD neurons in primarily mediating PE coupled reinforcement learning without encoding an intrinsic valence per se.

As activation of vPdRD neurons could not replace an instructive US during aversive fear learning by itself, we asked whether it may rather gate fear memory and associative learning in response to those contingencies that are novel and informative. We therefore examined whether vPdRD neuronal activity interferes with associative blocking of compound conditioning, a conditioning variant sensitive to aberrant reinforcement learning[25,35](Fig. 5d). Under normal conditions, linking a novel CS (CS B) to a US is blocked when the novel CS is co-presented with a CS (CS A) that is already associated with, and thus predicts, the subsequent US. This effect is also evident in our experiment, as controls froze significantly more to CS A than CS B, indicating successful blocking of the association between CS B and the US (Fig. 5d, *right*). In contrast, optogenetic activation of vPdRD neurons during compound CS-US presentations had two effects. It significantly increased the previously observed slow motion attend-like behavior (Fig. 5c) at the expense of freezing in that session (Fig. 5d, *middle*) and inverted the CS-response pattern during recall (Fig. 5e). Thus, artificially increasing PE and reinforcement learning during associative periods, results in establishing memories that are normally suppressed.

Taken together these experiments show that manipulation of stimulus-bound vPdRD neuronal activity – effectively simulating a larger or a smaller than actual PE at time of association - bidirectionally modulates fear learning. Thus, PE signals in vPdRD neurons, and DA reinforcement signals originating from vPdRD neurons positively gate associative learning.

Discussion

Learning from aversive experiences is one of the most basic and biomedically important brain functions. Here, we describe a circuit motif, reciprocally interconnecting vPdRD neurons with CE circuitry (Supplementary Fig. 14). It couples a positive aversive PE signal to DAergic reinforcement of an experience dependent memory trace at an amygdala fear synapse.

Amygdala nuclei are the canonical substrate for fear memory formation. However, the reinforcing mechanisms that rewire amygdala circuitry during learning are much less understood. Notwithstanding the known interaction between VTA DA and the amygdala, a longstanding missing element of fear learning was a dedicated DA system that allows aversive PE coupled reinforcement learning to modulate amygdala synaptic memory traces. In identifying vPdRD neurons as a major DA input to CE circuitry, we provide a circuit context that links vPAG/DR, which integrates nociceptive US-related information[36] and encodes PE information[26,37,38], to DA driven rewiring of BLA-CE connectivity.

In line with US responses of the vPAG region during acquisition of fear learning[26], we find that the response of vPdRD neurons shift from US to CS as learning progresses with conditioning. This re-orientation towards the predictive value of emotionally relevant information is in line with vPdRD neurons encoding PE coupled teaching signals. While PE coupled reinforcement signals are integral parts of several Pavlovian fear learning models, their neuronal implementation has not been fully resolved at the circuit level[25]. We propose that vPdRD neuronal activity and DA signals mirror features of the PE and of PE linked reinforcement signals of classical Rescorla-Wagner[39] and Pearce-Hall[40] models, positively encoding unpredicted aversive stimuli (Fig. 4i, Conditioning 1, Conditioning 2). As omissions of the shock-US in the non-reinforced session (Fig. 4i, Recall) were not positively signaled, most of vPdRD neurons implement a Rescorla-Wagner type PE. That said, some sets of cells in the vPdRD responded with delayed onset to the CS (Fig. 4i, Recall, middle cluster), which might assign a positive signal and Pearce-Hall type PE to US omissions. Thus, different vPdRD cells might encode segregated features of learning models as has been suggested for VTA[10]. This should inspire experiments dedicated at resolving the fine structure of PE signals in the vPdRD neurons and dissociate them from PE signals in VTA. A scenario in which VTA DA neuron activity signals positive reward prediction errors[10] whereas vPdRD cells signals positive fear prediction errors might be attractive, but is likely too simplistic.

Of note, DA release of vPdRD projections has been shown recently[21]. CE targeted retrograde tracing (Fig. 1c-f) identified vPdRD neurons as major DA neuronal input source whereas amygdalar projections from other dopaminergic areas beside vPdRD neurons appear to be rather sparse (Supplementary Fig. 2). Although contributions from these areas cannot be ruled out, these observations point to vPdRD neurons as a major origin of DA ergic modulation in CE and perhaps the whole amygdala. Accordingly, we hypothesize that vPdRD neurons emit a DAergic teaching signal that adapts to the predictive value of a given CS. The

CE, in turn, transforms this signal into fear memory. DA modulates synaptic plasticity of SST^+ neurons in the CEl via D1R dependent LTP. This D1R mediated synaptic plasticity might contribute to the underlying mechanism of the fear experience dependent reshaping of BLA synapses onto CEl SST^+ neurons (Fig. 3e)[5]. The fact that 6-OHDA lesions of vPdRD neurons can partially revert this effect, links aversive teaching signals from vPdRD neurons to DA mediated synaptic plasticity in the CEl. Since D1R potentiates BLA to CE synapses [13,14] and learning[41,42] and given that in our hands blocking of CE D2R signaling showed less behavioral consequences in fear conditioning (data not shown), we focused on D1Rs in our circuit model. However, we would like to point out that also D2R effects might contribute. In fact, our sequencing results show D2R expression in both CEl cell types (data not shown). Thus, CE D2R signalling may synergize with D1R activation to induce experience- and vPdRD neuron-dependent rewiring of BLA-CE $SST^+/PKC\delta^+$ connectivity. Importantly, such a mechanism integrates earlier work[43] into the circuit framework put forward by our study. The complexity of DA receptor signaling in the amygdala[43,44], demands further studies to dissociate the role of D1R vs. D2R dependent mechanisms.

It has recently been shown that CE feedback to the vlPAG controls fear learning, stimulus responsivity of vlPAG neurons and PE coding in the amygdala[38]. Our results extend the possible explanation for this observation as we find direct inhibitory synaptic connectivity of CE output from CEl $SST^+/PKC\delta^-$ cells and CEm to vPdRD neurons (Fig.4). During fear learning, this negative feedback projection could regulate vPdRD neurons and henceforth adapt PE signaling according to the neuronal activity state in CEl and CEm (e.g., suppression of US responding by a preceding predictive CS after CS learning by $SST^+/PKC\delta^-$ CEl neurons).

We used a combination of fear conditioning and an associative blocking design[25] to assess whether manipulation of vPdRD neuronal activity modulates associative learning. Silencing vPdRD neuronal activity during CS-US pairings, thereby simulating a PE that is smaller than actual, resulted in decreased CS-US associations. Conversely, increasing activity during CS-US compound pairings in associative blocking, simulating a PE that is larger than actual, facilitated the association of the novel CS (CS B). Thus, modulation of vPdRD activity, presumably representing PE coupled reinforcement, gates learning. In contrast to VTA DA neurons, where direct activation can induce behavioral conditioning[45] or reinforcement, our results demonstrate that this is not the case for sole activation of vPdRD neurons. This dissociates this class of DA neurons from VTA neurons. Moreover, it indicates that, besides vPdRD neuron activity, additional signals are required to write experiences into synaptic

long-term memory in CE circuitry. In the context of aversive experiences, these US pain related signal may come from other brainstem systems[46]. Hence, vPdRD neuron activity retains a primarily reinforcing nature but does not encode an intrinsic affective valence.

Regardless, activation of vPdRD neurons in a neutral context led to a mild behavioral switch, manifested as constant slow movement. This type of behavior has been described recently for the ventral PAG as 'slow motion' behavior[34]. Notably, it was able to override freezing behavior in our associative blocking assay (Fig. 5c), while increasing associative performance. Thus, vPdRD neurons may drive an own-standing distinct attentive-like behavioral state.

A notable aspect of our study being in line with recent findings[21], is the observation that vPdRD neurons can co-release glutamate in the CEl. The co-release of DA together with either one of the fast ionotropic neurotransmitters like GABA and glutamate has been observed for VTA DA neurons previously[47] but there is no satisfying theory about how it could affect behavior. Strikingly, blocking of DA in the CEl only affected fear testing (Fig. 3g-h), whereas optogenetic inhibition of vPdRD neurons, that most likely blocks the majority of DA and glutamate release in the CEl, affects short term fear memory during the conditioning phase as well (Fig. 5). One attractive hypothesis is, that glutamate co-release facilitates short term learning, which DA reinforces to long term synaptic memory, functionally dissociating these co-released neurotransmitters. Interestingly, glutamate activates $PKC\delta^{+}/SST^{-}$ neurons (Fig. 1k) which could drive short term learning by increasing attention-like states via the basal forebrain[48,49]. The 'slow motion' behavior evoked with very short delays after vPdRD neuron activation, likely driven largely by fast glutamate signaling from vPdRD neurons (rather than by the more slowly acting DA), may reflect such attention-like states.

Taken together, we identified a circuit motif, interconnecting vPdRD neurons and amygdala, that integrates the main components of associative learning (CS/US information, PE and synaptic memory) to shape an amygdala fear response. DA release in the CEl acts as a retrograde reinforcement signal by setting synaptic learning rules[7] to control Pavlovian memory traces. An inhibitory feedback-loop may inhibit reinforcement signals to prevent excessive associations. This delineates an intuitive model (Supplementary Fig. 14) on how the brain computes a learning problem. In the context of aversive learning, the vPdRD component integrates nociceptive US-related information and - via direct interaction with the CE - signals the PE to reinforce plasticity at a CEl fear synapse.

The dopaminergic identity of vPdRD neurons has previously been suggested[21,22] and our 6-OHDA lesion results further proof this notion. Thus, our study assigns a defined neuronal circuitry and behavioral function to vPdRD neurons, a hitherto relatively uncharted class of DA neurons in the mammalian brain.

In turn, we identify vPdRD neurons as a central component for negative reinforcement learning. Importantly, the CE is a critical component of reward conditioning[44] , which might point towards a more general role of vPdRD-CE circuitry also in positive reinforcement learning. Together with the fact that DA-ergic neurons in general[12] and the vPAG/DR region[25] play a key role in learning processes, vPdRD neurons might emerge as central gatekeepers of associative reinforcement learning.

From a biomedical point of view, signatures of aversive PEs have recently been detected in the human PAG[33]. Thus, dysregulation of vPAG/DR DA-CE circuitry could lead to inadequate fear memories observed in PTSD, and, given the pain sensing properties of vPAG/DR, the comorbidity of PTSD and chronic pain[50].

Accession codes: Neural population sequencing data (record GSE95154) are available at https://www.ncbi.nlm.nih.gov/geo/query/acc.cgi?token=oretwkoofbeppmp&acc=GSE95154.

Acknowledgements: We would like to thank Barbara Werner, Nadia Kaouane and the Next Generation Sequencing (NGS) Core at Vienna Biocenter Core Facilities GmbH (VBCF) for neuronal population sequencing and Simon Rumpel for scientific discussion and advice. We thank Manueal Pasieka of the Scientific computing unit at the Vienna Bio Campus (VBC), the Facility for Advanced Microscopy at the Vienna Bio Campus (VBC), in particular Pawel Pasierbek and Thomas Lendl for help with confocal microscopy. We further like to thank the Facility for Preclinical Phenotyping at the Vienna Biocenter Core Facilities GmbH (VBCF) and Mumna al Banchaabouchi, the IMP animal facility and Alexandra Stepanek for help with behavioral assays and animal research. We thank the HistoPathology at the VBCF for expertise and histological services. Boris Ferger (Boehringer Ingelheim, Germany) and Gunnar Filk (Brains On-Line LLC, San Francisco, USA) provided valuable discussions and microdialysis data, Lukasz Piszczek set up and analyzed FACS control experiments for D1R knockdown. We thank Mareike Roth and Julian Jude for advice in RNAi experiments. W. H. was supported by a grant from the European Community's Seventh Framework Programme (FP/2007-2013) / ERC grant agreement no. 311701, the Research Institute of Molecular Pathology (IMP), Boehringer Ingelheim and the Austrian Research Promotion Agency (FFG). S.M., T.M. and V.L. were supported by the DFG (TP B06 of SFB 779). The Vienna Biocenter Core Facilities GmgH (VBCF) preclinical Phenotyping Facility acknowledges funding from the Austrian Federal Ministry of Science, Research&Economy;and the City of Vienna.

Author Contributions: F.G. conceived, designed, performed and analyzed most of the experiments and wrote the manuscript. T.M. and S.M. performed whole-cell patch clamp and LFP recordings for LTP experiments. J.K. and P.P. performed and analyzed Ca^{2+} imaging experiments. J.G. performed mouse surgeries. D.K performed anatomical tracings and designed and tested AAVs for optogenetics, DREADDs and GCaMP6m.A.R. designed, performed and analyzed microdialysis experiments. S.B. and K.K. performed and analyzed SCH injections, fear conditioning, acute anxiety assays and pain tests. J. Z. designed RNAi viral vectors and supervised knock down experiments. V.L. co-supervised experiments and wrote the manuscript. W.H. initiated and conceived the project, designed, analyzed and supervised experiments and wrote the manuscript. All authors contributed to the experimental design and interpretation and commented on the manuscript.

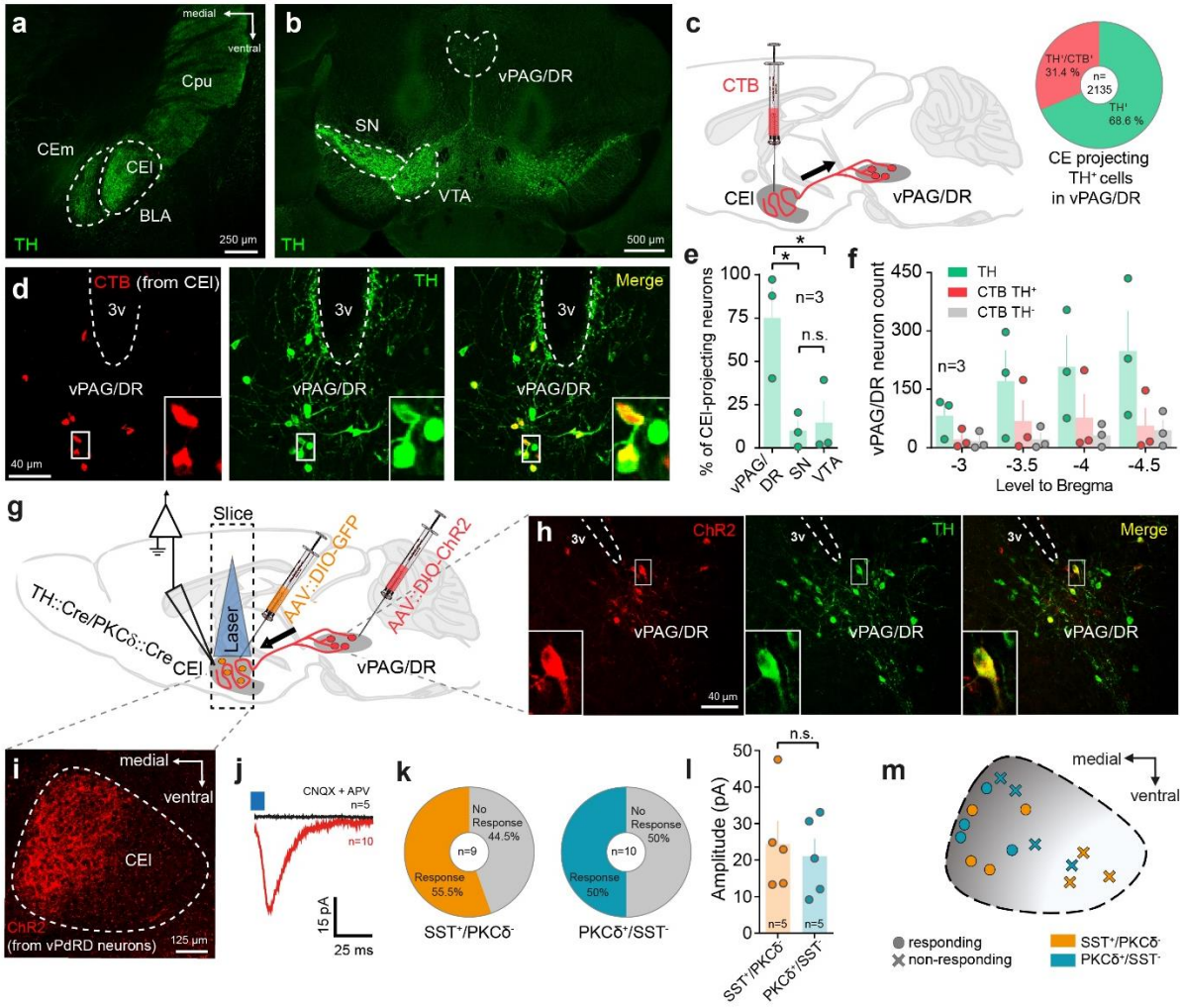

Figure 1 | vPAG/DR-CE circuitry is a major DA-ergic component in the fear pathway. Representative images of (a) CEl as a target of TH immunopositive terminals in the temporal lobe, of (b) TH immunopositive neurons in the midbrain and (c) of the identification of CEl DA sources by CTB retrograde tracing. Inset indicates fraction of CEl-projecting vPdRD neurons (d) CTB retrogradely labelled neurons in the vPAG/DR and co-localized with TH immunoreactivity. (e) Distribution of CEl projecting CTB^+/TH^+ neurons in the major midbrain DA regions (n = 3 animals; values from 3 sections/animal; one-way ANOVA F (2, 6) = 7.962, P = 0.0205; Holm-Sidak post-hoc test;) (f) Anterior to posterior distribution of TH^+/CTB^+ PAG neurons after CEl CTB injection. (g) Combined CTB/ChR2 optogenetic circuit mapping of vPdRD neurons in AAV::DIO-ChR2, AAV::DIO-GFP injected TH::Cre/PKCδ::Cre double transgenic animals. (h-i) $ChR2^+$ fibers of infected vPdRD neurons (h) innervate the CEl (i) (cf. TH^+ terminals in (a)). (j) Post-synaptic currents recorded in whole cell patch-clamp configuration from CEl neurons (red, average trace; n=10 neurons) induced by optogenetic activation of $ChR2^+$ fiber terminals of vPdRD neurons (i). PSC elicited in aCSF can be blocked by application of 10 µM CNQX + 50 µM APV (black, average trace; n=10 neurons). (k) Fraction of CEl $SST^+/PKC\delta^-$ and $PKC\delta^+/SST^-$ neurons responding to optogenetic activation in CEl. (l) Evoked ePSC amplitude of responding CEl $SST^+/PKC\delta^-$ and $PKC\delta^+/SST^-$ neurons (n=5 neurons; unpaired t-test, two-sided, t (8)= 0.4281, P =0.6799. (m) Spatial distribution of a subset of responding (l) and non-responding cells in CEl (cf. distribution of TH^+(a) and $ChR2^+$ (i) terminals). Representative images from at least three independent experiments (animals). Bars are means ± s.e.m. Significance levels between groups at * P<0.05.

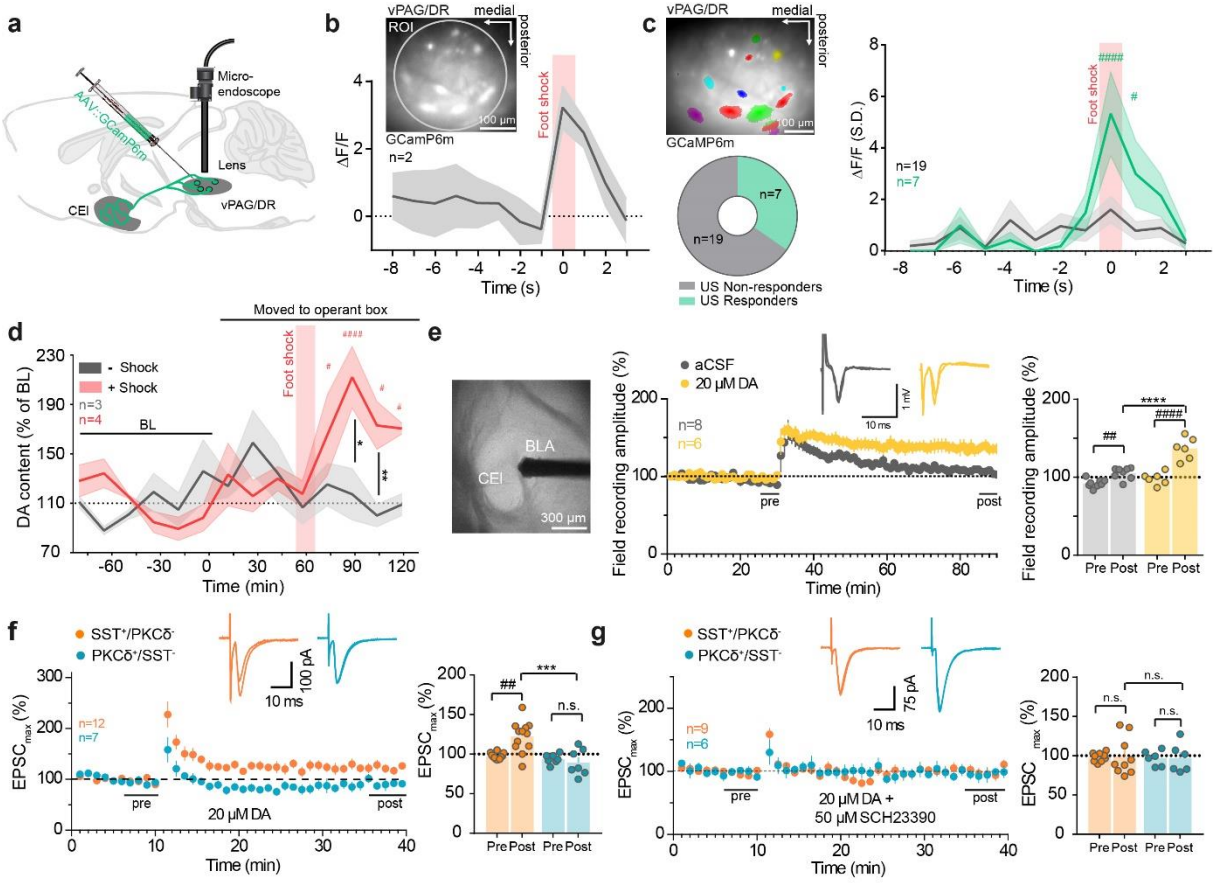

Figure 2 | Modulation of vPAG/DR-CE circuitry by shock and DA. (a) Deep brain Ca^{2+} imaging of vPAG/DR neurons. (b) Bulk Ca^{2+} imaging of vPAG/DR neuronal activity of freely moving mice in response to foot shock (n = 2 animals). Inset shows bulk imaging of vPAG/DR neurons expressing GCaMP6m. Circle indicates ROI used to calculate the bulk signal. (c) (*top left)* Representative example of vPAG/DR neuronal units expressing GCaMP6m (n= ROIs from 2 animals). Fraction of neuronal units responding (n = 7 cells) and non-responding (n = 19 cells) to foot shock (*bottom left*) and corresponding Ca^{2+} signals (*right*) (RM two-way ANOVA ($F_{interaction}$ (11, 264) = 3.141, P = 0.0005; F_{time} (11, 264) = 6.798, P < 0.0001; $F_{columns}$ (1, 24) = 3.235, P = 0.0847; Holm-Sidak post-hoc tests) (d) Microdialysis of DA release in the rat amygdala upon foot shock (n = 4 animals + shock session, n=3 animals -shock session; re-exposure; RM two-way ANOVA ($F_{interaction}$ (8, 40) = 4.26, P = 0.0009; F_{time} (8, 40) = 2.461, P = 0.0286; F_{groups} (1, 5) = 2.633, P = 0.1656; Holm-Sidak post-hoc tests). (e) CEl LFP recordings from acute slices with HFS (100 Hz, 1 s, 3 times, every 30 s) ± 20 µM DA (aCSF control group: n= 8 cells, DA group: n=6 cells; tests for LTP: RM two-way ANOVA $F_{interaction}$ (1, 12) = 20.2, P = 0.0007, F_{time} (1, 12) = 81.69, P < 0.0001; F_{groups} (1, 12) = 23.35, P = 0.0004; Holm-Sidak post-hoc tests). (f-g) LTP recordings of CEl neurons in the presence of (f) 20 µM DA ($SST^+/PKC\delta^-$ cells: n = 12, $SST^-/PKC\delta^+$ cells: n = 7; tests for LTP: RM two-way ANOVA $F_{interaction}$ (1, 14) = 9.052, P = 0.0094, F_{time} (1, 14) = 3.807, P = 0.0713; F_{groups} (1, 14) = 11.6, P = 0.0043; Holm-Sidak post-hoc tests) and (g) 20 µM DA + 50 µM SCH 23390 DA ($SST^+/PKC\delta^-$ cells: n = 9, $SST^-/PKC\delta^+$ cells: n = 6; tests for LTP: RM two-way ANOVA $F_{interaction}$ (1, 11) = 0.0001787 P = 0.9896, F_{time} (1, 11) = 0.0008886, P = 0.9768; F_{groups} (1, 11) = 0.01172, P = 0.9158; Holm-Sidak post-hoc tests). (c-g). Lines with shaded regions represent means ± upper and lower bounds (b) or s.e.m (c-d). Bars are means ± s.e.m. Significance levels between groups (*) and to baseline (BL) or pre-HFS (#) at */# P<0.05, **/## P<0.01, ***/### P<0.001 and ****/#### P<0.0001.

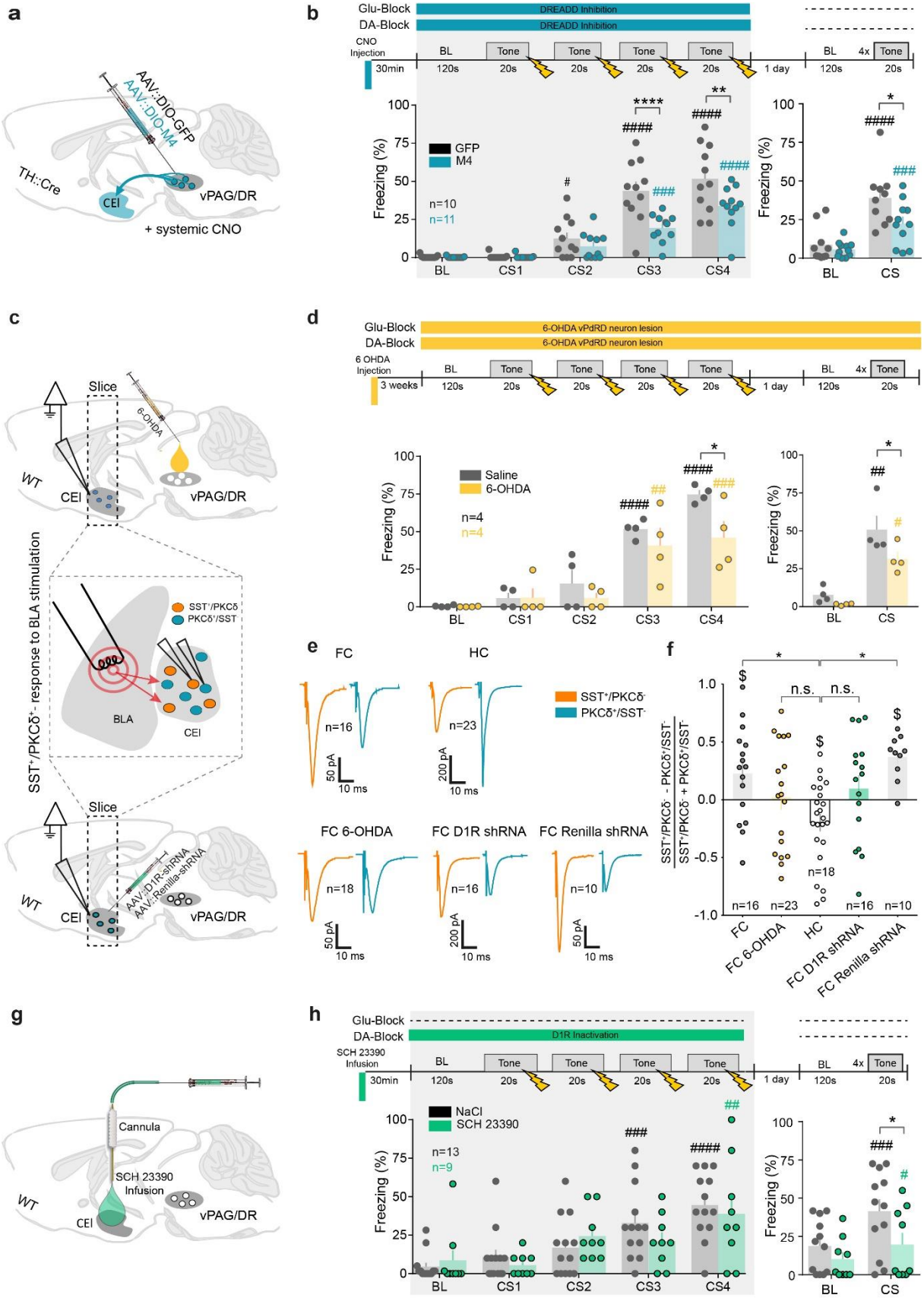

Figure 3 | vPdRD neurons support fear memory formation and amygdala rewiring. (a) AVV mediated Cre-dependent expression of DREADD M4 in vPdRD neurons of TH::Cre transgenic animals. (b) Fear conditioning protocol and freezing responses for systemic CNO injection and subsequent M4-receptor dependent tonic vPdRD neuron inhibition during conditioning (control group: n = 10 animals, M4 group: n = 11

animals; RM two-way ANOVA$_{conditioning}$ $F_{interaction}$ (4, 80) = 6.276, P = 0.002; F_{time} (4, 80) = 75.96, P = 0.0001; F_{groups} (1, 20) = 9.119, P = 0.0068; RM two-way ANOVA$_{recall}$ $F_{interaction}$ (1, 19) = 7.161, P = 0.0149; F_{time} (1, 19) = 83.32, P < 0.0001; F_{groups} (1, 19) = 3.717, P = 0.0689; Holm-Sidak post-hoc tests). (c) Experience dependent plasticity of BLA-CEl SST^+ synapses upon fear conditioning after either 6-OHDA ablation of vPdRD neurons (*top*) or AAV mediated D1R knock down in the CEl (*bottom*). (d) Freezing responses after 6-OHDA lesioning of vPdRD neurons during conditioning (control group: n = 4 animals, 6-OHDA lesion group: n = 4 animals; RM two-way ANOVA $_{conditioning}$ $F_{interaction}$ (4, 24) = 1.619, P = 0.2021; F_{time} (4, 24) = 34.05, P < 0.0001; F_{groups} (1, 6) = 6.029, P = 0.0494; Holm-Sidak post-hoc tests) and testing (RM two-way ANOVA$_{recall}$ $F_{interaction}$(1, 6) = 1.344, P = 0.2904, F_{time} (1, 6) = 40.88, P=0.0007; F_{groups}(1, 6) = 7.098, P = 0.0373; Holm-Sidak post-hoc tests). (e) Averaged whole-cell patch-clamp recordings of post-synaptic currents of CEl SST^+/$PKC\delta^-$ and $PKC\delta^+$/SST^- neurons next to each other (<60µm) in response to BLA stimulation of animals that underwent fear conditioning (FC, n = 16 cell pairs), that were naïve (home cage, HC, n = 23 cell pairs), that received 6-OHDA ablation of vPdRD neurons and underwent fear conditioning (FC 6-OHDA, n = 18 cell pairs), that received D1R knockdown virus in the CEl and underwent fear conditioning (FC D1R shRNA, n = 16 cell pairs) and that received a control virus and underwent fear conditioning (FC renilla shRNA, n = 10 cell pairs). (f) Ratio of CEl SST^+/$PKC\delta^-$ to $PKC\delta^+$/SST^- neuron post-synaptic currents after mice underwent a given behavioral paradigm as described in (e) (n = cell pair groups described in (e); One-way ANOVA$_{pairs}$ F_{groups} (4, 78) = 4.624 P = 0.0021; Dunnett's post-hoc). (g) Targeted pharmacological inhibition of CEl D1Rs by local infusion of SCH23390. (h) Freezing responses after CEl targeted SCH23390 infusion during conditioning (RM two-way ANOVA $_{conditioning}$ $F_{interaction}$ (4, 80) = 1.106, P=0.3593; F_{time} (4, 80) = 14.79, P < 0.0001; F_{groups} (1, 20) = 0.1926, P = 0.6655; Holm-Sidak post-hoc tests) and drug-free testing sessions (RM two-way ANOVA$_{recall}$ $F_{interaction}$(1, 19) = 6.164, P = 0.0225, F_{time} (1, 19) = 36.94, P<0.0001; F_{groups} (1, 19) = 2.88, P = 0.1060; Holm-Sidak post-hoc tests). Bars are means ± s.e.m. Significance levels between groups (*) and to baseline (BL) (#) at */# P<0.05, **/## P<0.01, ***/### P<0.001 and ****/#### P<0.0001.

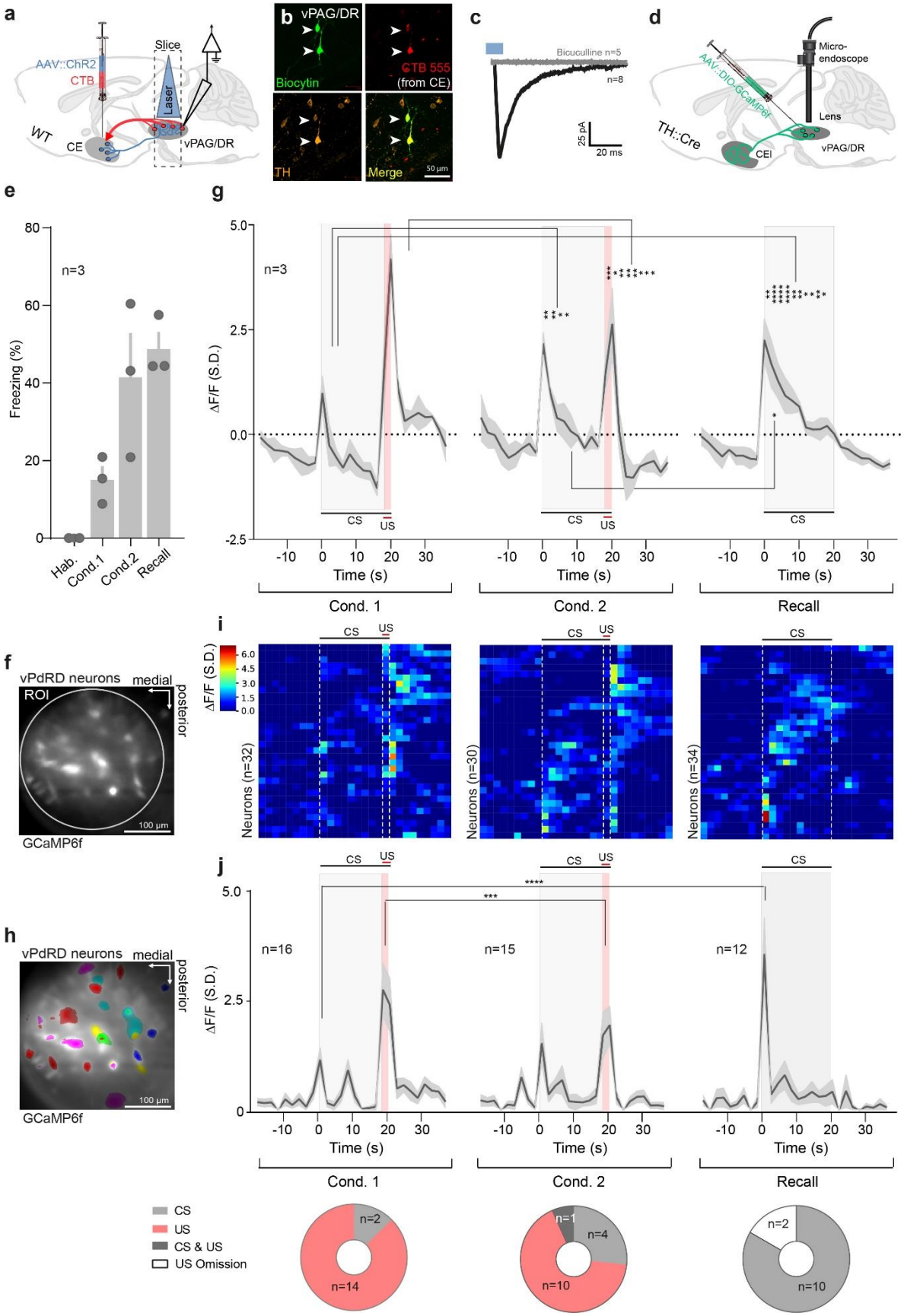

Figure 4 | vPdRD neurons encode PE linked teaching signals. (a) Combined CE CTB/ChR2 injections and whole cell patch-clamp recordings in the vPAG/DR. (b) Representative image of Biocytin-filled, TH$^+$ and CTB retrogradely labelled (derived from CE targeted CTB injections) vPdRD neurons. (c) Optogenetic activation of CE originating ChR2 fibers elicits iPSCs in vPdRD neurons (red, average trace, n = 8 cells) blocked by

application of 50 µM Bicuculline (black, average trace, n = 5 cells). (d) Expression of GCaMP6 in vPdRD neurons in TH::Cre animals injected with dependent AAV. (e) Freezing levels of Ca^{2+} imaged animals during fear conditioning and recall. (f) Bulk imaging of vPdRD neurons expressing GCaMP6f. Circle indicates ROI used to calculate the bulk signal. (g) Trial averages of bulk Ca^{2+} signals of vPAG/DR neuronal activity during fear conditioning and recall (n = ROIs from 3 animals; RM two-way ANOVA $F_{interaction}$ (54, 56) = 3.204, P<0.0001; F_{rows} (27, 28) = 3.434, F_{time} (2, 56) = 1.974, P=0.1484; Holm-Sidak post-hoc tests). (h) Representative example of vPdRD neuronal units expressing GCaMP6f. (i) Clustered traces of Ca^{2+} signals from vPdRD neuronal units from experiment shown in (g). (j) (*top*) Trail averages of Ca^{2+} event amplitudes of a CS and/or US responsive subset of vPdRD neurons (n = units from 3 animals; RM two-way ANOVA $F_{interaction}$ (54, 1080) = 3.749, P<0.0001; F_{time} (27, 1080) = 15.43, P<0.0001; F_{column} (2, 40) = 1.15, P = 0.3270; Holm-Sidak post-hoc tests). (*bottom*) Fraction of subsets of single units responding to either CS and/or US (n = units from 3 animals; Chi-Square (20.05, 4), P=0.005). Representative images from three independent experiments (animals). Bars and lines with shaded regions represent means ± s.e.m Significance levels between groups (*) at * *P*<0.05, ** *P*<0.01, *** *P*<0.001 and **** *P*<0.0001. Ca^{2+} signals and event amplitudes are derived from per ROI (g) or per cell (i-j) dF/F values, standardized over the whole experiment and given as units S.D.

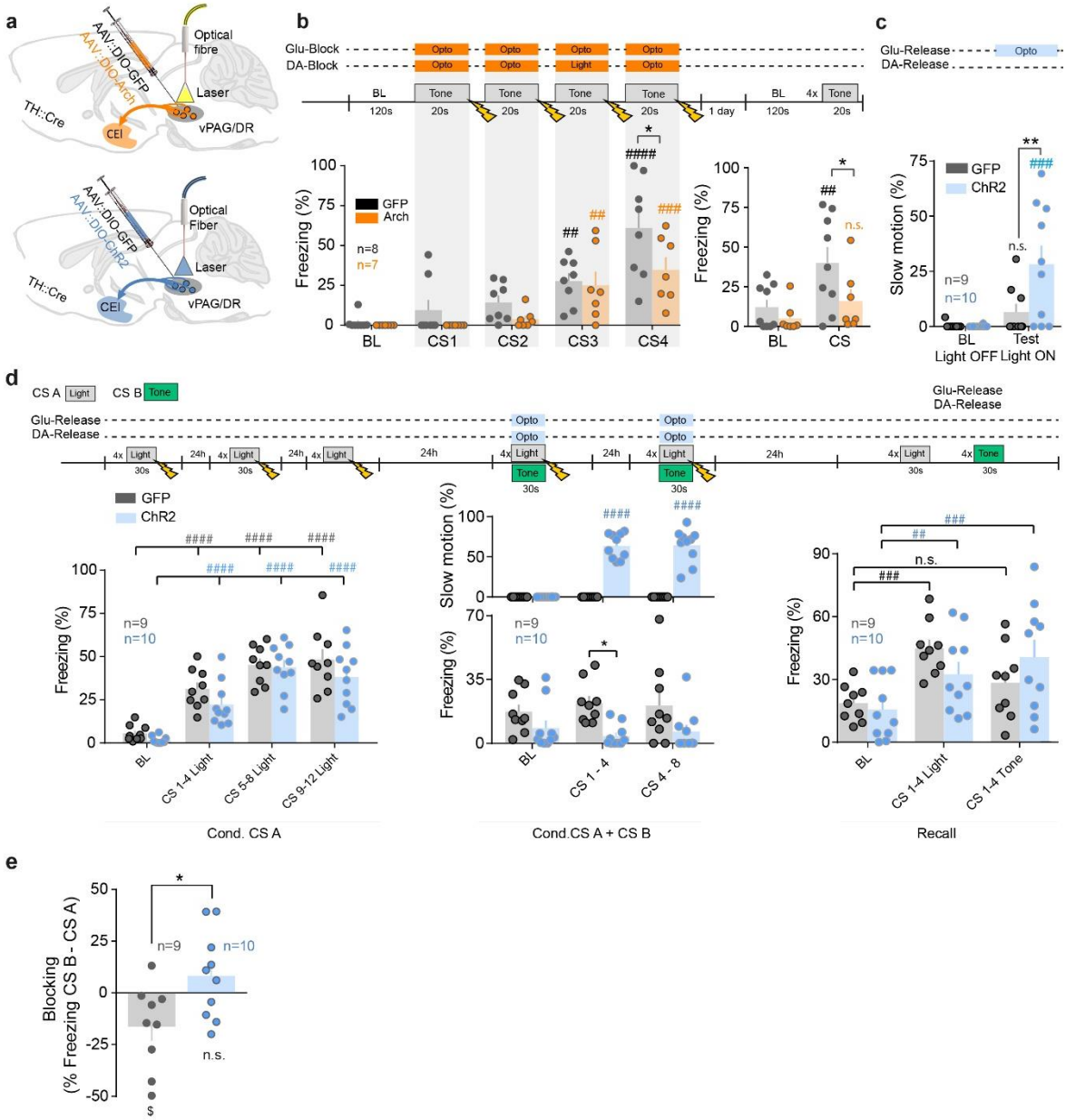

Figure 5 | vPdRD neuron reinforcement signals direct associative learning. Optogenetic targeting of vPdRD neurons in TH::Cre animals injected with AAV for Cre-dependent expression of (a) eArch3.0 or ChR2 (b) Freezing responses to neuronal inhibition by eArch3.0 during CS-US presentations (control group: n = 8 animals, Arch group: n = 7 animals; RM two-way ANOVA$_{conditioning}$ $F_{interaction}$ (4, 52) = 1.612, P = 0.1853; F_{time} (4, 52) = 24.97, P < 0.0001; F_{groups} (1, 13) = 4.189, P = 0.0615; two-way ANOVA$_{recall}$ $F_{interaction}$ (1, 14) = 2.846, P = 0.1137; F_{time} (1, 14) = 14.57, P = 0.0019; F_{groups} (1, 14) = 3.18, P = 0.0962; Holm-Sidak post-hoc tests). (c) Quantification of a slow motion behavioral state (cf. Fig. 5d) upon vPdRD neuron activation (control group: n = 9 animals, Chr2 group: n = 10 animals; RM two-way ANOVA $F_{interaction}$ (1, 17) = 5.309, P = 0.0341; F_{time} (1, 17) = 13.01, P=0.0022; F_{groups} (1, 17) = 4.969, P = 0.0396; Holm-Sidak post-hoc tests). (d) Design of associative blocking experiment (control group: n = 9 animals, Chr2 group: n = 10 animals). Acquisition of fear to CS A during first training session (RM two-way ANOVA $F_{interaction}$ (3, 51) = 0.6537, P = 0.5843, F_{time} (3, 51) = 57.27, P < 0.0001; F_{groups} (1, 17) = 2.927, P = 0.1053; Holm-Sidak post-hoc tests). Fear response and slow motion postures during compound conditioning phase (fear response: RM two-way ANOVA $F_{interaction}$ (2, 34) = 1.198, P = 0.3142; F_{time} (2, 34) = 0.03155, P = 0.9690; F_{groups} (1, 17) = 7.392, P = 0.0146; Holm-Sidak post-hoc tests; slow motion: RM two-way ANOVA $F_{interaction}$ (2, 34) = 54.57, P < 0.0001; F_{time} (2, 34) = 54.57, P < 0.0001; F_{groups} (1, 17) = 193.7, P < 0.0001; Holm-Sidak post-hoc tests) with presentation of CS A and CS B. Fear response during testing phase to alternating presentation of CS A and CS B (RM two-way ANOVA $F_{interaction}$ (2,

34) = 4.624, P = 0.0167; F_{time} (2, 34) = 15.68, P < 0.0001; F_{groups} (1, 17) = 0.02811, P = 0.8688; Holm-Sidak post-hoc tests). (e) Quantification of blocking effect from recall in c (unpaired t-test, two-sided t(17)= 2.58, $P_{Control\ vs\ ChR2}$ =0.0195; one-sample t-tests against zero t (8) = 2.407 $P_{Control}$ = 0.0427 ($) , t(9) = 1.235 P_{ChR2} = 0.2482)**.** Bars are means ± s.e.m. Significance levels between groups (*) and to baseline (BL) or between trials or sessions (#) at */# P<0.05, **/## P<0.01, ***/### P<0.001 and ****/#### P<0.0001.

References

1 LeDoux, J. The amygdala. *Current biology : CB* **17**, R868-874, doi:10.1016/j.cub.2007.08.005 (2007).

2 Gallistel, C. R. & Matzel, L. D. The neuroscience of learning: beyond the Hebbian synapse. *Annual review of psychology* **64**, 169-200, doi:10.1146/annurev-psych-113011-143807 (2013).

3 Ciocchi, S. *et al.* Encoding of conditioned fear in central amygdala inhibitory circuits. *Nature* **468**, 277-282, doi:10.1038/nature09559 (2010).

4 Haubensak, W. *et al.* Genetic dissection of an amygdala microcircuit that gates conditioned fear. *Nature* **468**, 270-276, doi:nature09553/10.1038/nature09553 (2010).[pii]

5 Li, H. *et al.* Experience-dependent modification of a central amygdala fear circuit. *Nature neuroscience* **16**, 332-339, doi:10.1038/nn.3322 (2013).

6 Cui, Y. *et al.* A Central Amygdala-Substantia Innominata Neural Circuitry Encodes Aversive Reinforcement Signals. *Cell reports* **21**, 1770-1782, doi:10.1016/j.celrep.2017.10.062 (2017).

7 Cassenaer, S. & Laurent, G. Conditional modulation of spike-timing-dependent plasticity for olfactory learning. *Nature* **482**, 47-52, doi:10.1038/nature10776 (2012).

8 Schultz, W. Behavioral dopamine signals. *Trends in neurosciences* **30**, 203-210, doi:10.1016/j.tins.2007.03.007 (2007).

9 Fiorillo, C. D. Two dimensions of value: dopamine neurons represent reward but not aversiveness. *Science* **341**, 546-549, doi:10.1126/science.1238699 (2013).

10 Cohen, J., Haesler, S., Vong, L., Lowell, B. & Uchida, N. Neuron-type-specific signals for reward and punishment in the ventral tegmental area. *Nature* **482**, 85-88, doi:10.1038/nature10754 (2012).

11 Hart, A. S., Rutledge, R. B., Glimcher, P. W. & Phillips, P. E. Phasic dopamine release in the rat nucleus accumbens symmetrically encodes a reward prediction error term. *The Journal of neuroscience : the official journal of the Society for Neuroscience* **34**, 698-704, doi:10.1523/JNEUROSCI.2489-13.2014 (2014).

12 Bromberg-Martin, E., Matsumoto, M. & Hikosaka, O. Dopamine in motivational control: rewarding, aversive, and alerting. *Neuron* **68**, 815-834, doi:10.1016/j.neuron.2010.11.022 (2010).

13 Silberman, Y. & Winder, D. G. Corticotropin releasing factor and catecholamines enhance glutamatergic neurotransmission in the lateral subdivision of the central amygdala. *Neuropharmacology* **70**, 316-323, doi:10.1016/j.neuropharm.2013.02.014 (2013).

14 Naylor, J. *et al.* Dopamine attenuates evoked inhibitory synaptic currents in central amygdala neurons. *The European journal of neuroscience* **32**, 1836-1842, doi:10.1111/j.1460-9568.2010.07457.x (2010).

15 Brischoux, F., Chakraborty, S., Brierley, D. I. & Ungless, M. A. Phasic excitation of dopamine neurons in ventral VTA by noxious stimuli. *Proceedings of the National Academy of Sciences of the United States of America* **106**, 4894-4899, doi:10.1073/pnas.0811507106 (2009).

16 Ungless, M. A., Magill, P. J. & Bolam, J. P. Uniform inhibition of dopamine neurons in the ventral tegmental area by aversive stimuli. *Science* **303**, 2040-2042, doi:10.1126/science.1093360 (2004).

17 Tan, K. *et al.* GABA neurons of the VTA drive conditioned place aversion. *Neuron* **73**, 1173-1183, doi:10.1016/j.neuron.2012.02.015 (2012).

18 Mileykovskiy, B. & Morales, M. Duration of inhibition of ventral tegmental area dopamine neurons encodes a level of conditioned fear. *The Journal of neuroscience : the official journal of the Society for Neuroscience* **31**, 7471-7476, doi:10.1523/JNEUROSCI.5731-10.2011 (2011).

19 Schultz, W. Neuronal Reward and Decision Signals: From Theories to Data. *Physiological reviews* **95**, 853-951, doi:10.1152/physrev.00023.2014 (2015).

20 Dougalis, A. *et al.* Functional properties of dopamine neurons and co-expression of vasoactive intestinal polypeptide in the dorsal raphe nucleus and ventro-lateral periaqueductal grey. *The European journal of neuroscience* **36**, 3322-3332, doi:10.1111/j.1460-9568.2012.08255.x (2012).

21 Matthews, G. A. *et al.* Dorsal Raphe Dopamine Neurons Represent the Experience of Social Isolation. *Cell* **164**, 617-631, doi:10.1016/j.cell.2015.12.040 (2016).

22 Lu, J., Jhou, T. C. & Saper, C. B. Identification of wake-active dopaminergic neurons in the ventral periaqueductal gray matter. *The Journal of neuroscience : the official journal of the Society for Neuroscience* **26**, 193-202, doi:10.1523/JNEUROSCI.2244-05.2006 (2006).

23 McDevitt, R. A. *et al.* Serotonergic versus nonserotonergic dorsal raphe projection neurons: differential participation in reward circuitry. *Cell reports* **8**, 1857-1869, doi:10.1016/j.celrep.2014.08.037 (2014).

24 Fibiger, H. C., LePiane, F. G., Jakubovic, A. & Phillips, A. G. The role of dopamine in intracranial self-stimulation of the ventral tegmental area. *The Journal of neuroscience : the official journal of the Society for Neuroscience* **7**, 3888-3896 (1987).

25 McNally, G. & Cole, S. Opioid receptors in the midbrain periaqueductal gray regulate prediction errors during pavlovian fear conditioning. *Behavioral neuroscience* **120**, 313-323, doi:10.1037/0735-7044.120.2.313 (2006).

26 Johansen, J. P., Tarpley, J. W., LeDoux, J. E. & Blair, H. T. Neural substrates for expectation-modulated fear learning in the amygdala and periaqueductal gray. *Nature neuroscience* **13**, 979-986, doi:10.1038/nn.2594 (2010).
27 de la Mora, M. P., Gallegos-Cari, A., Arizmendi-Garcia, Y., Marcellino, D. & Fuxe, K. Role of dopamine receptor mechanisms in the amygdaloid modulation of fear and anxiety: Structural and functional analysis. *Prog Neurobiol* **90**, 198-216, doi:10.1016/j.pneurobio.2009.10.010 (2010).
28 Swanson, L. W. The projections of the ventral tegmental area and adjacent regions: a combined fluorescent retrograde tracer and immunofluorescence study in the rat. *Brain research bulletin* **9**, 321-353 (1982).
29 Lee, H., Wheeler, D. & Holland, P. Interactions between amygdala central nucleus and the ventral tegmental area in the acquisition of conditioned cue-directed behavior in rats. *The European journal of neuroscience* **33**, 1876-1884, doi:10.1111/j.1460-9568.2011.07680.x (2011).
30 Edelmann, E. & Lessmann, V. Dopamine regulates intrinsic excitability thereby gating successful induction of spike timing-dependent plasticity in CA1 of the hippocampus. *Frontiers in neuroscience* **7**, 25, doi:10.3389/fnins.2013.00025 (2013).
31 Yu, K., Garcia da Silva, P., Albeanu, D. F. & Li, B. Central Amygdala Somatostatin Neurons Gate Passive and Active Defensive Behaviors. *The Journal of neuroscience : the official journal of the Society for Neuroscience* **36**, 6488-6496, doi:10.1523/JNEUROSCI.4419-15.2016 (2016).
32 Nagatsu, I., Karasawa, N., Kondo, Y. & Inagaki, S. Immunocytochemical localization of tyrosine hydroxylase, dopamine-beta-hydroxylase and phenylethanolamine-N-methyltransferase in the adrenal glands of the frog and rat by a peroxidase-antiperoxidase method. *Histochemistry* **64**, 131-144 (1979).
33 Roy, M. *et al.* Representation of aversive prediction errors in the human periaqueductal gray. *Nature neuroscience* **17**, 1607-1612, doi:10.1038/nn.3832 (2014).
34 Correia, P. A. *et al.* Transient inhibition and long-term facilitation of locomotion by phasic optogenetic activation of serotonin neurons. *eLife* **6**, doi:10.7554/eLife.20975 (2017).
35 Kamin, L. J. in *Punishment and aversive behavior* (ed Campbell & R.M. Church) 279-296 (Appleton-Century-Crofts, 1969).
36 Di Scala, G., Mana, M. J., Jacobs, W. J. & Phillips, A. G. Evidence of Pavlovian conditioned fear following electrical stimulation of the periaqueductal grey in the rat. *Physiology & behavior* **40**, 55-63 (1987).
37 McNally, G. P., Johansen, J. P. & Blair, H. T. Placing prediction into the fear circuit. *Trends in neurosciences* **34**, 283-292, doi:10.1016/j.tins.2011.03.005 (2011).
38 Ozawa, T. *et al.* A feedback neural circuit for calibrating aversive memory strength. *Nature neuroscience*, doi:10.1038/nn.4439 (2016).
39 Rescorla, R. A. & Wagner, A. R. *A theory of Pavlovian conditioning: variations in the effectiveness of reinforcement and nonreinforcement* 64-99 (Appleton-Century-Crofts, 1972).
40 Pearce, J. M. & Hall, G. A model for Pavlovian learning: variations in the effectiveness of conditioned but not of unconditioned stimuli. *Psychological review* **87**, 532-552 (1980).
41 Venniro, M. *et al.* The Anterior Insular Cortex-->Central Amygdala Glutamatergic Pathway Is Critical to Relapse after Contingency Management. *Neuron* **96**, 414-427 e418, doi:10.1016/j.neuron.2017.09.024 (2017).
42 Fadok, J. P., Dickerson, T. M. & Palmiter, R. D. Dopamine is necessary for cue-dependent fear conditioning. *The Journal of neuroscience : the official journal of the Society for Neuroscience* **29**, 11089-11097, doi:10.1523/JNEUROSCI.1616-09.2009 (2009).
43 De Bundel, D. *et al.* Dopamine D2 receptors gate generalization of conditioned threat responses through mTORC1 signaling in the extended amygdala. *Molecular psychiatry* **21**, 1545-1553, doi:10.1038/mp.2015.210 (2016).
44 Kim, J., Zhang, X., Muralidhar, S., LeBlanc, S. A. & Tonegawa, S. Basolateral to Central Amygdala Neural Circuits for Appetitive Behaviors. *Neuron* **93**, 1464-1479 e1465, doi:10.1016/j.neuron.2017.02.034 (2017).
45 Tsai, H.-C. *et al.* Phasic firing in dopaminergic neurons is sufficient for behavioral conditioning. *Science (New York, N.Y.)* **324**, 1080-1084, doi:10.1126/science.1168878 (2009).
46 Han, S., Soleiman, M. T., Soden, M. E., Zweifel, L. S. & Palmiter, R. D. Elucidating an Affective Pain Circuit that Creates a Threat Memory. *Cell* **162**, 363-374, doi:10.1016/j.cell.2015.05.057 (2015).
47 Tritsch, N. X., Granger, A. J. & Sabatini, B. L. Mechanisms and functions of GABA co-release. *Nature reviews. Neuroscience* **17**, 139-145, doi:10.1038/nrn.2015.21 (2016).
48 Gozzi, A. *et al.* A neural switch for active and passive fear. *Neuron* **67**, 656-666, doi:10.1016/j.neuron.2010.07.008 (2010).
49 Yu, K. *et al.* The central amygdala controls learning in the lateral amygdala. *Nature neuroscience* **20**, 1680-1685, doi:10.1038/s41593-017-0009-9 (2017).

50 Asmundson, G. J., Bonin, M. F., Frombach, I. K. & Norton, G. R. Evidence of a disposition toward fearfulness and vulnerability to posttraumatic stress in dysfunctional pain patients. *Behaviour research and therapy* **38**, 801-812 (2000).

Materials and Methods

Subjects. 2-4 months old male mice were group housed (2-5 animals) in a colony on 14 h light/10 h dark cycle starting at 07:00 with food and water *ad libitum*. All animal procedures were performed in accordance with institutional guidelines and were approved by the respective Austrian (BGBl nr. 501/1988, idF BGBl I no. 162/2005) and European authorities (Directive 86/609/EEC of 24 November 1986, European Community) and covered by the license M58/002220/2011/9. C57BL/6J wild-type mice were in-house bred and provided after weaning from the Research Institute of Molecular Pathology (IMP) mouse facility. Prkcd::GluClα-Cre BAC transgenic mice (PKCδ::Cre)[4], 7630403G23Rik$^{Tg(Th\text{-}cre)1Tmd}$ transgenice mice (TH::Cre, stock no008601, Jackson Laboratory), SOM-IRES-Cre transgenic mice (SST::Cre; stock no: 013044, Jackson Laboratory) and B6;129S6-*Gt(ROSA)26Sor*$^{tm9(CAG\text{-}tdTomato)Hze}$/J transgenic mice (Rosa::loxP-STOP-loxP-td-Tomato, stock no007909, Jackson Laboratory) were maintained heterozygous on a C57BL/6J background. Cohort sizes for neuroanatomical tracing approx. 30 2-4 months old male mice, slice electrophysiology approx. 50 1-3 months old male mice, microdialysis 4 adult male rats, GCaMP6m 2 2-3 months old male mice, GCaMP6f 4 2-3 months old male mice, SCH 23390 31 2-3 months old male mice, M4-DREAAD, 21 2-3 months old male mice, 6-OHDA lesion 8 2-3 months mice, Arch 15 2-3 months old male mice and ChR2 19 2-3 months male mice.

Stereotactic surgery for viral/toxin injections and cannula/light fiber implantation. Male mice 2-4 months old were deeply anaesthetized with isoflurane (5%, Abbot Laboratories) and placed in a stereotaxic frame (Kopf). Anesthesia was kept constant with 1.5 – 2% isoflurane supplied per anesthesia nosepiece and body temperature maintained at 36°C with a heating pad controlled by rectal thermometer (DC temperature controller). After injecting 0.1 ml of Lidocaine under the skin as analgesia, the skull was exposed and perforated with a stereotaxic drill at the desired coordinates relative to Bregma (Franklin & Paxinos 2007). For postoperative care, mice were supplied with drinking water containing 250mg/l Carprofen (Rimadyl, Pfizer) and 400 mg/l Enrofloxacin (Baytril, KVP pharma) for 14 days.

For optogenetic fibre implantation, one optic cannula (Doric lenses, 200-400 µm, 0.53NA) per mouse was implanted 0.5mm over the ventral PAG (AP = -4.5, ML = 0, DV = -2.7) for optogenetic manipulations. Placing a single fiber at midline ensured bilateral illumination of vPdRD neurons, which accumulate close to the midline under the 3rd ventricle.vPAG/DR (Supplementary Fig. 7c-d). Two guide cannulas (Bilaney, C316GS-4/SPC) were implanted bilaterally 0.5 mm over the CEl (AP = -4.5, ML = 0, DV = -2.7) for drug infusions. Both were fixed on the skull with dental cement (SuperBond C&B kit, Prestige Dental Products).

Micro4 Micro Syringe Pump controller (World Precision Instruments) was used to regulate injection volumes with a rate of 10 nl/min. The glass needle was left in place for 5 minutes after the injection volume was delivered. A detailed list of viral constructs is provided in Supplementary Fig. 15a.

Histological analysis. To verify virus expression (see Supplementary Fig.15a) and correct locations of optical fiber tips and cannulae**,** animals were sacrificed by a mixture of 10mg/ml Ketamine (OGRIS Pharma) and 1 mg/ml Medetomidine hydrochloride (Domitor, ORION Pharma) in 1 x PBS and tissue sectioning was performed as described under section

'Immunohistochemistry'. Expression of viral constructs and location of optical fiber tips/ cannulae were assessed for correct targeting (Supplementary Fig. 4, 7).

Fear Conditioning. Mice were handled on two different days prior to all behavioral training experiments. Fear Conditioning was separated into habituation, conditioning and testing phase and conducted on three different consequent days in a large sound-proof isolation cubicle that contained an adaptive mouse test cage (Coulbourn instruments). The context of the mouse test cage was modified to make the box distinct for different phases of the experiment. *Conditioning:* (Context A) the mouse test cage was adapted by a grey/white striped box formed on basis of a symmetric trapeze (15 x 12 x 7 cm), the floor texture consisted of the characteristic shock grid baseplate, box walls were swiped with lemon flavor. *Testing:* (Context B) test cage was adapted by a square white box, the floor consisted of a white flat baseplate, box walls were swiped with ethanol flavor. On day 1, mice individually underwent habituation phase in context B with each session taking 300 s. On day 2, mice were conditioned individually in context A with 4 pure tones (3 kHz, 70 dB, 20 s each) delivered at intervals with variable duration (80-120 s), each sound co-terminating with a 1 s, 0.5 mA foot shock, delivered by a precision regulated animal shocker H13-15 (Coulbourn Instruments). Testing of fear memory was performed 24h after conditioning on day 3 in context B by recording behavioral responses to 4 pure tones (3kHz, 70 dB, 20s each) delivered at variable intervals (80-120s). Matlab scripts were programmed to deliver foot shocks and tones. The isolation cubicle was illuminated in every phase of the experiment and the behavior was captured with a CCD camera at 25 fps and stored on PC. Test cages and test floors were thoroughly cleaned with water and dedicated flavor-alcohol mixtures in between mouse runs on a given day. Behavioral responses of all phases were analyzed off line by Ethovision software or visually by an observer blind to the experimental condition. A list of behavioral experiments and the experimental history of different cohorts is provided in Supplementary Fig. 15b.

Blocking experiment. The blocking experiment was performed as described earlier [25] with some modifications. The preparations and equipment were identical to fear conditioning (described above), but based on a different protocol (Figure 4). All blocking experiment phases took place in the dark without constant illumination. After Habituation phase on day 1 (identical as described in Fear Conditioning above), mice underwent three consecutive days of conditioning in context A on day 2 to day 4, each day consisting of a session where 30 s periods of 1 s house light pulses (CS A) at 1 Hz were presented 4 times, each period co-terminating with a 1s, 0.5 mA foot shock. The interval between these periods randomly varied from 80 to 120 s. Conditioning phase was followed by a two-day compound conditioning phase on day 5 and 6, again in context A, where animals received 4 times a compound CS on each session/day, composed of CS A accompanied by 1 Hz pulsed white noise (CS B) in random 80-120 s intervals, each presentation co-terminating with one 0.5 mA foot shock. The next day (day 7), behavioral responses to 12 CS A and 12 CS B presentations were recorded in one session. The CS presentation in this testing phase was designed in a way that two CSA were followed by two CSB, with a constant time interval of 60s between each CS (CSA-60s-CSA-60s-CSB-60s-CSB-…)

Systemic injections in behavioral experiments. For neuronal modulation of animals expressing DREADDs, Clozapine N-oxide (Sigma, 2.5mg/kg) was diluted in physiological

1xPBS and injected intraperitoneally 30 min before the start of the experimental session. Animals that received this treatment in experiments were habituated by PBS injections during handling sessions.

Optogenetic manipulation in behavioral experiments. Animals that had undergone stereotactic injection of optogenetic AAV virus for later neuronal modulation during behavior underwent habituation for attaching a fiber-optic patch cord (doric lenses) on implanted opto fibers. For ChR2 activation, laser trains of blue light (473nm) were delivered consisting 20 ms pulses delivered at 20 Hz (if not noted otherwise) at an intensity of 8-10 mW at the fiber tip. For Arch activation, laser trains of constant yellow light (568nm) were delivered at an intensity of 5-7 mW. Intensity of all laser stimulations were measured before every experiment at the tip of the optic fiber via Power Meter (Thorlabs, PM100D). Laser stimulation was controlled by MatLab scripts during conditioning experiments and by Arduino boards running customized scripts executed by any-maze software (Stoelting) during pain tests and baseline anxiety tests.

Intracranial drug delivery during behavioral experiments. Intracerebral drug administration was delivered through previously (2-4 weeks) implanted guide cannulas. Animals were handled once a day 5 min for 3 days. On day of the experiment, internal cannulas that protruded 1 mm beyond the edge of the guide cannula were inserted and either D1 receptor antagonist SCH23390 (Tocris) in saline or saline vehicle were infused bilaterally. 80ng doses of SCH23390 in 0.2 µl saline or saline alone were injected (0.2µl/side) over a period of 5 min using a syringe controlled by an infusion pump (Harvard Apparatus Pump 11). Behavioral tests were started 30 min after infusion.

Automated von Frey test. Touch sensitivity was tested with a dynamic plantar aesthesiometer (Ugo Basile S.R.L., Italy). Mice were habituated to the testing chambers for approx. 2 hours prior to testing. Then each hindpaw was tested 3 times with an increased force ranging from 0 to 10g with a 20sec ramp up time and at least 20sec between each trial on the same mouse. The average of 3 trials was calculated for each hindpaw. Read-out parameters were the force and latency at which the mouse lifted the hindpaw.

Hot plate test. Thermal sensitivity was tested 1 week after von Frey testing using a hot plate analgesia meter (IITC Life Science Inc., CA, USA). Mice were put on the hot plate at 45 °C and the temperature was increased from 45 to 55 °C within 2 minutes. The experiment was stopped as soon as the mice performed the first jump. Mice were videotaped and the latency and temperature of the first reaction (hindpaw shaking or licking) or jump recorded.

Elevated plus maze. Mice were placed in the center zone (6.5 x 6.5cm), facing an open arm of a custom-built elevated plus maze (elevated 54cm above the floor) with 2 open arms (OA, 30cm length, 7cm width) and 2 wall-enclosed arms (closed arms, CA, 30cm length, 6cm width, walls 14.5cm high) and let explore freely for 5 minutes. Their path was videotracked using Topscan software (Cleversys, Inc., VA, USA) and the amount of time spent and distance travelled in the open arms, closed arms and center zone were evaluated.

Light/Dark box. Mice were placed in the light zone and let explore the Light/Dark arena (open field arena from TSE-Systems modified with custom-built dark zone boxes) freely for 20 minutes. Their path was videotracked in the light zone using Videomot 2 software (V7.X, TSE-Systems GmbH, Germany) and the amount of time spent in the light versus dark zones and distance travelled in the light zone were evaluated, as well as the latency until they

escaped to the dark zone. Lux levels were 150 lux in the light zone and about 0 lux in the dark zone. Each zone (light zone and dark zone) was 24.5cm x 50cm in size.

Microdialysis. Experiments were performed by Brains-OnLine (Charles River Laboratories) following established amygdala microdialysis routines for awake behaving animals. Adult male rats were anesthetized using isoflurane (2%, 800 mL/min O2). Bupivacaine/epinephrine was used for local analgesia and carprofen was used for peri-/post-operative analgesia. The animals were placed in a stereotaxic frame (Kopf instruments, USA). Rats were implanted with a push-pull microdialysis probe (2 mm exposed surface, PEE membrane, BrainLink, the Netherlands) in the amygdala (AP = -3.3, ML = -4.5, DV = -9). Note that the stereotaxic position between BLA and posterior CE (Supplementary Fig. 5a) and the use of lateral exposed dialysis surfaces allows for sampling BLA and CE DA while preventing excessive CE tissue damage. After surgery, animals were housed individually in cages and provided food and water ad libitum. Microdialysis sampling was initiated approximately 24 hours after surgery. On the days of the sampling (Days 1and 2), the probes were connected with PAN tubing to a microperfusion pump (Harvard PHD 2000 Syringe pump, Holliston, MA or similar). Microdialysis probes were perfused with aCSF containing 147 mM NaCl, 3.0 mM KCl, 1.2 mM CaCl2 and 1.2 mM MgCl2, at a flow rate of 1.5 µL/min. Microdialysis samples were collected for 15-minute periods by an automated fraction collector (820 Microsampler, Univentor, Malta) into polystyrene (300 µl) mini-vials. All the dialysis samples were stored at -80°C for later analysis. After habituation, 15 minutes samples of baseline dialysate were collected for 90 minutes in the animals' home cage. Rats were then placed inside the test cages with grid floor shockers (Coulbourn Instruments, Lehigh Valley, PA) and dialysate samples were collected 1 hour before 2 shocks were administered (2x 1 sec shocks at 0.6 mA). Animals remained in the test cage for 30 minutes before being moved back to their home cages for the remainder of the experiment. The next day, animals underwent the same procedure as on day 1 except that the foot shock was omitted. After microdialysis, brains were fixed in 4 % PFA. Histological samples were visually inspected for correct probe placement.

Deep brain Ca^{2+} Imaging. Deep brain calcium imaging was conducted using the nVista HD 2.0 system (In Vivo Rodent Brain Imaging System, Inscopix, Inc). A microendoscope was implanted directly above the ventral PAG and a baseplate (BPL-2) was attached to the skull with dental cement 1 week later. Mice were habituated to camera mounting the day before the experiment. On experimental day, the microscope was attached to the baseplate before the start of the behavioral experiment. Ca^{2+} signals during behavioral testing were imaged with nVistaHD v2.0.32 at 20fps. We compensated for movement during video acquisition using custom ImageJ scripts and Mosaic v1.2 (Inscopix, Inc) software. The video was further analyzed in Mosaic analysis suite v1.2, first by applying a $\Delta F/F0$ normalization, where F0 was based on the entire length of the movie. Bulk signals were derived from the entire field of view and low-pass filtered at 0.5 Hz. Traces of individual units were extracted by principal/independent component analysis (PCA/ICA) and low-pass filtered at 0.5 Hz and manually sorted. Ca^{2+} events were detected automatically whenever the rise in the Ca^{2+} traces exceeded and amplitude of 3 SD and a τ of 0.5 s.

All further analysis was performed in Neuroexplorer software (Plexon Inc.) and Python scripts. Cells were classified as responders when their event counts during a 4s time window at CS and/or US presentation exceeded the > 95 % confidence interval for the expected mean firing rate. Bulk signals and unit traces were binned at 0.5-2 s, represented as population means and analyzed using parametric statistics throughout.

Immunohistochemistry. Animals were deeply anaesthetized with a mixture of 10mg/ml Ketamine (OGRIS Pharma) and 1mg/ml Medetomidine hydrochloride (Domitor, ORION Pharma) in 1xPBS and transcardially perfused with 10ml of cold 1xPBS followed by 25ml of 4% (PFA) in 1xPBS. Brains were immediately removed, postfixed in 4% PFA at 4°C overnight and transferred to 1xPBS at 4°C. 70-100µm vibratome sections were cut and transferred in PBS-T (1xPBS plus 0.1% Triton X-100). Non-specific binding was blocked with 1% BSA/ 2%NGS in PBS-T for 2 hours. Primary antibodies (goat anti SST (sc-7819; Santa Cruz; for amygdala SST^+ neurons[51]), mouse anti-PKC-δ (610398; BD Biosciences; for amygdala $PKC\delta^+$ neurons[4]), chicken anti-TH (AB9702; Millipore; for midbrain TH^+ neurons[52]) were diluted 1:500 – 1:1000 in blocking solution and incubated for 24h at 4°C. Standard secondary antibodies (Invitrogen) in blocking solution were incubated for 2h at room temperature, sections mounted with Fluoromount G (SouthernBiotech) and viewed under a Leica stereomicroscope and a Zeiss LSM 710 Spectral confocal microscope.

To identify recorded cells after acute brain slice electrophysiology, internal solution for patch-clamp recording contained 0.1% w/v biocytin (Sigma). Slices were transferred to 4% PFA in 1xPBS after recording and stained as described above including Fluorophore tagged Streptavidin (Sigma) to secondary antibody incubation.

Verification of M3-DREADD and M4-DREADD virus expression (both tagged with mCherry fluorophore) in behavior experiments that included the DREADD system was optimized with IHC against tdtomato as described above with anti-DsRed polyclonal antibody (Living Colors).

Combined CTB tracing/TH IHC experiments. CTB-Alexa Fluor 555 (Invitrogen) was delivered by stereotaxic injection. Animals were sacrificed 1 week after injection and brains processed for IHC as described above. Co-localization of CTB back-labelled neurons with either PKCδ (CEl) or TH (PAG) labelling was scored by an observer blind to the experimental condition.

6-OHDA vPAG lesions. 6-Hydroxydopamine Hydrobromide (Sigma) in saline containing 0.01% (w/v) ascorbic acid, was delivered by two stereotaxic 100nl injections into the rostral and caudal ventral PAG region at a concentration of 10µg/µl.

D1R Knockdown. To suppress D1R expression in the CEl we constructed an AAV-based vector expressing GFP and miRNA-adapted shRNAs in the optimized miR-E backbone[53] under control of the SFFV promoter (AAV-SFFV-GFP-miR; ASGE). Two independent shRNAs targeting D1R (guide sequences: 5'-TAGTA…[add 22mer guides]) were designed based on optimized design rules, cloned into miR-E and tested for knockdown potency at the protein level using an established two-color reporter assay[53]. In brief, NIH-3T3 cells were stably transfected with a construct expressing a td-Tomato transgene harboring target sites of D1R and several control shRNAs in its 3'UTR (name vector). Subsequently, cells were transduced with ASGE vectors harboring D1R and control shRNAs, and td-Tomato reporter knockdown in GFP-shRNA expressing cells was quantified using flow cytometry. Percentage

of knockdown was calculated as a ratio of the mean td Tomato signal in the GFP positive cell population to the mean td Tomato signal in the GFP negative cell population using the formula as follows:

$$\%\ knockdown = 100 - \frac{mean\ tdTomato\ GFP\ pos}{mean\ tdTomato\ GFP\ neg} * 100$$

Fiber density analysis. Transgenic SST::Cre and PKCδ::Cre mice received CEl targeted injections of AAV::ChR2-YFP. Brains were perfused, cut by vibratome and slices immunostained against TH to confirm correct targeting to the vPAG/DR region. The analysis was performed using Definiens Developer XD software on Maximum Intensity Projections of the 3D datasets. To segment the axons a 2D Bandpass Filter was applied and the resulting Image was thresholded. Objects low in contrast were removed and the total area of axons per image was measured.

Acute brain slice electrophysiology. Virally infected TH::Cre, SST::Cre and PKCδ::Cre single or double transgenic male mice (2 - 3 months old) were deeply anesthetized with Isoflurane, decapitated and their brains quickly chilled in sucrose-based dissection buffer, bubbled with 95% O_2/5% CO_2 containing the following (in mM): 220 Sucrose, 26 $NaHCO_3$, 2.4 KCl, 10 $MgSO_4$, 0.5 $CaCl_2$, 3 Sodium Pyruvate, 5 Sodium Ascorbate and 10 glucose[54]. Transverse coronal brain slices (300 μm) were cut in dissection buffer using a Vibratome (Leica, VT1000S) and immediately incubated for 15 min recovery phase in oxygenated artificial cerebrospinal fluid (aCSF) 126 NaCl, 2.5 KCl, 1.25 NaH2PO4, 26 NaHCO3, 2.5 CaCl2, 2.5 MgCl2, and 25 glucose in 95% O2/5% CO2 at 32°C. This was followed by a slice resting phase with oxygenated aCSF for at least 45 min at room temperature (RT).

Individual brain slices containing CEl were placed on the stage of an upright, infrared-differential interference contrast microscope (Olympus BX50WI) mounted on a X-Y table (Olympus) and visualized with a 40x water immersion objective by an infrared sensitive digital camera (Hamamatsu, ORCA-03). Slices were fully submerged and continuously perfused at a rate of 1-2 ml per min with oxygenated aCSF.

Optogenetic circuit mapping. $PKC\delta^+$ and SST^+ neurons in the CEl were identified by the presence of GFP fluorescence. Patch pipettes were pulled on a Flaming/Brown micropipette puller (Sutter, P-97) from borosilicate glass (1.5 mm outer and 0.86 mm inner diameter, Sutter) to final resistances ranging from 3 to 5MΩ. Internal solution for voltage-clamp recordings of responses to optogenetic stimulation contained (in mM): 135 Cesium Methanesulfonate, 5 KCl, 10 HEPES, 2 $MgCl_2$, 0.2 EGTA, 1 Na_2ATP, 0.4 NaGTP, 10 Na_2Phosphocreatine for excitatory responses in the CEl and 140 KCL, 10 HEPES, 2 $MgCl_2$, 0.2 EGTA, 1 Na_2ATP, 0.4 NaGTP, 10 Na_2Phosphocreatine for inhibitory responses in the PAG (280-290 mOsmol). Membrane currents were recorded with a Multiclamp 700B amplifier (Molecular Devices). Electrophysiological signals were low pass filtered at 3kHz, sampled at 10 kHz (Digidata 1440A, Axon Instruments) and stored on a PC for offline analysis with pClamp 10 software (Molecular Devices).

Cells were held at -70 mV. Cells were allowed to reestablish constant activity during 5 minutes waiting time after breaking the seal. Twenty ms blue light pulses were delivered through a 40x electrophysiology microscope objective, driven by a 120W mercury lamp (X-Cite 120 PC Q). The amplitude of 4 pulses, 5 seconds apart, was averaged as postsynaptic

response. Inhibitory responses were identified by adding 10 µM Bicuculline, excitatory responses by adding 10 µM CNQX + 50 µM D-APV (all Sigma) to the bath.

LTP experiments. Standard procedures were applied to prepare coronal slices from male C57Bl/6J mice (P28-P47). In brief, mice were deeply anaesthetized by inhalation of 4% isoflurane and killed by decapitation. A block of tissue containing the amygdala was rapidly removed and placed in a dissection buffer containing (mM): Sucrose 195; KCl, 2.4; NaH_2PO_4, 1.25; $NaHCO_3$, 24; $MgSO_4$, 10; $CaCl_2$, 0.5; glucose, 10; bubbled with 95% O_2/ 5% CO_2. Either, 400 µm coronal slices (field potential recordings) or 300 µm coronal slices (patch-clamp recordings) were prepared on a vibratome (Model 1000, The Vibratome Company, St. Louis, USA). Whole cell patch-clamp recordings of excitatory postsynaptic currents (EPSCs) were recorded in a submerged chamber with a patch-clamp amplifier (EPC-9, Heka, Lamprecht, Germany) at 30 ± 1°C. Standard artificial cerebrospinal fluid (aCSF) was composed of (in mM): NaCl, 119; KCl, 2.5; NaH_2PO_4, 1.25; $NaHCO_3$, 26; $MgSO_4$, 1; $CaCl_2$, 2; glucose, 20; bubbled with 95% O_2/5% CO_2. Picrotoxin (50 µM) was added to block $GABA_A$ receptors. Patch pipettes were pulled from borosilicate glass (GC150TF-10, Clark Electromedical Instruments, Pangbourne, UK) to resistances of 3 MΩ, and filled with (in mM): potassium gluconate, 135; KCl, 5; Hepes, 10; $MgCl_2$, 2; EGTA, 0.2; MgATP, 4; Na_3GTP, 0.4; K_3-phosphocreatine, 10; biocytin, 0.1; pH 7.2 (with KOH). A liquid junction potential of +10 mV of the pipette solution was corrected for. After obtaining the whole cell configuration, neurons were held at -70 mV. Electrodes were positioned as indicated for local field potentials. EPSCs were evoked every 15 s with stimulus intensities adjusted to generate EPSC amplitudes of approximately 150 pA. Peak current amplitudes of EPSCs were calculated by averaging four consecutive responses. LTP was induced by two trains of 100 Hz/1s separated by 20 s, paired with postsynaptic depolarization to –10 mV in voltage clamp mode. LTP was quantified by normalizing and averaging maximal EPSC amplitudes during the last 5 min of experiments (i.e. 30 min after LTP induction) relative to 10 min baseline. Recordings with changes in access resistance above 25% were discarded.

Local field potential recordings were conducted in an interface chamber at 32 °C ± 1 °C. aCSF was composed of (in mM): NaCl, 125; KCl, 2.5; NaH_2PO_4, 0.8; $NaHCO_3$, 25; $MgCl_2$, 1; $CaCl_2$, 2; glucose, 10; bubbled with 95% O_2/ 5% CO_2. Gabazine (0.1 µM) was added to reduce GABAergic inhibition. Recording pipettes were pulled from borosilicate glass (GC150TF-10, Clark Electromedical Instruments, Pangbourne, UK), filled with aCSF and sited at the lateral central amygdala. A concentric bipolar electrode (FHC Inc, Bowdoin, ME, USA) was positioned on the surface of the slice above the basal amygdala at the border to the capsular central amygdala. Field potentials were evoked by stimuli of 100 µs duration delivered by a stimulus isolator (Isoflex, AMPI, Jerusalem, Israel) at 0.016 Hz. Stimulus intensity was adjusted to evoke halfmaximal responses. Signals were amplified by a DAM-80 amplifier (WPI, Berlin, Germany) and digitized with a CED 1401plus interface (Cambridge Electronic Design, Cambridge, U.K). Signal amplitude was measured as the sum of the difference between onset and peak of the negative voltage deflection, and the difference of the peak of the negative voltage deflection and the succeeding positive peak, divided by two. To induce LTP, a high-frequency stimulation pattern (HFS) consisting of three trains of 100 stimuli at 100 Hz separated by 30 s was executed at time point zero. LTP was quantified by normalizing and averaging field potentials during the last 5 min of experiments (i.e. 55 - 60

min after LTP induction) relative to 30 min baseline. To verify significant differences induced by pharmacological manipulations, averaged field potential amplitudes during the last 5 min of recordings were compared.

Experience dependent synaptic plasticity. To evaluate experience dependent synaptic plasticity in the CEl, the male 6 OHDA lesioned and D1R Knock down cohort were sacrificed immediately after the fear testing step of our fear conditioning protocol and coronal slices prepared as described above. To obtain comparisons of the synaptic strength of BLA inputs onto SST^+ and PKC-δ^+ neurons, we performed subsequent whole-cell patch-clamp recordings of pairs of different neuronal subtypes next to each other (<60µm) to avoid an error due to different distances to the stimulation electrode. The Index of each pair as shown in the data represents the difference of the response amplitude to BLA electric stimulation in voltage clamp of a given pair of one SST^+ and one PKC-δ^+ neuron, divided by the sum of the same values.

Neuronal population sequencing. Amygdala punches (1 mm diameter, 300 µm thickness) of 6 week old males from PKCδ::Cre or SST::Cre animals crossed to Cre-dependent Rosa::td-Tomato lines were enzymatically dissociated and FACS sorted for approximately 10^3 td-$Tomato^+$ cells. SMARTer® smRNA-Seq Kit for Illumina® (Clontech, 78100 Saint-Germain-en-Laye, France) prepared libraries were submitted to deep sequencing on a HiSeq 2500 system (Illumina, San Diego, USA). The reads were mapped to the Mus musculus mm10 reference genome either with STAR (version 2.4.0d)[55] or TopHat (version 2.0.9)[56]. Reads aligning to rRNA sequences were filtered out prior to mapping. The read counts for each gene were detected using HTSeq (version 0.5.4p3)[57]. The counts were normalized using the TMM normalization from edgeR package in R. Prior to statistical testing the data was voom transformed and then the differential expression between the sample groups was calculated with limma package in R. The functional analyses were done using the topGO and gage packages in R. Complete data will be published elsewhere.

Sample sizes. No statistical methods were used to predetermine sample sizes. Sample size were similar as reported in previous publications[4,30,58,59].

Randomization. All animals and samples were randomly assigned to the experimental groups. Experimental conditions (Training and testing contexts, stimulus types) were fixed. Stimulus timing (CS, US) was applied in pseudorandom time intervals.

Blinding. Data collection and analysis were not performed blind to the conditions of the experiments. Data was acquired, processed and analyzed by automated workflows, except Fig. 1e, f, Supplementary Fig. 3a, Supplementary Fig. 4a,b, Supplementary Fig. 5a,b, Supplementary Fig. 7a,b,c,d, Supplementary Fig. 10e, Supplementary Fig. 11b.

Statistics. All statistics were performed in Graph Pad Prism ® (Version 6), unless otherwise indicated, and all statistical tests used are indicated in the figures legends. Experimental designs with one categorical independent variable (Fig. 1e,l, Fig. 3f, Fig. 5e, Supplementary Fig. 10c, Supplementary Fig. 11d) were assessed by Shapiro-Wilk normality tests. When normality test passed, parametric statistics (t-test, one-way ANOVA) were applied. In case of non-normal distributions, non-parametric statics (Mann-Whitney U-test and Wilcoxon Signed Rank test) were planned. Experimental designs with two categorical independent variables (Fig. 2c-g, Fig. 3b,d,h, Fig. 4e,g,j, Fig. 5b,c,d, Supplementary Fig. 3b, Supplementary Fig. 8a-h, Supplementary Fig. 13a,b, Supplementary Fig. 10f) were assumed to be normal and

analyzed by two-way ANOVA without formally testing normality. All significance levels are given as two-sided and were corrected for multiple comparisons, wherever applicable. Omnibus significance values were rounded up for values P <0.0001. Post-hoc significance values were rounded up and given as * for values P < 0.05, ** for values P < 0.01, *** for values P < 0.001 and **** for values P < 0.0001; where no significance was made explicit, the test did not reach a significance level of P < 0.05.

Data exclusion. For slice electrophysiology approximately 10 out 50 animals did not reach sufficient virus expression and/or missed injection targets and were excluded. Out of the SCH 23390 cohort, 9 out of 31 animals were excluded from the analysis due to misplaced or blocked infusion cannulae.

Data availability. The data that support the findings of this study (Fig. 1-5, Supplementary Figs. 3-5 and Supplementary Figs. 7-13) are available from the corresponding author upon reasonable request. Data Supporting Supplementary Figs. 1 & 2 are from Allen Mouse Brain Connectivity Atlas (http://connectivity.brain-map.org/). For data Supporting Supplementary Fig. 6 are Accession Codes section.

Code availability. The code for analysis is available from the corresponding author upon reasonable request.

For additional information please refer to the corresponding Life Sciences Reporting Summary.

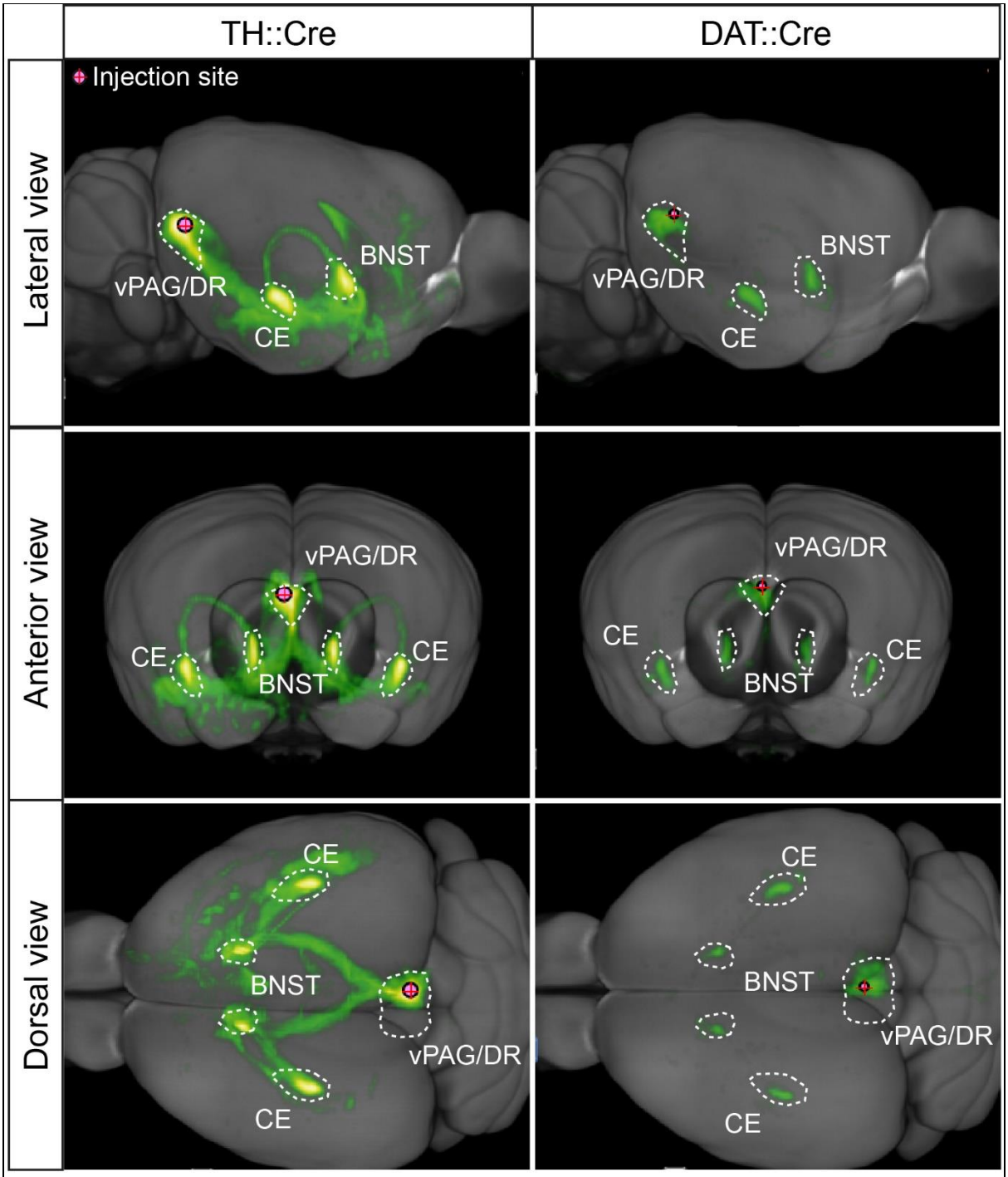

Source	Source function	Projection target	Projection target function
vPAG/DR	Pain modulation[60] Defensive behaviors[58]	CE	Associative fear learning[3,4,61,62]
		BNST	Sustained stress integration[61,62]

Supplementary Figure 1

Projections of vPdRD neurons

(*Top*) AAV::DIO-EGFP injections in the vPAG/DR of TH::Cre and DAT::Cre mice. Data from Allen Mouse Brain Connectivity Atlas; TH::Cre: Experiment number: 272699357; DAT::Cre: Experiment number: 272699357. Note that vPdRD neurons have only two major targets in the brain: Bed nucleus of the stria terminalis (BNST) and CE. (*Bottom*) Functional roles of vPdRD neuron projection targets. Note that of the

major projection targets, the CE is the target primarily associated with associative fear learning; thus, the most likely explanation for the observed effects of vPdRD neurons on Pavlovian conditioning is that they are mediated through their projections to the CE.

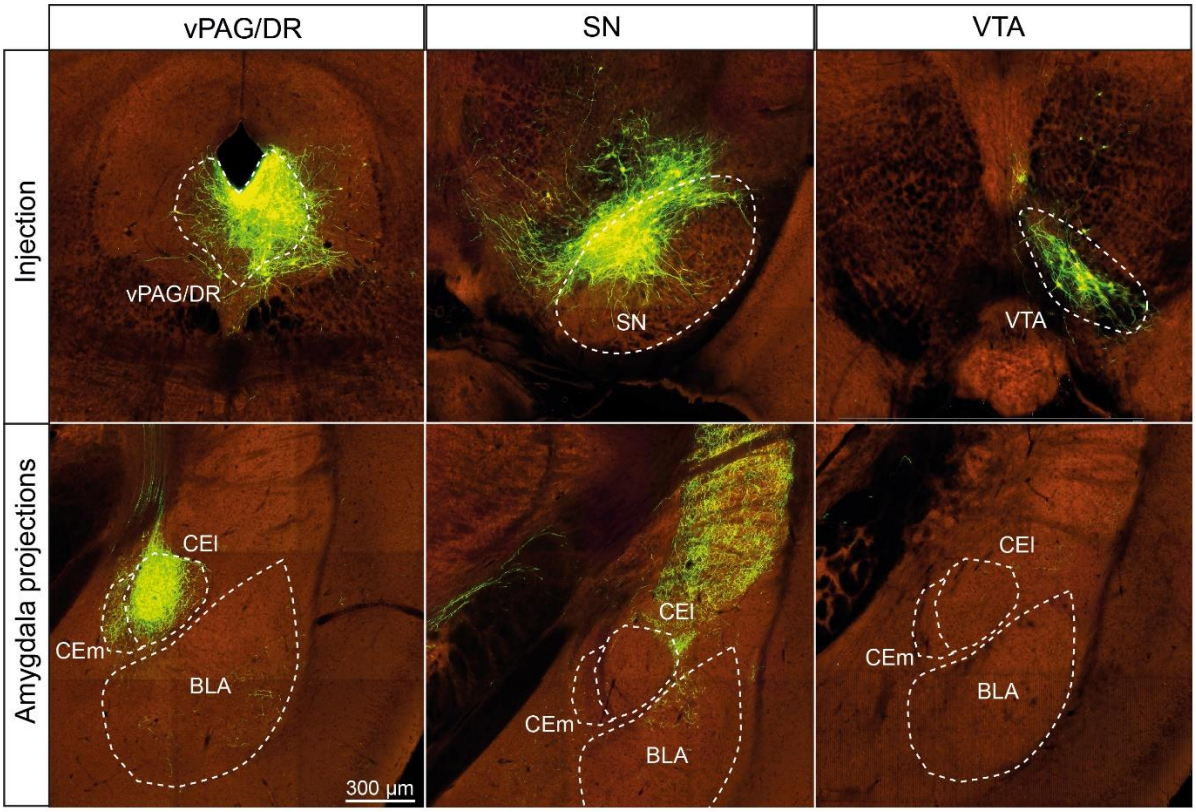

Supplementary Figure 2

Amygdala projections of midbrain DA regions

(*Top*) AAV::DIO-EGFP injections in the vPAG/DR of TH::Cre mice. Data from Allen Mouse Brain Connectivity Atlas; vPAG/DR: Experiment number: 272699357; SN: Experiment number: 304761539; SN: Experiment number: 304337288. Note that vPdRD neurons provide dense innervation to the CE (*left*), whereas amygdala projections from either SN (*middle*) or VTA (*right*) DA neurons appear rather sparse; thus, DA in CE seems to predominantly originate from vPdRD neurons.

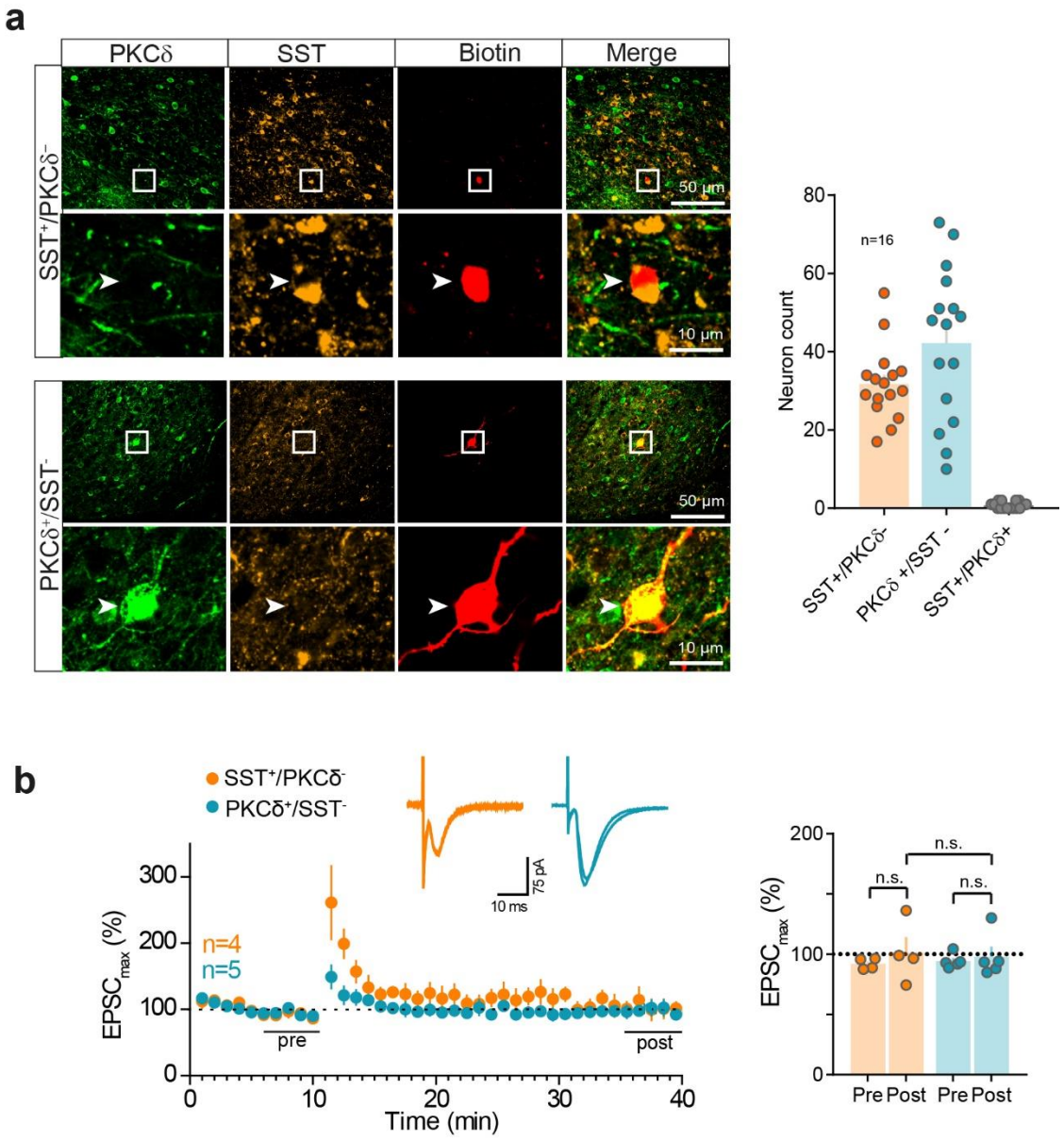

Supplementary Figure 3

DA is required for successful LTP at BLA-CEl synapses

(**a**) *Left* Representative images of histological identification of biocytin labelled cells after LTP recordings of CEl neurons in aCSF with electric HFS stimulation in the BLA. *Right* Quantification of immunohistochemically identified $SST^+/PKC\delta^-$, $PKC\delta^+/SST^-$ and $PKC\delta^+/SST^+$ cells (n = 16 animals; values from one section per animal) (**b**). Both cell types failed to undergo LTP without DA (n = 4 $SST^+/PKC\delta^-$ cells and 5 $PKC\delta^+/SST^-$ cells; tests for LTP: RM two-way ANOVA $F_{interaction}$ (1, 7) = 0.2202 P = 0.6532, F_{time} (1, 7) = 1.235, P = 0.3031; F_{groups} (1, 7) = 0.004483, P = 0.9485; Holm-Sidak post-hoc tests). Representative images are derived from experiments that have been repeated 5 times independently. Bars are means ± s.e.m.

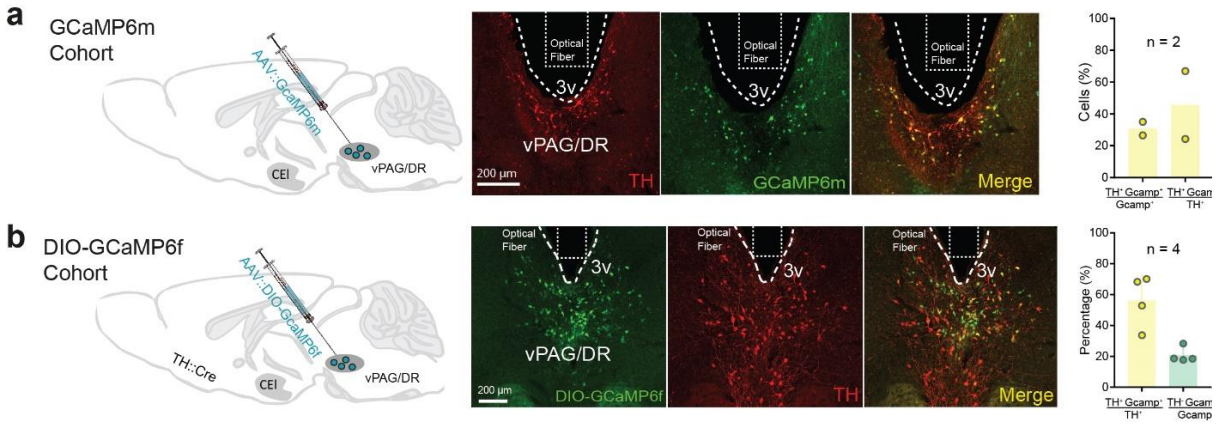

Supplementary Figure 4

GCaMP6 expression in vPAG/DR and vPdRD neurons

(**a**, *left*) Injection of AAV::GCaMP6m in the vPAG/DR of wild-type animals. (*Middle*) Representative IHC for extent and reliability of GCaMP6m expression in the vPAG/DR. (Right) Quantification over all animals within this cohort (n = 2 animals, values from 3 sections per animal). (**b**, *left*) Injection of AAV::DIO-GCaMP6f in the vPAG/DR of TH-Cre animals. (*Middle*) Representative IHC for extent and reliability of GCaMP6f expression in vPdRD neurons. (*Right*) Quantification over all animals within this cohort (n = 4 animals, values from 3 sections per animal). Representative images from two independent experiments (animals). Bars are means ± s.e.m.

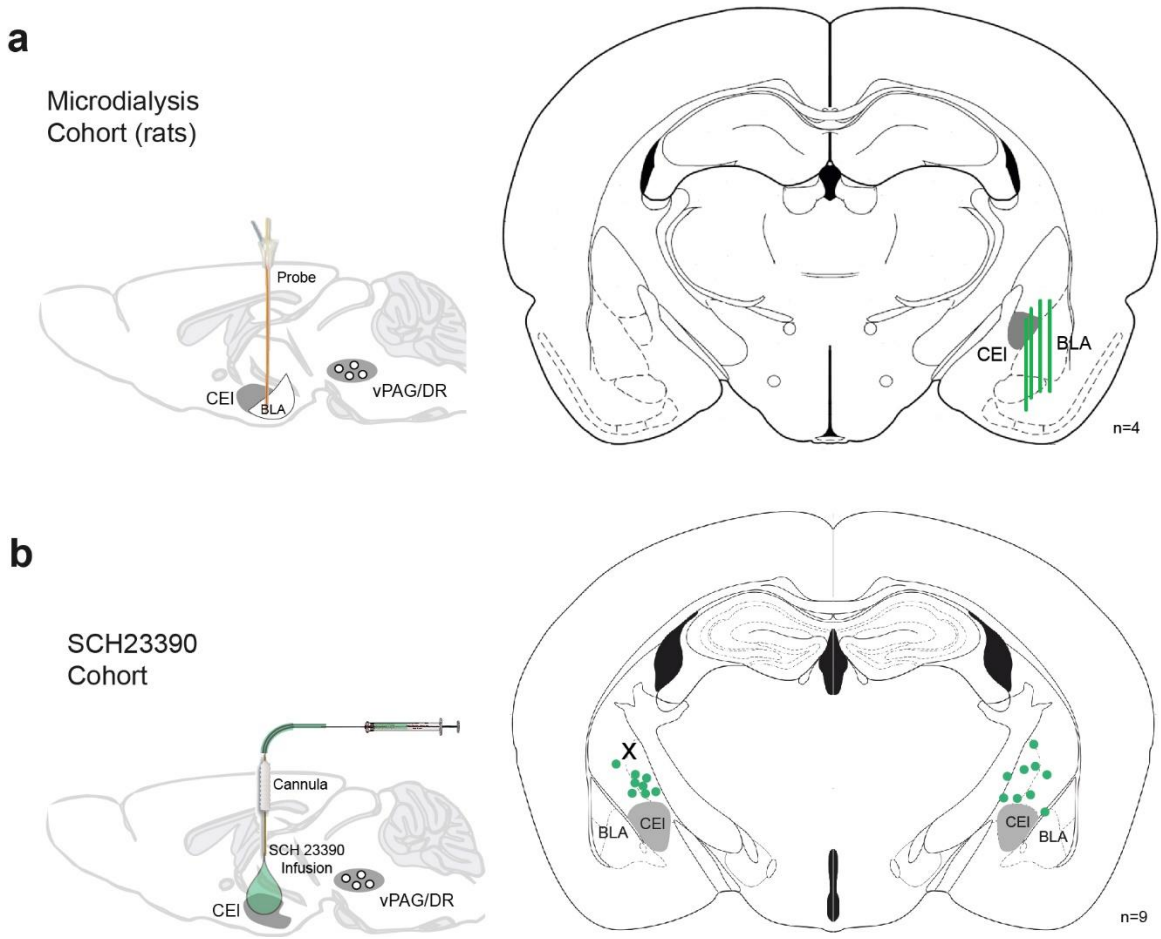

Supplementary Figure 5

Location of microdialysis probes and injection cannulas

(**a**, *left*) Implantation of microdialysis probes in the amygdala. (*Right*) Approximate position of the 2 mm lateral probe membranes (green) in and adjacent to the CEl. This configuration samples extracellular release from CEl and BLA. (**b**, l*eft*) Implantation of infusion cannulas over the CEl. (*Right*) Locations of the implantation sites (tip of the cannula) in the SCH23390 cohort. (x) indicates an implantation site anterior to that section.

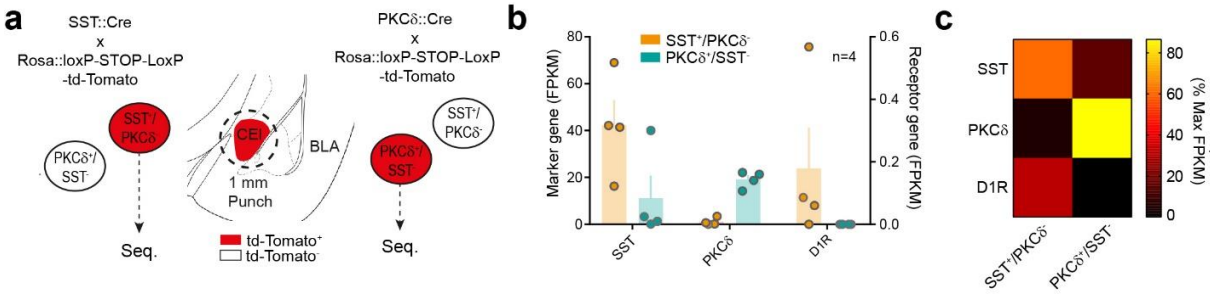

Supplementary Figure 6

Asymmetric expression of D1R in CEl neurons

(**a**) CEl neuronal types from SST::Cre or PKCδ::Cre crosses to Cre-dependent Rosa::td-Tomato reporter mice were FACS sorted. (**b**) Expression levels (Fragments per kilobase of transcript per million reads mapped, FPKM) of SST and PKCδ marker genes and D1R from combined deep sequencing results (n = 4 animals) (a). (c) Row-normalized expression values. Bars are means ± s.e.m.

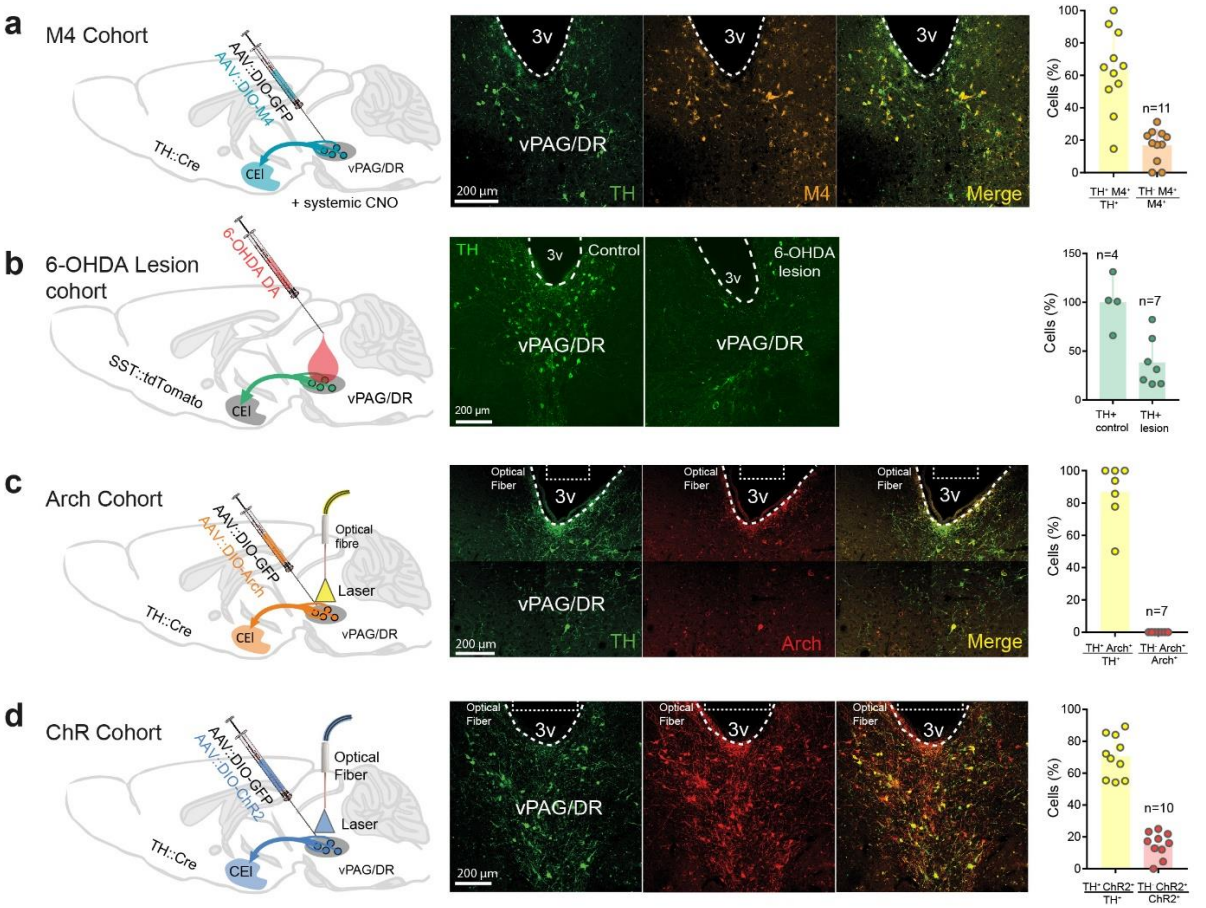

Supplementary Figure 7

vPAG/DR-CE circuit manipulations

(**a,** *left*) Injection of AAV::DIO-M4 in the PAG of TH-Cre animals for selective expression in vPdRD neurons. *Middle*, Representative IHC for extent and reliability of M4-expression in TH^+ neurons. *Right*, Quantification over all animals within this cohort (n = 11 animals, values from 3 sections per animal). (**b**, *left)* Injection of 6-OHDA in the vPAG/DR of SST-tdTomato animals. (*Middle)* Representative IHC for extent and reliability of vPdRD neuron lesioning by 6-OHDA. (*Right*) Quantification over all animals within this cohort (control group: n = 4, TH^+ lesion group: n = 7; values from 3 sections per animal). (**c**, *left*) Injection of AAV::DIO-Arch in the PAG of TH-Cre animals for selective expression in vPdRD neurons. (*Middle*) Representative IHC for extent and reliability of Arch-expression in TH^+ neurons. (*Right*) Quantification over all animals within this cohort (n = 7 animals; values from 3 sections per animal). (**d**, *left*) Injection of AAV::DIO- ChR2 in the PAG of TH-Cre animals for selective expression in vPdRD neurons. (*Middle*) Representative IHC for extent and reliability of M4-expression in TH^+ neurons. (*Right*) Quantification over all animals within this cohort (n = 10 animals; values from 3 sections per animal). Representative images from at least 4 experiments (animals). Bars are means ± s.e.m.

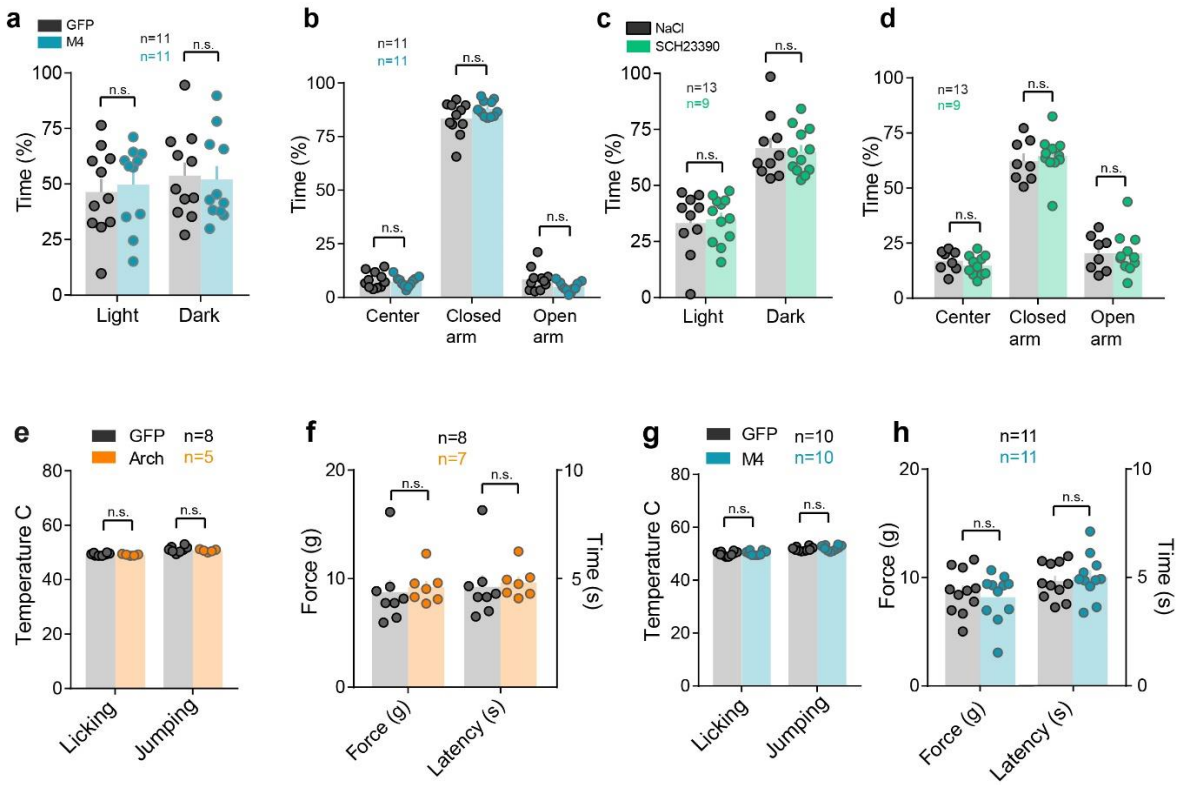

Supplementary Figure 8

Modulation of vPdRD neuronal activity or CEl D1R signalling does not affect anxiety or pain sensitivity

(**a**) Light/Dark transition test (control group: n = 11 animals, M4 group: n = 11 animals; RM two-way ANOVA$_{\text{Light/Dark}}$ $F_{\text{interaction}}$ (1, 20) = 0.09238, P = 0.7643; F_{time} (1, 20) = 0.3528, P = 0.5592; F_{groups} (1, 20) = 0.5466, P = 0.4683) and (**b**) Elevated plus maze (EPM) (control group: n = 11 animals, M4 group: n = 11 animals; RM two-way ANOVA$_{\text{EPM}}$ $F_{\text{interaction}}$ (2, 40) = 2.728, P = 0.0775; F_{time} (2, 40) = 1402, P < 0.0001; F_{groups} (1, 20) = 0, P > 0.9999; Holm-Sidak post-hoc tests) during M4 vPdRD neuron inactivation. (**c**) Light/Dark transition test (control group: n = 11 animals, SCH23390 group: n = 11 animals; RM two-way ANOVA$_{\text{Light/Dark}}$ $F_{\text{interaction}}$ (1, 20) = 0.08953, P = 0.7679; F_{time} (1, 20) = 37.73, P < 0.0001; F_{groups} (1, 20) = 0.7573, P = 0.3945) and (**d**) EPM (control group: n = 11 animals, SCH23390 group: n = 11 animals; RM two-way ANOVA$_{\text{EPM}}$ $F_{\text{interaction}}$ (2, 32) = 0.2519, P = 0.7787; F_{time} (2, 34) = 131.8, P < 0.0001; F_{groups}(1, 17) = 0.6561, P = 0.4291; Holm-Sidak post-hoc tests) during blocking of D1R signaling in the CEl by infusion of SCH 23390. (**e**) Hot Plate (control group: n = 8 animals, Arch group: n = 5 animals; RM two-way ANOVA$_{\text{HotPlate}}$ $F_{\text{interaction}}$ (1, 11) = 0.2614, P = 0.6192; F_{time} (1, 11) = 43.14, P < 0.0001; F_{groups} (1, 11) = 1.005, P = 0.3376; Holm-Sidak post-hoc tests) and (**f**) von Frey Filament test (control group: n = 8 animals, Arch group: n = 7 animals; unpaired t-test, two-sided, t(13) = 0.3113, $P_{\text{Control vs ARCH Force}}$ = 0.7605, t(13) = 0.3382, $P_{\text{Control vs ARCH Latency}}$ = 0.7406) during ARCH mediated silencing of vPdRD neurons. (**g**) Hot Plate (control group: n = 10 animals, M4 group: n = 10 animals; RM two-way ANOVA$_{\text{HotPlate}}$ $F_{\text{interaction}}$ (1, 18) = 0.1407, P = 0.7120; F_{time} (1, 18) = 110.9, P < 0.0001; F_{groups} (1, 18) = 1.254, P = 0.2774; Holm-Sidak post-hoc tests) and (**h**) von Frey filament test (control group: n = 11 animals, M4 group: n = 11 animals; unpaired t-test, two-sided, t(20) = 0.5277, $P_{\text{Control vs M4 Force}}$ = 0.6035; t(20) = 0.4701, $P_{\text{Control vs M4 Latency}}$ = 0.6433) during M4 mediated silencing of vPdRD neurons. Bars are means ± s.e.m.

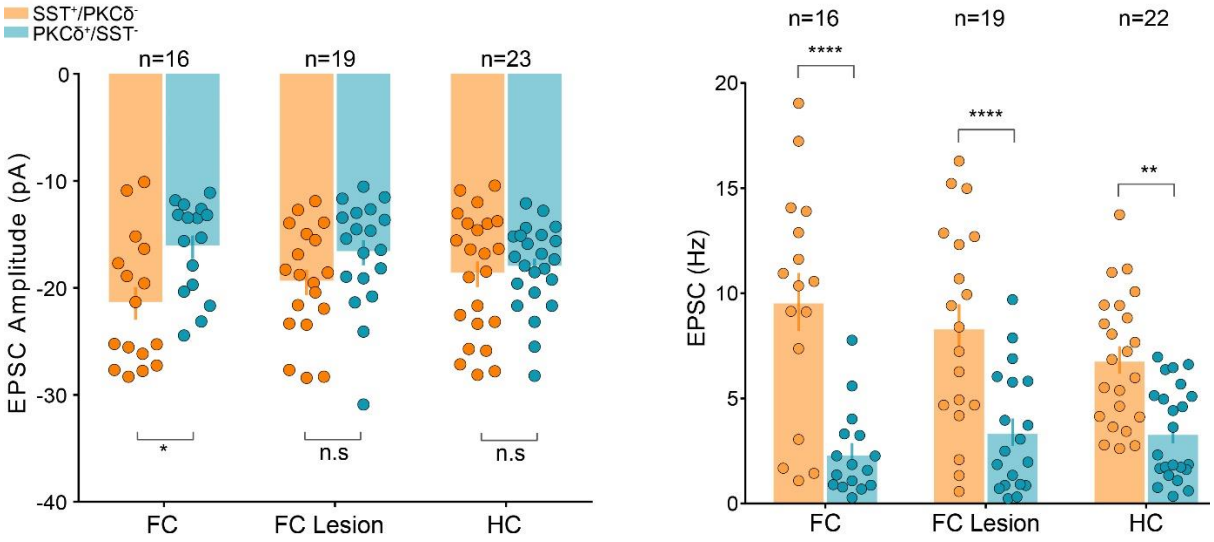

Supplementary Figure 9

6 OHDA lesion of vPdRD neurons affects CEl plasticity

(Left) Fear conditioning increases sEPSC amplitude of SST^+ neurons vs PKC-δ neurons (FC n = 16 cell pairs, FC lesion n = 19 cell pairs and HC n = 23 cell pairs; RM two-way $F_{interaction}(2, 110) = 1.939$, $P = 0.1487$; F_{time} (2, 110) = 0.1784, $P = 0.8369$; $F_{groups}(1, 110) = 9.12$, $P=0.0031$ Holm-Sidak post-hoc tests) in comparison to fear conditioned (FC) animals that underwent vPdRD neuron 6-OHDA lesioning as well as homecage (HC) animals. *(right)* Fear conditioning increases sEPSC frequency of SST^+ neurons vs PKC-δ neurons (FC n = 16 cell pairs, FC lesion n = 19 cell pairs and HC n = 22 cell pairs; RM two-way $F_{interaction}$ (3, 108) = 1.982, $P = 0.1210$; F_{time} (3, 108) = 0.5143, $P = 0.6733$ $F_{columns}$ (1, 108) = 49.18, $P=0.0001$; Holm-Sidak post-hoc tests). Significance levels between groups (*) at * P<0.05, ** P<0.01 and **** P<0.0001. Bars are means ± s.e.m.

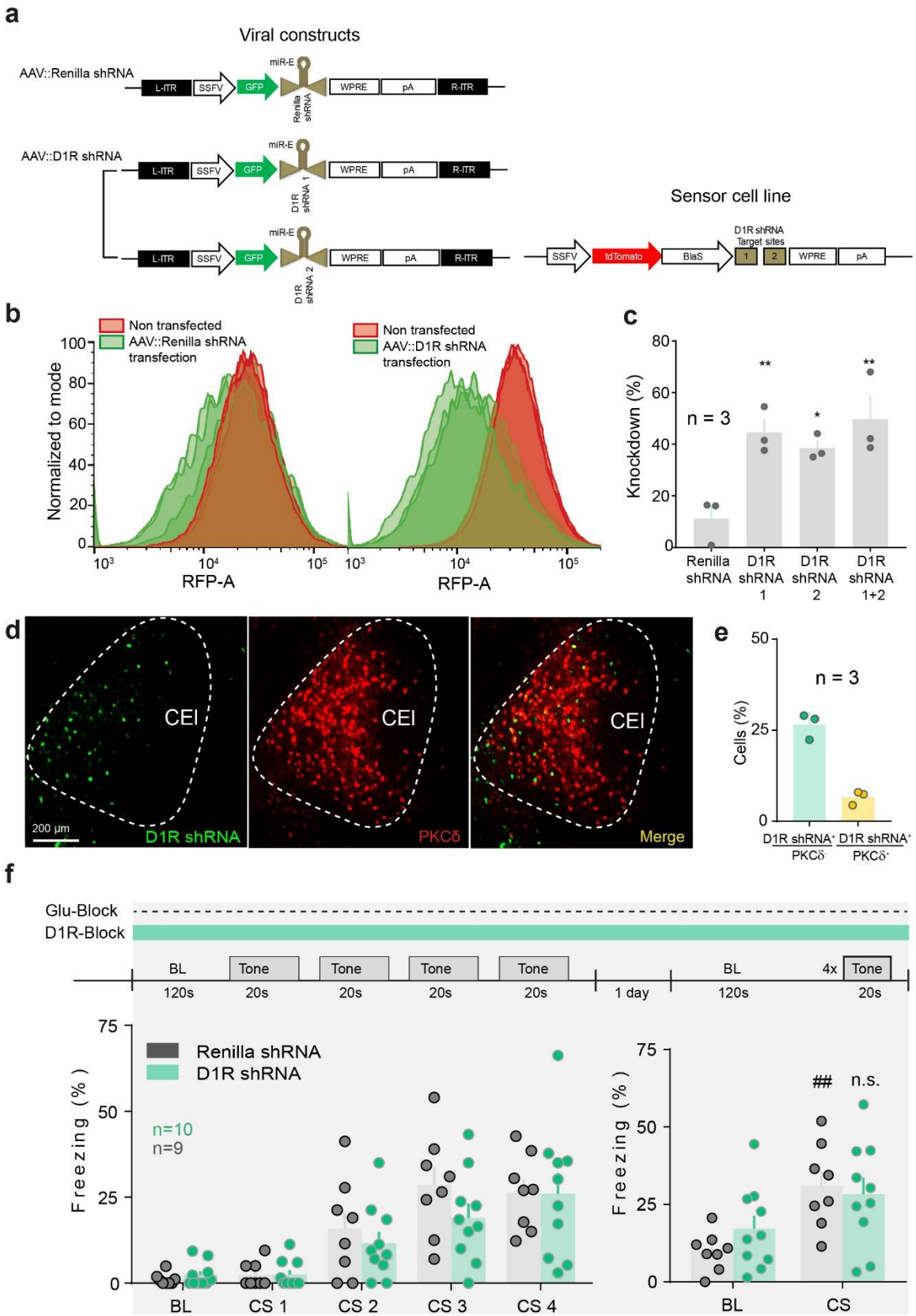

Supplementary Figure 10

RNAi mediated knock-down of D1R

(a) constructs of shRNAs and sensor cell line used in RNAi mediated D1R knock-down in the CEl (**b**) Reporter-

based evaluation of shRNA knockdown potency in NIH-3T3 cells expressing an expressing tdTomato transgene harboring shRNA target sites in the 3'UTR. Histograms depict tdTomato fluorescence intensity in reporter cells expressing control (green, left panel) or D1R shRNAs (green, right panel) compared to cells that were not transduced with shRNA (red). **(c)** Quantification of triplicate experiments in (**b**) (RM one-way ANOVA F (3, 8) = 8.05, $P = 0.0084$); (**d**) Representative IHC showing delivery and expression of GFP-shRNA transcripts in the CEl. (**e**) Quantification of D1R shRNA expression in PKCδ^- and PKCδ^+ neurons in the CEl (n = 3 animals, values are from 2 sections per animal). (**f**) Freezing responses to CS presentations during conditioning (RM two-way ANOVA$_{Conditioning}$ $F_{interaction}$ (4, 64) = 0.9245, $P = 0.4554$; F_{time} (4, 64) = 24.99, $P < 0.0001$, F_{groups} (1, 16) = 0.5751, $P = 0.4593$) and recall sessions (RM two-way ANOVA$_{Recall}$ $F_{interaction}$ (1, 16) = 1.444, $P = 0.2470$; F_{time} (1, 16) = 14.92, $P = 0.0014$; F_{groups} F (1, 16) = 0.2322, $P = 0.6364$; Holm-Sidak post-hoc tests). Quantification of (c) over all animals within this cohort. Representative images from two independent experiments (animals). Significance levels between groups (*) and to baseline (BL) (#) at */# $P<0.05$, **/## $P<0.01$, Bars are means ± s.e.m

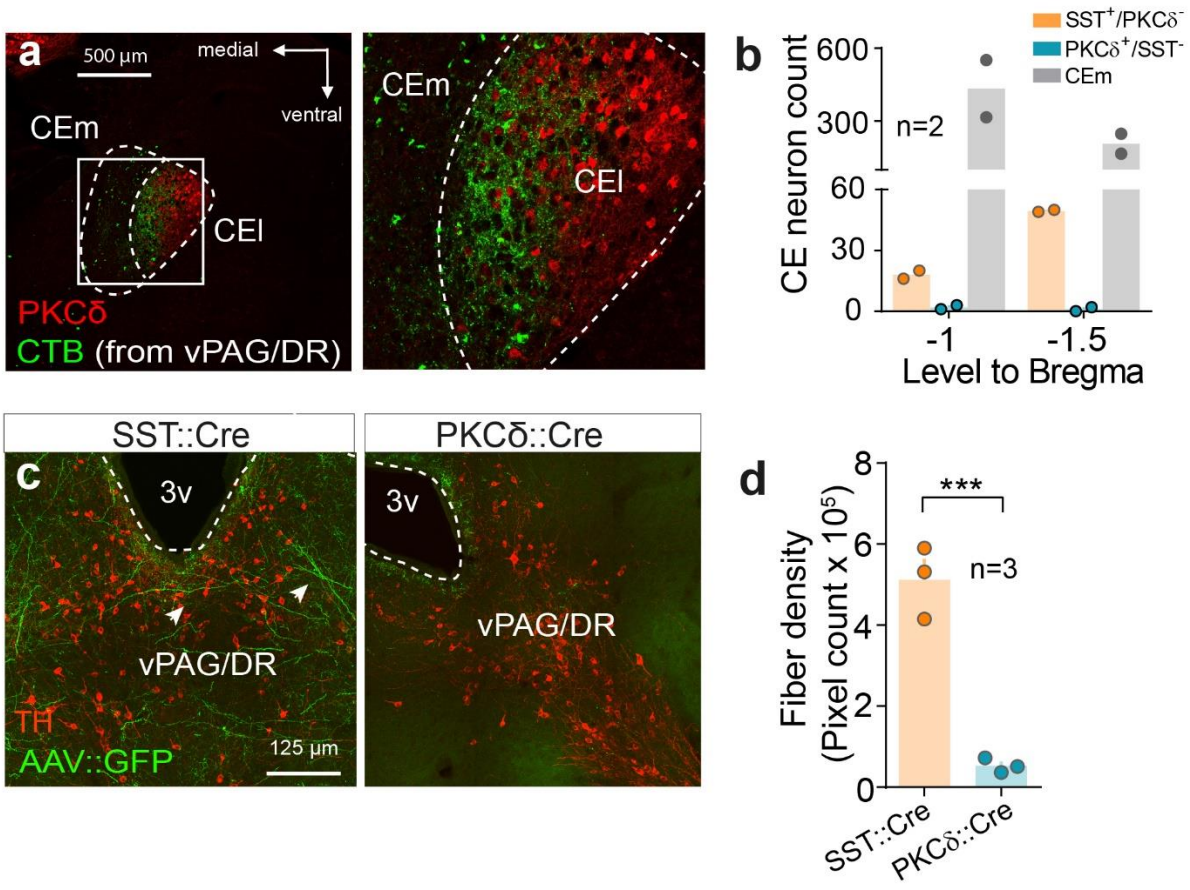

Supplementary Figure 11

Heterogeneity of vPAG/DR projecting CE output

(**a**) Representative image of CTB (injected into the vPAG/DR) retrogradely labelled neurons in the CEl and CEm. (**b**) Distribution of CTB retrogradely labelled CE neurons (n = 2 animals, values are from 3 sections per animal). (**c**) Representative image of cell-type specific projections (green) from CEl to TH^+ neurons in the vPAG/DR (red) in SST::Cre and PKCδ::Cre mice injected in CEl with AAV for Cre-dependent expression of GFP. (**d**) Density of projecting fibers originating from CEl $PKC\delta^+/SST^-$ or $SST^+/PKC\delta^-$ cells. (n = 3 animals, values are from 2 sections per animal; Unpaired t-test, two-sided, t(4) = 8.746, $P_{SST+/PKC\delta- \text{ vs } PKC\delta+/SST-} = 0.0009$). Representative images from at least two independent experiments (animals). Significance levels between groups (*) at *** P<0.001. Bars are means ± s.e.m.

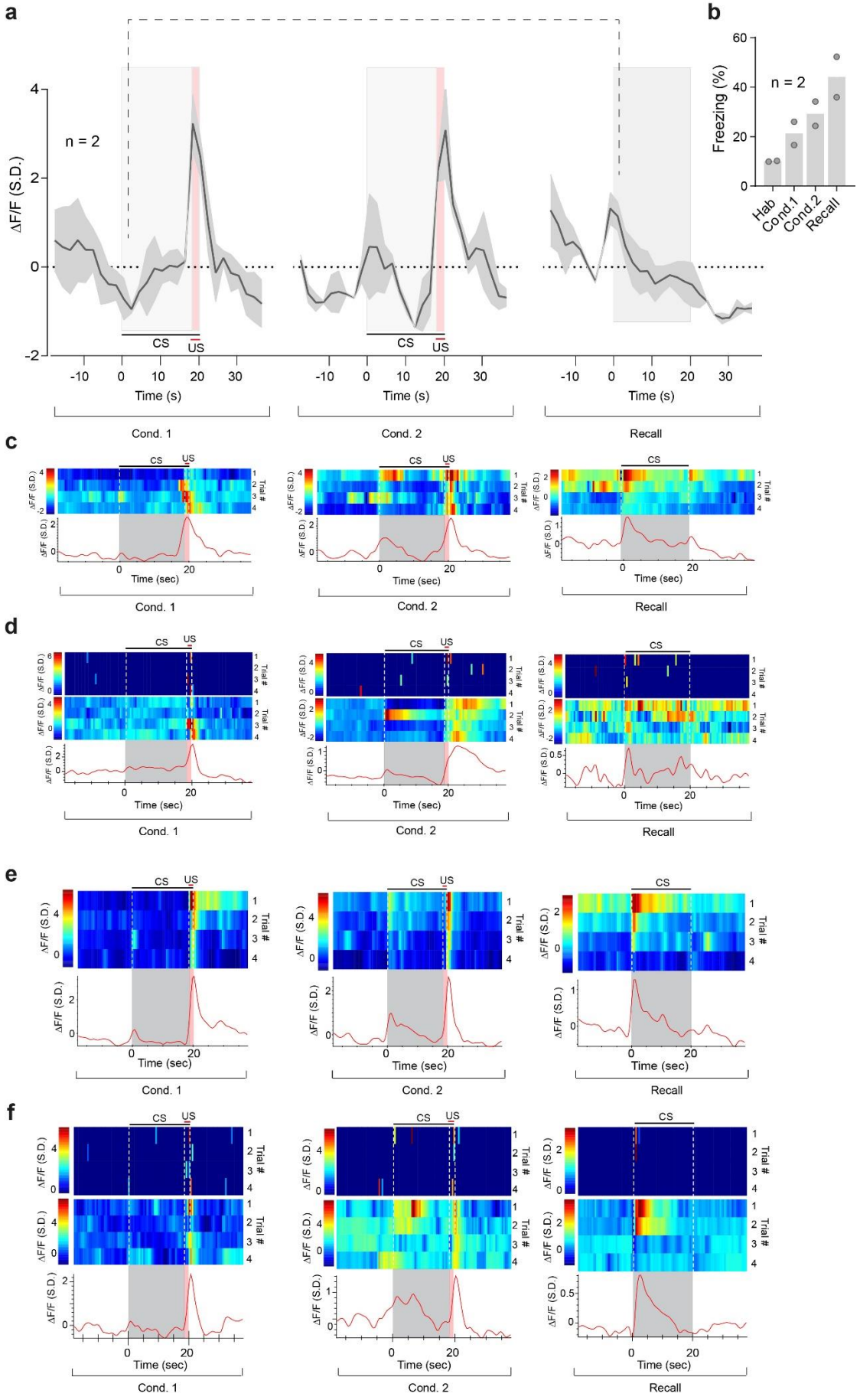
a
b
n = 2
ΔF/F (S.D.)
CS
US
Time (s)
Cond. 1
Cond. 2
Recall
Freezing (%)
Hab
Cond.1
Cond.2
Recall
c
d
e
f
Trial #
Time (sec)

Supplementary Figure 12

Modulation of vPAG/DR and vPdRD neuronal activity during associative learning

(**a**) Bulk Ca^{2+} signals of vPAG/DR neuronal activity of freely moving animals (b) during different phases of fear conditioning. Each trial within every session (conditioning day 1, conditioning day 2, recall day) consisted of 60s continuous Ca^{2+} imaging (20s pre-CS, 20s CS co-terminating into 1s foot shock and 20s post-CS, n = ROIs from 2 animals)(dashed line indicates CS response). (**b**) Freezing of Ca^{2+} imaged mice (n = 2 animals) during different phases of fear conditioning (**c**) Example traces of vPAG/ DR neuron bulk shown in **c**. Ca^{2+} signals of individual trials (*top*) and their trial averages (*bottom*). (**d**) Example traces of single vPAG/DR neuronal units during different phases of fear conditioning. Ca^{2+} signals of individual trials (middle), their trial averages (bottom) and Ca^{2+} events during individual trials (*top*). (**e**) Cell-type specific bulk Ca^{2+} imaging of vPdRD neurons of freely moving animals during different phases of fear conditioning as shown in Fig. 4f-i. Ca^{2+} signals of individual trials (*top*) and their trial averages (*bottom*). (**f**) Example traces of single vPdRD neuronal units from Ca^{2+} imaging shown in Fig. 4f-i**.** Ca^{2+} signals of individual trials (*middle*), their trial averages (*bottom*) and Ca^{2+} events during individual trials (*top*). Lines with shaded regions represent means ± upper and lower bounds. Ca^{2+} signals and event amplitudes are derived from per ROI (**a, c, e**) or per cell (**d, f**) dF/F values, standardized over the whole experiment and given as units S.D.

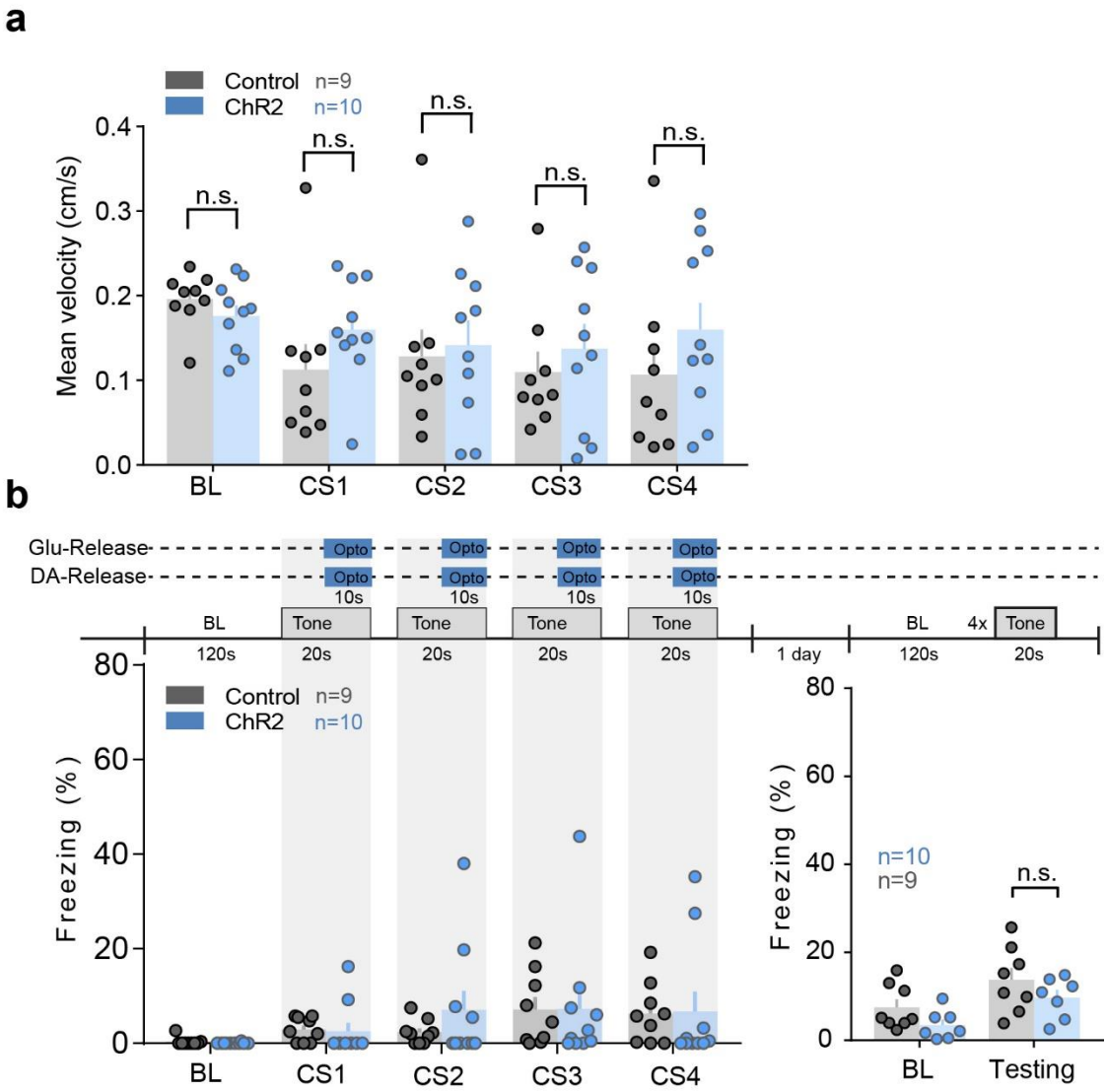

Supplementary Figure 13

Optogenetic activation of vPdRD neurons alone is not sufficient for fear conditioning

(**a**) Motor parameter mean velocity is unchanged during optogenetic activation of vPdRD neurons in TH::Cre mice injected with AAV for Cre-dependent expression of ChR2 (control group: n = 10 animals, ChR2 group: n = 9 animals; RM two-way $F_{interaction}$ (4, 68) = 1.781, P = 0.1428; F_{time} (4, 68) = 5.01, P = 0.0013; F_{groups} (1, 17) = 0.5832, P = 0.4555 Holm-Sidak post-hoc tests). (**b**) Freezing responses to CS presentations during conditioning (control group: n = 10 animals, ChR2 group: n = 9 animals; RM two-way $ANOVA_{Conditioning}$ $F_{interaction}$ (4, 52) = 0.3696, P = 0.8292; F_{time} (4, 52) = 2.691, P = 0.0410, F_{groups} (1, 13) = 2.066, P = 0.1743) and recall sessions (RM two-way $ANOVA_{Recall}$ $F_{interaction}$ (1, 13) = 0.0001412, P = 0.9907; F_{time} (1, 13) = 17.2, P = 0.0011; F_{groups} (1, 13) = 2.966, P = 0.1087; Holm-Sidak post-hoc tests). The shock-US was replaced with optogenetic activation of vPdRD neurons during second half of the 20s CS presentation. Bars are means ± s.e.m. BL, Baseline.

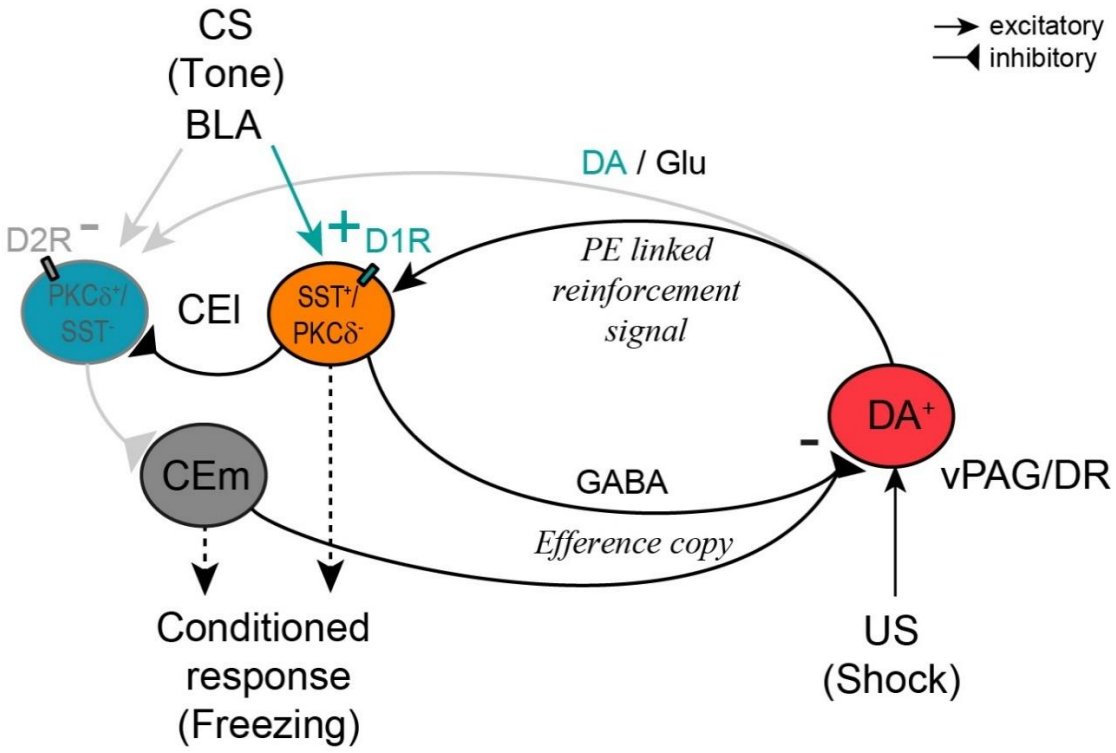

Supplementary Figure 14

Model of vPdRD neuron-amygdala circuit interactions during associative learning

Unpredicted US (shock) activates vPdRD neurons, which co-release glutamate and DA in the CEl. While glutamate activates both CEl PKCδ$^+$/SST$^-$ and SST$^+$/PKCδ$^-$ neurons, asymmetric D1R expression predominately reinforces CS (tone) signals at BLA-CEl SST$^+$/PKCδ$^-$ synapses. This potentiates CS-evoked responses of CEl SST$^+$/PKCδ$^-$ neurons (synergizing with D2R activity on PKCδ$^+$/SST$^-$ cells[43]) which together with CEm neurons jointly facilitate CS specific freezing. Of note, additional presynaptic mechanisms in BLA-CEl circuitry might contribute. Reinforcement signals from vPdRD neurons inversely correlate with stimulus (initially US, later CS) expectancy, linking the formation of associative memory traces in amygdala to PEs. Feedback inhibition from CEl SST$^+$/PKCδ$^-$ and CEm neurons controls activity of, and potentially encoding of PE in, vPdRD cells.

a

Virus	Short name	Manufacturer	Titer (GC/ml)
AAV2/5.Ef1a.DIO.hChR2(H134R).eYFP.WPRE (Addgene 20298P)	AAV::DIO-ChR2	BI Biberach	1 x 10^{13}
AAV2/5.DIO.eARCH3.0eYFP.WPRE	AAV::DIO-Arch	University of Pennsylvania	6 x 10^{12}
AAV5.Syn.DIO-hM4D.mCherry.WPRE.hGh	AAV::DIO-M4	University of Pennsylvania	1 x 10^{13}
AAV2/5.EF1a.DIO.GFP.WPRE	AAV::DIO-GFP	IMP	1 x 10^{11}
AAV9.hsyn.GCaMP6.WPRE	AAV::GCaMP6m	BI Biberach	1 x 10^{12}
AAV1.Syn.Flex.GCaMP6f.WPRE.SV40 AV-1-PV2819	AAV::DIO-GCaMP6f	PENN Vector	1 x 10^{13}
AAV2/5.SSFV.GFP.D1R-miR-E.WPRE	AAV::D1R-shRNA	IMP	1 x 10^{12}
AAV2/5.SSFV.GFP.Renilla-miR-E.WPRE	AAV::Renilla-shRNA	IMP	1 x 10^{12}

b

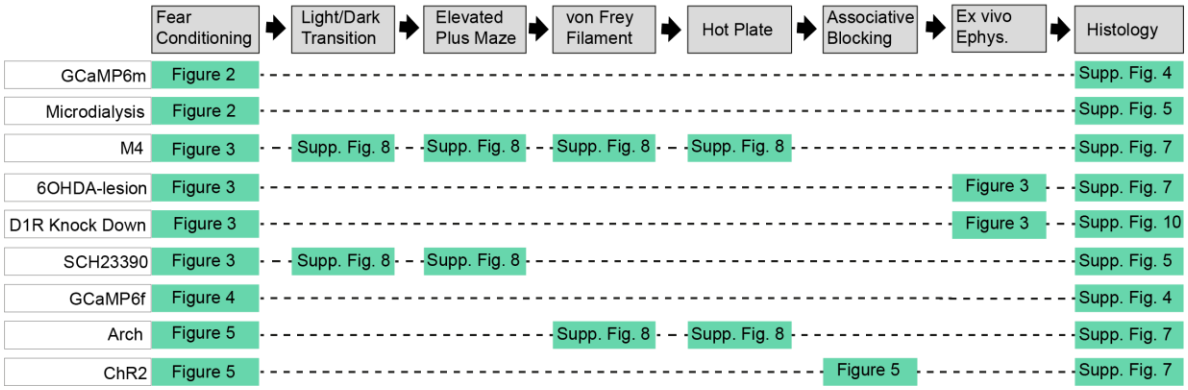

Supplementary Figure 15

Viral constructs and subject history

(**a**) Viral constructs, short names, manufacturer and titer as used in different experiments. (**b**) Subject history of different mouse cohorts.

Supplementary References

51 Bi, L. L. *et al.* Amygdala NRG1-ErbB4 is critical for the modulation of anxiety-like behaviors. *Neuropsychopharmacology* **40**, 974-986, doi:10.1038/npp.2014.274 (2015).

52 Grippo, R. M., Purohit, A. M., Zhang, Q., Zweifel, L. S. & Guler, A. D. Direct Midbrain Dopamine Input to the Suprachiasmatic Nucleus Accelerates Circadian Entrainment. *Current biology : CB* **27**, 2465-2475 e2463, doi:10.1016/j.cub.2017.06.084 (2017).

53 Fellmann, C. *et al.* An optimized microRNA backbone for effective single-copy RNAi. *Cell reports* **5**, 1704-1713, doi:10.1016/j.celrep.2013.11.020 (2013).

54 Meis, S., Endres, T. & Lessmann, V. Postsynaptic BDNF signalling regulates long-term potentiation at thalamo-amygdala afferents. *The Journal of physiology* **590**, 193-208, doi:10.1113/jphysiol.2011.220434 (2012).

55 Dobin, A. *et al.* STAR: ultrafast universal RNA-seq aligner. *Bioinformatics* **29**, 15-21, doi:10.1093/bioinformatics/bts635 (2013).

56 Kim, D. *et al.* TopHat2: accurate alignment of transcriptomes in the presence of insertions, deletions and gene fusions. *Genome biology* **14**, R36, doi:10.1186/gb-2013-14-4-r36 (2013).

57 Anders, S., Pyl, P. T. & Huber, W. HTSeq--a Python framework to work with high-throughput sequencing data. *Bioinformatics* **31**, 166-169, doi:10.1093/bioinformatics/btu638 (2015).

58 Tovote, P. *et al.* Midbrain circuits for defensive behaviour. *Nature* **534**, 206-212, doi:10.1038/nature17996 (2016).

59 Cho, J. R. *et al.* Dorsal Raphe Dopamine Neurons Modulate Arousal and Promote Wakefulness by Salient Stimuli. *Neuron* **94**, 1205-1219 e1208, doi:10.1016/j.neuron.2017.05.020 (2017).

60 Behbehani, M. M. Functional characteristics of the midbrain periaqueductal gray. *Prog Neurobiol* **46**, 575-605 (1995).

61 Davis, M. Neural systems involved in fear and anxiety measured with fear-potentiated startle. *The American psychologist* **61**, 741-756, doi:10.1037/0003-066X.61.8.741 (2006).

62 Davis, M., Walker, D. L., Miles, L. & Grillon, C. Phasic vs sustained fear in rats and humans: role of the extended amygdala in fear vs anxiety. *Neuropsychopharmacology* **35**, 105-135, doi:10.1038/npp.2009.109 (2010).

Discussion

IC subregions are functionally and anatomically divergent. Therefore, **hypothesis 1** states that they provide an ideal substrate for testing central propositions of IPP. We found IC subregions to represent an interoceptive hierarchical system, shaped by experience. Increased valence domain-generality in aIC is paralleled by predominantly unidirectional information flow from the general to the specific (aIC–pIC). aIC–pIC communication, signifying an encoded task model, is consistent with the IPP account and proposed information flow of prediction (top-down) and PE (bottom-up) in a hierarchical system (Barrett and Simmons, 2015; Seth et al., 2012).

At the onset of learning CE circuitry faces uncertainty about CS value. **Hypothesis 2** implicates the ascending CE–NBM–aIC pathway in signaling uncertainty. We found CE to actively recruit the interoceptive GM in IC through engagement of the cholinergic NBM, thereby overcoming CS value uncertainty.

The PAG encodes PE signals and responds to painful stimuli. **Hypothesis 3** states that the vPAG/DR provides a teaching signal to CE circuitry to drive affective learning. We found that the same signal used to build interoceptive value in the IC (the US) is used by the CE to retain CS salience and valence dimensions as long-term memory, constituting the GM in CE. The US ascends as a DAergic PE from vPAG/DR to tag US-predictive CS with salience.

The IC–CE represents a cortico-striatal circuit motif. **Hypothesis 4** states that this motif performs feature extraction of interoceptive GMs. We found CE extracting valence and salience dimensions from the GM, giving rise to interoception-based affective behavior and learning. This circuit operation is consistent with interoception-based decision-making proposed in the SMH (Damasio, 1994).

vPAG/DR drives learning in the CE. As the CE projects back to vPAG/DR, **hypothesis 5** states CE–vPAG/DR as a negative feedback loop preventing maladaptive learning in CE. We found acquired CS salience by CE subpopulations descends further to vPAG/DR, exerting inhibitory feedback onto DA neurons to prevent further PE signaling. This contributes to a DAergic belief state in vPAG/DR about acquired CS salience in CE.

Interoceptive predictions in the insular cortex

Intra-insular communication is shaped by experience and subsequent task performance. We infer the successful encoding of a task model by consistent stimulus-bound behavioral responding (Manuscript 1, suppl. Fig. 7c,h). Selective spike-field coherence (SFC) of aIC spikes to pIC local field potential (LFP), and not the converse, during CSs in a high-performing animal at recall, suggests hierarchical information flow from aIC to pIC, further underscored by congruent transfer entropy (TE) (Manuscript 1, Fig. 4). aIC–pIC coherence may represent an generalizable neural signature for precision signaling, the dynamic scaling of PE according to model certainty (Moran et al., 2013), since this phenomenon is absent in non-performing animals (Manuscript 1, suppl. Fig. 11b). In addition, we observe an inverse pIC–aIC SFC in discrete frequency bands during CSs in habituation (Manuscript 1, suppl. Fig. 11c). As TE consistently shows bottom-up signaling from pIC to aIC during surprising events, such as novel CSs at habituation and USs during conditioning (Manuscript 1, Fig. 5), pIC–aIC SFC may account for perceptual plasticity for model update in aIC.

The hierarchical predictive processing framework capitalizes on the systematic variation of laminar differentiation, which predicts laminar cortico-cortical connectivity patterns and gave rise to the structural model of cortical connectivity in primates (Barbas, 2015). The structural model captures rules of laminar origin and termination of axons, considering relative differences in laminar differentiation between connected areas (agranular-dysgranular-eulaminate). In essence, predictions are proposed to be issued from deep layers of agranular and terminate in supragranular eulaminate cortices (top-down), whereas supragranular layers from eulaminate cortices convey PE towards deep agranular layers (Barrett, 2015), creating supra- and infragranular counterstreams of information type and frequency (see below) (Markov et al., 2014). Although rodents exhibit variations in laminar differentiation as well, top-down and bottom-up projections are less specific in their laminar origins and targets, hence are organized in a more salt and pepper fashion (Berezovskii et al., 2011). Therefore, the precise laminar origin of recorded neurons in our IC dataset is less important, however, SFC and TE data is still in accord with top-down predictive and bottom-up PE information flow from aIC to pIC and pIC to aIC, respectively.

In primates, distinct frequency bands could be assigned to predictive and PE processes. Data mostly acquired in the primate visual system shows frequency bands in the beta range (~14-18Hz) predominantly carrying top-down (Bastos et al., 2015; von Stein et al., 2000), whereas gamma range synchronization (~60-80Hz) was particularly engaged during bottom-up

signaling, modulated by stimulus salience and attention (Bosman et al., 2012; Hadjipapas et al., 2015). This is paralleled by overall synchronization to gamma in supragranular (bottom-up) and beta-synchronization (top-down) in the infragranular layers, resonating with the structural model of connectivity (Buffalo et al., 2011). Although there are other examples, the intermediate frequency around 33Hz for top-down influences we observe in aIC–pIC SFC could reflect species differences and/or be a product of the less differentiated laminar projection specificity in rodents (Berezovskii et al., 2011). Another possibility is that the visual and interoceptive system represent two extremes at the level of hierarchical circuit complexity and number of dedicated cortical areas involved (Fig. 4 for comparison). The latter explanation would suggest that the strict hierarchical organization of the visual system requires dedicated frequency channels.

Overall, these data are in agreement with the conceptualization of limbic cortices (cortical areas lacking a granular layer, such as aIC) as the uppermost hierarchical layer within the cortex, above (dys)granular cortices (Chanes and Barrett, 2016), consequently they may accommodate the most domain-general model. Domain-generality was shown to be more prevailing in anterior cortices, as exemplified by the PFC (Badre, 2008). The aIC indeed displays higher valence domain-generality than the pIC, since the pIC shows greater intrinsic bias towards negative valence (Manuscript 1, suppl. Fig. 4b). This is consistent with the view that aIC conveys valence predictions to more valence-specific areas, i.e. the pIC, to interpret bottom-up sensory data (Barrett and Simmons, 2015). Further supporting this interpretation is the selective impairment of fear learning upon aIC–pIC and pIC–CE pathway inhibition (Manuscript 1, Fig. 4 and 2).

Central amygdala links learning models

Learning theories depict PE, the discrepancy between predicted and actual outcome, as the main driver for associative learning (Roesch et al., 2012). The change in associative strength should correspond to the magnitude of the PE, so learning is suppressed once the outcome can be fully predicted by a preceding cue. This type of associative learning is formalized in its most basic form in the Rescorla-Wagner (RW) model, wherein PEs are signed, strengthening or weakening associations proportionally (Rescorla and Wagner, 1972). Classically, DA neurons have been implicated in this type of learning, predominantly shown in appetitive paradigms (Schultz, 1997). The CE–vPAG/DR circuit module operates according to RW criteria (see above), since we show that phenomena predicted by the RW

model, such as associative blocking (Kamin, 1969), can be observed in CE–vPAG/DR circuitry (Manuscript 2, Fig. 5d,e). Once a stimulus (light in this case) accurately predicts the occurrence of a foot-shock, the association of a second stimulus (tone) with the foot-shock is weakened when the tone is co-presented with the light stimulus in a second conditioning session. This can be explained by the inhibitory modulation of the CE^{SST}/m projection onto the DAergic vPAG/DR neurons upon the light cue, curbing the bottom-up DAergic PE signal of the foot-shock for the tone.

CE lesions result in deficits in acquired orienting responses and attention (Holland and Gallagher, 1999) and CE is required for associative learning where CS-US contingencies are more unreliable, a relationship determining the 'associability' of a stimulus (Holland and Gallagher, 1993). Paradoxically, stimuli that are only partially reinforced (e.g. probabilistic conditioning), result in augmented associative learning rates (Hogarth et al., 2008; Kaye, 1984; Swan, 1988). This effect is attributed to uncertainty becoming a property of the stimulus, which in turn determines the amount of attentional resources devoted to its processing, thereby scaling its associability. These effects were formulated in the Pearce-Hall model of Pavlovian learning (Pearce and Hall, 1980). In the PH model, PEs are unsigned, strengthening associations independent of the direction of surprise. Uncertainty at variable hierarchical levels is implicit when learning the probabilistic structure of the environment. An elegant fMRI study explicitly mapped low-level PE (cue-outcome violations) to activity in the DAergic VTA/SN system, whereas high-level PE (change in cue-outcome contingencies, 'expected uncertainty' (Yu, 2005)) to the cholinergic basal forebrain. Early lesion studies implicated the CE–NBM pathway in mediating this surprise-induced enhancement of learning to overcome expected uncertainty (Han et al., 1999). Therefore, the CE may consolidate basic predictiveness (RW) and uncertainty as an additional scaling parameter for learning rate (PH) to mediate PL.

Previously, the posterior parietal cortex (PPC) was suggested as the functional target of CE–NBM signaling, since cholinergic denervation of the PPC resulted in similar attentional phenotypes (Bucci et al., 1998). However the PPC, together with the aIC and dlPFC, constitutes the CEN (Seeley et al., 2007), binding our and previous lines of evidence to a common network substrate. Our data implicates bottom-up recruitment of the IC by the CE–NBM pathway and adds a circuit mechanism to the proposed enhanced attentional processing mediated by CE. Consistent with data in humans showing enhanced coupling of IC and amygdala upon encounter of uncertain predictors (Sarinopoulos et al., 2010), stimulus uncertainty in CE recruits interoceptive models in IC via cholinergic NBM to resolve value

uncertainty (Manuscript 1, Fig. 3). Phasic acetylcholine (ACh) release was linked to detection of cues, rebranding ACh release rather deterministic than diffusely modulatory (Gritton et al., 2016; Sarter et al., 2014). ACh also rapidly reconfigures the mode of cortical network operation (Muñoz and Rudy, 2014). This suggests that ACh transients in IC, evoked by CE–NBM signaling, may flexibly assemble cortical ensembles into model representations across (but likely not only) IC subregions, evident by the striking stimulus-dependent coherence in the hierarchical aIC–pIC network. Coherence is indeed muscarinic 1 receptor (M1R)-dependent, a receptor implicated in the generation of gamma oscillations and cognition (Fisahn et al., 2002; Moran et al., 2018) and was further associated with autism spectrum disorder and schizophrenia (Perry et al., 2001; Yohn and Conn, 2018). A modulatory role of CE on cortical arousal has previously been described via putative $CE^{PKC\delta}$, although the IC was not detected (Gozzi et al., 2010). This discrepancy may have technical reasons. We stimulated $CE^{PKC\delta}$-NBM directly by optogenetics, whereas Gozzi et al. inferred putative $CE^{PKC\delta}$ activation by pharmacogenetic suppression of $CE^{PKC\delta}$-inhibiting putative CE^{SST} (Ciocchi et al., 2010). The inferred $CE^{PKC\delta}$ disinhibition may likely not fully recapitulate direct activation.

As indicated above, CE cell type function has remained ambiguous to some extent. State-dependency was proposed as an explanation for divergent behavioral effects observed upon neuronal activation (Fadok et al., 2018). Affective responses were mostly attempted to be reconciled in terms of local microcircuitry or downstream targets of CE. Our data offer a complementary explanation, whereby behavioral manifestations of e.g. $CE^{PKC\delta}$ stimulation are flexible depending on the model retrieved from upstream cortical areas. As the model in use is highly context-dependent, integrating environmental factors, internal goals and states (Pezzulo et al., 2018), so may be observed behaviors across the time of day, task conditions, laboratories and previous experience.

Top-down models facilitate adaptive behavior and learning

Interoceptive models in the insular cortex

In our work we show that the interoceptive IC represents and accumulates CS information over the course of a discriminatory Pavlovian learning (PL) paradigm, suggestive of the IC building internal models to infer the value of external stimuli. Cross-modal responses in unimodal sensory areas are an established phenomenon (Lakatos et al., 2007). The gustatory cortex, a subregion of the IC, similarly shows cross-modal responses to auditory cues. These however can be modified by associative learning, providing a basis for cross-modal inference (Vincis and Fontanini, 2016). By pairing of auditory cues with interoceptive USs (thirst-quenching water and mild foot-shock), the CSs become predictive of US-associated states by integrating the interoceptive value of the USs into CS representations (Manuscript 1, Fig. 1). By splitting animals into a performing and non-performing group at recall, we found striking differences in response magnitude to US at conditioning and CS at recall in IC. Non-performing animals displayed significantly dampened responses, providing a potential mechanistic link to human studies showing modulation of emotional memory performance by the ability to perceive one's bodily signals (interoceptive awareness) (Pollatos and Schandry, 2008). By assessing the similarity between CS and US, we demonstrate that CS representations in both the aIC and pIC become progressively similar to the respective US representations, the more CS-US pairings animals experience, a mechanism described previously (Grewe et al., 2017). This finding supports the interoceptive inference account of affective learning, whereby environmental stimuli are evaluated and categorized with respect to potential physiological change (Seth, 2013).

Although originally not interpreted according to the IPP framework, there is evidence that US responses do not necessarily represent sensory features of primary reinforcers per se, but may embody value predictions. Gore et al. (2015) labelled BLA neurons responsive to a rewarding nicotine or aversive foot-shock experience to express an optogenetic activator. Subsequent artificial activation of the same neurons evoked instrumental and Pavlovian behaviors by itself. This suggests US responsive ensembles do not (only) encode US features, but also comprise complex behavioral patterns to consummate value predictions, which are transferred onto CSs upon PL. The power of PL allows to classify CS-associated states as mere predictions for interoceptive states, based on past experience. It is reasonable to assume that this mechanism might be extendable to second- and higher-order conditioning, whereby CSs and associated values are used to further build more sophisticated models on complex

spatial and temporal relationships between mental objects. The resulting implicit associative structure might underpin the non-declarative basis of decision-making, put forward by the SMH (Damasio, 1994) and give rise to the colloquial ‘gut feeling’ where the origin of value is covert.

As the values of USs lie on opposing sides of the spectrum, R-CS and F-CS become more dissimilar from pre- to post-conditioning, allowing the system to discriminate and adjust behavior accordingly (Manuscript 1, Fig. 1). This is congruent with studies in humans, where IC lesioned patients report impaired valence and arousal ratings to positive and negative affective stimuli. Strikingly, in the same study amygdala lesioned patients did not show impaired valence ratings, however reported dampened arousal (Berntson et al., 2011). This dissociation highlights the role of the IC in generating meaning, with interoceptive inference as a potential mechanism, and suggests the IC to instruct hierarchically lower areas, blind to primary value, to fulfill allostatic loops. Recently, predicted physiological states upon exteroceptive stimulus presentations were indeed found in the IC (Livneh et al., 2020).

Model feature extraction in the central amygdala

CE cell populations exhibit excitatory responses to both USs, implying bottom-up information from the PAG may only provide a permissive salience signal and lacks instructive valence contrast (Manuscript 1, suppl. Fig. 7f). Nevertheless, it is possible that bottom-up USs signaling ascending from different sources, such as the ventral tegmental area (VTA; Hasue, 2002) may facilitate valence discrimination, concealed in the population response. However, consistent with the valence-free interpretation is that artificial activation of vPAG/DR DA neurons does neither evoke acute affective behaviors nor memory formation (Manuscript 2, suppl. Fig. 13). Concurrent bottom-up salience and top-down value may for this reason be a prerequisite for CE learning.

The presence of functional connectivity between interoceptive/allostatic cortical networks and dorsal amygdala (containing human CE) in humans, emphasizes the transferability of our findings in rodents with regard to IC-CE coupling as a defined circuit module (Kleckner et al., 2017). Given the disparity in circuit complexity between cortical IC and striatal CE, IC–CE projections may perform some form of feature extraction from high-dimensional cortical models. Along these lines, striatal function was suggested to serve as an efference synchronizer or filter to shape cortical output into a coherent stream of information for further downstream processing (Mesulam, 1998). The bidirectional modulation of affective decision-

making we observe in PL is in support of this model. aIC–CE and pIC–CE inhibition facilitate approach and avoidance behavior, respectively, while the same manipulations disinhibit the respective converse, suggesting that the CE arbitrates between various (cortical) inputs to gate behavior according to model output (Manuscript 1, Fig. 2). Importantly, the cortico-striatal IC-CE pathway represents a neural substrate for interoception-based decision-making proposed in the SMH (Bechara and Damasio, 2005).

In identifying features extracted from interoceptive models, we found valence and salience dimensions mapped onto $PKC\delta^{+}$ and SST^{+} populations in the CEl, respectively, which are both dependent on top-down IC activity (Manuscript 1, Fig. 5). Consistent with the role of the $PKC\delta^{+}$ population in discriminating valenced stimuli at the level of the CE, is the specific TE of aIC–$CE^{PKC\delta}$ differentiating between approach and avoidance behavior (Manuscript 1, Fig. 2). Further support can be derived from work on discriminatory threat conditioning, demonstrating pharmacological modulation by D2-receptors, predominantly expressed in $CE^{PKC\delta}$, to bidirectionally control fear generalization. Specifically, CE D2 agonism reverted CS generalization in a strong US regime, paralleled by D2-mediated phosphorylation of ribosomal proteins specifically in $CE^{PKC\delta}$. Notably, there are data inconsistent with the above evidence, showing tonic $PKC\delta^{+}$ neuron activity rather predicts and contributes to fear behavior/generalization and anxiety (Botta et al., 2015; Ciocchi et al., 2010; Kim et al., 2017). Potential explanations rest on assumptions about different circuit modes the CE operates in (e.g. tonic-phasic), as well as context dependency of behavioral effects (see above) (Fadok et al., 2018).

The projection targets of CE^{SST}, $CE^{PKC\delta}$ and CEm populations are highly divergent between PAG and the Nucleus Basalis of Meynert (NBM) (Manuscript 2, Suppl. Fig. 11; Manuscript 1; Suppl. Fig. 9), as $CE^{PKC\delta}$–PAG projections are virtually inexistent. Therefore, the acquisition of salience by CSs through the inhibitory SST^{+} population projecting directly onto DAergic vPAG/DR neurons represents a top-down prediction of a belief state, signaling sufficient evidence about CS value, which in turn shuts off bottom-up PE signaling by USs. (Manuscript 2, Fig. 4). In this way bottom-up PE can be scaled according to evidence about CS value. A related motif can be found in the ventral tegmental area (VTA), a site broadcasting DAergic reward PE. GABAergic interneuron activity in the VTA is proportional to reward expectancy (Cohen et al., 2012) and could thereby impose an inhibitory threshold onto DAergic neurons that has to be overcome by an actual reward (PE) to drive a teaching signal. This top-down prediction may originate from prefrontal areas distributing expected reward signals from its encoded task model (Takahashi et al., 2011). Collectively, the DA

system, including vPAG/DR and VTA, may integrate inferences about the state of the environment from multiple sources, constructing a belief state to broadcast DA transients upon belief violation. (Babayan et al., 2018; Sharpe et al., 2017)

The fact that DAergic vPAG/DR neurons acquire CS salience as well (Manuscript 2, Fig. 4i,j) has further functional implications. Firstly, it points towards a cascading top-down salience signal, fulfilling IC interoceptive predictions possibly down to spinal motor neurons targeting viscera and muscles (Tovote et al., 2016), making a case for active inference (Seth and Friston, 2016). Secondly, CS salience of vPAG/DR DA neurons further creates a mechanistic basis for second- and higher-order conditioning, where CSs may be repurposed as future reinforcers in CE and upstream. The observed absence of acquired salience by CEm neurons (Manuscript 1, Fig. 1), which also exhibit strong projections to the vPAG/DR, does not necessarily imply that the CEm–vPAG/DR projection does not convey CS salience. Since we infer salience acquisition as a direct transfer of US properties onto CS by individual neurons, it may simply suggest that CEm neurons responding to acquired CS and US salience are separate populations. The CEm population does respond to R-CS and F-CS at recall, arguing for acquired CS salience of the CEm population as well (Manuscript 1, suppl. Fig. 7h).

Model failure and psychopathologies

Psychiatric symptomologies are being increasingly reconceptualized as pathologies of (interoceptive) inference. Inappropriate use of priors, such as false inference, over-reliance (hyperpriors) or under-reliance on prior knowledge (hypopriors) may underlie conditions like depression, anxiety, autism and schizophrenia. (Seth, 2016).

Despite most well-known for deficits in social communication and interaction, autism is characterized by profound perceptual alterations (Lord et al., 2000; Mottron et al., 2006). Impairments in the social domain, encompassing the perhaps most demanding cognitive tasks brains are facing, might therefore be the earliest manifestations of problems in basic perception (Pellicano and Burr, 2012). Individuals on the autism spectrum (ASD) are less prone to experience illusory percepts than do neurotypical controls, suggesting they rely less on prior knowledge (Happé, 1999). Resulting detail-focused processing style reflects an inability to abstract and gives rise to exceptional sensory skills, along with sensory hypersensitivity and insistence on sameness (Happé and Frith, 2006). These characteristics

can be directly related to aberrant perceptual inference rooted in the absence of/inappropriate top-down signaling. Accordingly, in the absence of abstraction and context, bottom-up information is veridically mapped upstream the hierarchy (as PEs) and makes sensory learning increasingly difficult (Adams et al., 2013b). Functional and structural neuroanatomy established a contracted hierarchical architecture in ASD, especially in the DMN, while sensory-driven connectivity does not converge on transmodal areas, implying problems in building GMs (Hong et al., 2019). The DMN was proposed to signify top-down GM activity (Barrett, 2017) and the aIC, as part of the DMN, is indeed under-connected in ASD (Uddin and Menon, 2009). This highlights the role of limbic cortices such as the aIC for domain-general processing in explaining away bottom-up sensory input.

Our data ties into previous proposals on the etiology of ASD. Individuals must continuously modulate PE according to model evidence, a mechanism described as the precision account on ASD (Lawson et al., 2014). Therefore, dampened precision results in persistent underweighting of previous knowledge (hypopriors) at the face of sensory input and thereby lead to overestimation of the volatility of environmental statistics (i.e. overestimation of the volatility of cue-outcome contingencies). This was indeed demonstrated for individuals on ASD (Lawson et al., 2017). We introduce a pathway from $CE^{PKC\delta}$–NBM–aIC to modulate precision as a function of uncertainty by adjusting aIC model gain via SFC with downstream areas (i.e. pIC). Individuals on ASD show functional underconnectivity of anterior-posterior cortical connections, as well as diminished aIC–amygdala coupling (Cherkassky et al., 2006; Ebisch et al., 2011), implicating aberrant $CE^{PKC\delta}$–NBM–aIC signaling in an inability to recruit interoceptive models. Corroborating this view is recent data on the benzodiazepine (BDZ) action in the CEl, where $CE^{PKC\delta}$ is disinhibited by BDZ-mediated increased inhibitory drive onto CE^{SST} (Griessner et al., 2018). Resulting anxiolysis may be explained by augmented model recruitment, supported by evidence showing BZD-mediated acute rescue of social interaction behavior in a mouse model of autism (Defensor et al., 2011; Han et al., 2014). Along the same lines, the role of oxytocin (OXT) in ASD as a modulator of PE gain was discussed (Quattrocki, 2014). The prosocial effects of OXT as well as the enhanced emotional discrimination by OXT in CE (Ferretti et al., 2019) may also be in part $CE^{PKC\delta}$-mediated, as the OXT receptor is predominantly expressed on $CE^{PKC\delta}$ and increases firing of this cells type (Gozzi et al., 2010; Haubensak et al., 2010).

We tested this role of $CE^{PKC\delta}$ by ablating CEl cell types by ectopically expressing Caspase3 and subjecting mice to discriminatory PL. We found $CE^{PKC\delta}$-ablation impaired behavioral

discrimination compared to control animals (Fig. 8, left), arguing for failure in model recruitment in discriminatory learning.

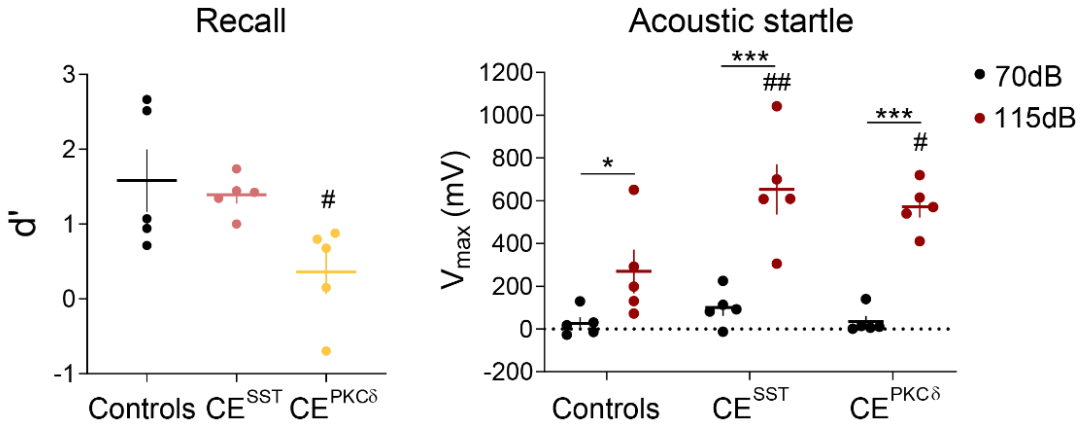

Figure 8 | Supplementary Data. Cell-type specific ablation in CEl by AAV-mediated caspase3 expression results in impairments in behavioral valence discrimination and sensorimotor gating. (Left) Discriminatory PL paradigm equivalent to Manuscript 1, Fig 1. Sensitivity index d' quantifes the behavioral discrimination between R-CS and F-CS, where zero means no difference. d' for approach behavior (port visits during R-CS vs F-CS) and avoidance behavior (freezing during F-CS vs R-CS) was averaged. $CE^{PKC\delta}$ show impairment in behavioral discrimination compared to controls. The effect was stronger in the avoidance domain (data not shown). One-way ANOVA, Holm-Sidak post hoc, #p<0.05. **(Right)** Auditory startle response assessing sensorimotor gating. CE^{SST} and $CE^{PKC\delta}$ display augmented startle responses, compared to controls. V_{max} quantifies the jumping force acting on the platform and is normalized to a baseline period. Two-way ANOVA, Holm-Sidak post hoc, * and # indicate significant differences within and between treatment groups, respectively, */#p<0.05, ##p<0.01, ***p.0.001.

The inability to recruit models may result in pervasive environmental salience and persistent PE signaling (Den Ouden et al., 2012). Individuals on the ASD do display sensory hyperreactivity and augmented startle responses (Kohl et al., 2014). By testing the acoustic startle reflex in CE^{SST}- and $CE^{PKC\delta}$-ablated cohorts we found augmented startle responses in both CEl populations, implicating the CEl in sensory gating (Fig. 8, right). This is in agreement with our observation that silencing the interoceptive GM in aIC results in enhanced salience of CSs during conditioning along with impaired CS discrimination (Manuscript 1, Fig. 5iii,iv). Collectively, we provide a mechanism for the established dysregulation in the salience network, a common neural signature of affective distress in many psychiatric disorders (McTeague et al., 2020).

Anxiety conditions have been associated with elevated PE signaling in the interoceptive system previously (Paulus and Stein, 2006, 2010), indicating an inability to build or recruit meaningful GMs, which may render withdrawal from the environment an adaptive behavioral strategy. Anxiety conditions are characterized by hyperactivity of aIC and amygdala in

humans (Stein et al., 2007), which at first glance is counterintuitive to the notion of aIC encoding the most domain-general GM. Possible explanations for aIC hyperactivity may be increased PE signaling in aIC itself, which could lead to functional network alterations, as observed in anxiety states (Tan et al., 2018). Under baseline conditions IC coupling is relatively stronger to the CE versus the bed nucleus of the stria terminalis (BNST) (Gorka et al., 2018), a region associated with anxiety and tonic fear (Davis et al., 2010; Walker and Davis, 2008; Yassa et al., 2012). To hypothesize, the inability to resolve uncertainty via the IC–CE pathway may lead to persistent PE signaling and subsequent relative switch to the IC–BNST pathway. The BNST is known to coordinate autonomic responses constituting an anxiety state (Kim et al., 2013). Therefore, tonic BNST engagement may represent a shift to 'model-free' anticipation of events that cannot be predicted and increase allostatic load. This hypothesis is supported by studies showing elevated BNST activity in anticipatory states and increase in IC–BNST coupling upon unpredictable shock in humans (Kinnison et al., 2012; Klumpers et al., 2017). Collectively, comorbid anxiety could be explained by the inability to build or recruit models for adaptive decision-making.

Concluding model of hierarchical affective learning

PL illustrates how brains create motivational drive in their interaction with the environment. Associative learning links pleasure and pain with increasingly complex predictive stimuli and patterns to navigate the world in behavioral episodes of approach and avoidance across timescales. This thesis proposes IPP across hierarchical levels as the core of affective states (Seth et al., 2012). Interoceptive predictions are being reduced in dimensionality into discrete stimulus features descending the hierarchy. This gives rise to PE minimization by active inference, manifesting in binary approach and avoidance behavior. In a sense, the IPP is at the interface between James-Lange and Schachter-Singer's two-factor theory of affect, as matching top-down predictions with bottom-up sensory input can be viewed as single-process appraisal mechanism (Quadt et al., 2018). At the same time, bottom-up information does carry meaning, however inferred from an interoceptive GM.

In this framework, learning is driven by errors in prediction, ascending from bottom up. The IC constructs GM by relating sensory events in the environment (CS, US). Unexpected sensory input (CS) drives $CE^{PKC\delta}$ recruitment of (a)IC via the cholinergic NBM, signaling value uncertainty. Subsequently, uncertainty is resolved by extraction of salience and valence

from the IC GM. Salience and valence dimensions, associated with the CS, are retained in the CE once deemed predictive of a significant event (CS-US pairing) by virtue of synaptic plasticity. The implementation of a successful US-predictive GM in the CE prevents further PE signaling by explaining away bottom-up information in the vPAG/DR.

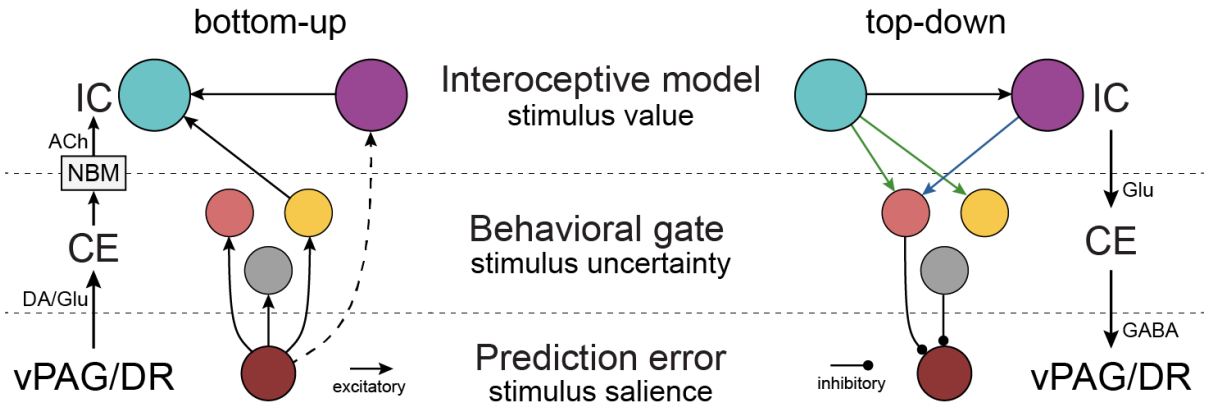

Figure 9 | Circuit operation and information flow during unexpected events (bottom-up) and model-based decision-making (top-down).

References

(Bud) Craig, A.D. (2009). How do you feel — now? The anterior insula and human awareness. Nat. Rev. Neurosci. *10*, 59–70.

Adams, R.A., Shipp, S., and Friston, K.J. (2013a). Predictions not commands: Active inference in the motor system. Brain Struct. Funct.

Adams, R.A., Stephan, K.E., Brown, H.R., Frith, C.D., and Friston, K.J. (2013b). The Computational Anatomy of Psychosis. Front. Psychiatry.

Adams, W.J., Graf, E.W., and Ernst, M.O. (2004). Experience can change the "light-from-above" prior. Nat. Neurosci. *7*, 1057–1058.

Akatsuka, K., Wasaka, T., Nakata, H., Kida, T., and Kakigi, R. (2007). The effect of stimulus probability on the somatosensory mismatch field. Exp. Brain Res.

Anderson, A.K., and Phelps, E.A. (2001). Lesions of the human amygdala impair enhanced perception of emotionally salient events. Nature *411*, 305–309.

Arnold, M.B. (1960). Emotion and Personality: Psychological Aspects (vol.1).

Azzalini, D., Rebollo, I., and Tallon-Baudry, C. (2019). Visceral Signals Shape Brain Dynamics and Cognition. Trends Cogn. Sci. *23*, 488–509.

Babayan, B.M., Uchida, N., and Gershman, S.J. (2018). Belief state representation in the dopamine system. Nat. Commun. *9*, 1891.

Badcock, P.B., Friston, K.J., Ramstead, M.J.D., Ploeger, A., and Hohwy, J. (2019). The hierarchically mechanistic mind: an evolutionary systems theory of the human brain, cognition, and behavior. Cogn. Affect. Behav. Neurosci. *19*, 1319–1351.

Badre, D. (2008). Cognitive control, hierarchy, and the rostro-caudal organization of the frontal lobes. Trends Cogn. Sci. *12*, 193–200.

Baldeweg, T. (2006). Repetition effects to sounds: Evidence for predictive coding in the auditory system [1]. Trends Cogn. Sci.

Balleine, B.W., and Killcross, S. (2006). Parallel incentive processing: an integrated view of amygdala function. Trends Neurosci. *29*, 272–279.

Bar, M., Kassam, K.S., Ghuman, A.S., Boshyan, J., Schmidt, A.M., Dale, A.M., Hämäläinen, M.S., Marinkovic, K., Schacter, D.L., Rosen, B.R., et al. (2006). Top-down facilitation of visual recognition. Proc. Natl. Acad. Sci. U. S. A. *103*, 449–454.

Barbas, H. (2015). General Cortical and Special Prefrontal Connections: Principles from Structure to Function. Annu. Rev. Neurosci. *38*, 269–289.

Barbas, H., and Rempel-Clower, N. (1997). Cortical structure predicts the pattern of corticocortical connections. Cereb. Cortex *7*, 635–646.

Barrett, L.F. (2011). Was darwin wrong about emotional expressions? Curr. Dir. Psychol. Sci. *20*, 400–406.

Barrett, L.F. (2017). The theory of constructed emotion: an active inference account of interoception and categorization. Soc. Cogn. Affect. Neurosci. *12*, 1–23.

Barrett, L.F., and Simmons, W.K. (2015). Interoceptive predictions in the brain. Nat. Rev. Neurosci. *16*, 419–429.

Barto, A., Mirolli, M., and Baldassarre, G. (2013). Novelty or Surprise? Front. Psychol. *4*.

Bastos, A.M., Vezoli, J., Bosman, C.A., Schoffelen, J.M., Oostenveld, R., Dowdall, J.R., DeWeerd, P., Kennedy, H., and Fries, P. (2015). Visual areas exert feedforward and feedback influences through distinct frequency channels. Neuron *85*, 390–401.

Bechara, A. (2004). The role of emotion in decision-making: Evidence from neurological patients with orbitofrontal damage. Brain Cogn.

Bechara, A., and Damasio, A.R. (2005). The somatic marker hypothesis: A neural theory of economic decision. Games Econ. Behav. *52*, 336–372.

Bechara, A., Damasio, A.R., Damasio, H., and Anderson, S.W. (1994). Insensitivity to future consequences following damage to human prefrontal cortex. Cognition *50*, 7–15.

Bechara, A., Tranel, D., Damasio, H., Adolphs, R., Rockland, C., and Damasio, A. (1995). Double dissociation of conditioning and declarative knowledge relative to the amygdala and hippocampus in humans. Science (80-.). *269*, 1115–1118.

Bechara, A., Tranel, D., Damasio, H., and Damasio, A.R. (1996). Failure to respond autonomically to anticipated future outcomes following damage to prefrontal cortex. Cereb. Cortex *6*, 215–225.

Bechara, A., Damasio, H., Tranel, D., and Damasio, A.R. (1997). Deciding advantageously before knowing the advantageous strategy. Science (80-.). *275*, 1293–1295.

Bechara, A., Damasio, H., Tranel, D., and Anderson, S.W. (1998). Dissociation of working memory from decision making within the human prefrontal cortex. J. Neurosci.

Berezovskii, V.K., Nassi, J.J., and Born, R.T. (2011). Segregation of feedforward and feedback projections in mouse visual cortex. J. Comp. Neurol. *519*, 3672–3683.

Berkes, P., Orbán, G., Lengyel, M., and Fiser, J. (2011). Spontaneous cortical activity reveals hallmarks of an optimal internal model of the environment. Science (80-.).

Berntson, G.G., Norman, G.J., Bechara, A., Bruss, J., Tranel, D., and Cacioppo, J.T. (2011). The insula and evaluative processes. Psychol. Sci. *22*, 80–86.

Berntson, G.G., Gianaros, P.J., and Tsakiris, M. (2018). Interoception and the autonomic nervous system: Bottom-up meets top-down. In The Interoceptive Mind: From Homeostasis to Awareness Manos, p.

Bosman, C.A., Schoffelen, J.M., Brunet, N., Oostenveld, R., Bastos, A.M., Womelsdorf, T., Rubehn, B., Stieglitz, T., De Weerd, P., and Fries, P. (2012). Attentional Stimulus Selection through Selective Synchronization between Monkey Visual Areas. Neuron.

Botta, P., Demmou, L., Kasugai, Y., Markovic, M., Xu, C., Fadok, J.P., Lu, T., Poe, M.M., Xu, L., Cook, J.M., et al. (2015). Regulating anxiety with extrasynaptic inhibition. Nat. Neurosci. *18*, 1493–1500.

Bucci, D.J., Holland, P.C., and Gallagher, M. (1998). Removal of cholinergic input to rat posterior parietal cortex disrupts incremental processing of conditioned stimuli. J. Neurosci.

Buchel, C., Morris, J., Dolan, R.J., Friston, K.J., and Street, R. (1998). Brain Systems Mediating Aversive Conditioning: an Event-Related fMRI Study. *20*, 947–957.

Buffalo, E.A., Fries, P., Landman, R., Buschman, T.J., and Desimone, R. (2011). Laminar differences in gamma and alpha coherence in the ventral stream. Proc. Natl. Acad. Sci. U. S. A.

Cabanac, M. (2002). What is emotion? Behav. Processes *6357*, 69–83.

Cacioppo, J.T., and Gardner, W.L. (1999). EMOTION. 191–214.

Cai, H., Haubensak, W., Anthony, T.E., and Anderson, D.J. (2014). Central amygdala PKC-δ+ neurons mediate the influence of multiple anorexigenic signals. Nat. Neurosci. *17*, 1240–1248.

Calder, A.J., Lawrence, A.D., and Young, A.W. (2001). Neuropsychology of fear and loathing. Nat. Rev. Neurosci. *2*, 352–363.

Cannon, W.B. (1927). The James-Lange Theory of Emotions: A Critical Examination and an Alternative Theory. Am. J. Psychol.

Cannon, W.B. (1931). Again the James-Lange and the thalamic theories of emotion. Psychol. Rev.

Cannon, W.B. (1939). The wisdom of the body, 2nd ed.

Ceunen, E., Vlaeyen, J.W.S., and Van Diest, I. (2016). On the origin of interoception. Front. Psychol. *7*, 1–17.

Chanes, L., and Barrett, L.F. (2016). Redefining the Role of Limbic Areas in Cortical Processing. Trends Cogn. Sci. *20*, 96–106.

Chen, T., Michels, L., Supekar, K., Kochalka, J., Ryali, S., and Menon, V. (2015). Role of the anterior insular cortex in integrative causal signaling during multisensory auditory-visual attention. Eur. J. Neurosci. *41*, 264–274.

Cherkassky, V.L., Kana, R.K., Keller, T.A., and Just, M.A. (2006). Functional connectivity in a baseline resting-state network in autism. Neuroreport *17*, 1687–1690.

Cho, J.R., Treweek, J.B., Robinson, J.E., Xiao, C., Bremner, L.R., Greenbaum, A., and Gradinaru, V. (2017). Dorsal Raphe Dopamine Neurons Modulate Arousal and Promote Wakefulness by Salient Stimuli. Neuron *94*, 1205–1219.e8.

Ciocchi, S., Herry, C., Grenier, F., Wolff, S.B.E., Letzkus, J.J., Vlachos, I., Ehrlich, I., Sprengel, R., Deisseroth, K., Stadler, M.B., et al. (2010). Encoding of conditioned fear in central amygdala inhibitory circuits. Nature *468*, 277–282.

Clark, A. (2013). Whatever next? Predictive brains, situated agents , and the future of cognitive science. Behav. Brain Sci. 181–253.

Cobos, P., Sánchez, M., García, C., Vera, M.N., and Vila, J. (2002). Revisiting the James versus Cannon debate on emotion: Startle and autonomic modulation in patients with spinal cord injuries. Biol. Psychol.

Cohen, J.Y., Haesler, S., Vong, L., Lowell, B.B., and Uchida, N. (2012). Neuron-type-specific signals for reward and punishment in the ventral tegmental area. Nature.

Collin, S.H.P., Milivojevic, B., and Doeller, C.F. (2015). Memory hierarchies map onto the hippocampal long axis in humans. Nat. Neurosci. *18*, 1562–1564.

Corbit, L.H. (2005). Double Dissociation of Basolateral and Central Amygdala Lesions on the General and Outcome-Specific Forms of Pavlovian-Instrumental Transfer. J. Neurosci. *25*, 962–970.

Craig, A.D. (2002). How do you feel? Interoception: the sense of the physiological condition of the body. Nat. Rev. Neurosci. *3*, 655–666.

Craig, A.D. (2003). Interoception: The sense of the physiological condition of the body. Curr. Opin. Neurobiol. *13*, 500–505.

Craig, A.D.B. (2011). Significance of the insula for the evolution of human awareness of feelings from the body. Ann. N. Y. Acad. Sci. *1225*, 72–82.

Craig, A.D., Chen, K., Bandy, D., and Reiman, E.M. (2000). Thermosensory activation of insular cortex. Nat. Neurosci.

Critchley, H.D. (2005). Neural mechanisms of autonomic, affective, and cognitive integration. J. Comp. Neurol. *493*, 154–166.

Critchley, H.D., and Garfinkel, S.N. (2017). Interoception and emotion. Curr. Opin. Psychol. *17*, 7–14.

Critchley, H.D., and Harrison, N.A. (2013). Visceral Influences on Brain and Behavior. Neuron *77*, 624–638.

Critchley, H.D., Corfield, D.R., Chandler, M.P., Mathias, C.J., and Dolan, R.J. (2000a). Cerebral correlates of autonomic cardiovascular arousal: A functional neuroimaging investigation in humans. J. Physiol. *523*, 259–270.

Critchley, H.D., Elliott, R., Mathias, C.J., and Dolan, R.J. (2000b). Neural activity relating to generation and representation of galvanic skin conductance responses: A functional magnetic resonance imaging study. J. Neurosci. *20*, 3033–3040.

Critchley, H.D., Mathias, C.J., and Dolan, R.J. (2001). Neuroanatomical basis for first-and second-order representations of bodily states. Nat. Neurosci. *4*, 207–212.

Critchley, H.D., Mathias, C.J., and Dolan, R.J. (2002). Fear Conditioning in Humans: The Influence of Awareness and Autonomic Arousal on Functional Neuroanatomy. Neuron *33*, 653–663.

Critchley, H.D., Wiens, S., Rotshtein, P., Öhman, A., and Dolan, R.J. (2004). Neural systems supporting interoceptive awareness. Nat. Neurosci. *7*, 189–195.

Damasio, A. (1994). Descartes' error: Emotion, rationality and the human brain. New York Putnam.

Damasio, A. (2003). Feelings of emotion and the self. In Annals of the New York Academy of Sciences, p.

Damasio, A.R. (1998). Emotion in the perspective of an integrated nervous system. Brain Res. Rev. *26*, 83–86.

Darwin, C. (1872). The Expression of the Emotions in Man and Animals (Chicago: Fontana Press).

Davis, M., Walker, D.L., Miles, L., and Grillon, C. (2010). Phasic vs sustained fear in rats and humans: role of the extended amygdala in fear vs anxiety. Neuropsychopharmacology *35*, 105–135.

Deen, B., Pitskel, N.B., and Pelphrey, K.A. (2011). Three Systems of Insular Functional Connectivity Identified with Cluster Analysis.

Defensor, E.B., Pearson, B.L., Pobbe, R.L.H., Bolivar, V.J., Blanchard, D.C., and Blanchard, R.J. (2011). A novel social proximity test suggests patterns of social avoidance and gaze aversion-like behavior in BTBR T+ tf/J mice. Behav. Brain Res.

Dickinson, A., and Pearce, J.M. (1977). Inhibitory interactions between appetitive and aversive stimuli. Psychol. Bull.

Dolan, R.J. (2002). Emotion, Cognition, and Behavior. *298*, 1191–1195.

Dunn, B.D., Dalgleish, T., and Lawrence, A.D. (2006). The somatic marker hypothesis: A critical evaluation. Neurosci. Biobehav. Rev. *30*, 239–271.

Duvarci, S., Popa, D., and Paré, D. (2011). Central amygdala activity during fear conditioning. J. Neurosci. *31*, 289–294.

Ebisch, S.J.H., Gallese, V., Willems, R.M., Mantini, D., Groen, W.B., Romani, G.L., Buitelaar, J.K., and Bekkering, H. (2011). Altered intrinsic functional connectivity of anterior and posterior insula regions in high-functioning participants with autism spectrum disorder. Hum. Brain Mapp.

Ekman, P. (1992). An Argument for Basic Emotions. Cogn. Emot.

Engel, A.K., Fries, P., and Singer, W. (2001). Dynamic predictions: Oscillations and synchrony in top–down processing. Nat. Rev. Neurosci.

Ernst, M., Bolla, K., Mouratidis, M., Contoreggi, C., Matochik, J.A., Kurian, V., Cadet, J.L., Kimes, A.S., and London, E.D. (2002). Decision-making in a risk-taking task: A PET study. Neuropsychopharmacology.

Eslinger PJ, and Damasio AR (1985). Severe disturbance of higher cognition after bilateral frontal lobe ablation: patient EVR. Neurology.

Fadok, J.P., Krabbe, S., Markovic, M., Courtin, J., Xu, C., Massi, L., Botta, P., Bylund, K., Müller, C., Kovacevic, A., et al. (2017). A competitive inhibitory circuit for selection of active and passive fear responses. Nature *542*, 96–99.

Fadok, J.P., Markovic, M., Tovote, P., and Lüthi, A. (2018). New perspectives on central amygdala function. Curr. Opin. Neurobiol. *49*, 141–147.

Feldman, H., and Friston, K.J. (2010). Attention , uncertainty , and free-energy. *4*, 1–23.

Felleman, D., and Van Essen, D. (1991). Distributed hierarchical processing in the primate cerebral cortex. Cereb. Cortex *1*, 1–47.

Ferretti, V., Maltese, F., Contarini, G., Nigro, M., Bonavia, A., Huang, H., Gigliucci, V., Morelli, G., Scheggia, D., Manago`, F., et al. (2019). Oxytocin Signaling in the Central Amygdala Modulates Emotion Discrimination in Mice. Curr. Biol. *In press*, 1938–1953.

Fisahn, A., Yamada, M., Duttaroy, A., Gan, J.W., Deng, C.X., McBain, C.J., and Wess, J. (2002). Muscarinic induction of hippocampal gamma oscillations requires coupling of the M1 receptor to two mixed cation currents. Neuron *33*, 615–624.

Konorski, J. (1967). Integrative Activity of the Brain. An Interdisciplinary Approach. Q. Rev. Biol.

Friston, K. (2003). Learning and inference in the brain. Neural Networks.

Friston, K. (2005). A theory of cortical responses. Philos. Trans. R. Soc. B Biol. Sci. *360*, 815–836.

Friston, K. (2008). Hierarchical models in the brain. PLoS Comput. Biol. *4*.

Friston, K. (2009). The free-energy principle: a rough guide to the brain? Trends Cogn. Sci. *13*, 293–301.

Friston, K. (2010). The free-energy principle: A unified brain theory? Nat. Rev. Neurosci. *11*, 127–138.

Friston, K., Kilner, J., and Harrison, L. (2006). A free energy principle for the brain. J. Physiol. Paris *100*, 70–87.

Friston, K.J., Shiner, T., FitzGerald, T., Galea, J.M., Adams, R., Brown, H., Dolan, R.J., Moran, R., Stephan, K.E., and Bestmann, S. (2012). Dopamine, affordance and active inference. PLoS Comput. Biol.

Gallagher, M., Graham, P., and Holland, P. (1990). The amygdala central nucleus and appetitive Pavlovian conditioning: lesions impair one class of conditioned behavior. J. Neurosci. *10*, 1906–1911.

Gendron, M., and Feldman Barrett, L. (2009). Reconstructing the past: A century of ideas about emotion in psychology. Emot. Rev. *1*, 316–339.

Geuter, S., Boll, S., Eippert, F., and Büchel, C. (2017). Functional dissociation of stimulus intensity encoding and predictive coding of pain in the insula. Elife *6*, 1–22.

Ghaziri, J., Tucholka, A., Girard, G., Boucher, O., Houde, J.-C., Descoteaux, M., Obaid, S., Gilbert, G., Rouleau, I., and Nguyen, D.K. (2018). Subcortical structural connectivity of insular subregions. Sci. Rep. *8*, 8596.

Goosens, K.A. (2001). Contextual and Auditory Fear Conditioning are Mediated by the Lateral, Basal, and Central Amygdaloid Nuclei in Rats. Learn. Mem. *8*, 148–155.

Gore, F., Schwartz, E.C., Brangers, B.C., Aladi, S., Stujenske, J.M., Likhtik, E., Russo, M.J., Gordon, J.A., Salzman, C.D., and Axel, R. (2015). Neural Representations of Unconditioned Stimuli in Basolateral Amygdala Mediate Innate and Learned Responses. Cell *162*, 134–145.

Gorka, A.X., Torrisi, S., Shackman, A.J., Grillon, C., and Ernst, M. (2018). Intrinsic functional connectivity of the central nucleus of the amygdala and bed nucleus of the stria terminalis. Neuroimage *168*, 392–402.

Gozzi, A., Jain, A., Giovanelli, A., Bertollini, C., Crestan, V., Schwarz, A.J., Tsetsenis, T., Ragozzino, D., Gross, C.T., and Bifone, A. (2010). A neural switch for active and passive fear. Neuron *67*, 656–666.

Grewe, B.F., Gründemann, J., Kitch, L.J., Lecoq, J.A., Parker, J.G., Marshall, J.D., Larkin, M.C., Jercog, P.E., Grenier, F., Li, J.Z., et al. (2017). Neural ensemble dynamics underlying a long-term associative memory. Nature *543*, 670–675.

Griessner, J., Pasieka, M., Böhm, V., Grössl, F., Kaczanowska, J., Pliota, P., Kargl, D., Werner, B., Kaouane, N., Strobelt, S., et al. (2018). Central amygdala circuit dynamics underlying the benzodiazepine anxiolytic effect. Mol. Psychiatry.

Griffith, J.L. (1998). Disorders of Affect Regulation: Alexithymia in Medical and Psychiatric Illness. Psychosomatics.

Grinband, J., Hirsch, J., and Ferrera, V.P. (2006). A neural representation of categorization uncertainty in the human brain. Neuron *49*, 757–763.

Gritton, H.J., Howe, W.M., Mallory, C.S., Hetrick, V.L., Berke, J.D., and Sarter, M. (2016). Cortical cholinergic signaling controls the detection of cues. Proc. Natl. Acad. Sci. *113*, E1089–E1097.

Groessl, F., Munsch, T., Meis, S., Griessner, J., Kaczanowska, J., Pliota, P., Kargl, D., Badurek, S., Kraitsy, K., Rassoulpour, A., et al. (2018). Dorsal tegmental dopamine neurons gate associative learning of fear. Nat. Neurosci.

Hadjipapas, A., Lowet, E., Roberts, M.J., Peter, A., and De Weerd, P. (2015). Parametric variation of gamma frequency and power with luminance contrast: A comparative study of human MEG and monkey LFP and spike responses. Neuroimage.

Han, J.S., Holland, P.C., and Gallagher, M. (1999). Disconnection of the amygdala central nucleus and substantia innominata/nucleus basalis disrupts increments in conditioned stimulus processing in rats. Behav. Neurosci. *113*, 143–151.

Han, S., Tai, C., Jones, C.J., Scheuer, T., and Catterall, W.A. (2014). Enhancement of inhibitory neurotransmission by GABAA receptors having α2,3-subunits ameliorates behavioral deficits in a mouse model of autism. Neuron.

Han, W., Tellez, L.A., Rangel, M.J., Motta, S.C., Zhang, X., Perez, I.O., Canteras, N.S., Shammah-Lagnado, S.J., van den Pol, A.N., and de Araujo, I.E. (2017). Integrated Control of Predatory Hunting by the Central Nucleus of the Amygdala. Cell *168*, 311–324.e18.

Hangya, B., Ranade, S.P., Lorenc, M., and Kepecs, A. (2015). Central Cholinergic Neurons Are Rapidly Recruited by Reinforcement Feedback. Cell *162*, 1155–1168.

Happé, F. (1999). Autism: Cognitive deficit or cognitive style? Trends Cogn. Sci.

Happé, F., and Frith, U. (2006). The weak coherence account: Detail-focused cognitive style in autism spectrum disorders. J. Autism Dev. Disord. *36*, 5–25.

Harris, J.A., Mihalas, S., Hirokawa, K.E., Whitesell, J.D., Choi, H., Bernard, A., Bohn, P., Caldejon, S., Casal, L., Cho, A., et al. (2019). Hierarchical organization of cortical and thalamic connectivity. Nature *575*, 195–202.

Harrison, N.A., Gray, M.A., Gianaros, P.J., and Critchley, H.D. (2010). The embodiment of emotional feelings in the brain. J. Neurosci. *30*, 12878–12884.

Hartley, N.D., Gaulden, A.D., Báldi, R., Winters, N.D., Salimando, G.J., Rosas-Vidal, L.E., Jameson, A., Winder, D.G., and Patel, S. (2019). Dynamic remodeling of a basolateral-to-central amygdala glutamatergic circuit across fear states. Nat. Neurosci. *22*, 2000–2012.

Hasue, R.H., and Shammah-Lagnado, S.J. (2002). Origin of the dopaminergic innervation of the central extended amygdala and accumbens shell: A combined retrograde tracing and immunohistochemical study in the rat. J. Comp. Neurol.

Haubensak, W., Kunwar, P.S., Cai, H., Ciocchi, S., Wall, N.R., Ponnusamy, R., Biag, J., Dong, H.-W., Deisseroth, K., Callaway, E.M., et al. (2010). Genetic dissection of an amygdala microcircuit that gates conditioned fear. Nature *468*, 270–276.

Heims, H.C., Critchley, H.D., Dolan, R., Mathias, C.J., and Cipolotti, L. (2004). Social and motivational functioning is not critically dependent on feedback of autonomic responses: Neuropsychological evidence from patients with pure autonomic failure. Neuropsychologia.

Helmholtz, H. von (1867) Handbuch der physiologischen Optik. Leopold Voss.

Herbert, B.M., Herbert, C., and Pollatos, O. (2011). On the relationship between interoceptive awareness and alexithymia: Is interoceptive awareness related to emotional awareness? J. Pers. *79*, 1149–1175.

Hesse, C., and Floyd, K. (2008). Affectionate experience mediates the effects of alexithymia on mental health and interpersonal relationships. J. Soc. Pers. Relat.

Hill, E., Berthoz, S., and Frith, U. (2004). Brief report: Cognitive processing of own emotions in individuals with autistic spectrum disorder and in their relatives. J. Autism Dev. Disord.

Hochstein, S., and Ahissar, M. (2002). View from the top: Hierarchies and reverse hierarchies in the visual system. Neuron.

Hogarth, L., Dickinson, A., Austin, A., Brown, C., and Duka, T. (2008). Attention and expectation in human predictive learning: The role of uncertainty. Q. J. Exp. Psychol.

Hohwy, J. (2007). Functional integration and the mind. Synthese.

Holland, P.C., and Gallagher, M. (1993). Amygdala Central Nucleus Lesions Disrupt Increments, But Not Decrements, in Conditioned Stimulus Processing. Behav. Neurosci.

Holland, P.C., and Gallagher, M. (1999). Amygdala circuitry in attentional and representational processes. Trends Cogn. Sci. *3*, 65–73.

Hong, S.J., de Wael, R.V., Bethlehem, R.A.I., Lariviere, S., Paquola, C., Valk, S.L., Milham, M.P., Di Martino, A., Margulies, D.S., Smallwood, J., et al. (2019). Atypical functional connectome hierarchy in autism. Nat. Commun.

Hubel, D.H., and Wiesel, T.N. (1959). Receptive fields of single neurones in the cat's striate cortex. J. Physiol.

Isosaka, T., Matsuo, T., Yamaguchi, T., Funabiki, K., Nakanishi, S., Kobayakawa, R., and Kobayakawa, K. (2015). Htr2a-Expressing Cells in the Central Amygdala Control the Hierarchy between Innate and Learned Fear. Cell *163*, 1153–1164.

James, W. (1884). What is an emotion? Mind *9*, 188–205.

Joffily, M., and Coricelli, G. (2013). Emotional Valence and the Free-Energy Principle. PLoS Comput. Biol. *9*.

Kamin, L.J. (1969). Predictability, surprise, attention and conditioning. Punishm. Aversive Behav.

Kaye, H., and Pearce, J.M. (1984). The strength of the orienting response during Pavlovian conditioning. J. Exp. Psychol. Anim. Behav. Process.

Keller, G.B., and Mrsic-Flogel, T.D. (2018). Predictive Processing: A Canonical Cortical Computation. Neuron *100*, 424–435.

Kim, J., Zhang, X., Muralidhar, S., LeBlanc, S.A., and Tonegawa, S. (2017). Basolateral to Central Amygdala Neural Circuits for Appetitive Behaviors. Neuron *93*, 1464–1479.e5.

Kim, S.Y., Adhikari, A., Lee, S.Y., Marshel, J.H., Kim, C.K., Mallory, C.S., Lo, M., Pak, S., Mattis, J., Lim, B.K., et al. (2013). Diverging neural pathways assemble a behavioural state from separable features in anxiety. Nature *496*, 219–223.

Kinnison, J., Padmala, S., Choi, J.M., and Pessoa, L. (2012). Network analysis reveals increased integration during emotional and motivational processing. J. Neurosci. *32*, 8361–8372.

Kleckner, I.R., Zhang, J., Touroutoglou, A., Chanes, L., Xia, C., Simmons, W.K., Quigley, K.S., Dickerson, B.C., and Feldman Barrett, L. (2017). Evidence for a large-scale brain system supporting allostasis and interoception in humans. Nat. Hum. Behav. *1*.

Klumpers, F., Kroes, M.C.W., Baas, J.M.P., and Fernández, G. (2017). How Human Amygdala and Bed Nucleus of the Stria Terminalis May Drive Distinct Defensive Responses. J. Neurosci. *37*, 9645–9656.

Koechlin, E., and Jubault, T. (2006). Broca's Area and the Hierarchical Organization of Human Behavior. Neuron *50*, 963–974.

Kohl, S., Wolters, C., Gruendler, T.O.J., Vogeley, K., Klosterkötter, J., and Kuhn, J. (2014). Prepulse inhibition of the acoustic startle reflex in high functioning autism. PLoS One *9*.

Lakatos, P., Chen, C.M., O'Connell, M.N., Mills, A., and Schroeder, C.E. (2007). Neuronal Oscillations and Multisensory Interaction in Primary Auditory Cortex. Neuron.

Lamm, C., and Singer, T. (2010). The role of anterior insular cortex in social emotions. Brain Struct. Funct.

de Lange, F.P., Heilbron, M., and Kok, P. (2018). How Do Expectations Shape Perception? Trends Cogn. Sci. *22*, 764–779.

Lawson, R.P., Rees, G., and Friston, K.J. (2014). An aberrant precision account of autism. Front. Hum. Neurosci. *8*, 1–10.

Lawson, R.P., Mathys, C., and Rees, G. (2017). Adults with autism overestimate the volatility of the sensory environment. Nat. Neurosci. *20*, 1293–1299.

LeDoux, J. (1995). Emotion: clues from the brain. Annu. Rev. Psychol. *46*, 209–235.

LeDoux, J. (2003). The emotional brain, fear, and the amygdala. Cell. Mol. Neurobiol. *23*, 727–738.

LeDoux, J.E. (2000). Emotion circuits in the brain. Annu. Rev. Neurosci. *23*, 155–184.

LeDoux, J.E., Iwata, J., Cicchetti, P., and Reis, D.J. (1988). Different projections of the central amygdaloid nucleus mediate autonomic and behavioral correlates of conditioned fear. J. Neurosci. *8*, 2517–2529.

Leweke, F., Leichsenring, F., Kruse, J., and Hermes, S. (2011). Is alexithymia associated with specific mental disorders? Psychopathology *45*, 22–28.

Li, H., Penzo, M. a, Taniguchi, H., Kopec, C.D., Huang, Z.J., and Li, B. (2013). Experience-dependent modification of a central amygdala fear circuit. Nat. Neurosci.

Livneh, Y., Sugden, A.U., Madara, J.C., Essner, R.A., Flores, V.I., Sugden, L.A., Resch, J.M., Lowell, B.B., and Andermann, M.L. (2020). Estimation of Current and Future Physiological States in Insular Cortex. Neuron 1–18.

Lord, C., Risi, S., Lambrecht, L., Cook, E.H., Leventhal, B.L., Dilavore, P.C., Pickles, A., and Rutter, M. (2000). The Autism Diagnostic Observation Schedule-Generic: A standard measure of social and communication deficits associated with the spectrum of autism. J. Autism Dev. Disord.

Lyvers, M., Duric, N., and Thorberg, F.A. (2014). Caffeine Use and Alexithymia in University Students. J. Psychoactive Drugs.

Ma, W.J., Beck, J.M., Latham, P.E., and Pouget, A. (2006). Bayesian inference with probabilistic population codes. Nat. Neurosci. *9*, 1432–1438.

MacLean, P.D. (1949). Psychosomatic disease and the visceral brain; recent developments bearing on the Papez theory of emotion. Psychosom. Med. *11*, 338–353.

Mailis-Gagnon, A., and Furlan, A.D. (2002). Sympathectomy for neuropathic pain. In Cochrane Database of Systematic Reviews, p.

Manes, F., Sahakian, B., Clark, L., Rogers, R., Antoun, N., Aitken, M., and Robbins, T. (2002). Decision-making processes following damage to the prefrontal cortex. Brain.

Markov, N.T., Vezoli, J., Chameau, P., Falchier, A., Quilodran, R., Huissoud, C., Lamy, C., Misery, P., Giroud, P., Ullman, S., et al. (2014). Anatomy of hierarchy: Feedforward and feedback pathways in macaque visual cortex. J. Comp. Neurol. *522*, 225–259.

Mazzola, L., Isnard, J., Peyron, R., and Mauguire, F. (2012). Stimulation of the human cortex and the experience of pain: Wilder Penfield's observations revisited. Brain *135*, 631–640.

McTeague, L.M., Rosenberg, B.M., Lopez, J.W., Carreon, D.M., Huemer, J., Jiang, Y., Chick, C.F., Eickhoff, S.B., and Etkin, A. (2020). Identification of Common Neural Circuit Disruptions in Emotional Processing Across Psychiatric Disorders. Am. J. Psychiatry.

Menon, V., and Uddin, L.Q. (2010). Saliency, switching, attention and control: a network model of insula function. Brain Struct. Funct. 1–13.

Mesulam, M.M. (1998). From sensation to cognition. Brain *121*, 1013–1052.

Moran, R.J., Campo, P., Symmonds, M., Stephan, K.E., Dolan, R.J., and Friston, K.J. (2013). Free energy, precision and learning: The role of cholinergic neuromodulation. J. Neurosci.

Moran, S.P., DIckerson, J.W., Cho, H.P., Xiang, Z., Maksymetz, J., Remke, D.H., Lv, X., Doyle, C.A., Rajan, D.H., Niswender, C.M., et al. (2018). M1-positive allosteric modulators lacking agonist activity provide the optimal profile for enhancing cognition. Neuropsychopharmacology *43*, 1763–1771.

Morel, A., Gallay, M.N., Baechler, A., Wyss, M., and Gallay, D.S. (2013). The human insula: Architectonic organization and postmortem MRI registration. Neuroscience.

Mottron, L., Dawson, M., Soulières, I., Hubert, B., and Burack, J. (2006). Enhanced perceptual functioning in autism: An update, and eight principles of autistic perception. J. Autism Dev. Disord. *36*, 27–43.

Muñoz, W., and Rudy, B. (2014). Spatiotemporal specificity in cholinergic control of neocortical function. Curr. Opin. Neurobiol. *26*, 149–160.

Murray, J.E., Belin-Rauscent, A., Simon, M., Giuliano, C., Benoit-Marand, M., Everitt, B.J., and Belin, D. (2015). Basolateral and central amygdala differentially recruit and maintain dorsolateral striatumdependent cocaine-seeking habits. Nat. Commun. *6*, 1–9.

Nemiah, J.C., Freyberger, H.J., and Sifneos, P.E. (1976). Alexithymia: A view of the psychosomatic process. In Modern Trends in Psychosomatic Medicine, p.

Nieuwenhuys, R. (2012). The insular cortex. A review. (Elsevier B.V.).

Nowakowski, M.E., McFarlane, T., and Cassin, S. (2013). Alexithymia and eating disorders: A critical review of the literature. J. Eat. Disord.

Den Ouden, H.E.M., Friston, K.J., Daw, N.D., McIntosh, A.R., and Stephan, K.E. (2009). A dual role for prediction error in associative learning. Cereb. Cortex.

Den Ouden, H.E.M., Kok, P., and de Lange, F.P. (2012). How prediction errors shape perception, attention, and motivation. Front. Psychol. *3*, 1–12.

Parr, T., and Friston, K.J. (2017). Uncertainty, epistemics and active Inference. J. R. Soc. Interface.

Paulus, M.P., and Stein, M.B. (2006). An Insular View of Anxiety. Biol. Psychiatry *60*, 383–387.

Paulus, M.P., and Stein, M.B. (2010). Interoception in anxiety and depression. Brain Struct. Funct. *214*, 451–463.

Pavlov, I. (1911). The Work of the Digestive Glands. J. Am. Med. Assoc. *LVI*, 1349.

Pearce, J.M., and Hall, G. (1980). A model for Pavlovian learning: Variations in the effectiveness of conditioned but not of unconditioned stimuli. Psychol. Rev.

Pellicano, E., and Burr, D. (2012). When the world becomes “too real”: A Bayesian explanation of autistic perception. Trends Cogn. Sci. *16*, 504–510.

Pendl, S.L., Salzwedel, A.P., Goldman, B.D., Barrett, L.F., Lin, W., Gilmore, J.H., and Gao, W. (2017). Emergence of a hierarchical brain during infancy reflected by stepwise functional connectivity. Hum. Brain Mapp. *38*, 2666–2682.

Penfield, W., and Faulk, M.E. (1955). The insula: Further observations on its function. Brain.

Penzo, M.A., Robert, V., and Li, B. (2014). Fear conditioning potentiates synaptic transmission onto long-range projection neurons in the lateral subdivision of central amygdala. J. Neurosci. *34*, 2432–2437.

Perry, E.K., Lee, M.L.W., Martin-Ruiz, C.M., Court, J.A., Volsen, S.G., Merrit, J., Folly, E., Iversen, P.E., Bauman, M.L., Perry, R.H., et al. (2001). Cholinergic activity in autism: Abnormalities in the cerebral cortex and basal forebrain. Am. J. Psychiatry *158*, 1058–1066.

Pessoa, L. (2008). On the relationship between emotion and cognition. Nat. Rev. Neurosci. *9*, 148–158.

Peters, A., Payne, B.R., and Budd, J. (1994). A numerical analysis of the geniculocortical input to striate cortex in the monkey. Cereb. Cortex.

Pezzulo, G., Rigoli, F., and Friston, K.J. (2018). Hierarchical Active Inference: A Theory of Motivated Control. Trends Cogn. Sci.

Phan, K.L., Wager, T., Taylor, S.F., and Liberzon, I. (2002). Functional neuroanatomy of emotion: A meta-analysis of emotion activation studies in PET and fMRI. Neuroimage *16*, 331–348.

Pollatos, O., and Schandry, R. (2008). Emotional processing and emotional memory are modulated by interoceptive awareness. Cogn. Emot.

Quadt, L., Critchley, H.D., and Garfinkel, S.N. (2018). Interoception and emotion: Shared mechanisms and clinical implications (Oxford University Press).

Quattrocki, E., and Friston, K. (2014). Autism, oxytocin and interoception. Neurosci. Biobehav. Rev. *47*, 410–430.

Ramachandran, V.S. (1988). Perceiving shape from shading. Sci. Am.

Rauss, K., and Pourtois, G. (2013). What is bottom-up and what is top-down in predictive coding. Front. Psychol. *4*, 1–8.

Rescorla, R.A., and Wagner, A.R. (1972). A Theory of Pavlovian Conditioning: Variations in the Effectiveness of Reinforcement and Nonreinforcement BT - Clasical conditioning II: current research and theory. Clasical Cond. II Curr. Res. Theory.

Rickenbacher, E., Perry, R.E., Sullivan, R.M., and Moita, M.A. (2017). Freezing suppression by oxytocin in central amygdala allows alternate defensive behaviours and mother-pup interactions. Elife *6*, 1–17.

Roesch, M.R., Esber, G.R., Li, J., Daw, N.D., and Schoenbaum, G. (2012). Surprise! Neural correlates of Pearce-Hall and Rescorla-Wagner coexist within the brain. Eur. J. Neurosci. *35*, 1190–1200.

Roy, M., Shohamy, D., Daw, N., Jepma, M., Wimmer, G.E., and Wager, T.D. (2014). Representation of aversive prediction errors in the human periaqueductal gray. Nat. Neurosci. *17*, 1607–1612.

Russel, J. (1980). A Circumplex Model of Affect. J. Pers. Soc. Psychol. *39*, 1161–1178.

Sanford, C.A., Soden, M.E., Baird, M.A., Miller, S.M., Schulkin, J., Palmiter, R.D., Clark, M., and Zweifel, L.S. (2017). A Central Amygdala CRF Circuit Facilitates Learning about Weak Threats. Neuron *93*, 164–178.

Saper, C.B. (2002). The Central Autonomic Nervous System: Conscious Visceral Perception and Autonomic Pattern Generation. Annu. Rev. Neurosci. *25*, 433–469.

Sarinopoulos, I., Grupe, D.W., Mackiewicz, K.L., Herrington, J.D., Lor, M., Steege, E.E., and Nitschke, J.B. (2010). Uncertainty during anticipation modulates neural responses to aversion in human insula and amygdala. Cereb. Cortex *20*, 929–940.

Sarter, M., Lustig, C., Howe, W.M., Gritton, H., and Berry, A.S. (2014). Deterministic functions of cortical acetylcholine. Eur. J. Neurosci. *39*, 1912–1920.

Schachter, S., and Singer, J. (1962). Cognitive, social, and physiological determinants of emotional state. Psychol. Rev.

Schandry, R. (1981). Heart Beat Perception and Emotional Experience. Psychophysiology.

Schulkin, J., and Sterling, P. (2019). Allostasis: A Brain-Centered, Predictive Mode of Physiological Regulation. Trends Neurosci. *42*, 740–752.

Schultz, W. (1997). Dopamine neurons and their role in reward mechanisms. Curr. Opin. Neurobiol.

Seeley, W.W., Menon, V., Schatzberg, A.F., Keller, J., Glover, G.H., Kenna, H., Reiss, A.L., and Greicius, M.D. (2007). Dissociable Intrinsic Connectivity Networks for Salience Processing and Executive Control. J. Neurosci. *27*, 2349–2356.

Segerdahl, A.R., Mezue, M., Okell, T.W., Farrar, J.T., and Tracey, I. (2015). The dorsal posterior insula subserves a fundamental role in human pain. Nat. Neurosci. *18*, 499–500.

Sepulcre, J., Sabuncu, M.R., Yeo, T.B., Liu, H., and Johnson, K.A. (2012). Stepwise connectivity of the modal cortex reveals the multimodal organization of the human brain. J. Neurosci. *32*, 10649–10661.

Seth, A.K. (2013). Interoceptive inference, emotion, and the embodied self. Trends Cogn. Sci. *17*, 565–573.

Seth, A.K., and Critchley, H.D. (2013). Extending predictive processing to the body: Emotion as interoceptive inference. Behav. Brain Sci.

Seth, A.K., and Friston, K.J. (2016). Active interoceptive inference and the emotional brain. Philos. Trans. R. Soc. B Biol. Sci. *371*, 20160007.

Seth, A.K., Suzuki, K., and Critchley, H.D. (2012). An Interoceptive Predictive Coding Model of Conscious Presence. Front. Psychol. *2*, 1–16.

Shabel, S.J., and Janak, P.H. (2009). Substantial similarity in amygdala neuronal activity during conditioned appetitive and aversive emotional arousal. Proc. Natl. Acad. Sci. *106*, 15031–15036.

Shah, P., Catmur, C., and Bird, G. (2016). Emotional decision-making in autism spectrum disorder: the roles of interoception and alexithymia. Mol. Autism *7*, 43.

Shallice, T., and Burgess, P. (1991). Deficits in strategy application following frontal lobe damage in man. Brain *114*, 727–741.

Sharpe, M.J., Chang, C.Y., Liu, M.A., Batchelor, H.M., Mueller, L.E., Jones, J.L., Niv, Y., and Schoenbaum, G. (2017). Dopamine transients are sufficient and necessary for acquisition of model-based associations. *20*.

Sherrington, C. (1907). The Integrative Action of the Nervous System. J. Nerv. Ment. Dis.

Shipp, S., Adams, R.A., and Friston, K.J. (2013). Reflections on agranular architecture: Predictive coding in the motor cortex. Trends Neurosci. *36*, 706–716.

Shizgal (1999). On the Neural Computation of Utility: Implications from Studies of Brain Stimulation Reward. In Well-Being: The Foundations of Hedonic Psychology, p.

Sigurdsson, T., Doyère, V., Cain, C.K., and LeDoux, J.E. (2007). Long-term potentiation in the amygdala: a cellular mechanism of fear learning and memory. Neuropharmacology *52*, 215–227.

Sridharan, D., Levitin, D.J., and Menon, V. (2008). A critical role for the right fronto-insular cortex in switching between central-executive and default-mode networks. Proc. Natl. Acad. Sci. U. S. A. *105*, 12569–12574.

Stein, M.B., Simmons, A.N., Feinstein, J.S., and Paulus, M.P. (2007). Increased amygdala and insula activation during emotion processing in anxiety-prone subjects. Am. J. Psychiatry.

von Stein, A., Chiang, C., and Konig, P. (2000). Top-down processing mediated by interareal synchronization. Proc. Natl. Acad. Sci. *97*, 14748–14753.

Sterling, P. (2012). Allostasis: A model of predictive regulation. Physiol. Behav. *106*, 5–15.

Swan, J.A., and Pearce, J.M. (1988). The Orienting Response as an Index of Stimulus Associability in Rats. J. Exp. Psychol. Anim. Behav. Process.

Takahashi, Y.K., Roesch, M.R., Wilson, R.C., Toreson, K., O'Donnell, P., Niv, Y., and Schoenbaum, G. (2011). Expectancy-related changes in firing of dopamine neurons depend on orbitofrontal cortex. Nat. Neurosci.

Tan, Y., Wei, D., Zhang, M., Yang, J., Jelinčić, V., and Qiu, J. (2018). The role of mid-insula in the relationship between cardiac interoceptive attention and anxiety: evidence from an fMRI study. Sci. Rep.

Terburg, D., Scheggia, D., Triana del Rio, R., Klumpers, F., Ciobanu, A.C., Morgan, B., Montoya, E.R., Bos, P.A., Giobellina, G., van den Burg, E.H., et al. (2018). The Basolateral Amygdala Is Essential for Rapid Escape: A Human and Rodent Study. Cell *175*, 723–735.e16.

Thorberg, F.A., Young, R.M.D., Sullivan, K.A., and Lyvers, M. (2009). Alexithymia and alcohol use disorders: A critical review. Addict. Behav.

Todorovic, A., and de Lange, F.P. (2012). Repetition suppression and expectation suppression are dissociable in time in early auditory evoked fields. J. Neurosci.

Tovote, P., Esposito, M.S., Botta, P., Chaudun, F., Fadok, J.P., Markovic, M., Wolff, S.B.E., Ramakrishnan, C., Fenno, L., Deisseroth, K., et al. (2016). Midbrain circuits for defensive behaviour. Nature.

Tranel, D., and Damasio, H. (1994). Neuroanatomical correlates of electrodermal skin conductance responses. Psychophysiology *31*, 427–438.

Tse, P.U., and Cavanagh, P. (2000). Chinese and Americans see opposite apparent motions in a Chinese character. Cognition.

Uddin, L.Q. (2014). Salience processing and insular cortical function and dysfunction. Nat. Rev. Neurosci. *16*, 55–61.

Uddin, L.Q., and Menon, V. (2009). The anterior insula in autism: Under-connected and under-examined. Neurosci. Biobehav. Rev. *33*, 1198–1203.

Van Der Velde, J., Swart, M., Van Rijn, S., Van Der Meer, L., Wunderink, L., Wiersma, D., Krabbendam, L., Bruggeman, R., and Aleman, A. (2015). Cognitive alexithymia is associated with the degree of risk for psychosis. PLoS One *10*, 1–13.

Vincis, R., and Fontanini, A. (2016). Associative learning changes cross-modal representations in the gustatory cortex. Elife *5*, 1–24.

Walker, D.L., and Davis, M. (2008). Role of the extended amygdala in short-duration versus sustained fear: a tribute to Dr. Lennart Heimer. Brain Struct. Funct. *213*, 29–42.

Wundt, W. (1894). Grundzuge der Physiologischen Psychologie. Am. J. Psychol.

Yassa, M.A., Hazlett, R.L., Stark, C.E.L., and Hoehn-Saric, R. (2012). Functional MRI of the amygdala and bed nucleus of the stria terminalis during conditions of uncertainty in generalized anxiety disorder. J. Psychiatr. Res.

Yohn, S.E., and Conn, P.J. (2018). Positive allosteric modulation of M1 and M4 muscarinic receptors as potential therapeutic treatments for schizophrenia. Neuropharmacology *136*, 438–448.

Yu, A.J., and Dayan, P. (2005). Uncertainty, neuromodulation, and attention. Neuron *46*, 681–692.

Zaki, J., Davis, J.I., and Ochsner, K.N. (2012). Overlapping activity in anterior insula during interoception and emotional experience. Neuroimage *62*, 493–499.

Zhang, K., Chen, C.D., and Monosov, I.E. (2019). Novelty, Salience, and Surprise Timing Are Signaled by Neurons in the Basal Forebrain. Curr. Biol. *29*, 134–142.e3.

Zhang, S., Xu, M., Kamigaki, T., Do, J.P.H., Chang, W.C., Jenvay, S., Miyamichi, K., Luo, L., and Dan, Y. (2014). Long-range and local circuits for top-down modulation of visual cortex processing. Science (80-.).

Zimmerman, C.A., Lin, Y.C., Leib, D.E., Guo, L., Huey, E.L., Daly, G.E., Chen, Y., and Knight, Z.A. (2016). Thirst neurons anticipate the homeostatic consequences of eating and drinking. Nature *537*, 680–684.